

Alma Mater Studiorum – Università di Bologna

**DOTTORATO DI RICERCA IN
SCIENZE E TECNOLOGIE DELLA SALUTE**

Ciclo XXXIV

Settore Concorsuale: 09/G2 BIOINGEGNERIA

Settore Scientifico Disciplinare: ING-IND/34 BIOINGEGNERIA INDUSTRIALE

PLANNING AND ASSESSMENT TECHNIQUES FOR SPINE SURGERIES

Presentata da: Jennifer Fayad

Coordinatore Dottorato:
Prof. Marco Viceconti

Supervisore:
Prof. Luca Cristofolini

Co-Supervisore:
Rita Stagni, PhD
Peter Endre Eltes, MD, PhD
Aron Lazary, MD, PhD

Esame finale anno 2022

Abstract

The rate of diagnosis and treatment of degenerative spine disorders is increasing, as a result, the need for surgical intervention is on the rise. Posterior spine fusion is one of these surgical interventions used to treat various spine degeneration pathologies. However, as the rate of fusion surgeries increases, we're seeing an increase in the rate of complications, requiring reoperation in extreme cases.

To minimize the risk of complications and provide patients with positive outcomes, preoperative planning and postsurgical assessment are necessary. Image-based approaches for spine surgery remain the diagnostic tool of choice to plan surgery and to measure the postoperative outcome. However, these approaches aren't enough to provide surgeons with information on the patients' mobility, the complexity of the spine degeneration and the effect of instrumentation on the biomechanics of the spine.

This PhD aimed to investigate techniques for the surgical planning and assessment of spine surgeries. This project assessed three main techniques that could be used in a clinical setting, and these were: stereophotogrammetric motion analysis, 3D printing of complex spine deformities and finite element analysis of the thoracolumbar spine.

The first part of the thesis focused on reviewing the literature to find the currently available spine kinematics protocol. From this review, a comprehensive motion analysis protocol to measure the multi-segmental spine motion was developed. Using this protocol, the patterns of spine motion in patients before and after posterior spine fixation was mapped. These patterns could be further used to assess the relation between spinal fixation and the risk of biomechanical complications.

The second part investigated the use of virtual and 3D printed spine models for the surgical planning of complex spine deformity correction. Compared to usual radiographic images, the physical model of the deformed spine allowed surgeons to plan the optimal surgical intervention, reduced surgical time and provided better surgeon-patient communication.

The third part assessed the use of polyetheretherketone (PEEK) rods auxiliary to titanium rods to reduce the stiffness of posterior spine fusion constructs and decrease the risk factors related to proximal junctional kyphosis. Using a finite element model of the thoracolumbar spine, the PEEK rods system showed an increase in intervertebral rotation, a decrease in pedicle screw stresses and a decrease in the overall stress of the uppermost instrumented vertebra when compared to regular fixation approaches.

Finally, a retrospective biomechanical assessment of a lumbopelvic reconstruction technique was investigated to assess the patients' gait following the surgery, the implant deformation over the years and the extent of bony fusion between spine and implant. Through this assessment approach, a computer-based assessment methodology was developed that could be applied to assess complex spine surgical procedures.

In conclusion, the present study highlighted the need to provide surgeons with new planning and assessment techniques to get a better understanding of postsurgical complications. The three methodologies investigated in this project can be used in the future to establish a patient-specific planning protocol.

Table of Contents

ABSTRACT	3
TABLE OF CONTENTS	5
INTRODUCTION	7
THESIS OUTLINE:	9
CHAPTER 1: BACKGROUND	11
1.1 SPINE DEGENERATION, POSTERIOR SPINE FUSION, AND PROXIMAL JUNCTIONAL KYPHOSIS	11
1.2 MULTI-SEGMENTAL SPINE KINEMATICS MEASUREMENT APPROACHES	17
<i>Abstract:</i>	17
<i>Introduction:</i>	19
<i>Methods:</i>	20
<i>Results:</i>	23
<i>Discussion:</i>	44
<i>Conclusions</i>	48
1.3 3D PRINTING OF ANATOMICAL SPINE MODELS.....	50
1.4 FEA OF THE THORACOLUMBAR SPINE:.....	54
CHAPTER 2: QUANTIFYING MULTI-SEGMENTAL SPINE KINEMATICS IN HEALTHY PARTICIPANTS	57
ABSTRACT	57
INTRODUCTION:.....	59
METHODS:	59
<i>Participants:</i>	59
<i>Experimental Assessment:</i>	60
<i>Data Analysis:</i>	62
RESULTS:	65
<i>Measurement Reliability:</i>	65
<i>Characterization of multi-segmental spine motion:</i>	67
DISCUSSION:.....	71
<i>Measurement Reliability:</i>	71
<i>Motion Characterization:</i>	73
CONCLUSION:	74
CHAPTER 3: MULTI-SEGMENT SPINE MOTION OF PATIENTS BEFORE AND FOLLOWING POSTERIOR SPINE FUSION	76
ABSTRACT	76
INTRODUCTION:.....	78
METHODS:	79
<i>Participants:</i>	79
<i>Radiographic Evaluation:</i>	79
<i>Motion Data Collection:</i>	80
<i>Data Analysis:</i>	80
RESULTS:	82
<i>Radiographic Evaluation:</i>	82
<i>Patient Cohorts Comparisons:</i>	85
<i>Before and After Surgery Comparison:</i>	87
<i>Healthy Participants and Patient cohorts' comparisons:</i>	92
DISCUSSION:.....	93
CONCLUSION:	96
CHAPTER 4: THE USE OF 3D VIRTUAL AND PRINTED MODELS TO PLAN DEFORMITY CORRECTION SURGERIES	97
ABSTRACT	97
INTRODUCTION:.....	99

CASE PRESENTATION:.....	99
<i>Medical history</i>	99
<i>Evaluation and analysis</i>	100
<i>Analysis of spinopelvic alignment in terms of surgical correction</i>	100
<i>Virtual and 3D printed models of the surgery</i>	102
<i>Surgical treatment and outcome</i>	103
DISCUSSION:.....	105
CONCLUSION:	106
SUPPLEMENTARY MATERIALS	107
CHAPTER 5: THE EFFECT OF PEEK RODS ON THE BIOMECHANICS OF PROXIMAL JUNCTIONAL KYPHOSIS	109
ABSTRACT:	109
INTRODUCTION.....	111
MATERIALS AND METHODS	112
<i>Intact T7-L5 Model:</i>	112
<i>Model Validation:</i>	114
<i>Instrumented models:</i>	114
<i>Data analysis:</i>	115
RESULTS:	116
<i>Model validation:</i>	116
<i>Intervertebral Rotations:</i>	118
<i>Von Mises Stress in Screw Bodies:</i>	120
<i>Stress Distribution in the UIV:</i>	122
DISCUSSION.....	122
CONCLUSION	125
CHAPTER 6: GAIT ANALYSIS AND MAPPING BONY FUSION TO ANALYSE THE OUTCOME OF THE CLOSED LOOP RECONSTRUCTION TECHNIQUE	126
ABSTRACT	126
INTRODUCTION.....	128
METHODS:	129
<i>Clinical Case:</i>	129
<i>Post-Surgical Evaluation:</i>	130
RESULTS	134
<i>Gait Analysis:</i>	134
<i>Segmentation Accuracy:</i>	137
<i>Evaluation of implant alignment:</i>	138
<i>Implant Deformation:</i>	138
<i>Mapping of the bony fusion:</i>	138
DISCUSSION.....	139
CONCLUSION	140
CONCLUSIONS.....	142
LIST OF FIGURES	144
LIST OF TABLES	145
ACRONYMS	146
ACKNOWLEDGEMENTS.....	147
BIBLIOGRAPHY.....	148

Introduction

With the gradual increase in the age and life expectancy of the population, the rate of diagnosis and treatment of degenerative spine disorders are increasing¹⁻⁴. Low back pain (LBP) is such a disorder that is currently the leading cause of years lived with disability in the world^{5,6}. LBP could be classified into specific or non-specific⁶. Specific LBP is characterized by a detectable somatic cause such as disc herniation, spine deformity, osteoporosis to name a few⁶. Following diagnosis, the first step in the management of LBP is conservative therapy such as medication and physiotherapy to alleviate the pain^{5,7}; and that is often the treatment of choice for the older population⁷. However, when LBP is accompanied by persistent pain and a localized pain source, more invasive therapy options are considered such as targeted injections or ultimately surgical interventions^{5,7}.

Posterior spine fusion (PSF) is one of these surgical interventions used to treat various spine degeneration pathologies⁴. The surgery entails the fusion of two or more vertebrae that become one solid structure holding them together by transpedicular screws and rods⁸. PSF surgeries are needed to stop the motion of painful vertebrae, correct deformities, achieve neural decompression and restore spine balance in the sagittal and coronal planes³. Following long PSF, complications have been seen to occur in the spinal segment adjacent to the instrumented vertebrae adversely affecting both the patient and surgeons⁹. Proximal junctional kyphosis (PJK) is one such complication^{2,10,11}, where an abnormal kyphotic deformity occurs just above the uppermost instrumented vertebrae^{2,12-14}.

To minimize the risk of these complications, achieve sagittal balance and provide patients with positive surgical outcomes; extensive preoperative planning is needed¹⁵. Image-based planning for spine surgery remains the diagnostic tool of choice to evaluate the spine. Current preoperative planning is mainly based on the analysis of the spino-pelvic alignment of the spine using standing full-spine radiographs including at least the femoral heads¹⁶. Dedicated software is then used to measure the spino-pelvic parameters, simulate the surgical procedures and establish the objectives of the correction¹⁶. To evaluate the bony structures of the spine and plan appropriate screw placement location for PSF surgeries, computed tomography (CT) scans could be used, while magnetic resonance imaging (MRI) is used to characterize the intervertebral disc, vertebral endplates and nerve impingements¹⁷. However, these measurements aren't enough to provide a complete understanding of the spine and its pathology due to (a) the effect of motion on the spine and its alignment¹⁸, (b) the complex

nature of the spine degeneration ¹⁹, (c) the effect of the fusion level and the implants used on the biomechanics of the spine ¹⁴.

Motion abnormalities in spine pathology patients have been linked to the prevalence and the recurrence of spine ailments ^{20,21}. Motion analysis could provide information on the dynamic sagittal alignment of the patient ²², the compensatory mechanisms the patient employs ²³, the coordination between the spine segments and between the spine and the lower limbs ²⁴. Currently, various motion analysis protocols exist to measure and characterize the motion of the spine, however, a standard multi-segmental spine motion analysis protocol is still missing ^{25,26}. A standard is needed to provide 1) reliable data on spine motion in terms of the repeatability and accuracy of the measurement, 2) a suitable measurement approach for the spine in a clinical setting, 3) clinically significant outcome measures to help in surgical planning and treatment choice.

In addition to motion abnormalities, complex anatomical changes are seen in extreme degenerative cases at the level of the affected spine segment ²⁷, causing unique geometrical irregularities and proving to be a great hurdle for regular surgical planning approaches as the surgeons are unable to properly visualize the geometrical problem from onscreen x-ray images ²⁸. Virtual and printed three-dimensional models of the spine have been found to improve surgical outcomes and performance however patient-specific models are still very rare worldwide ²⁹.

When looking at improving surgical outcomes and decreasing the risk of PJK in PSF patients through pre-surgical planning, understanding the biomechanics of the spine and the implants to be used provides additional information on the reasons for the failure mechanism ^{8,13}. In order to achieve this, finite element (FE) analysis of spine models is now widely accepted to simulate the effect of PSF on the spine ³⁰. However, currently, most FE simulations are based on lumbar spine models with reliable models of the thoracolumbar spine being very limited ^{31,32}. Following long PSF of the thoracolumbar spine, the upper instrumented vertebrae fall in the thoracic region; hence simulating the effect of PSF in the thoracic spine could help in understanding the biomechanical risk factors causing PJK ¹⁴.

In addition to helping plan spine surgeries, some of these techniques could also be used to assess surgical outcomes and measure the success of the surgery. Motion analysis and in particular, gait analysis could be used to measure how gait parameters were affected due to surgery or how the surgical intervention helped improve the motion of the patient. On the other hand, defining the three-dimensional (3D) geometry of the spine and implant construct could be used to measure bony fusion and implant deformation following surgery.

This PhD aims to introduce and investigate techniques for the surgical planning and assessment of spine surgeries that can provide physicians with information on the patient's motion abilities, the accurate geometry of the spine, the risk of complication following surgery and the surgical outcome. The project assesses three methods for surgical planning and assessment that could become essential techniques used in everyday clinical settings and personalized medicine in the future.

The thesis activities are organised as follows: first, the literature was assessed on the available methods for multi-segmental spine motion analysis, from there a motion analysis protocol was developed and used to measure the motion of PSF patients before and after surgery and of healthy participants. The reliability and advantages of 3D printed anatomical models of the spine to be used as a surgical planning technique were also investigated in addition to the effect of transitional rods on the biomechanics of the spine following PSF using FE simulations was assessed to understand its effect on the onset of PJK. Finally, a post-operative assessment approach was developed to assess the mobility, bony fusion and implant deformation in a patient following the closed loop reconstruction technique.

Thesis Outline:

Chapter 1 focuses on providing background information on the project and is separated into four sections: 1) PSF, PJK and current surgical planning techniques, 2) spine-kinematic measurement approaches, 3) 3D printed anatomical models and 4) finite element analysis of surgical implants. First, we go over the PSF surgery, its indications, patients benefitting from the surgery, its complications such as PJK to then explain the current technique employed in everyday surgical planning. Second, a review of the literature was developed to investigate the spine motion analysis protocols that currently exist and ultimately find common grounds between these different protocols from which a standard method for measuring spine kinematics could be agreed upon. This chapter finally goes over the current state of 3D printing of anatomical models for pre-surgical planning and FE simulations of spine segments and surgeries.

Chapter 2 introduces the developed protocol to measure multi-segmental spine motion in healthy participants. This method focused on providing a reliable, suitable, and clinically significant approach for spine motion allowing for measurement comparability. It also aimed at establishing the reference motion patterns of the spine segments when completing several tasks.

Chapter 3 assessed the motion of PSF patients before and after their surgery. The patient cohort was split into two categories, patients undergoing long PSF and those undergoing short PSF. The spine motion of patients while completing activities of daily living tasks was then compared to the reference motion patterns established in Chapter 2, while the changes to the motion patterns before and after the surgery were also highlighted.

Chapter 4 introduces the second surgical planning technique of this PhD project. The use of 3D virtual and printed anatomical models of the spine was assessed to help develop a surgical plan for a complex flat back deformity correction. The 3D printed model helped the surgeons visualize the complex anatomy of the patient and resulted in a successful surgery, paving the way for its use in more personalized medicine in the future.

The third surgical planning technique introduced in this thesis was described in Chapter 5. Using FE simulations, the effects of polyetheretherketone (PEEK) rods on the biomechanics of the thoracolumbar spine were assessed and compared to regular PSF procedures, in an aim to ultimately investigate the biomechanical risk factors leading to PJK.

Chapter 6 introduces an approach to assess surgical outcome. Using gait analysis and CT scans, the biomechanics of the closed loop reconstruction surgery were measured to assess the changes to the instrumentation over 6 years and its effect on the patients' mobility.

The project was carried out in collaboration with the National Center for Spinal Disorders, Buda Health Center, Budapest as part of the SPINNER ITN. Motion acquisitions were made at the Department of Orthopaedics of the Semmelweis University, Budapest, and the University of Bologna.

Chapter 1: Background

1.1 Spine Degeneration, Posterior Spine Fusion, and Proximal Junctional Kyphosis

The increase in life expectancy due to the advancements in healthcare have led to an increase in the prevalence of spinal degeneration disorders with back pain becoming one of the most frequent complaints of older people ^{2,33}. Degeneration of the spine induces anatomical changes to different structures at the level of the bone, disc, ligaments and facet joints ³³. These alterations could be seen as osteoporosis in the vertebrae, disc degeneration or impairments at the level of the back muscles ³⁴; ultimately causing pain, disability and postural changes in patients ¹.

When looking at the pain and disability caused by spine degenerative diseases, LBP is found to be the most common musculoskeletal condition affecting the older population ^{33,35} causing major social and economic problems and responsible for the most years lived with disability in the world ^{5,6,35}. Many anatomical sources could be causing LBP symptoms from nerve roots, spine muscles, intervertebral discs, bones, or joints ³⁵; proving to be a challenge for physicians to diagnose especially as imaging findings are usually weakly linked to patient symptoms ^{35,36}. In general, LBP is referred to as non-specific pain however some of the pain sources could be attributed to either the facet joint, disc degeneration, the sacro-iliac joint or spinal stenosis ³⁵.

Beyond pain and disability, adult spinal deformity (ASD) is another highly prevalent outcome of spine degenerative diseases in people over the age of 65 with incidence rates ranging between 32% and 68% in that age group ¹⁹. The causes of ASD are diverse, from new-onset deformity to progressive development of a pre-existing deformity or the accelerated progression of a deformity due to spinal surgery ¹⁹. The degeneration usually starts at the level of the intervertebral disc causing changes to the disc's anatomy and biomechanical properties ¹⁹. These changes lead to pathological changes in the load-bearing abilities of the spine and start affecting the facet joints and intervertebral space promoting bone remodelling at these joints ¹⁹. This bone remodelling cycle keeps progressing to cause instability in the joint and the ligaments surrounding it and ultimately leading to spinal deformity ¹⁹.

Different treatment options exist to address LBP and ASD ³⁷. These can be classified as non-invasive treatment, and surgical interventions ³⁷. Non-operative treatments are the first

1.1 Spine Degeneration, Posterior Spine Fusion, and Proximal Junctional Kyphosis

to be suggested following a diagnosis such as physical therapy, non-steroidal anti-inflammatory drugs, and injection therapy³⁸. The goal of these treatments is to alleviate back pain and provide a way for patients to manage the disease and maintain functional abilities³⁸. Once conservative treatment options have been exhausted, surgical intervention could then be considered³⁸. The main aim of these surgeries is to restore coronal and sagittal balance and achieve the needed neural decompressions³⁸.

Multiple surgical procedures have been used to treat spine degenerative diseases including i) decompression surgeries to address pain-related spine degeneration such as discectomy and laminectomy³⁹, ii) osteotomy to correct sagittal or coronal imbalances such as pedicle screw osteotomy and vertebral column resection³⁸, iii) simple fusion and iv) complex fusion³⁹. With some corrections involving a combination of decompression, fusion and osteotomies to address spine malalignment⁴⁰. Fusion surgeries can be achieved either from an anterior approach known as anterior spinal fusion (ASF) or from a posterior approach referred to as posterior spine fusion (PSF) or a combination of both approaches⁴¹. However, in most cases, PSF is the gold standard of choice for the treatment of spine degenerative diseases^{38,41}.

When looking at fusion surgeries, simple fusion surgeries involve a single surgical approach and are also referred to as short fusion surgeries as only 1-2 disc levels are involved; while complex fusion surgeries could involve more than one approach or involve the fusion of more than 2 disc levels and are then referred to as long fusion surgeries³⁹. The main aim of fusion surgeries is to achieve a balanced spine and address the instability in the functional spine unit while avoiding any neurological deficit and maintaining as much motion in the remaining spinal segments as possible^{42,43}. The functional spinal unit (FSU) is held together by transpedicular screws and metal rods (Figure 1).

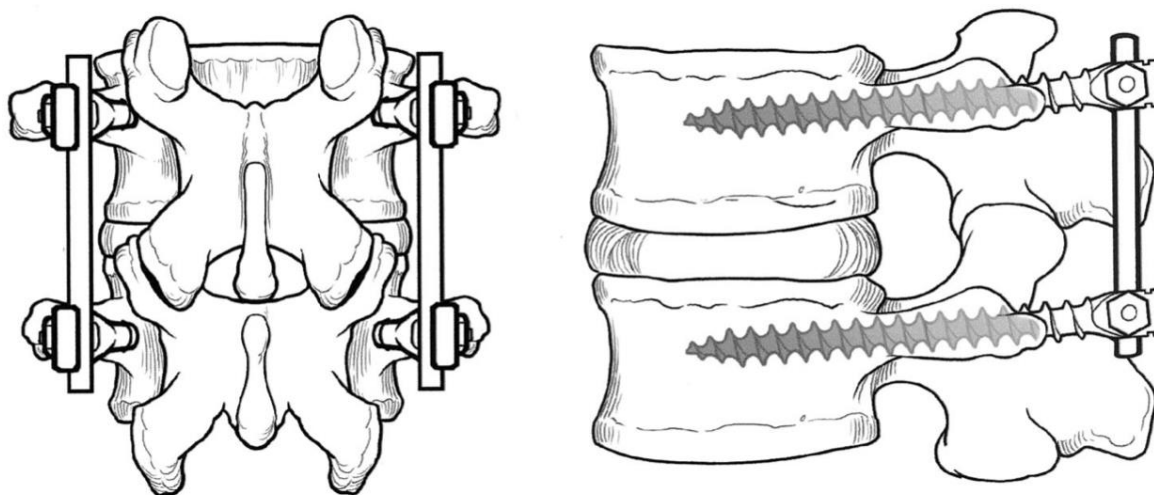


Figure 1 Posterior Spine fusion instrumentation showing an FSU with transpedicular screws and rods. From Ferrara LA, Secor JL, Jin BH, Wakefield A, Inceoglu S, Benzel EC: A biomechanical comparison of facet screw fixation and pedicle screw fixation: Effects of short-term and long-term repetitive cycling. *Spine* 28(12):1226–1234, 2003⁴⁴

The efficiency and safety of fusion surgeries have long been demonstrated^{41,45}, however, given the extensive dissection needed to place the implants and the longer operative time compared to spine decompression surgeries^{8,46} fusion surgeries are associated with the highest rate of post-operative complications when compared to other kinds of spine surgeries⁸. The most common complications reported after fusion are infection, neurological injury, instrument failure occurring in up to 7% of cases such as implant loosening, vascular complication for patients with various comorbidities, and mispositioning of hardware^{8,46}. Following the successful fusion of the spine segments, changes to the mechanics of the spine are seen in the adjacent segments⁴⁶. Due to the loss of mobility in the fused segments, high-stress localities are seen to occur in the adjacent vertebra. This occurrence is called adjacent segments disease or junctional failure⁴⁶. In particular, proximal junctional kyphosis (PJK) is one such complication that occurs in 20-40% of cases following spinal fusion, especially during long PSF surgeries^{2,46}.

PJK is a slow-developing symptom showing an abnormal kyphotic or forward bending occurring at the uppermost instrumented vertebrae, defined by 1) a sagittal Cobb angle greater than 10° between the inferior endplate of the uppermost instrumented vertebrae (UIV) and the upper endplate of the vertebrae two levels above the UIV (UIV+2), 2) a postoperative sagittal Cobb angle between the UIV and UIV+2 at least 10° greater than preoperative measurements^{2,12-14} (Figure 2). It could go on to be asymptomatic or develop a proximal junctional failure associated with pain, walking disturbances due to nerve impingement or spine imbalance, and a need for reoperation¹⁰.

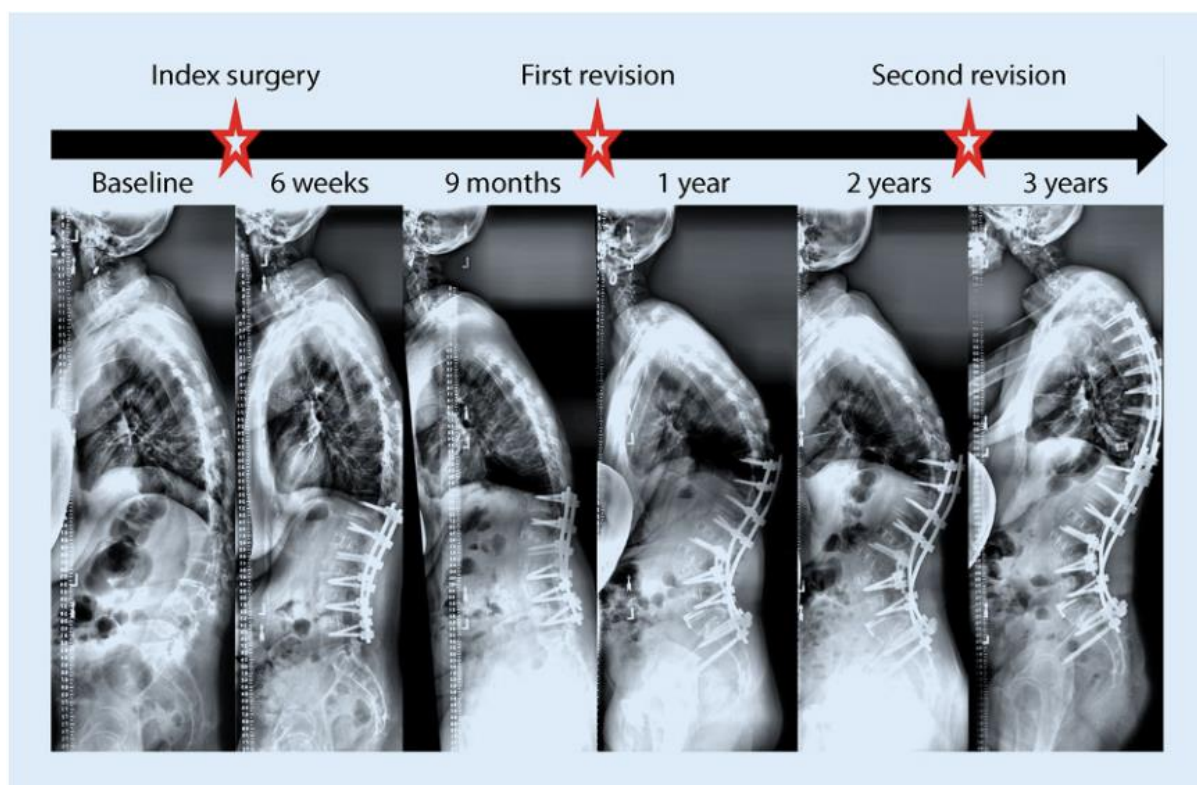


Figure 2 Patient with PJK requires 2 revision surgeries to address the mechanical complication From Diebo BG, Shah N V, Boachie-Adjei O, et al. Adult spinal deformity. Lancet. 2019;394(10193):160-172¹³.

Various risk factors have been associated with the development of PJK⁴⁷. Older age, high body mass index, decrease in bone mineral density, overcorrection of sagittal alignment and fusion to the sacrum have all been reported as risk factors for PJK^{13,14,48}. Conflicting evidence exists to suggest that the choice of UIV and the number of vertebrae fused influence the prevalence of PJK^{13,48}. The aetiology of PJK is complex^{2,48}, suggested failure mechanisms include altered biomechanics of the spine due to the change in rigidity between the UIV and the cranial spine segments^{9,14}, recurrence of the deformity due to the process of natural ageing in ASD patients⁴⁸, surgical disruption to the spinal muscles and ligaments at the UIV level^{9,13,48}. The global sagittal alignment or sagittal vertical axis (SVA) is also a great risk factor related to PJK, where an inadequate SVA change following spine fusion greater than 50mm was associated with higher PJK incidence^{2,10}. Currently, PJK is diagnosed using static radiographic techniques by calculating the Cobb angle between the uppermost instrumented vertebrae and T2 and by calculating the changes in the sagittal vertical axis².

In order to minimize surgical complications and optimize the surgical plan, adequate preoperative planning is needed^{6,15} to calculate the surgical correction required⁶, and predict the effect of the correction and instrumentation on the global balance of the spine¹⁵. Image-based techniques such as x-rays, CTs and MRIs are the tools of choice to diagnose spine

1.1 Spine Degeneration, Posterior Spine Fusion, and Proximal Junctional Kyphosis

pathologies and plan surgical corrections^{16,17}. Simple radiographs are the most commonly used in clinical practice to evaluate the patients' symptoms and serve as the first diagnostic tool for spine pathologies¹⁷. From standing x-rays of the patient, the spino-pelvic parameters can be measured to assess the sagittal and coronal balance and measure the degree of correction needed in the case of ASD¹⁷. Using dedicated software such as Surgimap (Nemaris Inc., New York, NY, USA), spinopelvic parameters are measured (Figure 3). The sagittal spino pelvic parameters commonly measured are Pelvic Incidence (PI), Pelvic Tilt (PT), Sacral Slope (SS), Lumbar Lordosis (LL), Thoracic Kyphosis (TK), Sagittal vertical axis (SVA), T1 spinopelvic inclination (T1SPi), T9 spinopelvic inclination (T9SPi), T1 pelvic angle (TPA), T1 slope (T1S), C2–C7 cervical lordosis, and C2–C7 SVA⁴⁹. For the coronal plane, the Cobb angle is measured in addition to the distance between the centre of the C7 vertebral body and the central sacral vertical line (CSVL)⁵⁰.

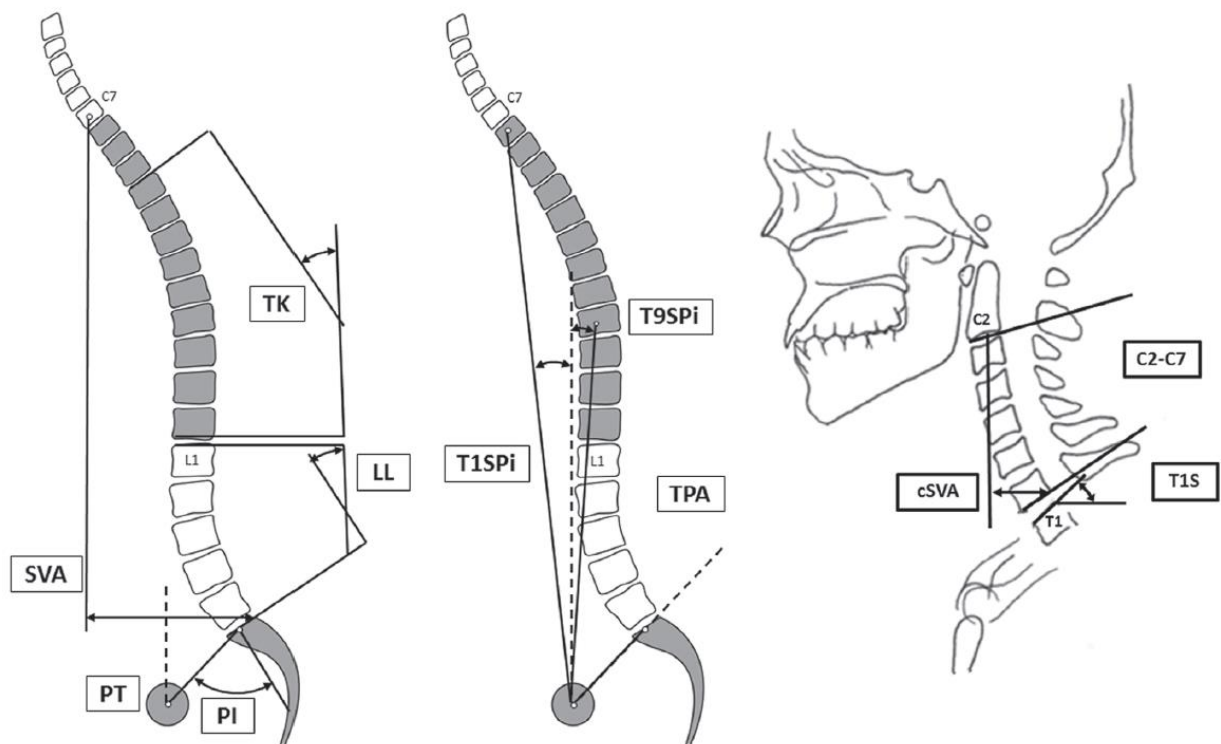


Figure 3 Sagittal spino-pelvic parameters. From Lafage R, Ferrero E, Henry JK, Challier V, Diebo B, Liabaud B, et al. Validation of a new computer-assisted tool to measure spino-pelvic parameters. *Spine J.* (2015) 15:2493–502⁴⁹

The assessment of these spino-pelvic parameters before surgical correction plays a crucial role in optimizing the surgery, and the instrumentation to be used⁶. From these, particular attention has been paid to three clinically relevant parameters: SVA, PT and the mismatch between PI and LL (PI-LL)^{6,17}. Targets are set for the corrective realignment to have an SVA < 40 or 50 mm, a PT < 20°, and a PI-LL < 10°⁶. These parameters are then adjusted to

1.1 Spine Degeneration, Posterior Spine Fusion, and Proximal Junctional Kyphosis

the patient's age to avoid overcorrection⁴⁹. When these values fall outside of the accepted ranges, poor postoperative alignment is seen associated with disability and mechanical complications⁶.

Beyond simple radiography, CT and MRI scans are used for additional information on the state of the pathological spine especially as these can provide higher resolution images than simple radiography¹⁷. CT scans can provide reconstructed three-dimensional images of the spine to evaluate the bony structures, particularly in the case of spine fusion where CT scans are used to plan pedicle screw location and assess the vertebra's anatomy¹⁷. When it comes to MRIs, these are used particularly to diagnose disc degeneration, herniation, infections, fractures, and tumours¹⁷. Currently, MRIs are the diagnostic procedure of choice due to the low radiation exposure and their ability to visualise both the vertebral and soft tissue elements of the spine¹⁷. Although imaging-based techniques have been the tool of choice for the diagnosis of spine pathologies and the planning of surgical interventions, insufficient correlation is found between the diagnostic images and the clinical symptoms⁵¹. Dynamic changes to the spine during loading or motion cannot be measured using simple imaging techniques although these changes could play a significant role in the onset of spine degenerative diseases⁵¹. When looking at ASD patients, in particular, extensive geometrical irregularities are seen in the spine anatomy due to various reasons (prior surgery, scoliosis, degenerative disc disease, sagittal degeneration)¹⁹. To visualize these irregularities, screen-based images are not enough for the surgeon to have a complete idea about the anatomical changes to the spine and what is to be expected during the surgery⁵². Likewise, the choice of instrumentation and the levels of fusion during PSF surgeries could also affect the surgical outcome and the risk for mechanical complications such as PJK. To this end, simulating the surgery using finite element analysis could also provide vital information for pre-surgical planning. These three aspects of surgical planning would be further discussed in the next points of this chapter.

1.2 Multi-Segmental spine kinematics measurement approaches

From the manuscript:

Jennifer Fayad, Peter E. Eltes, Aron Lazary, Luca Cristofolini, Rita Stagni.

Stereophotogrammetric approaches to multi-segmental kinematics of the thoracolumbar spine: A Systematic Review to submitted to BMC Musculoskeletal Disorders

Abstract:

Background: Spine disorders are becoming more prevalent in today's ageing society. Motion abnormalities have been linked to the prevalence and recurrence of these disorders. Various protocols exist to measure thoracolumbar spine motion, but a standard multi-segmental approach is still missing. This study aims to systematically evaluate the literature on stereophotogrammetric motion analysis approaches to quantify thoracolumbar spine kinematics in terms of measurement reliability, suitability of protocols for clinical application and clinical significance of the resulting functional assessment.

Methods: Electronic databases (PubMed, Scopus and ScienceDirect) were searched until February 2022. Studies published in English, investigating the intersegmental kinematics of the thoracolumbar spine using stereophotogrammetric motion analysis were identified. All information relating to measurement reliability; measurement suitability and clinical significance was extracted from the studies identified.

Results: Seventy-four studies met the inclusion criteria. 33% of the studies reported on the repeatability of their measurement. In terms of suitability, only 35% of protocols were deemed suitable for clinical application. The spinous processes of C7, T3, T6, T12, L1, L3 and L5 were the most widely used landmarks. The spine segment definitions were, however, found to be inconsistent among studies. Activities of daily living were the main tasks performed. Comparable results between protocols are however still missing.

Conclusion: The literature to date offers various stereophotogrammetric protocols to quantify the multi-segmental motion of the thoracolumbar spine, without a standard guideline being followed. From a clinical point of view, the approaches are still limited. Further research is needed to define a precise motion analysis protocol in terms of segment definition and clinical relevance.

1.2 Multi-Segmental spine kinematics measurement approaches

Keywords: Thoracolumbar spine, Stereophotogrammetry, Multi-Segment, Motion.

Introduction:

Spinal disorders such as low back pain (LBP) and adult spine deformity (ASD) are becoming more prevalent in today's ageing society ^{2,53}, with LBP being the leading global cause of years lived with disease ^{54,55} and ASD prevalence rates ranging between 32% and 68% in individuals over the age of 60 ^{56,57}. Patients could present with mild to severe symptoms ⁵⁸ impairing their mobility from gait disturbances to limitations in the spine range of motion (ROM) ^{18,22}. Treatment for spinal disorders depends on the severity of the disease ², when non-operative treatments are exhausted, surgical interventions are needed to provide pain relief or correct deformity ^{2,13}; however, the failure rates remain high following surgery ranging between 10% and 46% ⁵⁸ due to instrumentation failure or sagittal imbalance ^{13,58}. These disorders include a wide range of clinical and radiographical characteristics ⁵⁷. However, current research suggests that movement abnormalities impact the prevalence of spinal disorders and the recurrence of the disease following treatment ^{20,21}, hence the need for a better understanding of spine kinematics to improve treatment decisions and outcomes ^{59,60}.

Different quantification methods are available to quantitatively characterize spine kinematics and posture. i) Spinal alignment angles in the frontal and sagittal planes are quantified in static conditions by means of imaging techniques ⁶¹, such as X-rays, CT or MRI scans ^{18,61,62}. These angles are commonly used in clinical practice to support diagnosis, surgical planning, and pre- and post-intervention assessment ¹⁸, but do not provide any characterization of spine function in dynamic conditions ⁶². Static measurements are also affected by the limited repeatability of the measurements ⁶¹ with up to 20% change in lumbar lordosis values in subjects inter-session ⁶³. ii) Intervertebral 3D kinematics can be quantified using video-fluoroscopy [15, 16]. This technique is highly accurate, detecting intervertebral ROM with a measurement error varying between 0.32° and 0.52° in the coronal and sagittal plane, respectively ⁶⁶, but it is not exploited in clinical practice due to the small imaging volume preventing the analysis of spine segments, and due to the critical ionizing radiations exposure ⁶⁷. iii) Spine 3D angles can be quantified non-invasively using stereophotogrammetric motion analysis ⁶⁸ without field of view limitations, allowing also for the assessment during daily living activities ^{69,70}, but can potentially be affected by significant experimental errors ²⁶.

Stereophotogrammetric motion analysis is extensively used for the assessment of body segment kinematics during gait and other functional tasks ^{71,72}; although specific protocols and biomechanical models used for the assessment can differ ⁷³. Body segments (i.e. trunk, pelvis

1.2 Multi-Segmental spine kinematics measurement approaches

and limb segments) and joint definitions are consistent among protocols^{74,75}, while, for spine kinematics, a standard multi-segmental approach is still missing^{25,26}.

To assess thoracolumbar spine kinematics in an everyday clinical setting, reliable, clinically significant, and comparable data need to be reported by spinal motion protocols to provide a functional assessment of each spine segment and supply clinicians with a tool to characterize thoracolumbar kinematics changed by different pathologies. To achieve this, a set of standards and guidelines need to be agreed upon with recommendations on the motion tasks to carry out, optimal segment definitions, data to be generated and requirements for a protocol to be suitable for clinical application. Some previous review papers assessing spine motion analysis partially covered the clinical significance of thoracolumbar spine kinematic protocols^{26,76–79} or provided methodological information on the protocols available^{26,71}. However, this review aims to provide a complete assessment of available protocols in terms of 1) reliability of the measurement, 2) suitability of the protocol for clinical application and 3) clinical significance of the reported results to unravel comparable outcomes between the protocols found and ultimately provide recommendations on the standards needed for thoracolumbar motion analysis.

The review uncovers information relating to the measurement repeatability and accuracy approaches, number of markers used, segment definitions, degrees of freedom assessed, motion analysis system used, task choice, number of participants included, main measurements reported, pathologies assessed, and clinical findings.

Methods:

This systematic review was conducted in accordance with the PRISMA 2020 statement⁸⁰.

Study Selection and Research Criteria:

Article search was completed on the 7th of February 2022 on Scopus, PubMed, and Science Direct databases. The research keywords were customised to match each of the databases. Details of the research strings on each of the databases could be seen in Table 1.

1.2 Multi-Segmental spine kinematics measurement approaches

Table 1 Search Strings used on each database

Database	Research String
Scopus	TITLE-ABS-KEY (spine OR trunk OR back OR kinematics OR lumbar OR thoracic) AND TITLE-ABS-KEY ("motion analysis" OR "movement analysis") AND ABS (segment*) AND NOT TITLE-ABS (knee OR ankle OR cervical OR head OR inertial OR wireless OR gait)
PubMed	((("Motion analysis"[Title/Abstract] OR "movement analysis"[Title/Abstract])) AND (spine [Title/Abstract] OR back [Title/Abstract] OR trunk [Title/Abstract] OR kinematics [Title/Abstract] OR lumbar [Title/Abstract] OR thoracic [Title/Abstract]) AND (segmental [Title/Abstract] OR segment [Title/Abstract])) NOT (cervical [Title/Abstract] OR head [Title/Abstract] OR knee [Title/Abstract] OR ankle [Title/Abstract] OR gait [Title/Abstract] OR inertial [Title/Abstract] OR wireless [Title/Abstract])
Science Direct	("motion analysis" OR "movement analysis") AND (spine OR spinal OR back OR trunk OR lumbar OR thoracic) and (segment OR segmental) NOT (Cervical OR head OR ankle OR knee OR gait) NOT (wireless OR inertial)

The outcomes of the searches on the different databases were merged into a single list.

Studies were included in the review if they met the following inclusion criteria:

- 1) journal papers written in English,
- 2) assessing the intersegmental motion of the thoracolumbar spine,
- 3) using stereophotogrammetric motion analysis,

Articles passing inclusion criteria were retained as full-text documents.

Quality assessment:

The quality of the included studies was assessed using a customised quality assessment questionnaire including 19 questions. Questions 1-12 were designed to appraise the general quality of the studies in terms of study design and reproducibility of the method used. Questions 13 to 19 were specifically designed to assess the reliability of the measurement approach, the suitability of the approach to be used in a clinical setting and the clinical significance of the measurement. Quality assessment questions are listed in Table 2.

Table 2 Quality Assessment questionnaire used to evaluate the quality of the studies included in the review.

Quality Assessment Questionnaire:
1) Are the research objectives clearly stated?
2) Were the eligibility criteria of participants clearly defined?
3) Did the description of the method used, allow for a replication of the measurement?
4) Is the motion analysis system and setup described?
5) Are marker locations clearly described?
6) Were the spine segments chosen clearly stated and defined?
7) Was the population information and anthropometric data provided?

1.2 Multi-Segmental spine kinematics measurement approaches

8) Were the movement tasks chosen clearly described?
9) Were the statistical tests used clearly defined?
10) Were the main measurements and their calculations clearly described?
11) Are the main outcomes of the study clearly stated?
12) Were the limitations of the study clearly stated?
13) Was the repeatability of the measurement assessed?
14) Are errors from marker attachment considered?
15) Was the accuracy of the marker setup assessed?
16) Were the marker setups chosen easily applicable in a clinical setting?
17) Was the reason for choosing the motion task justified?
18) Did the participant cohorts include subjects with spine pathology?
19) Were the measurement outcomes clinically relevant?

Each question was scored on a three-level basis: 2= yes, 1= limited detail, 0= no, for an overall score of up to 38 possible points for each article. Bishop *et al.* (2012) rating score was used to classify studies by their quality: high quality was associated with articles with a score higher than 80% (31/38), medium quality articles had a score between 51% and 79% (19-30/38) while low quality was associated with a score lower than 50% (18/39).

Data extraction

A standardised extraction form was used to identify and report relevant information from each study. The extraction form points are listed in Table 3.

Table 3 Standardised extraction form used to extract relevant information from the studies collected.

Extraction Form:
1. Repeatability of the measurement
2. Accuracy of marker setup
3. Validation technique used
4. Number of markers used
5. Segments defined
6. Degrees of freedom studied
7. Motion analysis system used
8. Task Choice
9. Number of participants included
10. Pathologies assessed
11. Main measurements reported
12. Clinical findings

The study details extracted could be divided into three categories: reliability of the measurement (points 1 to 3), suitability of the approach to be used in a clinical setting (points 4 to 9) and the clinical significance of the results reported (points 10 to 12). Some of the data extracted were related to more than one category; this was the case for points 4,5,6,8 which related to both the repeatability and suitability of the measurement, points 9 and 10 related to both the suitability of the measurement and the clinical significance of the reported results.

1.2 Multi-Segmental spine kinematics measurement approaches

Since none of the studies assessed in this review reported on the suitability of the measurement to be used in a clinical setting in terms of time needed to attach the markers and the ease of use of their data processing approach by clinicians, the number of markers used, segments defined, and degrees of freedom studied were reported instead to determine this suitability. Studies using the same protocol as previous ones were grouped into a separate list.

Results:

Data Acquisition and research strategy:

The selection process identified a total of 10465 records, resulting in 8937 after duplicate removal. After screening titles and abstracts, 8827 studies were excluded as they were deemed irrelevant for the purposes of this review. Inclusion criteria were applied to 110 full-text articles. Seventy-four papers were found to match the inclusion criteria established while 36 studies were excluded as these did not report information on their marker setup, did not use an optoelectronic technique or defined the spine as one moving segment. The process for study selection is shown in the PRISMA flow chart (Figure 4). Of the 74 articles found, 44 articles proposed new protocols for multi-segments spine motion analysis.

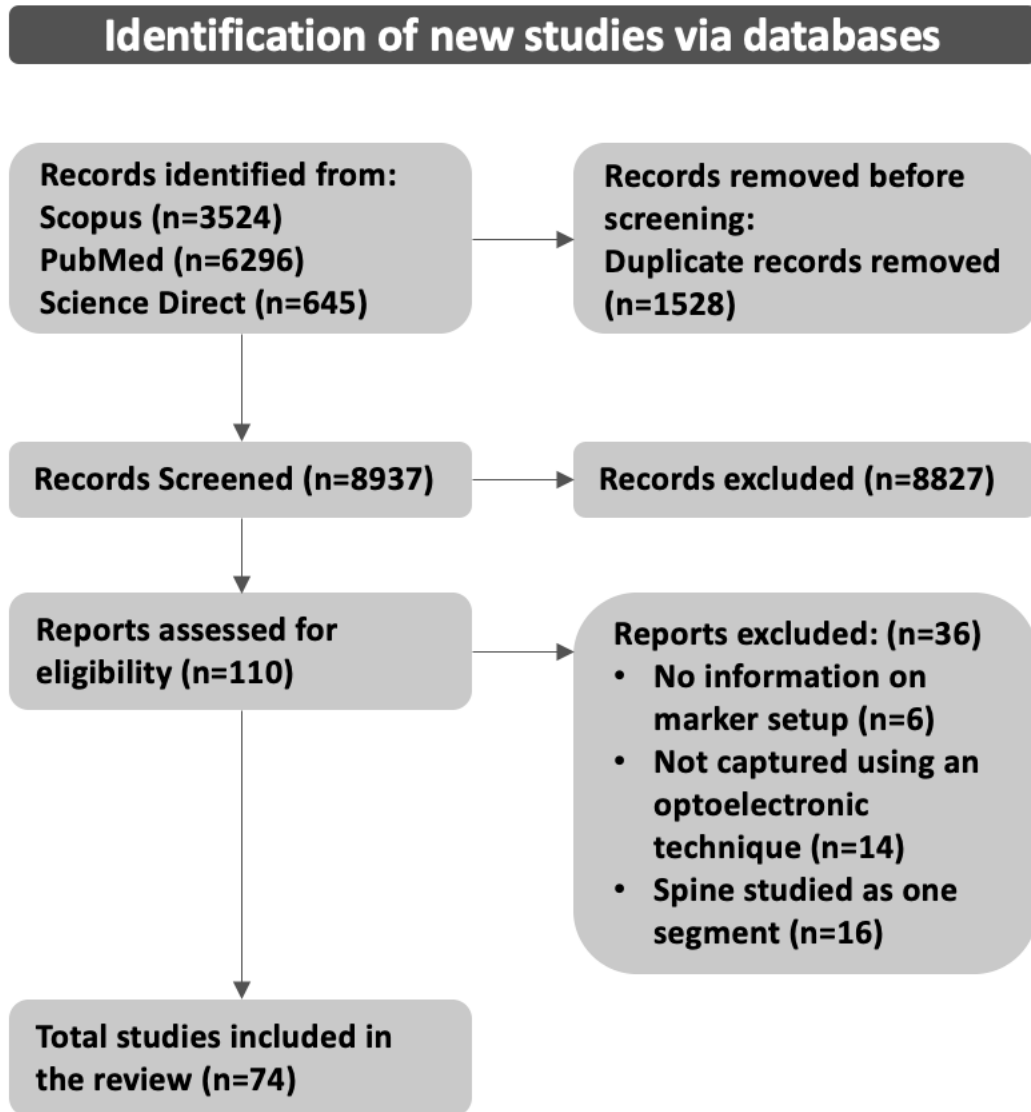


Figure 4 PRISMA flow chart representing the review process.

Quality Assessment:

The 74 articles were assessed using the quality assessment questionnaire. Of those, 12 studies^{20,59,60,82-90} were found to be of high quality. Sixty studies^{23-25,70,72,91-137} were deemed as medium quality studies and 2 studies^{138,139} had a low-quality score below 50% (Figure 5).

1.2 Multi-Segmental spine kinematics measurement approaches

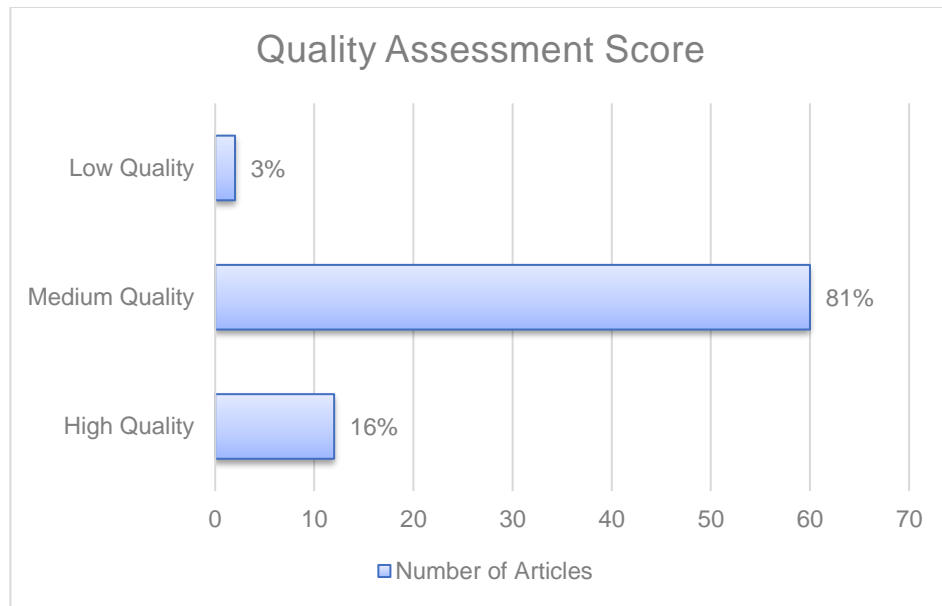


Figure 5 Quality Assessment Score of Articles included in the review Studies were scored as high, medium, or low-quality papers.

The number of articles answering yes to the quality assessment questions could be seen in Figure 6.

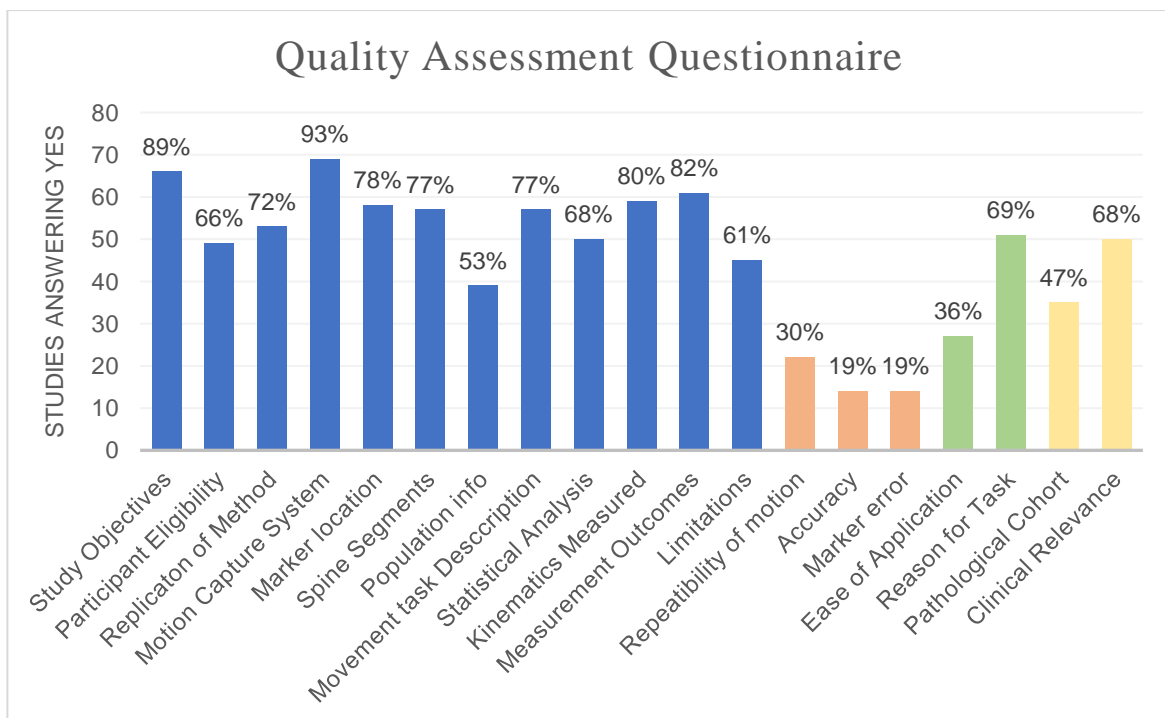


Figure 6 Quality Assessment Questionnaire. The number of articles answering yes to each of the questions. Blue bar plots indicate overall quality questions, orange bar plots indicate reliability-related questions, green bar plots indicate suitability related questions and yellow bar plots indicate clinical relevance related questions.

The details and study characteristics obtained from the extraction form of the 74 articles reviewed could be found in Tables 4 and 5.

1.2 Multi-Segmental spine kinematics measurement approaches

Table 4 Characteristics of included studies as retrieved from the data extraction form.

Study	NO. of Markers	Spine segments analysed	Kinematic variable assessed	System used	No. of Participants	Task performed
Alemi et al., 2021	35	3 (T1-T5, T5-T9, T9-L1, L1-S1)	Frontal, Sagittal, and transverse plane angles between the segments	10-camera VICON System	7	Flexion-extension, lateral bending, axial rotation
Arshad et al., 2018	47	5 (L1L2, L2L3, L3L4, L4L5, L5S1)	ROM in the sagittal, frontal, and transverse planes	10-camera VICON System, NEXUS	6	Walking trials
Choi et al., 2007	18	5 (Cervical, UT, LT, UL, LL)	ROM in the sagittal, frontal, and transverse planes	6-camera VICON 460 system, VICON NEXUS	6	Walking Trials
Christe et al., 2016	20	4 (UT, LT, UL, LL)	ROM in the sagittal plane	VICON system at 120HZ, MATLAB	21	Sit-to-Stand
Claus et al., 2016	5	3 (T5-T10, T10-L3, L3-S2)	Thoracolumbar angle in the sagittal plane	VICON system at 30Hz, VICON NEXUS, MATLAB	50	Spontaneous sitting position, correct sitting position, typical standing posture
Crosbie et al., 1997	15	4 (UT, LT, lumbar, pelvis)	Frontal, Sagittal, and transverse plane angles between the segments	4-camera Motion Analysis Corporation System	108	Walking trials
Frigo et al., 2003	12	3 (M1-M3, M3-M6, M6-M8)	Sagittal and frontal plane angles between the segments	4-camera ELITE system motion analyser at 100Hz	18	Walking trials
Ghasemi et al., 2021	42	2 (thoracic, lumbar)	ROM and lumbopelvic rhythm in sagittal, frontal, and transverse planes	10-camera VICON system, NEXUS	18	Flexion forward, extension backwards, lateral bending, spine rotation, load handling tasks
Gombatto et al., 2015	10	4 (UT, LT, UL, LL)	ROM in the sagittal, frontal, and transverse planes	9-camera VICON system, NEXUS, VISUAL 3D	36	Walking trials
Hemming, 2018	30	4 (UT, LT, UL, LL)	ROM of the Sagittal plane	8-camera VICON 512 at 100 Hz, MATLAB	79	Reach up, sit-to-stand, stand-to-sit, step up, step down, box lift, box replace, bend to retrieve pen from the floor
Hidalgo et al., 2012	9	5 (UT, LT, UL, LL, Lumbar)	Frontal, Sagittal, and transverse plane angles between the segments	8-camera BTS System	50	Flexion forward, lateral bending, flexion with left and right rotation while in a seated position
Holewijn et al., 2018	40	2 (proximal and distal parts of the fused spine)	ROM in the sagittal, transverse, and frontal planes	10-camera VICON system at 100Hz, NEXUS	12	Walking on a treadmill at a speed of 1.35m/s
Ignasiak et al., 2017	75	8 (thoracic, lumbar, C7-T3, T3-T5, T5-T7, T7-T9, T9-T11, T11-L1)	ROM in the sagittal plane	12-camera VICON MX system at 100Hz, NEXUS	42	Full range flexion forward with a return to upright posture
Kakar et al., 2019	19	3 (upper trunk, middle trunk, lower trunk)	ROM in the sagittal, transverse, and frontal planes	7-camera VICON M MX System at 240Hz, NEXUS	20	Running on a treadmill at speeds between 2.2-3.8m/s
Konz et al., 2006	5 + 8 marker triads	3 (cervical, thoracic, lumbar)	Frontal, sagittal, and transverse angles between segments	8-camera EAGLE digital real-time measurement system	10	Walking at 5 selected speeds
Kuai et al., 2018	8	5 (L1L2, L2L3, L3L4, L4L5, L5S1)	Frontal, sagittal, and transverse angles between segments	NDI OPTOTRAK CERTUS motion analysis system at 100Hz, MATLAB	33	Walking trials, stair climbing, max flexion
Kudo et al., 2018	70	1 (trunk), 2 (C7-T9, T9-S1), 3 (C7-T6, T6-T12, T12-S1), 6 (C7-T3, T3-T6, T6-T9, T9-T12, T12-S1)	Sagittal, frontal, and transverse plane angles between segments	23-camera Motion Analysis Corporation System at 250Hz, MATLAB	10	Max flexion, lateral bending and axial rotation posture held for 5s. Walking trials.
Kuwahara et al., 2016	24	2 (thoracic, lumbar)	Sagittal plane angles between segments	16-camera VICON MX system at 100Hz	20	Walking trials

1.2 Multi-Segmental spine kinematics measurement approaches

Study	NO. of Markers	Spine segments analysed	Kinematic variable assessed	System used	No. of Participants	Task performed
Leardini et al., 2011	14	5 (C7-T12, T12-MA1, MA1-L1, L1-L3, L3-L5)	Sagittal, frontal, and transverse plane angles between segments	8-camera VICON 612 at 100Hz, NEXUS, MATLAB	10	Chair rising and sitting, step up and down, walking trials
Lin et al., 2020	39 + 6 marker triads	5 (UT, Middle thoracic, Thoracolumbar, UL, LL)	ROM in the sagittal plane, angular velocity	10-camera VICON MX system, NEXUS, MATLAB	24	Box lifting
List et al., 2013	71	2 (thoracic, lumbar)	Sagittal, frontal, and transverse plane angles between segments	12-camera VICON MX system at 100Hz, MATLAB	30	Restricted and unrestricted squats
Marich et al., 2017	35	2 (thoracic, lumbar)	Sagittal plane angles between segments	8-camera VICON system at 120Hz, VISUAL 3D, MATLAB	48	Object pick-up at different heights and distances
Mason et al., 2014	14	2 (thoracic, Lumbar)	ROM in the sagittal, transverse, and frontal planes, angles between segments	12-camera Qualisys Pro-reflex system at 240Hz, Visual 3D, MATLAB	12	Running at a speed of 5.6m/s
Needham et al., 2015	3	3 (UT, LT, Lumbar)	Frontal, sagittal, and transverse angles between segments	8-camera VICON system at 100fps, VISUAL 3D	10	Walking trials
Papi et al., 2019	24	4 (UT, LT, UL, LL)	ROM in the sagittal, transverse, and frontal planes	10-camera VICON system at 100Hz, MATLAB	40	Walking trials, sit-to-stand transitions, lifting a 5kgs box
Patel et al., 2018	20	2 (Thorax, Pelvis)	Frontal Plane angles between segments	7-camera VICON 512	15	Walking trials, rotation of the spine
Peharec et al., 2007	15	4 (UT, LT, UL, LL)	Sagittal and coronal plane angles between segments	9-camera Smart BTS system	63	Flexion/extension, lateral bending from standing
Pesenti et al., 2020	36	2 (Thoracic, Lumbar)	Spine curvatures, CVA, SVA	6-camera VICON system at 100Hz	62	Walking Trials
Pollock et al., 2008	4	3 (UT, LT, UL)2	Sagittal plane angles between the segments	7-camera VICON at 100Hz	8	Walking on a treadmill for 60 minutes
Preuss and Popovic, 2010	24	7 (UT, MUT, MLT, LT, UL, LL, Sacral)	Frontal, sagittal, and transverse angles between segments	6-camera VICON 512 system at 120Hz	11	Leaning towards targets while seated
Rozumalski et al., 2008	6 marker triads	5 (L1-L2, L2-L3, L3-L4, L4-L5, L5-S1)	ROM of all three anatomical planes	12-camera VICON MX system	10	Maximum voluntary spine ROM, walking trials, jogging, sit-to-stand, lifting
Ryan and Bruno, 2017	14	2 (UL, LL)	Frontal, sagittal, and transverse angles between segments	6-camera VICON T-series system at 100Hz, NEXUS, VISUAL 3D	17	Walking trials, alternately raise the leg to a height of 20cm while keeping the knee extended
Saad et al., 2020	18	6 (C2-T1, T1-4, T4-6, T6-8, T8-10, T10-12)	Sagittal and coronal plane angles between segments	10-camera Motion Analysis Corporation system, MATLAB	10	Sit to stand, stand to flexion motions
Schinkel-ivy and Drake, 2015	5 marker triads	5 (C7-T3, T3-T6, T6-T9, T9-T12, T12-L5)	Frontal, sagittal, and transverse angles between segments	VICON MX system, VISUAL 3D, MATLAB	30	Max flexion, max lateral bending, max twist, slumped standing, thoracic flexion, thoracic lateral bend, thoracic twist
Schmid et al., 2015	56	3 (Cervical, thoracic, lumbar)	Thoracic and Lumbar curvature	12-camera MXT20 VICON system at 200-300Hz, NEXUS, MATLAB	10	Walking trials
Seay et al., 2008	35	2 (Thoraco-lumbar, Lumbo-Sacral)	Frontal, sagittal, and transverse angles between segments, segment moments	8-camera MC240 QUALISYS System at 240Hz, QTM, Visual 3D	10	Running at a speed of 3.83m/s
Seerden et al., 2019	45	6 (UT, Middle Thoracic, Thoracolumbar, UL, LL, lumbosacral)	ROM in the sagittal plane	10-camera VICON MX system at 100Hz, NEXUS, MATLAB	18	Return from forward flexion, box lifting

1.2 Multi-Segmental spine kinematics measurement approaches

Study	NO. of Markers	Spine segments analysed	Kinematic variable assessed	System used	No. of Participants	Task performed
Severijns et al., 2020	47 + 6 marker triads	2 (Thoracic, Lumbar)	Spine curvatures, SVA	10-camera VICON system	41	Sit-To-Stand
Sung et al., 2016	34	3 (Lumbar, LT, UT)	Spine rotation	EvaRT: Motion analysis corporation, MATLAB	44	Lateral Bending to dominant and non-dominant sides while holding a bar overhead
Sung et al., 2020	44	3 (Lumbar, LT, UT)	Spine Rotation	6-camera Motion analysis corporation, CORYEX software	32	Trunk rotation from left to right while holding a bar
Swain et al., 2018	17	4 (LL, UL, LT, UT)	ROM in frontal and transverse planes	9-camera MX13+ VICON, NEXUS, VISUAL 3D	60	Max trunk rotation, max side bend
Tojima et al., 2013	8	2 (Pelvis, Lumbar)	ROM in the sagittal, transverse, and frontal planes	7-camera VICON, MATLAB	7	Max flexion/extension, Max lateral bending, axial rotation
Wilk et al., 2006	2 marker triads	2 (lumbar, Thoracic)	ROM in the sagittal and coronal planes	8-camera VICON system at 120 Hz	91	Forward, Backward, and lateral bending
Zwambag et al., 2018	21	2 (thoracic, lumbar)	Frontal, sagittal, and transverse angles between segments	Optitrack motion analysis system	4	Full forward flexion, lateral bending, axial rotation to reach a virtual target

1.2 Multi-Segmental spine kinematics measurement approaches

Table 5 Characteristics of studies extracted from the literature search with marker setups adapted from papers in Table 4.

Study	No. of Markers	Spine segments analysed	Kinematic variable assessed	System used	Participants	Task Performed	Adapted From
Al Eisa <i>et al.</i> , 2006	13	3 (UT, LT, Lumbar, Sacral)	ROM in the transverse and frontal planes	5-camera Qualisys Motion analysis System, MATLAB	113	Lateral Flexion and axial rotation	Crosbie <i>et al.</i> , 1997
Alijanpour <i>et al.</i> , 2021	40	3 (UT, LT, Lumbar)	ROM in sagittal, frontal, and transverse planes, segment coordination	7-camera VICON system at 200Hz, NEXUS	14	Rowing	Needham <i>et al.</i> , 2015
Bagheri <i>et al.</i> , 2017	13	2 (thoracic, lumbar)	Frontal, sagittal, and transverse angles between segments	6-camera Qualisys System, QTM, MATLAB	30	Walking trials with and without load carrying	Seay <i>et al.</i> , 2008 Hidalgo <i>et al.</i> , 2012
Beaudette <i>et al.</i> , 2019	57	2 (thoracic, lumbar)	ROM in the sagittal plane	Optitrack motion analysis system	51	Flexion Extension Motion	Zwambag <i>et al.</i> , 2018
Breloff <i>et al.</i> , 2015	22	7 (UT, MUT, MLT, LT, UL, LL, Sacral)	ROM in sagittal, frontal, and transverse planes	10-camera Motion analysis corporation, MATLAB	10	Seated anterior and lateral bending, level-ground walking	Preuss and Popovic, 2010
Christe <i>et al.</i> , 2017	20	4 (UT, LT, UL, LL)	ROM in the sagittal plane	VICON at 120HZ, MATLAB	22	Walking Trials	Christe <i>et al.</i> , 2016
Christe <i>et al.</i> , 2020	20	4 (UT, LT, UL, LL)	ROM in sagittal, frontal, and transverse planes	14-camera VICON at 120HZ, MATLAB	21	Step up on boxes of different heights	Christe <i>et al.</i> , 2016
Deane <i>et al.</i> , 2020	23	3 (UT, LT, Lumbar)	Peak joint angles in the sagittal, transverse, and frontal planes	10-camera VICON system at 100Hz, NEXUS, MATLAB	10	Walking trials, sit-to-stand transitions	Papi <i>et al.</i> , 2019
Gilleard <i>et al.</i> , 2013	15	2 (thoracic, lumbar)	ROM in sagittal, frontal, and transverse planes	8-camera camera Motion analysis corporation	9	Walking Trials	Crosbie <i>et al.</i> , 1997
Glover <i>et al.</i> , 2021	63	3 (upper trunk, middle trunk, lower trunk)	Error profile of spine markers, tracking error of musculoskeletal models	7-camera VICON M MX System at 120Hz, OpenSim	7	Running Trials	Kakar <i>et al.</i> , 2019
Gombatto <i>et al.</i> , 2017	10	4 (UT, LT, UL, LL)	Frontal, sagittal, and transverse angles between segments	9-camera VICON system, NEXUS, VISUAL 3D	35	Picking up a small object from the ground	Gombatto <i>et al.</i> , 2015
Hagins <i>et al.</i> , 2021	31	4 (LL, UL, LT, UT)	ROM in the sagittal, transverse, and frontal planes	8-camera Motion analysis corporation, VISUAL 3D	59	Dance movements	Swain <i>et al.</i> , 2018
Hernandez <i>et al.</i> , 2019	10	4 (UT, LT, UL, LL)	ROM in sagittal, frontal, and transverse planes	9-camera VICON system, NEXUS, VISUAL 3D	36	Step Down	Gombatto <i>et al.</i> , 2015
Hooker <i>et al.</i> , 2021	35	2 (thoracic, lumbar)	Lumbar curvature angle	8-camera VICON system at 120Hz, NEXUS, MATLAB	154	Preferred sitting posture, flexed, and extended sitting	Gombatto <i>et al.</i> , 2015 Marich <i>et al.</i> , 2017
Ignasiak <i>et al.</i> , 2018	75	8 (thoracic, lumbar, C7-T3, T3-T5, T5-T7, T7-T9, T9-T11, T11-L1)	Maximum compressive loads on thoracolumbar spine, ROM in the sagittal plane	12-camera VICON MX system at 100Hz, NEXUS	44	Full Flexion Forward, Stand-to-Sit, Sit-to-Stand	Ignasiak <i>et al.</i> , 2017
Knechtle <i>et al.</i> , 2021	58	2 (thoracic, lumbar)	Angular displacement in Sagittal plane, lumbar lordosis curvature	20-camera VICON at 200Hz, NEXUS, MATLAB	61	Bending forward, sit-to-stand transitions, object pick-up	Schmid <i>et al.</i> , 2015
Marich <i>et al.</i> , 2020	35	2 (thoracic, lumbar)	Angular displacement in Sagittal plane	8-camera VICON system at 120Hz, NEXUS, MATLAB	48	Forward bending, object pick-up	Marich <i>et al.</i> , 2017
Muller <i>et al.</i> , 2016	24	3 (UT, LT, Lumbar)	ROM in sagittal, frontal, and transverse planes	8-camera VICON system at 200Hz	10	Treadmill walking trials with perturbations	Preuss and Popovic, 2010
Niggli <i>et al.</i> , 2021	58	3 (Cervical, thoracic, lumbar)	Thoracic and Lumbar curvature	10-camera VICON at 200Hz, NEXUS	20	Walking, running, sit-to-stand, object pickup, vertical jump	Schmid <i>et al.</i> , 2015
Noamani <i>et al.</i> , 2018	21	7 (UT, MUT, MLT, LT, UL, LL, Sacral)	ROM in sagittal, frontal, and transverse planes	6-camera Vicon System at 120Hz	11	Anterior and side Seated Bending	Preuss and Popovic, 2010
Papi <i>et al.</i> , 2020	24	4 (UT, LT, UL, LL)	ROM in the sagittal, transverse, and frontal planes	VICON system at 100Hz, NEXUS, MATLAB	40	Walking trials, sit-to-stand transitions, lifting a 5kgs box	Papi <i>et al.</i> , 2019
Pelegrinelli <i>et al.</i> , 2020	18	2 (Thoracic, Lumbar)	ROM in the sagittal, transverse, and frontal planes	10-camera Oqus 400 Qualisys system at 240 Hz, MATLAB	26	Running on a treadmill at 3.3m/s	Mason <i>et al.</i> , 2014
Preece <i>et al.</i> , 2016	14	2 (Thoracic, Lumbar)	ROM in the sagittal, transverse, and frontal planes	12-camera Qualisys Pro-reflex system at 240Hz, Visual 3D, MATLAB	15	Running at a speed of 5.6m/s	Mason <i>et al.</i> , 2014
Rouhani <i>et al.</i> , 2016	22	7 (UT, MUT, MLT, LT, UL, LL, Sacral)	ROM in sagittal, frontal, and transverse planes	6-camera Vicon System at 120Hz	11	Anterior and side Seated Bending	Preuss and Popovic, 2010
Sayers <i>et al.</i> , 2020	77	2 (thoracic, lumbar)	Spine Curvatures	22-camera VICON MX system at 100Hz, MATLAB	20	High-bar squat at 2 different heel elevations	List <i>et al.</i> , 2013

1.2 Multi-Segmental spine kinematics measurement approaches

Schmid et al., 2016	56	3 (Cervical, thoracic, lumbar)	ROM in the sagittal, transverse, and frontal planes	12-camera MXT20 VICON system at 200-300Hz, NEXUS, MATLAB	29	Walking trials	Schmid et al., 2015
Seerden et al., 2021	45	6 (UT, Middle Thoracic, Thoracolumbar, UL, LL, lumbosacral)	ROM in sagittal, frontal, and transverse planes, motion velocity	13-camera VICON MX system at 100Hz, NEXUS, MATLAB	43	Forward Flexion, Lateral Bending, Spine Rotation	Seerden et al., 2019
Simonet et al., 2020	58	3 (Cervical, thoracic, lumbar)	ROM of the Lumbar Lordosis	10-camera VICON system at 200Hz, NEXUS, MATLAB	33	Standing for 10s, Walking, Running at self-selected speeds	Schmid et al., 2015
Stoll et al., 2016	12	3 (UT, LT, Lumbar)	ROM in sagittal, frontal, and transverse planes	8-camera VICON system at 200Hz	15	Lifting different weights from the ground	Preuss and Popovic, 2010
Sugaya et al., 2016	22	7 (UT, MUT, MLT, LT, UL, LL, Sacral)	ROM in sagittal, frontal, and transverse planes, Muscle forces	VICON system at 200Hz	11	Ipsilateral Rotation	Preuss and Popovic, 2010

1.2 Multi-Segmental spine kinematics measurement approaches

Reliability of the Motion Capture Setup:

Repeatability:

Thirty-one studies asked their participants to repeat the motion tasks three times^{20,59,60,84–88,91,93,99,100,103–106,109–111,113,124,125,131,134}, 12 studies did 5 repetitions of the motion tasks^{72,83,90,92,98,112,118,119,122,130,135,139}, 7 studies had 10 repetitions^{24,25,70,97,115,127}, 1 study only asked participants to complete the motion task once¹²⁸ while 12 studies did not mention the number of task repetitions made^{82,89,94,95,102,108,116,117,133,136–138}. Ten studies reported their intra-subject repeatability measures^{70,82,90,92,112,113,115,127,135,145}, 3 studies measured their inter-rater reliability^{82,92,124} while 5 studies assessed the repeatability of the findings when measured across different days^{25,72,82,124,133}.

Accuracy:

Fifteen studies evaluated the accuracy of their marker setups^{23,72,82,98,99,101,104,107,111,112,116,118,124,126,129,137}. The soft tissue artefact associated with the motion was quantified using imaging techniques in 3 studies^{98,107,124}. Two studies used electromagnetic sensors along with passive markers to cross-check the values generated by both systems^{126,137}. Two studies compared the kinematic variables collected from participants to those collected from markers placed on custom-built mechanical models of the spine^{72,98}. One study used the *medimouse* apparatus to compute spinal angles and cross-check with the values generated by the motion analysis²³. Only 1 study inserted wires into the vertebral body to quantify soft tissue artefact (STA)¹¹¹.

Suitability of the Approach:

Marker Setup:

Most studies used clusters of single markers for their setups, only 7 studies used marker triads to define spine segments^{82,98,100,111,115,125,130}. The spinous processes of C7, T3, T6, T12, L1, L3 and L5 were the most widely used. All studies reported marker positioning by palpation of the anatomical landmark surface. Two studies positioned markers following the curvature of the spine, at the points of most thoracic kyphosis and lumbar lordosis^{70,108}. Information on the time needed to position the markers was not reported by any of the studies.

1.2 Multi-Segmental spine kinematics measurement approaches

Segment Definition:

The majority of studies^{24,59,60,84,85,89,91,94,102,103,107,109,110,120,123,124,129,132,135,138} used 4 markers to define a spinal segment using 2 markers on the spinous processes and 2 lateral markers midway between these to form a diamond shaped segment. Eleven studies^{23,82,83,87,96,99,100,108,115,118,122,131,137,139,141} used only 2 markers on the spinal processes to form a segment line. While 12 other studies^{20,70,72,86,88,95,98,101,113,114,121,125,130,136} used 3 markers to define their segments by using 1 marker on the spine and 2 lateral markers to form a triangular shape. It is worth noting that 12 studies used anterior markers on the sternum to define their spinal segments^{25,70,90,97,101,114,116,119,127–129,133}.

The most common segment definition used was dividing the kinematic model of the spine into 2 distinct segments, either the thoracic and lumbar spines^{24,25,89,94,95,101,106,107,114,117,125–128,134} or the upper lumbar and lower lumbar spines^{112,124}.

Another common segment definition was dividing the back into 3 parts and these were: Upper thoracic, Lower Thoracic and Lumbar^{72,84,91,92,97,102,108,120–122,129,130}. Some studies further divided the lumbar spine into upper and lower lumbar, to have a total of 4 segments^{20,59,60,85–88,91,104,105,123,132,139}. Only 5 papers defined the cervical spine and analysed it in their models^{90,116,119,133,136}. Three studies considered each lumbar vertebra as a single segment^{99,111,131}.

Data Processing:

The kinematic data collected from markers was low pass filtered using Butterworth Filters with a cut-off frequency ranging between 2Hz and 10Hz depending on the motion capture setup. Most studies defined the pelvis as the local coordinate system for their data analysis^{20,23–25,59,60,70,72,82,85–91,93–104,106–110,112–118,120–125,131,134–139}. The Grood and Suntay convention was mentioned in 14 studies to calculate intersegmental angles to obtain the flexion/extension, lateral bending, and axial rotations of the defined segments in all 3 anatomical planes^{59,60,69,70,72,91,92,96,104,105,112,136,150,151}.

Some studies reported subtracting the static standing trial of participants from the dynamic trials to normalize the angle of motion^{59,60,85,105,119}. None of the studies included in this review commented on the ease of use of their data processing procedure for use in clinical practice.

Participant Cohorts:

Thirty-five studies had only healthy participants in their cohorts^{23,25,70,72,91–94,96,101–103,108–115,117,118,120,124,126,127,129,131,133–139}. Twenty-seven studies compared pathological participants to

1.2 Multi-Segmental spine kinematics measurement approaches

healthy participants^{20,59,60,82–90,97,100,104–106,119,121–123,125,128,130,132} while only 3 studies assessed the motion of only pathological subjects^{95,107,116}. Details of participant cohorts can be found in Table 6.

Table 6 Study participants sample size and characteristics (M= male, F= female, AEP= active extension pattern, FP= flexion pattern, AK= ankylosed axial spondyloarthritis, Inf= Inflamed axial spondyloarthritis)

Study	Subjects										
	Total	Healthy					Pathological				
	No.	Gender	Age	Height(m)	Weight(kg)	No.	Gender	Age	Height(m)	Weight(kg)	
Al Eisa <i>et al.</i> , 2006	113	59	25M 34F	31.1±6.9	-	-	54	27M 27F	33.4±7.2	-	-
Alemi <i>et al.</i> , 2021	7	7	3M 4F	42±14	1.72±0.07	69.6±11.1	-	-	-	-	-
Alijanpour <i>et al.</i> , 2021	14	6	3M 3F	25.03±4.5	1.8±0.09	70.83±14.6	8	4M 4F	24.12±4.9	1.83±0.09	77.87±13.2
Arshad <i>et al.</i> , 2018	6	6	6M	24-33	1.8±0.04	75±8.03	-	-	-	-	-
Bagheri <i>et al.</i> , 2017	30	15	-	-	-	-	15	-	-	-	-
Beaudette <i>et al.</i> , 2019	51	51	-	24±3.3	1.8±0.07	80.4±11	-	-	-	-	-
Brelloff <i>et al.</i> , 2015	10	10	5M 5F	26.8±3.8	1.8±0.02	67.7±11.6	-	-	-	-	-
Choi <i>et al.</i> , 2007	6	6	6M	23.8±0.4	1.76±0.04	67.8±1.6	-	-	-	-	-
Christe <i>et al.</i> , 2016	21	11	6M 5F	38.2±6.7	1.72±0.07	65.6±9.8	10	5M 5F	36.7±5.4	1.74±0.05	69.5±9.8
Christe <i>et al.</i> , 2017	21	11	6M 5F	36.7±5.4	1.74±0.05	69.5±9.8	10	6M 4F	38.7±7.2	1.74±0.07	67.8±8.9
Christe <i>et al.</i> , 2020	21	11	6M 5F	36.7±5.4	1.74±0.05	69.5±9.8	10	6M 4F	38.7±7.2	1.74±0.07	67.8±8.9
Claus <i>et al.</i> , 2016	50	50	21M 29F	22±4 21±3	1.72±0.07 1.64±0.06	66±12 55±8	-	-	-	-	-
Crosbie <i>et al.</i> , 1997	108	108	50M 58F	46±18 45±18	1.72±0.08 1.61±0.07	73.7±10.5 59.6±9.8	-	-	-	-	-
Deane <i>et al.</i> , 2020	10	10	4M 6F	30.8	-	-	-	-	-	-	-
Friego <i>et al.</i> , 2003	18	18	18F	12.3	1.56	49.2	-	-	-	-	-
Ghasemi <i>et al.</i> , 2021	18	9	9M	23.6±1.1	1.78±0.057	75.9±7.1	9	9M	26.9±3.9	1.76±0.04	110.1±10.6
Gilleard <i>et al.</i> , 2013	9	9	9F	32.6±4.3	1.63±0.06	66.8±10.3	-	-	-	-	-
Glover <i>et al.</i> , 2021	7	7	4M 3F	49.9±12.2	1.72±0.11	-	-	-	-	-	-
Gombatto <i>et al.</i> , 2015	36	18	8M 10F	27.6±12.4	1.67±0.12	72±14.5	18	7M 11F	28.1±13.1	1.69±0.11	71.2±15.3
Gombatto <i>et al.</i> , 2017	35	17	7M 10F	25.6±8.7	1.67±0.13	71.1±14.4	18	7M 11F	28.1±13.1	1.69±0.11	71.2±15.3
Hagins <i>et al.</i> , 2021	59	24	2M 21F	24.9±6.1	1.66±0.09	62.1±9.7	33	9M 26F	24.9±6.1	1.66±0.09	62.1±9.7
Hemming, 2018	77	28	12M 16F	38.5±11.2	1.69±0.07	72.9±15.2	23AEP 27FP	4M/1 9F 21M/ 6F	43.7±11.2 41±10	1.69±0.1 1.75±0.87	68.9±18 82.5±14.6
Hernandez <i>et al.</i> , 2019	36	18	8M 10F	26.1±8.6	-	-	19	7M 11F	28.1±13.1	-	-
Hidalgo <i>et al.</i> , 2012	50	25	10M 15F	40±11	-	-	25	12M 13F	42±9	-	-
Holewijn <i>et al.</i> , 2018	12	-	-	-	-	-	12	12F	15.2±1.7	-	-
Hooker <i>et al.</i> , 2021	154	-	-	-	-	-	154	59M 95F	42.6±1.8 5	-	-
Ignasiak <i>et al.</i> , 2017	42	21Young 21Elderly	16M/26F	27±3.97 70.1±3.85	1.73±0.09 1.68±0.08	68.3±13.7 67.4±11.3	-	-	-	-	-
Ignasiak <i>et al.</i> , 2018	44	23Young 21Elderly	17M/27F	27.13±3.79 70.1±3.85	1.73±0.09 1.68±0.08	68.3±13.7 67.4±11.3	-	-	-	-	-
Kakar <i>et al.</i> , 2019	20	10	4M 6F	20.6±1.5	1.72±0.08	66.4±10.9	10	4M 6F	17.4±1.3	1.69±0.09	65.5±12.2
Knechtle <i>et al.</i> , 2021	61	61	31M 31F	29.5±6.9	-	-	-	-	-	-	-
Konz <i>et al.</i> , 2006	10	10	-	27±4	1.71±0.06	71.9±12.2	1	1M	-	-	-

1.2 Multi-Segmental spine kinematics measurement approaches

Kuai <i>et al.</i> , 2018	33	26	-	-	-	-	7	-	-	-	-	
Kudo <i>et al.</i> , 2018	10	10	10M	22.6±1.5	1.7±0.05	64.6±6	-	-	-	-	-	
Kuwahara <i>et al.</i> , 2016	20	10	6M 5F	62±19.1	1.62±0.08	60.7±11.7	10	5M 5F	75.3±3.9	1.58±0.08	63.4±6	
Leardini <i>et al.</i> , 2011	10	10	5M 5F	24.7±0.8	1.71±0.08	62.4±9.3	-	-	-	-	-	
Lin <i>et al.</i> , 2020	24	15	10M 5F	48.2±14.46	1.76±0.09	76.3±14.7	9	8M 1F	53.9±9.3	1.7±0.05	72.6±11.4	
List <i>et al.</i> , 2013	30	30	-	25±4	1.74±0.08	67±11	-	-	-	-	-	
Marich <i>et al.</i> , 2017	48	16	6M 10F	37.4±11	1.7±0.13	68.6±14.6	-	16low LBP 16high LBP	6M 10F 6M 10F	38.6±13 36.2±11	1.71±0.11 1.71±0.09	68.9±15.1 71.6±9.6
Marich <i>et al.</i> , 2020	48	16	7M 9F	32.1±9.4	1.72±0.12	71.8±11.1	32	17M 15F	33.8±10	1.72±0.1	74.3±15.3	
Mason <i>et al.</i> , 2014	12	12	11M 1F	23.25±4.3	1.64±0.06	60.45±8.13	-	-	-	-	-	
Muller <i>et al.</i> , 2016	10	10	5M 5F	29±3	1.79±0.11	74±14	-	-	-	-	-	
Needham <i>et al.</i> , 2015	10	10	-	-	-	-	-	-	-	-	-	
Niggli <i>et al.</i> , 2021	20	20	9M 11F	31±9	1.73±0.1	69±13	-	-	-	-	-	
Noamani <i>et al.</i> , 2018	11	11	7M 4F	28.5±3.3	0.75±0.04	69.9±13.7	-	-	-	-	-	
Papi <i>et al.</i> , 2019	40	20	10M 10F	28±7.6	1.72±0.11	66.2±12	20	16M 4F	41±10.7	1.68±0.1	74.1±19.5	
Papi <i>et al.</i> , 2020	40	20	10M 10F	28±7.6	1.72±0.11	66.2±12	20	16M 4F	41±10.7	1.68±0.1	74.1±19.5	
Patel <i>et al.</i> , 2018	28	13	6M 7F	16.6	1.62	64	15	5M 10F	14.3	1.62	58.3	
Peharec <i>et al.</i> , 2007	63	63	40M 23F	35	-	-	-	-	-	-	-	
Pelegrinelli <i>et al.</i> , 2020	26	13	-	-	-	-	13	-	-	-	-	
Pesenti <i>et al.</i> , 2020	62	-	-	-	-	-	62	8M 54F	15.5±2.1	-	-	
Pollock <i>et al.</i> , 2008	8	8	8M	22±3.9	1.72±0.07	76±8.9	-	-	-	-	-	
Preece <i>et al.</i> , 2016	15	15	15M	25±5	1.78±0.0689	63.1±6.1	-	-	-	-	-	
Preuss <i>et al.</i> , 2010	11	11	7M 4F	28.5±3.3	-	-	-	-	-	-	-	
Rouhani <i>et al.</i> , 2016	11	11	7M 4F	28.5±3.3	-	-	-	-	-	-	-	
Rozumalski <i>et al.</i> , 2008	10	10	-	-	-	-	-	-	-	-	-	
Ryan <i>et al.</i> , 2017	17	17	10M 7F	26.5±5.4	1.68±0.09	67.9±10.5	-	-	-	-	-	
Saad <i>et al.</i> , 2020	10	10	10M	-	-	-	-	-	-	-	-	
Sayers <i>et al.</i> , 2020	20	10Novice 10Pro	5F/5M 5F/5M	26.1±4.9 27.6±3.6	1.73±0.1 1.71±0.09	67.6±12.4 66±10.7	-	-	-	-	-	
Schinkel-ivy <i>et al.</i> , 2015	30	30	15M 15F	25±3.8 22.8±2.7	1.8±0.05 1.66±0.05	79±8 59±6	-	-	-	-	-	
Schmid <i>et al.</i> , 2015	10	-	-	-	-	-	10	2M 8F	14.8±1.3	1.65±0.1	55.3±12.7	
Schmid <i>et al.</i> , 2016	29	15	8M 7F	14.1	1.62	54.2	14	2M 12F	15.2	1.66	55.6	
Seay <i>et al.</i> , 2008	10	10	-	26.2	1.72±0.14	66.2±10.2	-	-	-	-	-	
Seerden <i>et al.</i> , 2019	18	18	11M 7F	45.8±14.8	1.76±0.09	74±14.5	-	-	-	-	-	
Seerden <i>et al.</i> , 2021	43	23	16M 7F	45.2±13.4	1.77±0.09	75.2±14	12 AK 8 Inf	11M, 1F 7M, 1F	50.4±11.4 37.6±13.7	1.73±0.06 1.79±0.08	77.3±12.9 87.3±15.9	
Severijns <i>et al.</i> , 2020	41	18	6M 12F	61.4±10.5	1.65±0.07	63.8±12	23	4M 19F	61.8±10	1.62±0.07	60.6±9.5	
Simonet <i>et al.</i> , 2020	33	20	9M 11F	31.4±9.2	1.73±0.09	68.9±12.9	13	8M 5F	38±11.6	1.74±0.07	67±12	
Stoll <i>et al.</i> , 2016	10	10	6M 4F	29±3	1.79±0.09	75±14	-	-	-	-	-	
Sugaya <i>et al.</i> , 2016	11	11	11M	26.5±3.3	1.73±0.04	65.4±3.9	-	-	-	-	-	

1.2 Multi-Segmental spine kinematics measurement approaches

Sung <i>et al.</i> , 2016	44	24	18M 6F	39.7±18.7	-	-	20	12M 8F	43.1±17.	-	-
Sung <i>et al.</i> , 2020	32	18	4M 12 F	14.22±0.73	-	-	14	2M 12F	14.79±1.	05	-
Swain <i>et al.</i> , 2018	60	27	-	-	-	-	33	-	-	-	-
Tojima <i>et al.</i> , 2013	7	7	7M	30.3±4.9	1.7±0.05	64.4±6.6	-	-	-	-	-
Wilk <i>et al.</i> , 2006	91	25	25F	15-28	-	-	66	66F	15-28	-	-
Zwambag <i>et al.</i> , 2018	4	4	4M	27±1.7	1.8±0.1	85±10.3	-	-	-	-	-

Tasks Conducted:

The majority of studies ^{20,59,60,70,72,85–96,98–100,102,104–108,111,112,116,118–120,128,131,133,135–137} looked at the motion of the spine segments during activities of daily living (ADL), as these were considered routine and repetitive motions where the spine plays a key role to assure equilibrium and are affected in spine pathology cases. Some of these studies ^{20,72,85,89–95,98,99,104–108,111,112,116,119,131,136} looked in particular at the active role the spine segments play during gait to maintain equilibrium and the compensation mechanism used by patients to achieve it.

When it comes to the studies that recruited patients undergoing spine surgery ^{89,95,97,98,106,125}, ADL tasks were used to assess improvement or deterioration of neurological symptoms, changes in motion patterns and the compensation mechanisms involved in the motion.

Twenty-two studies ^{23,83,84,96,103,106,109–111,115,118,121–126,128,134,135,138,139} included spine range of motion tasks such as forward flexion, lateral bending, or spine rotation. These tasks were implemented to report normal spine segment kinematics, investigate the role of each spine segment in spine motion and assess the reliability of motion capture setups. Eight studies ^{24,25,97,117,119,127,129,133} looked at the motion of the spine during running trials while 2 studies ^{101,114} assessed spine motion during the squat exercise, 2 studies ^{123,132} assessed spine motion while their participants performed dancing tasks while 1 study assessed the motion of the spine during rowing ¹³⁰.

- *Patient Considerations:*

Studies involving patients and healthy subjects ^{20,59,60,82–90,97,100,104–106,119,121–123,125,128} had the same tasks for both cohorts. Participants were asked to perform their tasks at their self-selected speed. One study involving patients asked their participants to perform a lifting task only in their most comfortable approach ¹⁰⁰.

Main Measurements:

Eighteen studies calculated the angles between the spine segments defined ^{70,72,86,91–93,98,101,106,108,109,112,113,115,117,126,132,133,137,139} while 33 studies ^{20,23–25,59,60,83–85,87,88,90,94–97,100,102–}

1.2 Multi-Segmental spine kinematics measurement approaches

^{105,110,111,118,120,124,125,127,128,130,131,134,136,138} calculated the range of motion of the segments during the tasks conducted.

The ROM of segments during walking tasks ranged from 2.3° to 7.9° in the sagittal plane, 1.8° to 10.8° in the frontal plan while most of the motion was recorded in the transverse plane ranging from 2.6° to 13.5°. Detailed ROMs of the spine segments defined in the studies extracted can be found in Table 7.

Four studies ^{107,114,116,119} reported the angle of inclination between the segments and as such calculated the angles of lumbar lordosis or thoracic kyphosis.

Of the 24 studies that conducted walking trials ^{20,72,85,89–95,98,99,104–108,111,112,116,119,131,133,136}, only 5 assessed the kinematics of the lower limbs and reported the gait parameters generated.

Table 7 Range of Motion of the spine segments during the various tasks reported in the studies extracted.

Task	Study	Cohort	Spine Segment	Plane	Angle°	SD°
Walking	Choi <i>et al.</i> , 2007	Control	UT/LT	Sagittal	2.3	1.1
				Frontal	2.8	1.4
				Transverse	2.6	1.8
			LT/UL	Sagittal	3.8	1.5
				Frontal	2.5	0.4
				Transverse	7.9	1.3
			UL/LL	Sagittal	3.6	1.3
				Frontal	5.6	1.4
				Transverse	5.3	1.2
			LL/Pelvis	Sagittal	4.8	1.8
				Frontal	7.9	1.8
				Transverse	5	1.3
	Christe <i>et al.</i> , 2017	Control	UT/LT	Sagittal	4.45	-
			UL/LL	Sagittal	6.55	-
			LL/Pelvis	Sagittal	7.97	-
		LBP	UT/LT	Sagittal	4.46	-
			UL/LL	Sagittal	4.45	-
			LL/Pelvis	Sagittal	6.55	-
	Crosbie <i>et al.</i> , 1997	Control	LT	Sagittal	2.5	1.5
				Frontal	7	3
				Transverse	4	2.5
			Lumbar	Sagittal	3.5	2
				Frontal	9	3.5
				Transverse	4.5	2
			Pelvis	Sagittal	3.5	1.5
				Frontal	6	2.5
				Transverse	4	2.5
	Gombatto <i>et al.</i> , 2015	Control	UL	Sagittal	7.9	-
				Frontal	2.9	-
				Transverse	5.5	-
			LL	Sagittal	4.5	-
				Frontal	1.8	-
				Transverse	2.2	-
LBP		UL	Sagittal	5.8	-	

1.2 Multi-Segmental spine kinematics measurement approaches

			LL	Frontal	2.7	-
				Transverse	4.7	-
				Sagittal	4.5	-
				Frontal	2	-
				Transverse	3.7	-
	Holewijn <i>et al.</i>, 2018	AIS	Proximal Spine	Sagittal	5.5	2.7
				Frontal	8.3	2.9
				Transverse	12.2	4
			Distal Spine	Sagittal	8	0.3
				Frontal	8.2	3.4
				Transverse	13.5	1.7
	Konz <i>et al.</i>, 2006	Control	Thoracic	Sagittal	5.7	0.9
				Frontal	7.1	2.4
				Transverse	8.7	2.5
			Lumbar	Sagittal	6.8	1.4
				Frontal	10.8	2.4
				Transverse	11.5	1.3
		AIS	Thoracic	Sagittal	7.1	2.4
				Frontal	8.7	2.5
				Transverse	6.8	1.4
			Lumbar	Sagittal	10.8	2.4
				Frontal	11.5	1.3
				Transverse	4.1	0.9
	Leardini <i>et al.</i>, 2011	Control	Thoracic	Sagittal	4.2	4.7
Frontal				5.1	2.1	
Transverse				8.3	3.1	
Muller <i>et al.</i>, 2016	Control	UT	Sagittal	5.8	2.6	
			Frontal	3.8	0.9	
			Transverse	12.8	2.9	
		LT	Sagittal	6.9	1.5	
			Frontal	3.8	1.1	
			Transverse	12.6	3.3	
		Lumbar	Sagittal	6	1.2	
			Frontal	3.4	1.1	
			Transverse	13.9	3.4	
Needham <i>et al.</i>, 2015	Control	UT	Sagittal	2.21	0.83	

1.2 Multi-Segmental spine kinematics measurement approaches

			LT	Frontal	5.6	1.93
				Transverse	11.34	4.68
				Sagittal	3.74	1.74
			Lumbar	Frontal	5.54	2.43
				Transverse	5.5	1.56
				Sagittal	3.22	0.63
	Ryan and Bruno, 2017	Control	UL	Frontal	6.5	2.11
				Transverse	7.39	2
				Sagittal	4	0.9
			LL	Frontal	3.15	0.5
				Transverse	8.3	1.4
				Sagittal	5.1	1.1
	Schmid et al., 2016	Control	Thoracic	Frontal	4.27	0.54
				Transverse	9.9	1.3
				Sagittal	4	1.6
			Lumbar	Frontal	4.3	1.6
				Transverse	7.3	2.7
				Sagittal	4.3	1.3
AIS		Thoracic	Frontal	5.2	1.9	
			Transverse	9.3	3.3	
			Sagittal	4.8	1	
		Lumbar	Frontal	3.7	1.4	
			Transverse	6.7	1.7	
			Sagittal	4.3	0.9	
Forward Bending	Ghasemi et al., 2021	Control	Trunk	Sagittal	125	-
			Lumbar	Sagittal	45	-
			Pelvis	Sagittal	50	-
		Obese	Trunk	Sagittal	118	-
			Lumbar	Sagittal	45	-
			Pelvis	Sagittal	55	-
	Marich et al., 2020	Control	Lumbar	Sagittal	33.8	7.1
		LBP	Lumbar	Sagittal	35.1	9.3
	Seerden et al., 2021	Control	UT	Sagittal	12.4	5.4
			MUT	Sagittal	4.7	3

1.2 Multi-Segmental spine kinematics measurement approaches

			LT	Sagittal	8.7	3.8	
			UL	Sagittal	18.6	6.5	
			LL	Sagittal	28	8.6	
			Control	Thoracic	Sagittal	25	10
				Lumbar	Sagittal	63	10
			Fused Spine	Thoracic	Sagittal	18	10
Lumbar	Sagittal	57		12			
Seated Bending	Brelloff <i>et al.</i> , 2015	Control	UL/LT	Sagittal	10.53	10.16	
			LL/UL	Sagittal	11.93	7.56	
			LL/Sacrum	Sagittal	18.31	8.52	
	Hidalgo <i>et al.</i> , 2012	Control	UT	Sagittal	122.4	15.2	
			LT	Sagittal	110.4	14.1	
			UL	Sagittal	81.9	15.9	
			LL	Sagittal	73.1	15.8	
		LBP	UT	Sagittal	100.1	22	
			LT	Sagittal	85.4	20.4	
			UL	Sagittal	60.9	16.8	
			LL	Sagittal	53.8	16.3	
	Rouhani <i>et al.</i> , 2016	Control	LT/UL	Sagittal	7.5	-	
				Frontal	1.8	-	
				Transverse	2.2	-	
			UL/LL	Sagittal	15.1	-	
				Frontal	1.8	-	
				Transverse	2.2	-	
	Lateral Bending	Ghasemi <i>et al.</i> , 2021	Control	Trunk	Frontal	50	-
Lumbar				Frontal	88	-	
Pelvis				Frontal	72	-	
Obese			Trunk	Frontal	55	-	
			Lumbar	Frontal	95	-	
			Pelvis	Frontal	62	-	
Seerden <i>et al.</i> , 2021		Control	UT	Frontal	6.9	3.1	
			MUT	Frontal	7.2	3.5	
			LT	Frontal	9.1	4.6	
	UL		Frontal	10.1	4.2		
	LL		Frontal	10.3	5.3		
Wilk <i>et al.</i> , 2006	Control	Thoracic	Frontal	56	10		

1.2 Multi-Segmental spine kinematics measurement approaches

		Fused Spine	Lumbar	Frontal	52	10
			Thoracic	Frontal	32	14
Axial Rotation	Ghasemi <i>et al.</i> , 2021	Control	Lumbar	Frontal	42	8
			Trunk	Transverse	88	-
			Lumbar	Transverse	72	-
		Obese	Pelvis	Transverse	30	-
			Trunk	Transverse	95	-
			Lumbar	Transverse	62	-
	Seerden <i>et al.</i> , 2021	Control	Pelvis	Transverse	30	-
			UT	Transverse	9.6	6
			MUT	Transverse	11.3	6.5
			LT	Transverse	15.3	10.3
			UL	Transverse	7.4	5.2
	Sugaya <i>et al.</i> , 2016	Control	LL	Transverse	7.9	4.3
			UT	Transverse	39	8
			MUT	Transverse	35	7
			MLT	Transverse	27	6
LT			Transverse	18	4	
UL			Transverse	11	3	
Stand-to-sit	Al Eisa <i>et al.</i> , 2006	Control	Thoracic	Frontal	37.1	9
				Transverse	43.4	11.4
			Lumbar	Frontal	17	8.2
				Transverse	32.3	8
	Hemming, 2018	Control	UL	Sagittal	10.7	10.9
			LL	Sagittal	9.9	11.2
			UT	Sagittal	22.5	7.8
			LT	Sagittal	20.6	7.4
Sit-to-Stand	Al Eisa <i>et al.</i> , 2006	Control	Thoracic	Frontal	26	7.6
				Transverse	39.9	14.2
			Lumbar	Frontal	20.4	7.9
				Transverse	34.8	9.7
	Christe <i>et al.</i> , 2016	Control	UT/LT	Sagittal	5.7	-
			UL/LL	Sagittal	10.3	-
LBP	LL/Pelvis	Sagittal	21.8	-		
			UT/LT	Sagittal	3.3	-

1.2 Multi-Segmental spine kinematics measurement approaches

			UL/LL	Sagittal	5.7	-		
			LL/Pelvis	Sagittal	10.3	-		
			Hemming, 2018	Control	UT	Sagittal	20.6	7.4
					LT	Sagittal	10.7	10.9
					UL	Sagittal	9.9	11.2
					LL	Sagittal	-6.3	7.6
Marich et al., 2020	Control	Lumbar	Sagittal	21.3	4.7			
	LBP	Lumbar	Sagittal	24.9	7.2			
Object Pickup	Stoll et al., 2016	Control	UT	Sagittal	103.8	14.7		
				Frontal	5	18		
				Transverse	56.4	13.77		
			LT	Sagittal	110.5	18		
				Frontal	23.3	9.4		
				Transverse	33.1	10.3		
			Lumbar	Sagittal	84.33	15.7		
				Frontal	22.5	7.1		
				Transverse	30	7.86		

1.2 Multi-Segmental spine kinematics measurement approaches

Clinical Significance:

Pathologies Assessed:

The majority of studies involving pathology assessed subjects with low back pain (LBP) or chronic low back pain (CLPB)^{20,24,59,60,84–88,104,105,119,121,123,130,132}. Eight studies had teenagers with adolescent idiopathic scoliosis (AIS)^{90,95,97,106,107,116,122,125}. Two studies assessed adult spinal deformity (ASD)^{82,98}. One study assessed ankylosing spondylitis¹⁰⁰, another focused only on lumbar disc herniation subjects⁹⁹, 1 study assessed lumbar spinal stenosis patients⁸⁹ and one study assessed patients with axial spondyloarthritis (axSpa) with two patient cohorts in the active inflammation or the bone formation phases⁸³. Only one study assessed the changes in spine motion due to obesity¹²⁸.

Six studies assessed patients undergoing spine surgery, 5 of them had patients who underwent posterior spinal fusion surgery^{95,97,98,106,125} while 1 study had patients undergoing two different decompression surgery approaches⁸⁹.

Four studies assessed patient motion before and after surgery. One study measured patients before and 1 month after⁸⁹, other measured patients before, 3 months and 12 months after surgery⁹⁵, Patel *et al.*¹⁰⁶ measured patients before and 12 months following surgery while Konz *et al.*⁹⁸ analysed their subjects before and 6 months after surgery.

Clinical Findings:

The studies including patients assessed the kinematics of the multi-segmental spine to help clinical decisions, provide more information on motion compensation, evaluate treatment, and monitor pathology outcome. Kuwahara *et al.*⁸⁹ used the multi-segmental motion approach to compare two decompression surgery techniques and measure the improvement of neurological symptoms following surgery of the two-patient cohort. Hemming *et al.*⁸⁷ found evidence to support subgrouping LBP patients to better refine intervention approaches. Christe *et al.*⁶⁰ suggested that CLBP patient rehabilitation could benefit from targeting specific motion deficits in functional activities.

Of the 29 studies assessing patients, 3 studies^{84,85,106} reported motion asymmetry at the levels of the lumbar and thoracic spine between the patient and control cohorts, Christe *et al.*⁸⁵ reported a 20% increase in transverse plane asymmetry in CLBP patients (Table 7) while Patel *et al.*¹⁰⁶ reported asymmetric axial plane motion in LBP patients. 4 studies assessed spine rotation abilities depending on the pathology, 3 of these^{20,85,86} reported up to 15% decrease in

1.2 Multi-Segmental spine kinematics measurement approaches

segment rotation either after a surgical intervention or due to LBP (Table 7). Only 1 study¹²¹ reported an increase in lumbar and thoracic rotations in patients with LBP. The motion profile of axial spondylopathy patients was seen to be similar to the maladaptive motion profiles of patients with CLBP with a significant decrease in motion velocity when compared to controls⁸³.

When it comes to the motion of the lumbar spine, 3 studies reported a decrease in lumbar spine flexion in LBP patients^{59,85,88} (Table 7), while 1 study⁸⁶ reported a decrease in lower lumbar flexion but an increase in upper lumbar flexion. One study¹⁰⁵ found an increase in the upper lumbar and lower lumbar ROM during walking, sit-to-stand and running tasks in patients with LBP (Table 7).

Five studies reported the motion coordination present between the spinal segments^{24,100,104,122,130}. Of these, two studies^{104,122} found a lack of coordination between the lumbar and thoracic segments in LBP and AIS patients. One study²⁴ found that the pattern of coordination between segments is different for LBP patients when compared to the control and 1 study¹⁰⁰ found evidence of coordination between the upper lumbar, thoracic and pelvis to stabilize the trunk in ankylosing spondylitis patients. One study assessing the motion of rowers with CLBP¹³⁰ found a lack of coordination between the spinal segments when the intensity of the motion is increased while also finding that the lower spine segments could not work as supports for the upper segments.

Five studies^{70,82,90,107,116} reported the changes in spine curvature during dynamic trials when compared to static posture. These were able to show that curvature angles of the spine could be measured with high accuracy and that regional differences exist depending on the pathology. One study¹¹⁹ reported a decrease in the lumbar lordosis angle during walking and running in patients with non-specific LBP. Two studies^{95,125} reported the motion of the spine following fusion surgery, one with AIS patients and the other with ASD patients, both did not report any hypermobility in the unfused spinal segment. Only one study¹²³ found no significant spine kinematic differences between the LBP group and the control group.

Discussion:

Motion abnormalities of the spine impact the onset and recurrence of spinal disorders^{20,21}, therefore analysing the kinematics of the thoracolumbar spine gives an insight into the causes of these disorders and aids in the choice of treatment^{59,60}. Stereophotogrammetric motion analysis could objectively quantify this motion^{69,70}, however numerous methods and protocols

1.2 Multi-Segmental spine kinematics measurement approaches

are found in the literature. The current review aims to evaluate these studies and assess their reliability, suitability in a clinical setting and clinical significance. Seventy-four articles were identified focusing on the multi-segmental motion of the thoracolumbar spine of which 44 articles proposed a different protocol to quantify this motion. These protocols differed in the number of markers used, segments defined, participant cohorts recruited, disorders analysed, kinematic variables assessed, and outcome measurements reported highlighting the need for a set of standard principles to provide reliable and reproducible kinematic information on various motions, spine segments and spine disorders.

Reliability of the Motion Capture Setup:

The reliability of the identified studies was first evaluated. It was defined as the repeatability and accuracy of the measurement approach in addition to the analysis of sources of error. Most studies did not report on these three reliability aspects scoring 32%, 18% and 18% respectively in the quality assessment questionnaire. To quantify the repeatability of the measurement, we first looked at task repetitions; most studies asked their participants to repeat the motion at least three times^{20,24,25,59,60,70,72,83–88,90–93,97–100,103–106,109–113,115,118,119,122,124,125,127,131,134,135,139} and ultimately based their measurements on the average of trials, however, the repetitions of tasks were unrelated to the number of participants in the cohorts. Some of the studies succeeded in analysing the repeatability of the outcome measurement either by studying the intra-subject variability^{70,82,90,92,112,113,115,127,135,145}, the inter-rater reliability^{82,92,124} or the repeatability of the findings when measured across different days^{25,72,82,124,133}. When it comes to the accuracy of the optoelectronic protocol, 11 studies^{72,90,98,99,107,111,114,116,124,126,131} compared their results to more conventional imaging techniques to show the accuracy of the marker setup and their reported outcomes; however, the remaining studies did not report on these differences as they were investigating the changes in spine motion between cohorts and were not reporting the absolute angle of motion of spinal segments^{20,59,60,82,84–90,100,104,106,121–123,125}. Deane *et al.*⁹² was the only study to quantify the standard error associated with spine motion ranging between 0.8° and 5.5° for gait and between 1° and 12.6° for sit-to-stand motion compared to imaging techniques that account for a <1° of error during static measurements⁶⁶. Only 9 studies^{23,82,84,91,98,110,116,126,129} reported the marker placement error associated with the setup, this is especially important as the spine region is greatly affected by STA¹¹⁵ and hence would be expected to be more thoroughly reported. None of the studies identified in this review however was found to report on all three reliability aspects assessed in the quality questionnaire. These

shortcomings affect the reliability of the protocols suggested and make implementing a standard protocol in a clinical setting even more difficult.

Suitability of the Approach:

When assessing the suitability of the protocols suggested for a clinical setting, we looked at marker configurations, segment definitions, participant cohorts, tasks conducted outcome measures and the ease of use of the methodology in a clinical setting. Major differences in marker setups were seen across studies, with different numbers of markers on the thoracolumbar spine and their location on the anatomical landmarks; the most common anatomical landmarks to attach the markers on were C7/T1, T6/T7, T12/L1, L3, L5. Only 11 studies^{25,70,90,97,101,114,116,119,127–129} reported positioning of markers anteriorly to the spine on the sternum to decrease the effect of STA on the measurement while the majority of the studies positioned markers laterally to the spine^{24,59,60,84,85,89,91,94,102,103,107,109,110,120,123,124,130,135,138}. Some of these marker setups were seen to be very complex for a clinical setting and are more suited for research purposes as they require more time to position due to the high number of marker^{23,82,90,96,100,101,111,116,121,122,130–133}, other studies^{20,59,60,70,83,85–88,91,102–104,108–110,118,123,136,139} were seen to be successful in limiting the number of markers on the spine or by using 3D clusters. This limitation was mentioned by Glover *et al.*,¹²⁹ who saw that a higher number of markers on the spine decreases marker tracking error but the implementation of the protocol and processing the data would take a significantly longer time. A poor consistency was found in terms of thoracolumbar segment definition. These changed depending on the study cohorts and tasks of interest. The majority of studies tried to define at least the thoracic and lumbar spines^{24,25,89,94,95,101,106,107,114,117,125–128,134}, the lumbar spine was further divided into upper and lower segments^{20,59,60,85–88,91,104,105,123,132,139} especially when investigating patients with LBP due to the changes in motion seen at each level^{20,86,87,104,105,132}. The thoracic spine was also divided into upper and lower segments to have a better understanding of the less studied kinematics of the thoracic spine and help in the investigation of kyphotic and scoliotic spines^{23,59,60,70,85,101,123,132}. When it comes to participant considerations, most of the studies tried to match the age of participants with only 9 studies including participants with an age range difference exceeding 10 years^{82,83,87,89,91,93,100,118,121}. More than half of the studies investigated ADLs such as lifting, sit-to-stand, stair climbing and walking. These tasks had been seen to present a challenge to spine pathology patients and could highlight the differences in segment ROM and coordination when compared to controls^{59,60,70,76,85}. The angle between

1.2 Multi-Segmental spine kinematics measurement approaches

the defined segment was the main outcome reported by studies independent of the tasks conducted, marker setup used, or segments defined. Despite ROM being a straightforward indication of motion ability and is easily estimated even in a clinical setting, it can limit our understanding of motion contribution, compensation mechanisms and coordination between the spine segments⁷⁶. The coordination between the segments wasn't as widely reported although evidence has been found to show changes in coordination due to age and spine pathology^{24,100,104,122,130}. None of the studies in this review reported on the time needed for each measurement or the ease of use of their processing approach in a clinical setting. Hence after assessing the suitability of the studies found, ADLs remain the most useful tasks to understand spine motion and its pathologies^{59,60,70,76,85} while more investigations are needed to agree on marker setups and segments definitions to be used in a clinical setting in addition to what to report when it comes to outcome measurements.

Clinical Significance:

When it comes to the clinical significance of the studies evaluated, this was defined as the relevancy of the study and its outcome measurements to a certain spine pathology. Different kinematic findings were reported by the studies depending on the spine pathology, the multi-segmental approach and the marker setup used. When considered as one moving segment, the lumbar spine flexion was seen to decrease overall in subjects with LBP^{59,85,88}; however, when further dividing the lumbar spine into upper and lower segments, motion contribution by the UL was seen to be greater than the LL segment^{20,86}. As such, segment definition plays a key role in understanding the effects of pathology on spine motion; it is advised to divide the spine into more than 2 segments to be able to describe the motion of the whole spine and understand the contribution of each segment⁹⁰. Besides, grouping patients into subcategories depending on their motion impairments⁸⁷ or surgical treatments⁸⁹ could reveal the similarities in the kinematic findings against healthy controls⁷⁶. Considerations for the changes in spine motion due to age were limited. Only 2 studies reported the differences in spine ROM between older and younger adults^{23,96} while the majority of the studies reported the motion of the spine in healthy younger adults under the age of 35^{70,92-94,98,101-103,109,110,114,115,120,124,131,134,135,137-139}. Significant age-related lumbar segment reductions in motions have however been reported in the literature⁷⁷, it is therefore advised to investigate the spine motion of both older and younger adults and spine pathology subjects to define the motions of each segment of the spine and the coordination between the segments. When looking at the differences between patients and

1.2 Multi-Segmental spine kinematics measurement approaches

controls, distinct motion perturbations were found in the axial and sagittal plane during spine motion in addition to transverse plane asymmetry in subjects with spine pathologies^{20,59,60,83–86,88,121,122,130}. Hence it is advised to investigate the motion of the defined segments in the three dimensions of motion in addition to studying the coordination between spine segments and to the pelvis to ultimately define distinct motion characteristics for LBP, AIS, ASD or spine surgery patients. The use of a multi-segmental spine motion protocol was seen to be successful in a clinical setting to accurately assess spine curvature^{70,82,90,107,116} and the effect of surgical treatment on the patient motion^{89,95,125}. Evidence has been found in this review to support the use of a multi-segmental approach for spine motion analysis to help clinicians in the diagnosis and treatment of spine disorders.

Limitations:

The present study has a few limitations. Only three research databases were queried for articles published in a peer-reviewed journal and only in English. Hence, a publication or language bias might have occurred. The quality assessment questionnaire developed was not assessed for objective reliability and validity although it was constructed using prior assessments found in the literature^{76,81}. Additionally, the review only included studies using passive markers and an optoelectronic system. Studies assessing multi-segmental spine motion using inertial markers or wearable technology were not assessed due to the high signal to noise ratio linked to these sensors especially when attached to a vertebral landmark¹⁰⁹.

Conclusions

The current review showed a shortage in standard protocols to assess spine motion using optoelectronic techniques to identify and support clinical investigations. The findings mentioned in the review could be used when trying to choose the most fitting protocol to assess the motion of the thoracic and lumbar spines however, information on the motion of the cervical spine was not as elaborate. Based on the studies assessed in the review, separating each of the thoracic and lumbar segments into upper and lower parts is essential to accurately describe the motion of the spine. Markers attached to C7/T1, T6/T7, T12/L1, L3, L5 in addition to anterior markers on the sternum are needed to describe this motion. This limited number of markers would allow for easier application in a clinical setting. In terms of instrumentation, a motion analysis system made up of at least 6 cameras is needed. However, no study in this review mentioned the cost incurred by such an analysis and a cost effectiveness study would

1.2 Multi-Segmental spine kinematics measurement approaches

need to be completed to assess the feasibility of using spine motion analysis in a clinical setting. Additionally standardizing the marker setups, segment definitions and tasks conducted as part of a multicentric study could prove to help identify more accurate clinical applications for spine motion analysis.

1.3 3D Printing of Anatomical Spine Models

Surgeons rely on two-dimensional image-based techniques such as x-rays, CTs and MRIs to understand a patient's pathology and plan out surgical interventions ¹⁵². This approach to preoperative planning depends heavily on the surgeon's visualisation skills and the quality of the image ¹⁵². 3D printing can help overcome this limitation by producing patient-specific medical models ¹⁵³. Using patient-specific CT or MRI data, the 3D printed models visualize the patient's anatomical variations and helps in diagnosis, surgical planning, medical education and patient communication ^{154,155}. 3D printing has been used in various medical fields such as cardiology, orthopaedics (hip, knee and shoulder surgeries), maxillofacial surgeries and spine surgeries ^{152,153,156}.

The process to create a 3D printed model is the same for the different medical fields and the different anatomical regions of interest ¹⁵⁷ (Figure 7). The first step to generating a 3D model is to acquire a patient's CT or MRI scans ¹⁵². These data sets would need to be of high resolution to allow for the accurate isolation of the geometry ¹⁵³. After acquiring the medical images, the region of interest needs to be segmented using a segmentation software such as Materialise Mimics (Materialise Research, Leuven, Belgium) or the open-source software 3D slicer (Brigham and Women's Hospital, Boston, MA, USA) ^{153,157}. The segmentation process entails the partition of the image into different labelled regions using thresholding depending on the pixel intensity of the tissue as such bone has a high density and can be separated from the lungs for example as they have a very low density ¹⁵⁷. The advances in segmentation software have allowed for the easy extraction of the surface structures from radiographic images to a point where the process could be considered automatic or semi-automatic ¹⁵⁷.

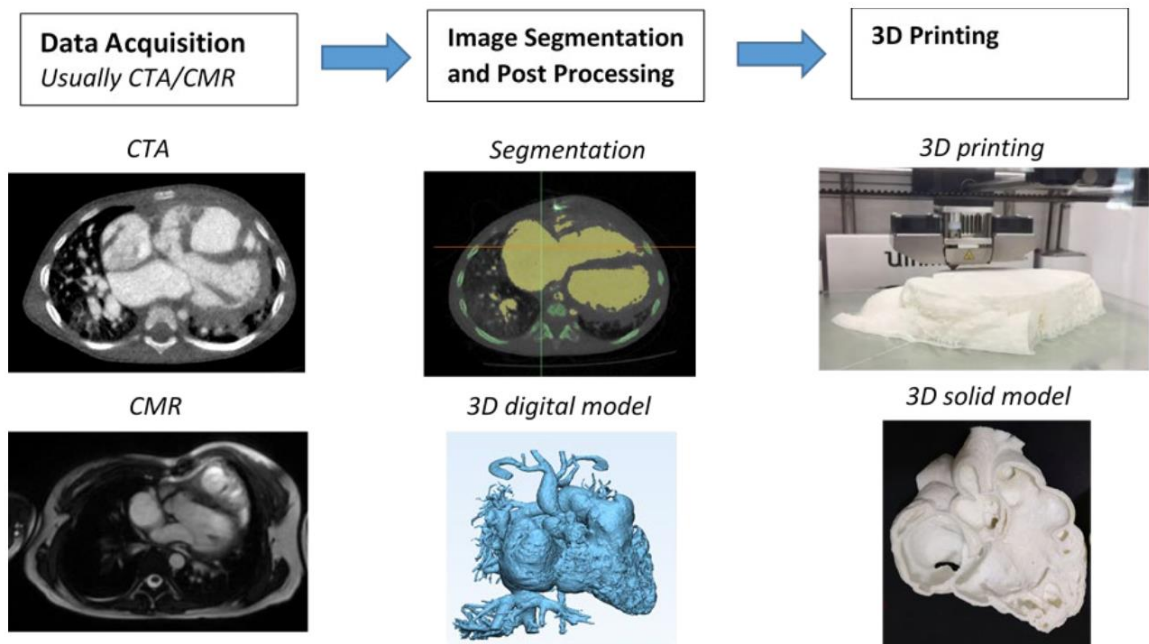


Figure 7 Steps needed for the fabrication of a 3D printed anatomical model of the heart. CTA (Computed Tomographic Angiography), CMR (Cardiac Magnetic Resonance) from Sun, Lau, Wong, Yeong. *Personalized Three-Dimensional Printed Models in Congenital Heart Disease*. *J Clin Med*. 2019;8(4):522. doi:10.3390/jcm8040522 ¹⁵³.

The surface mesh of the segmented geometry can then be refined for 3D printing ^{155,157}. Using different computer-aided design (CAD) tools and software such as Materialise 3Matic (Mimics Research, Materialize, Leuven, Belgium) and Mesh Lab 1.3.2 (CNR, Pisa, Italy), the segmented geometry could be repaired, smoothed, or appended ¹⁵⁷. These design tools can repair the surface mesh from any small errors, smooth the surface to discard resolution irregularities and append the surface to remove unwanted parts or add certain components ^{155,157}.

To print the model generated, different 3D printing technologies currently exist. These could be divided into 3 commonly used methods: 1) extrusion printing such as fused deposition modelling (FDM), 2) photopolymerization such as digital light processing (DLP) and 3) powder-based printing such as selective laser sintering (SLS) ¹⁵⁷. Using FDM, a thin polymer filament is melted and deposited slice by slice on a moving platform using an extrusion head ¹⁵⁵. The printed geometry is supported by a simultaneously printed scaffold ¹⁵⁵. For DLP, a UV light directed at a liquid resin polymerizes and solidifies the resin to form the model ^{155,158}. In the case of SLS, a heat-generating CO₂ laser is used to draw the 3D model layer by layer using a heat-fusible powder ¹⁵⁸. FDM 3D printers are considered to be the fastest and most economical however they do not provide the accuracy of the DLP and SLS printers ¹⁵⁹.

The most vital part of creating an anatomical 3D model is to ensure that the model accurately describes the pathology being investigated and the changes to the anatomical structures of the patient ¹⁵³. To measure the accuracy between model and anatomy, different methods are used

- Measuring the 3D printed models using callipers to compare them to the radiographic image measurements ¹⁵³.
- Conducting CT scans on the printed model to create a new segmented version saved as an STL file that can then be compared to the original segmented geometry ¹⁵³.
- The use of the Dice Similarity Index (DSI) to measure the accuracy of the segmentation. The DSI measures the overlap in mask volume between two or more segmented geometries with values ranging between 0 ± 1 . With a value of 1 denoting a perfect match. In this case, the segmentation of the radiographic image is completed by 2 or more investigators and compared using the DSI to ensure the accurate depiction of the patients' geometry ¹⁵⁵.

Once an accurate 3D printed model is created, it can be used in various medical fields. Looking at the application of 3D printing for spine surgery, 3D printed anatomical models have been found to help surgeons in their pre-operative planning ^{155,158,159}. Surgeons dealing with spine deformities often encounter complex problems intra-operatively due to the deformity such as vertebral rotation, distorted or absent pedicles and changes to the anatomical landmarks of the spine restricting pedicle insertion ¹⁵⁹. A 3D printed model of the patient's spine would hence provide surgeons with tactile feedback on the complexity of the anatomy and on the technical challenges that might be encountered during the surgery ^{159 160}. It also gives surgeons an idea of 1) the optimal screw trajectory needed for the spinal fixation ^{156,159}, 2) the supplemental bony reconstructions needed in the case of vertebral osteotomies ¹⁵⁹ and 3) the optimal degrees of correction required to restore spine balance ^{156,161}. In addition to these specific spine surgical benefits, 3D printing of anatomical models has been associated with a decreased operative time, a decrease in blood loss during the surgery and a decrease in intra-operative radiation used ¹⁵⁹⁻¹⁶¹.

Although 3D printing has evident advantages in spine surgery it is still affected by the time and cost needed to create accurate models ^{159,161}. The time needed to plan and create the 3D printed model varies anywhere from 2 hours to 2 days with an average of 10 to 12 hours typically ^{159,161}. This long process makes the use of 3D printing impractical for emergency surgical interventions ¹⁵⁹. On the other hand, the cost to produce highly accurate 3D models of the spine is still very costly with one vertebra costing approximately 250\$. This is due to the complex

manufacturing process of the SLS and DLP printing techniques in addition to the special software needed, the cost of the printer and the need for a trained professional to create the model. However, a study by Eltes et al. (2020) showed that FDM printing could be used to create fast and low cost printed models with enough accuracy for the surgeon to plan the surgery without paying extra for DLP or SLS. Currently, 3D printing for spine surgeries isn't used as widely however if time- and cost-efficient approaches are presented to surgeons, the advantages are plenty ¹⁶².

1.4 FEA of the Thoracolumbar Spine:

As the number of PSF surgeries is increasing¹⁻⁴, different new motion-preserving fixation techniques are being used to improve the long-term outcomes of the surgical procedure^{163,164}. To biomechanically test these new treatment approaches different measurement approaches are available¹⁶³. First, the in-vitro measurement of spinal segments in a laboratory setting using cadaveric specimens have long been used to compare different fixation techniques however they are limited in terms of availability of cadaveric specimen, changes to tissue hydration and variability between specimens^{163,164}. The second method is the in-vivo measurement approach which provides accurate information on the spinal segments in their natural state however these are very restricted due to their high invasiveness¹⁶³. The last method used is in-silico testing which has now gained widespread acceptance such as finite element analysis (FEA)¹⁶³.

FEA can be used to 1) investigate the biomechanical effect of surgeries on both healthy and pathological models of the spine allowing for greater population variation^{164,165}, 2) understand the mechanical behaviour of the spine due to degeneration, adjacent segment disease or scoliosis^{165,166} and 3) design and develop spinal instrumentation¹⁶⁷. In contrast to in-vitro measurement methods, FEA can predict the stresses in the vertebrae and instrumentation, intradiscal pressure (IDP) and the detailed range of motion^{165,167}.

The first step in FEA is creating the 3D structure of the spine to be analysed^{32,166}. Most of the current spine models use CT and MRI data to build their 3D models as these can provide accurate and high-resolution images of the bone geometry^{32,166}. Using segmentation software, each vertebra of the spinal model can be thus created³². The segmented vertebrae are then imported into CAD software to create the complex geometries of the vertebra including the vertebral body, the trabecular core, and the posterior elements³². The vertebrae are then stacked on top of each other to create the spinal segment desired³². Additional spine components are then added such as the intervertebral disc (IVD), the facet joints, and the ligaments³² (Figure 8). Material properties of the bony tissue the IVD and the ligament can then be assigned in addition to the interactions between the components¹⁶³. Using dedicated FE software, the biomechanical evaluation can be initiated under different loading conditions³².

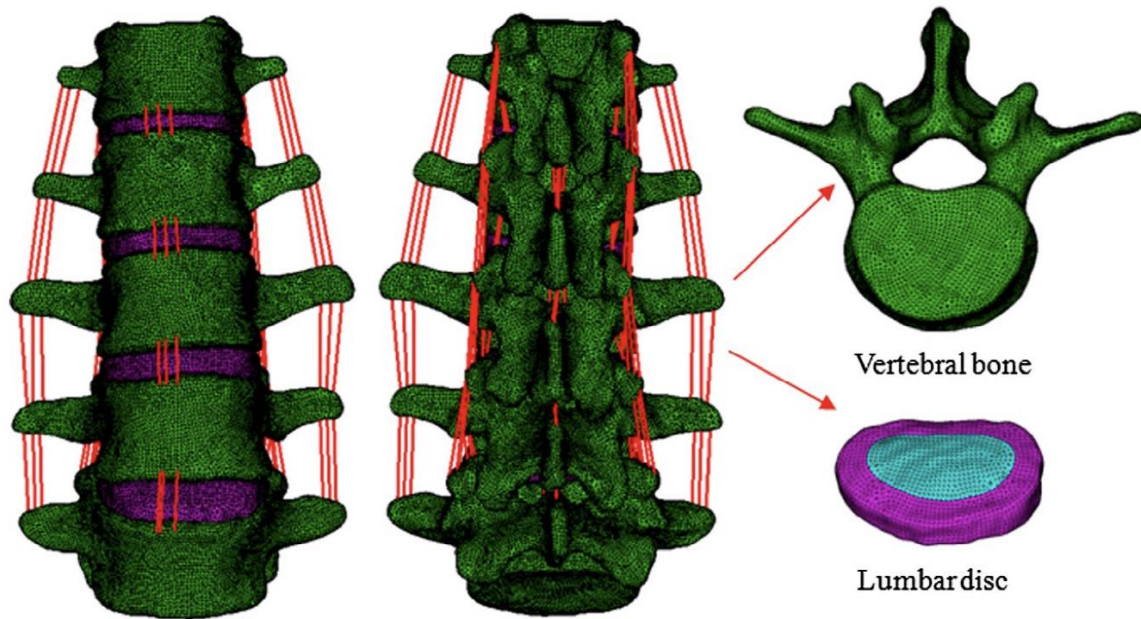


Figure 8 FE model of the lumbar spine From Zhang Z, Fogel GR, Liao Z, Sun Y, Liu W. Biomechanical analysis of lumbar interbody fusion cages with various lordotic angles: a finite element study. *Comput Methods Biomech Biomed Engin.* 2018;21(3):247-254 ¹⁶⁸

Once the final geometry of the 3D model is created and before reporting the outcomes of the range of motion, IDP and stresses in the vertebra or instrumentation; three key elements need to be first checked ¹⁶³:

- Verification implies the assessment of the numerical accuracy of the geometry created and the effect of the mesh resolution on the numerical outputs of the model.
- Sensitivity analysis: assesses the sensitivity of the numerical outputs measured to the input variables of the model. This step provides information on the contribution of the input variable to the overall errors of the model.
- Validation: compares the numerical outputs generated by the model to real-life outputs from in-vitro measurements.

Looking in particular at the kinds of FE models generated for the spine, a clear division can be found separating the models into different sections: 1) vertebral body models, 2) IVD and motion segment models, 3) lumbar spine models, 4) cervical spine models, 5) thoracolumbar spine models and 6) whole spine models which are usually more simplified models than the remaining sections ^{32,167}. Lumbar spine models are currently the most reported on in the literature due to the high incidence of low back pain ^{32,169}.

In contrast, FE models of the thoracolumbar spine remain limited but are slowly increasing ^{14,31,32,170,171}. The main reasoning behind the creation of these models is to assess the effect of various spinal fixation approaches on the onset of proximal junctional kyphosis (PJK)

^{14,30,31,170,172–175}. Due to PJK occurring just above the uppermost instrumented vertebra (UIV), the abnormal kyphotic bend usually appears in the thoracolumbar spine ¹⁰. Hence, simulating long PSF surgeries in a thoracolumbar spine model could provide information on the biomechanical risk factors associated with PJK ¹⁴.

One particular risk factor that is increasingly being investigated for the onset of PJK, is the notion of rod stiffness ¹⁷⁶. Due to the high stiffness exhibited by the metal rods used in PSF surgeries, a mismatch locality is appearing between the instrumented spine segment and the non-instrumented part ^{14,176}. Using FE models of the thoracolumbar spine, the effect of various spinal fixations can be simulated to assess their effect on the onset of PJK. Bess *et al.* (2017) ¹⁴ assessed the effect of using posterior tethers above the UIV on the onset of PJK and found that these tethers did indeed allow for a more gradual transition in the stiffness of the construct. Cahill *et al.* (2012) ³¹ tested the effect of using smaller diameter transition rods above the UIV on the onset of PJK and found a decrease in implant stress at the UIV to diminish the incidence of PJK. Flexible instrumentations of interest could be polyetheretherketone (PEEK) rods. Although these have not been investigated before, PEEK has stiffness characteristics closer to the physiological environment of the spine ^{176,177} and hence can provide a transition phase if used above the UIV level.

Chapter 2: Quantifying multi-segmental spine kinematics in healthy participants

From the manuscript:

Jennifer Fayad, György Szőke, Tamás Terebessy, Peter E. Eltes, Aron Lazary, Luca Cristofolini, Rita Stagni. *A comprehensive protocol to quantify multi-segmental spine kinematics* to be submitted to *Gait and Posture*.

Abstract

Introduction: Abnormalities in spine motion have been linked to the incidence and recurrence of spine pathologies. To assess the motion of the spine, various protocols exist in the literature that includes different marker sets, spine segments and angle definitions limiting the comparability in the outcome measures reported. This study aimed to develop a comprehensive protocol for spine motion analysis that allows for results comparability and has clinical significance while also assessing its reliability in terms of marker misplacement.

Methods: Twenty-two healthy participants were enrolled in this study. Fourteen markers were attached to anatomical landmarks of the spine most notably at C7, T3, T7, T12 and L3. To assess the reliability of the protocol, a second marker placement technique was analysed. The spine was divided into upper thoracic, lower thoracic, upper lumbar and lower lumbar segments. The participants were asked to complete three range of motion tasks and three activities of daily living. The measurements were recorded in three laboratories. To synchronise the motion of the spine, key events were identified in each motion task. Following synchronisation, the differences in motion timings, range of motion and contribution of each segment were reported to characterize the motion of the spine and to compare the effect of marker misplacement on the measured outcomes.

Results: Marker misplacement affected both the joint angle distributions and the timing of key events of each task, however, no difference was found in the range of motion or contribution of each segment. The synchronisation approach provided consistent key events for each segment defined for all participants. The lowest intersegmental range of motion was detected between the Upper Thoracic and Lower thoracic segments, while the upper lumbar-lower lumbar segment contributed the most to the motion of the spine.

Conclusion: The comprehensive spine motion protocol developed in this study was able to investigate the reliability of the measurement in terms of marker misplacement, characterize the motion of the spine in healthy adults and provide a synchronisation approach for spine motion. The findings of this study could be used in a clinical setting to assess the effect of spine pathologies on the motion of the multi-segmental spine.

Introduction:

Motion abnormalities at the level of the spine have been linked to the prevalence and recurrence of various spine pathologies^{20,21,88} such as low back pain⁵⁹ and spine degenerative diseases¹⁰⁴. Quantifying and analysing the kinematics of the spine in-vivo can provide a better understanding of spine function to support diagnosis, surgical planning, treatment, and characterize the motion of the spine during activities of daily living (ADL)^{23,88}.

The spine is a multi-articulate structure²⁵ with distinct motion patterns found at the level of the upper and lower lumbar segments^{59,85,86,104} and between the upper and lower levels of the thoracic spine^{23,72,130}. Currently, more than 40 different protocols have been proposed to assess multi-segmental spine motion, designed to analyse different spine pathologies from low back pain^{20,24,59,60,84–88,104,105,119,121,123,130,132} to scoliosis^{90,95,97,106,107,116,122,125}, to adult spine deformity^{82,98}. Although these protocols all aim to describe the complex motion of the spine¹⁰⁹, they include different markers set-up, segment, joint, and angle definitions^{69,178}, limiting the comparability of the resulting kinematic outputs¹⁷⁸. Intra-, inter-subject comparability, reliability, and clinical significance of the outputs, in addition to ease of use, are fundamental characteristics of any motion analysis protocol to be used for functional assessment in clinics.

The present work aimed to define a comprehensive protocol for the functional assessment of spine kinematics, combining design criteria and solutions of previously proposed protocols to guarantee results comparability and clinical significance, taking also into account usability by minimising the number of markers^{101,104,109}. The reliability of the proposed protocol was also assessed, analysing, in particular, the effect of marker placement.

Methods:

Participants:

Twenty-two healthy participants were recruited (12M, 10F, age:26±4, height:175±7cm, weight:71±14kg). Participants had no history of back pain or musculoskeletal affections, nor had undergone any spine surgery. Ethical approval was obtained from the National Ethics Committee of Hungary (OGYÉI/163-4/2019). The study was explained to all participants before they signed informed consent.

Experimental Assessment:

Fourteen markers were attached on anatomical landmarks of the trunk (10 markers) and pelvis (4 markers) (Figure 9), chosen as a combination of common landmarks used in clinically relevant protocols^{23–25,70,87,89,93,95,98–102,104,107,109,122,131,134–136}, and are listed in Table 8(A), as well as the corresponding body segments.

Twelve markers were also attached on landmarks of the lower limbs listed in Table 8 (B), to allow synchronous assessment of lower limb kinematics walking trials.

Skin markers were attached while participants were standing upright, by the same operator for all subjects.

Table 8 Marker Setup

Marker Placement on the trunk (A), pelvis (A) and lower limbs (B) to describe the body segments defined, the markers and their position on anatomical landmarks, the segments each marker defined and the studies they were originally used in.

A

Body Part	Marker	Anatomical Landmark	Segment Definition	Adapted From
Trunk	RA/LA	Right/Left Acromia	Shoulders	Davis Marker Set ¹⁷⁹
	IJ	Clavicle	Shoulders, Upper Thoracic	24,25,70,82,90,95,101,116,180
	XP	Xiphoid Process	Lower Thoracic, Upper Lumbar, Lower Lumbar	24,25,70,82,95,180
	C7	7 th Cervical Vertebrae	Upper Thoracic, Shoulders	23,25,70,87,89,93,95,98–102,131,134–136
	T3	3 rd Thoracic Vertebrae	Upper Thoracic	23,82,109,116
	T7	7 th Thoracic Vertebrae	Upper Thoracic, Lower Thoracic	23,101,104,116
	T12	12 th Thoracic Vertebrae	Lower Thoracic, Upper Lumbar	24,104,107,109,122
	L3	3 rd Lumbar Vertebrae	Upper Lumbar, Lower Lumbar	23,59,104,107,109,118,123
	SACR	Sacrum Virtual Marker	Lower Lumbar	122,180–182
Pelvis	RASIS/LASIS	Right/Left Anterior Superior Iliac Spine	Pelvis	Davis Marker Set ¹⁷⁹
	RPSIS/LPSIS	Right/Left Posterior Superior Iliac Spine	Pelvis	

B

Body Segment	Marker	Anatomical Landmark	Segment Definition	Adapted From
Lower Limbs	RTHI/LTHI	Right/Left Thigh	Thigh	Davis Marker Set ¹⁷⁹
	RTIB/LTIB	Right/Left Tibia	Shank	
	RKNE/LKNE	Right/Left Knee	Thigh, Shank	
	RANK/LANK	Right/Left Ankle	Shank, Foot	
	RTOE/LTOE	Right/Left Toe	Foot	
	RHEE/LHEE	Right/Left Heel	Foot	

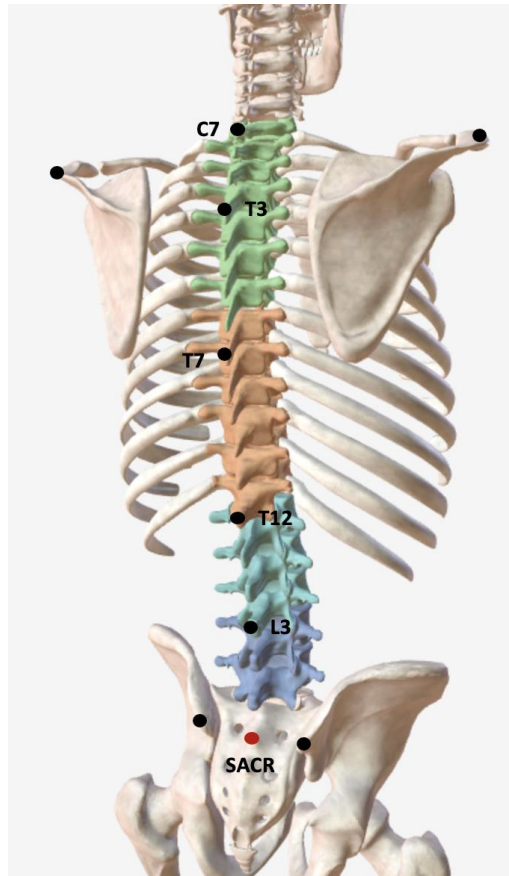


Figure 9 Marker Setup on spine anatomical landmarks

Participants were asked to complete 7 tasks:

- Upright standing
- Three functional tasks:
 - Full Flexion
 - Thoracic Flexion
 - Lateral Bending
- Three activities of daily living (ADL):
 - Sit-to-Stand (STS) (stool height controlled to have thigh parallel, shank and trunk orthogonal to the ground while sitting)
 - Ball Pick-up (m=3kg, radius=6.75cm) placed on a stool (height=47-69cm))
 - Walking at a self-selected speed along a straight path

Three repetitions were acquired per task.

Marker trajectories were acquired using stereophotogrammetry in 3 laboratories, details of each lab system can be found in Table 9.

Chapter 2: Quantifying multi-segmental spine kinematics in healthy participants

Table 9 Motion Capture Systems in the 3 laboratories used.

For each lab, the motion capture system, sampling rate, camera sensor resolution, capture space diagonal and participant characteristics were reported.

Lab	System	Sampling Rate	Sensor Resolution	Capture Volume Diagonal	Participants			
					No.	Age	Height	Weight
1	6-camera VICON MXT40	100Hz	4 Mpixels	3.8m	7M 7F	26±4	175±8cm	72±14kg
2	6-camera BTS SMART-D500	200Hz	0.5 Mpixels	3.5m	3M, 2F	27±2	177±4cm	71±10kg
3	10-camera BTS SMART-DX7000	250Hz	2.2 Mpixels	4.7m	2M, 1F	29±2	176±8cm	71±17kg

To assess the sensitivity of the protocol to marker misplacement, a subset of 10 participants (7M, 3F age=26±3, height=176±6cm, weight=72±13kg) underwent a second marker placement: attaching the spine markers with the subject at maximal forward flexion, before performing the 3 functional tasks again.

Data Analysis:

Marker trajectories were filtered using a Woltring filter with 10Hz cut-off frequency.

Four spinal functional segments were defined in addition to the shoulders and pelvis. Segment name, the protocol they were adapted from, landmark choice and axis definition are reported in Table 10.

Table 10 Segments of the spine defined The table shows the study they were priorly mentioned in, the landmarks used to define them, and the axis definition used for each segment.

Segment	Adapted From	Markers	Axis Definition
Upper Thoracic (C7) (UT/C7)	87,120	C7, T7, IJ	x-axis= orthogonal to C7, T7, IJ plane, pointing to the left y-axis= T7→C7 z-axis= $x \times y$
Upper Thoracic (T3) (UT/T3)	20,86,87,104	T3, T7, IJ	x-axis= orthogonal to T3, T7, IJ plane, pointing to the left y-axis= T7→C7 z-axis= $x \times y$
Lower Thoracic (LT)	20,86,104	T7, T12, XP	x-axis= orthogonal to T7, T12, XP plane, pointing to the left y-axis= T12→T7 z-axis= $x \times y$

Upper Lumbar (UL)	20,86,87,104	T12, L3, XP	x-axis= orthogonal to T12, L3, XP plane, pointing to the left y-axis= L3→T12 z-axis= $x \times y$
Lower Lumbar (LL)	20,86,87,104	L3, SACR, XP	x-axis= orthogonal to L3, SACR, XP plane, pointing to the left y-axis= SACR→L3 z-axis= $x \times y$
Shoulders	70,87	RA, LA, C7, IJ	y-axis= orthogonal to LA, RA, IJ plane, pointing upwards x-axis= LA→RA z-axis= $x \times y$
Pelvis	70,87	RASIS, LASIS, RPSIS, LPSIS	y-axis= orthogonal to LASIS, RASIS, RPSIS plane, pointing upwards x-axis= LPSIS→RPSIS z-axis= $x \times y$

Two different conventions were defined for the upper thoracic segment based on previous protocols ^{20,86,87,104,120}.

Three-dimensional intersegmental joint and segment-pelvis angles were calculated following Grood and Suntay ¹⁸³ convention in accordance with ISB recommendations ¹⁶¹. For each task, 18 intersegmental angles and 18 segment-pelvis were generated in the sagittal, coronal, and frontal planes.

Motion Synchronisation:

For intra- and inter-subject motion data comparability, key functional events were identified in each repetition of each motor task. The start and end timings of each joint angle repetition were adjusted to match the start and stop motions of the C7 marker in the plane of motion.

Then, 3 functional events were identified within each joint angle. These events corresponded to key turning points (TP) in the first derivative of each joint angle in the plane of motion. The TPs matched the time at which the derivative was equal to a maximum absolute value or was equal to 0. For each task and each joint, TPs conveyed what was occurring in the first half (TP1), the middle (TP2) and the second half (TP3) of the motion task (Figure 10). Details of TP choice for each motion task can be found in Table 11.

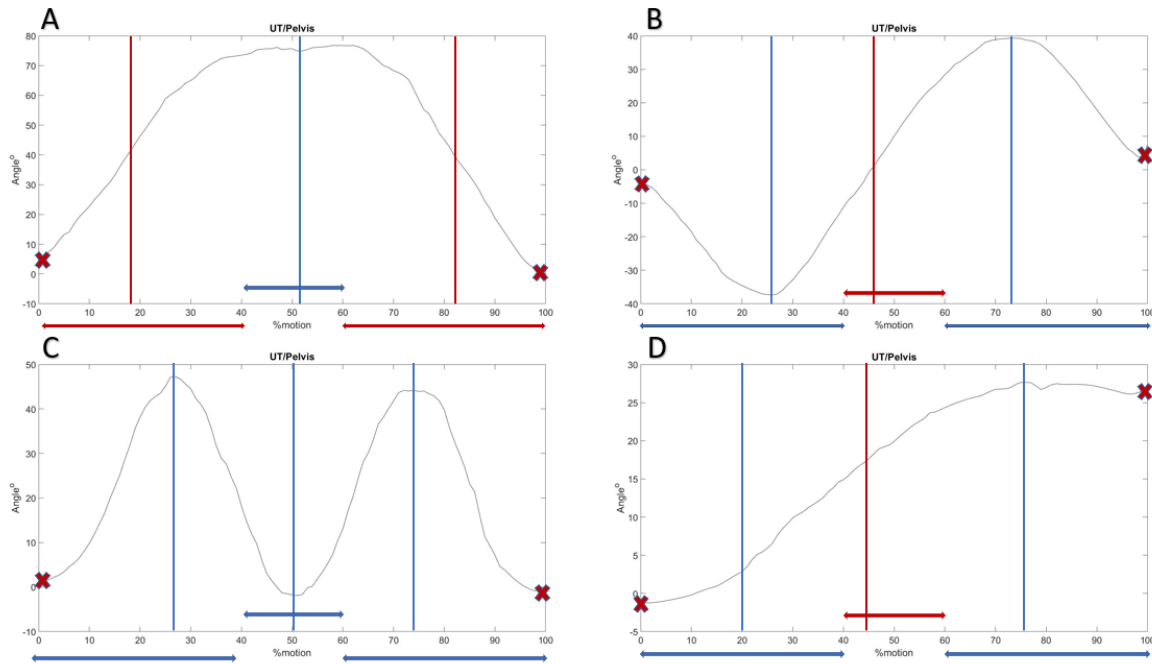


Figure 10 Turning points identified in the UT/pelvis joint angle for each motion task. A= Full flexion, B= Lateral Bending, C= Ball pick-up, D= Sitting. A, C, D depict the joint angle in the sagittal plane, B depicts the angle in the coronal plane. X= Beginning and end of the motor task identified from the motion of the C7 marker. Red vertical lines corresponded to the timing of the maximum absolute value of the joint angle first derivative. Blue vertical lines correspond to the timing of the minimum value of the first derivative. \leftrightarrow = time window chosen to detect the key event.

Table 11 TPs defined for each motion task from the first derivative of the joint angles.

Task	First Derivative		
	TP1	TP2	TP3
Full Flexion	Maximum Absolute value	Equal to 0	Maximum Absolute value
Thoracic Flexion	Maximum Absolute value	Equal to 0	Maximum Absolute value
Lateral Bending	Equal to 0	Equal to 0	Equal to 0
STS	Equal to 0	Maximum Absolute value	Equal to 0
Ball Pickup	Equal to 0	Equal to 0	Equal to 0

After defining the beginning, end and 3 TPs, the joint angles of each repetition were time-stretched to the median TPs of the UT/pelvis joint. The UT/pelvis was chosen as it showed consistent TPs for all repetition and all tasks. The time stretch was completed twice, first for intra-subject synchronisation and then for inter-subject. Joint angles were time normalized to 100 points. The median and dispersion around the median (25th-75th percentiles and 10th-90th percentiles) of the time at which the peak motion value occurs were then compiled for all joint angles and tasks.

Definition of Spine Parameters:

In addition to the timing of peak motion, 2 angular parameters were calculated for each joint angle and reported as median and dispersion:

- 1) ROM: maximum-minimum value.
- 2) Percent contribution of the joint to the overall motion of the shoulders with respect to the pelvis: $\frac{Joint\ ROM}{ShoulderPelvis\ ROM} * 100$.

Measurement Reliability:

To assess measurement reliability in terms of marker placement, the influence of lab measurement and marker configuration of the UT segment; comparisons were made between 1) the 2 marker placement cohorts of 10 participants each, 2) each of the lab cohorts and the 2 remaining ones and 3) each of the joints that included the UT segment in the 22-participant cohort. Independent t-tests were performed to assess the differences between group demographics in terms of age, height, and weight.

Pairwise comparisons were made between the joint angle distributions at each of the 100-time points and for each of the measured angles using independent t-tests.

Comparisons were also made between the groups to assess differences in the timed parameters and the angular parameters (ROM and %Contribution) of each joint angle. To assess the differences between these parameters for all groups, data normality was first checked using the Lilliefors test, depending on the data distribution the ANOVA or Kruskal Wallis tests were then applied to test for significant differences ($\alpha=0.05$).

Results:

Measurement Reliability:

Effect of marker Placement:

Significant differences in the joint angle distributions were found between the marker placements groups occurring before and after peak flexion is achieved for full flexion and thoracic flexion. For lateral bending the significant difference occurred when participants returned to standing following left bending and at the time of peak right lateral bend. Table 12 shows the angle distribution of the intersegmental joints over the task durations.

Chapter 2: Quantifying multi-segmental spine kinematics in healthy participants

Table 12 Angle Distribution around the median of the intersegmental joints over the 3 ROM tasks between the 2 marker placement approaches. Significant differences are indicated with (*)

Task	Segment	Time (s)	Angle Distribution around the median (\pm°)		p
			Placement 1	Placement 2	
Full Flexion	UT/LT	1-16	16 – 20	23 – 30.5	p> 0.059
		17-20*	16	21 – 22	p<0.047
		21-100	12 – 18	17 – 24.5	p>0.051
	LT/UL	1-39	22.5 – 43	13 – 26	p>0.05
		40-49*	20 – 22	12 – 16	p<0.048
		50-60	20 – 21	10 – 14	p>0.054
		61-90*	17 – 24	11 – 30	p<0.049
		91-100	25 – 32	24 – 32	p>0.079
	UL/LL	1-17	40 – 48	22 – 32	p>0.051
		18-34*	41 – 52	22 – 31	p<0.045
		35-100	40 – 53	22 – 47	p>0.065
	Thoracic Flexion	UT/LT	1-5	20	10 – 12
6-39*			20 – 31	13 – 23	p<0.044
40-100			28 – 40	11 – 29	p>0.051
LT/UL		1-46	7 – 14	8 – 12	p>0.052
		47-85*	7 – 13	7 – 11	p<0.047
		86-100	7 – 10	10 – 18	p>0.054
Lateral Bending	UT/LT	1-38	11 – 25	12 – 24	p>0.07
		39-65*	16 – 22	13 – 21	p<0.047
		66-72	15 – 18	12 – 13	p>0.056
		73-96*	11 – 20	8 – 17	p<0.03
		97-100	12 – 14	7 – 10	p>0.054
	LT/UL	1-38	11 – 25	11 – 24	p>0.056
		39-65*	17 – 26	10 – 22	p<0.037
		66-80	27 – 31.5	21 – 24	p>0.058
		81-89*	27.5 – 31	18 – 21	p<0.027
		90-100	17 – 27	12 – 19	p>0.052
	UL/LL	1-39	13 – 21	10 – 19	p>0.075
		40-59*	18 – 24	13 – 23.5	p<0.006
		60-78	22 – 24	22 – 26	p>0.07
		79-86*	23 – 27.5	19 – 21	p<0.024
		87-100	21 – 28	17 – 19	p>0.06

In terms of motion peak timing, significant differences ranging between 3%-8% of total motion were detected during lateral bending for all the joint angles measured.

No differences were found in the ROM or the % contribution of all joint angles defined.

Influence of Lab Setting and Motion Capture System:

Looking at the 3 range of motion tasks, joint angle distributions showed the greatest differences when comparing Lab 1 to Labs 2&3, and when comparing Lab 3 to Labs 1&2. Joint angle distributions showed significant differences between all 3 labs during the ball pickup motion that coincided with the timing of the 3TPs.

For the motion peak timing, no significant differences were detected between the labs during lateral bending or thoracic flexion. However, differences in motion timing were found when looking at the remaining tasks.

In terms of ROM, on average, a median significant increase of 20° (range 17° to 24°) was found between all the segment-pelvis joint angles of Lab 1 when compared to Labs 2&3. No significant differences were seen between the remaining tasks.

Marker Configuration of UT segment:

Joint angle distributions showed significant differences between the 2 marker configurations of the Shoulder/UT joint during lateral bending and sitting tasks when peak motion occurred. Significant differences were also detected between the 2 marker configurations of the UT/LT joint during full flexion, lateral bending, ball pickup and STS. No significant differences were found for thoracic flexion or the UT/Pelvis joint.

No significant differences were detected for any of the timed parameters measured.

ROM of the UT/LT joint showed a median significant increase of 3° (range 2° to 4°) when using the C7 marker for lateral bending and STS.

Characterization of multi-segmental spine motion:

Timing of the Motion Peak

Looking at the timing of the motion peak, a delayed motion was seen at the level of UT/LT angle (median +12.75%) when compared to the remaining intersegmental angles during full flexion. The motion peak of the UT/LT angle was however achieved quicker during the sitting motion (median -14.5%) when compared to the remaining intersegmental angles. The LL/pelvis angle showed a median delay of +5% when compared to the remaining segment-pelvis angles of lateral bending.

Motion Pattern

The motion patterns of full flexion (Figure 11, A), lateral bending (Figure 11, B), and ball pick-up (Figure 11, C) can be seen in Figure 11. For full flexion, thoracic flexion, ball-pick up, and sit-to-stand, the highest motion recorded between the segment-pelvis joints were in the sagittal plane ranging between -20° to $+126^{\circ}$. For lateral bending, the highest motion between the segment-pelvis joints was registered in the coronal and frontal planes ranging between -49° to $+55^{\circ}$ and -20° to $+22^{\circ}$ respectively.

When looking at the intersegmental angle, the UT/LT segment exhibited the least motion (between -16° and $+20^{\circ}$) for full flexion, Ball Pickup and STS in the sagittal plane.

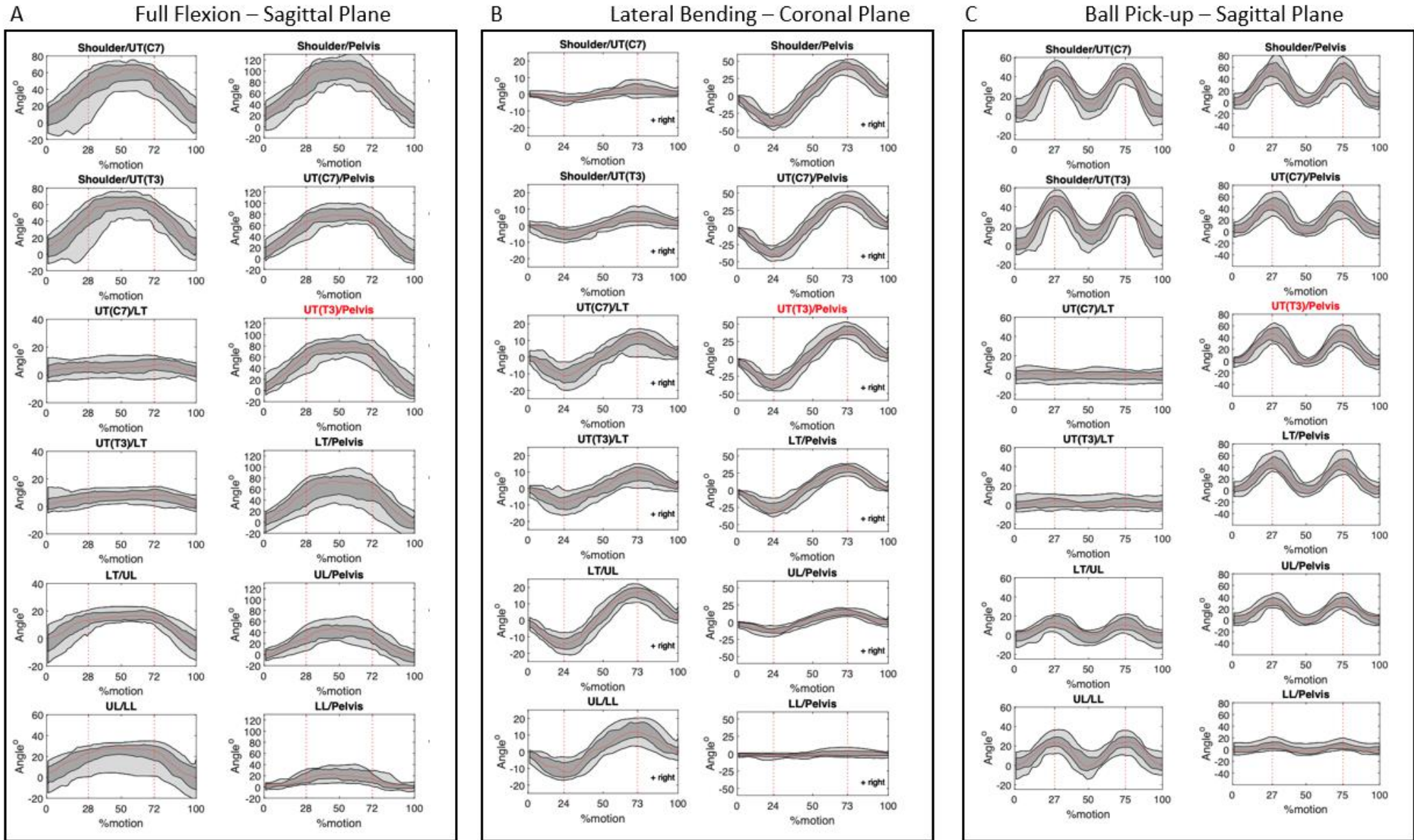


Figure 11 Joint angle curves between the segments defined and between the segments and the pelvis. Vertical dotted lines correspond to key events 1 and 3 in the motion of the UT(T3)/Pelvis joint. Curves show the median (red), 25-75th percentile range (dark grey) and the 10th-90th percentile range (light grey).

ROM

The highest intersegmental ROM was registered between the shoulders and UT segment in the sagittal plane for full flexion (median 56.9°), thoracic flexion (median 16.6°), STS (median 23.7°), and ball pick-up (median 48.9°). The lowest intersegmental ROM was seen at the UT/LT segment registering less than 12° for full flexion, thoracic flexion, STS, and ball pickup. When looking at STS, the sitting motion exhibited a higher ROM between the segments and pelvis when compared to the standing motion with a median difference of 12.8° (between +3.3° and +14°) (Figure 12).

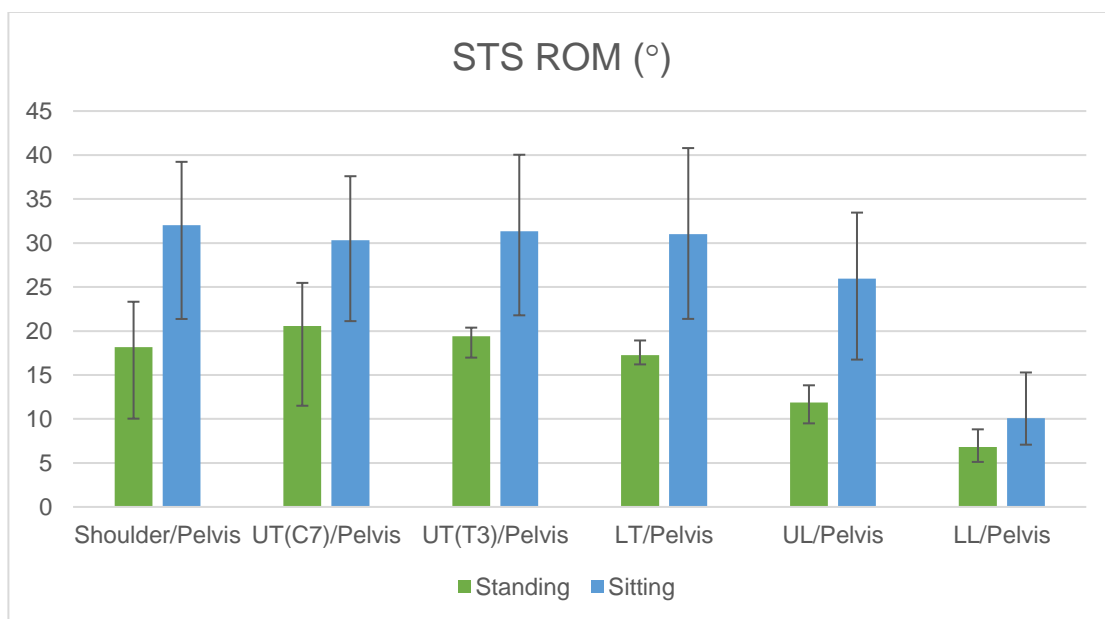


Figure 12 Segment to Pelvis ROM in the sagittal plane during the standing and sitting tasks. Bar Plots show the 25th percentile, median and 75th percentile values

Percent Contribution of Segments:

The UT/LT segment had the least contribution to the motion for all tasks except thoracic flexion with a median contribution of 15% (range from 10% to 23%). The UL/LL segment had the most contribution to the motion during full flexion, STS, and ball pickup with a median contribution of 46% (range from 31% to 55%). The LT/UL segment contributed the most to the thoracic flexion and lateral bending tasks with a median contribution of 47% (Figure 13).

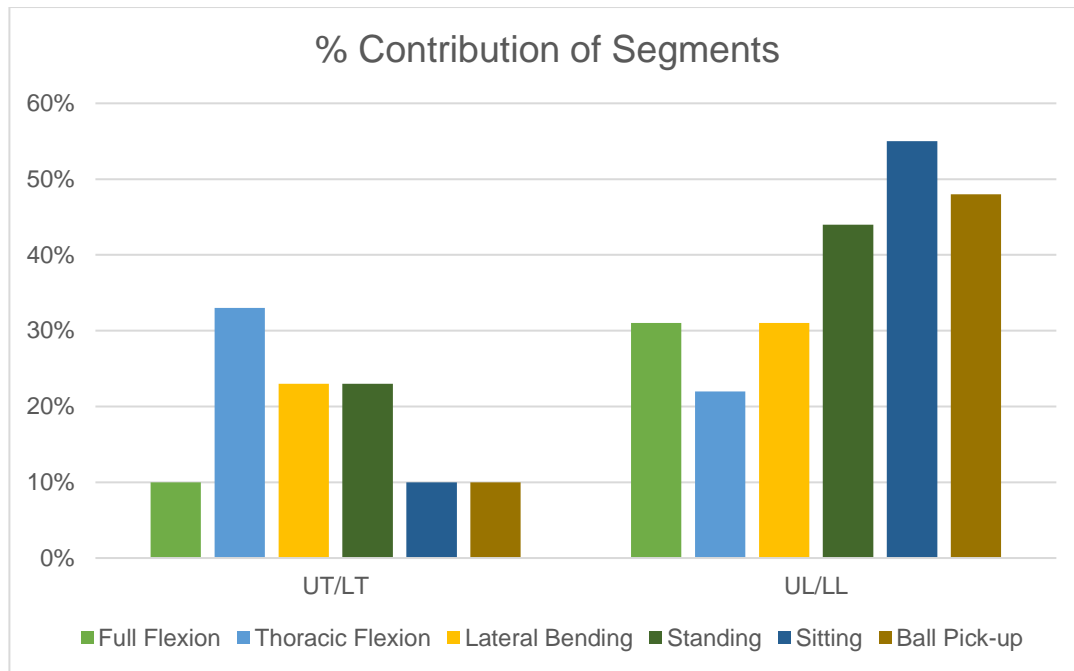


Figure 13 Percent Contribution of the UT/LT and UL/LL segments with the reference for the overall motion being the Shoulder/Pelvis joint.¹⁸⁴

Discussion:

The functional assessment of spine motion has been found to help in the identification and diagnosis of various spine pathologies^{59,104}. However, to have a motion analysis tool readily used in a clinical setting it needs to be reliable, suitable for clinical application and provides comparable data across participants and clinics. The first step in achieving such a tool resides in identifying the healthy motion of the spine segments. In this study, a multi-segmental spine motion analysis protocol was developed from a combination of previously introduced protocols^{23–25,70,87,89,93,95,98–102,104,107,109,122,131,134–136} and tested for its reliability on a cohort of 22 healthy participants.

Measurement Reliability:

The reliability of the protocol developed was tested on three aspects: 1) the effect of marker misplacement on the measurements reported, 2) the influence of the lab on the measurement and 3) the effect of marker choice on the measurements of the upper thoracic spine segment. Looking at marker misplacement, differences were found between the timing parameters (i.e., TP and motion peak timing) of the two marker placement techniques. These differences occurred when maximal motion was required from the participants such as during the full flexion task in the sagittal plane and lateral bending in the coronal plane. No significant differences were noted for the angular parameters measured (i.e., ROM and % segment

contribution). Marker misplacement is a source of error often associated with spine marker placements as the bony landmarks of the vertebrae are not as prominent as those of the lower limbs^{110,116,185}. In a study by Severijns *et al.*¹⁸⁵, an increased marker misplacement effect was detected for mediolaterally placed spine markers when compared to markers placed on vertebral bony landmarks as was used in this study. The timing parameter differences detected in this study support the findings of Visscher *et al.*¹⁸⁶, where marker misplacement affected the gait event timings of the lower limbs. Studies reporting on marker misplacement on spine kinematics did not report, however, on the effect the misplacement had on the motion event timings^{82,110,116,180,185,187}. In a study by Rouhani *et al.*¹¹⁰, marker misplacement was found to significantly affect the intersegmental ROM in the coronal and axial planes during seated trunk flexion. In the case of our study, this difference was not detected as the motion in those two planes was very small that a significant change could not be seen. Studies conducted by Zemp *et al.*¹⁸⁰ and Schmid *et al.*¹¹⁶ found that the marker misplacement negatively affected the measurement of the absolute amount of spine curvature however, it did not affect the relative change in spine shape (lordosis/kyphosis). Following these findings, an explanation as to why no significant difference was detected in the angular parameters measured in this study could be hypothesized as the ROM measured was calculated from relative angles between the segments rather than absolute angle measurements.

To further assess the reliability of the protocol, this study provided preliminary data on the effect of lab setting and instrumentation on spine kinematic outcomes. The angular parameters exhibited the highest differences between labs with up to 24° difference in the ROM of the segment-pelvis joints of lab 1 when compared to those of lab 2&3. To our knowledge, this is the first study to attempt to test the reliability of spine kinematic measurements across different labs. Inter-laboratory comparisons have been however carried out for gait analysis measurements^{188,189}. In a study by Kaufman *et al.*¹⁸⁹, high-quality reliable gait data were obtained across different labs, marker sets and instrumentations as long as the segment definition remained identical. Similarly, Scalona *et al.*¹⁸⁸, found high levels of repeatability in the sagittal plane kinematics of gait across 2 labs, however, the pelvis was found to be the segment with the lowest repeatability. The decrease in repeatability of the pelvis segment could have played a part in the differences seen in the segment-pelvis ROM of this study nonetheless, further testing is needed as part of a multi-centric study where the same participants are tested across different labs.

With regards to spine segment reliability in particular that of the upper thoracic segment, two marker configurations were tested. We found that the choice of the C7 or the T3 marker did not affect the measurement significantly in terms of the TP timings, the timing of the motion peak or the percent contribution of the upper thoracic joint. The significant differences were detected in the joint angle distributions of the Shoulder/UT and UT/LT joints in addition to an increase in the ROM of the UT segment when using the C7 marker. In a study by Saad *et al.*¹¹³, to assess the contribution of the cervical and thoracic segment to STS motion, a correlation was found between the motions of the T1-T4 segment and the cervical spine. In contrast, the T4-T6 segment exhibited motions closer to those of the lower thoracic segments and hence provided a better description of motion. Schinkel-Ivy *et al.*¹¹⁵ preferred the use of the C7 marker over the T3 marker in their study. When the C7 marker was associated with markers on T6, T12 and L5, a complete description of spine motion could be achieved with high repeatability. While the C7 marker is widely used in spine kinematic protocols, it is highly affected by the motion of the shoulders¹¹³. As Leardini *et al.*¹⁵⁰ have pointed out, high intersegmental angles are exhibited between the shoulder and thoracic segments during spine flexion. To decrease this source of error and guarantee that the motion detected at the level of the upper thoracic segment is entirely originating from the spine, the use of the T3 marker would be thus recommended.

Motion Characterization:

With regards to the output of the comprehensive protocol developed, this study was able to characterize the motion patterns of the various spine segments defined. In terms of the suitability of the protocol to be used in clinical practice, the marker setup added 3 markers to the conventional VICON plug-in-gait marker set and as such it could easily be added to routine tests. The spine markers were all placed on the bony vertebral landmarks which have been found to exhibit decreased marker palpation error when compared to mediolaterally placed markers on the spine¹⁸⁵. The limited number of markers on the spine was still able to provide ample information on the segmental motion of the spine and this agrees with the findings of Schinkel-Ivy *et al.*¹¹⁵ and Needham *et al.*⁷² who found that 3 to 4 markers on the spine are enough to describe the motion of the multi-segmental spine with good reproducibility.

To tackle the problem of data comparability in spine motion, the introduction of TPs to the data processing step helped in the synchronisation of the spine motion for all participants. The identification of key events in spine motion is essential to achieve comparable data across

protocols as is the case for gait analysis¹⁸⁴. The choice of which parameter to pick to synchronise the spine motion to has varied from study to study, Christie *et al.*⁵⁹ used the anterior displacement of the C7 and L5 markers, Papi *et al.*¹⁰⁴ used the displacement and change in velocity of the PSIS and T1 markers while studies assessing spine kinematics during walking and running used the heel strike event to synchronise their motion to. This study adapted the same approach taken by Seerden *et al.*⁸³ by choosing the key events following the change in the first derivative of the angular position and as such minimizing the source of error linked to individual marker displacements¹¹⁶. Following synchronisation, the angular outcomes of the protocol demonstrated how each spinal segment has its own motion pattern. The findings supported those of Papi *et al.*¹⁰⁴ that the UL and LL segments do in fact move differently. This difference in motion pattern was detected in the ROM of the two segments but also in the timing of the motion detected, where the UL segment achieved peak motion before that of the LL. For the two thoracic segments, the ROM calculated was well within the range of results reported by previous studies^{20,23,118}. In particular, the intersegmental motion between the UT/LT joint exhibited the least motion for all tasks except the thoracic flexion where it was responsible for more than 30% of the motion. The shoulder segment had a considerable effect on the thoracic segment, wherein identifying if motion seen in the UT/LT joint during thoracic flexion task was originating from the shoulder segment. This source of error has been also reported in previous studies^{113,150}.

There are limitations to consider when interpreting the findings of this study. The first concern is the small sample size of participants. Although the findings of the study were consistent with previous literature, a larger participant cohort is needed to reliably characterize the motion patterns of the spine and derive clinical conclusions. The 10-participant subset would also need to be increased to fully understand the effect of marker misplacement on the measurement outcomes. Second, to assess the influence of the lab on the measurement, a larger multi-centric study would need to be carried out with the same participants and the same motion analysis instrumentation. Lastly, the current study focused on tasks mainly carried out in the sagittal plane and one carried out in the coronal plane. Assessment of spine rotation tasks would be beneficial to provide a complete characterization of healthy spine motion patterns.

Conclusion:

In conclusion, this study showed that a comprehensive protocol with limited spine markers was able to characterize the multi-segmental motion of the spine. The small sensitivity of the

protocol to marker misplacement showed that it could be used routinely in the clinic with a minimal effect on the angular outcomes of the measurement. The optimal marker configuration for the UT segment was the one including the T3 rather than the C7 marker. Additionally, the synchronisation technique developed here permits the comparability of spine kinematic data between different marker sets, task choice and lab settings.

Chapter 3: Multi-Segment Spine Motion of Patients before and following Posterior Spine Fusion

From the manuscript:

Jennifer Fayad, Ferenc Bereczki, György Szőke, Tamás Terebessy, Peter E. Eltes, Aron Lazary, Luca Cristofolini, Rita Stagni. *Multi-Segment Spine Motion of patients before and following posterior spine fusion.*

Abstract

Introduction: As the average life expectancy increases, the prevalence of spine pathologies is on the rise. While abnormalities in spine motion have been linked to the incidence and recurrence these pathologies. Using motion analysis, the kinematics of the spine could be quantified to analyse the effect of pathology and surgery on the motion of the spine. This study aimed to assess the spine kinematics of patients undergoing various levels of posterior spine fusion surgeries by assessing the differences in kinematics between patient cohorts, pre-and post-surgery and between patients and a control cohort.

Methods: Thirty patients undergoing posterior spine fusion surgeries were recruited and split into a long fusion cohort (n=10) and a short fusion cohort (n=20) while twenty-two healthy participants as the control group. Patients were measured one day before surgery and at the 6-month follow up. Standing x-rays of patients were taken during the two measurement days to assess the change in spinopelvic parameters. For each measurement, markers were attached to anatomical landmarks of the spine at C7, T3, T7, T12 and L3. The spine was divided into upper thoracic, lower thoracic, upper lumbar and lower lumbar segments. Both patient cohorts and the control group were asked to complete sit-to-stand, stand-to-sit and ball pickup motion tasks. Following the measurement, the differences in motion peak timing, range of motion and contribution of each segment were reported to quantify the changes to spine kinematics before and after the surgery.

Results: Twenty-three patients returned for their post-surgery measurement. Upon radiographic analysis, 8 patients had a GAP score equivalent to a severely disproportionate

spine pre-surgery. Pre-surgery patients in the long fusion cohort exhibited decreased ranges of motion and contributions to the overall motion when compared to the short fusion cohort especially the segment/pelvis joints. Following surgery, patients in the long fusion cohort showed an increase in ROM for the segment/pelvis joints. Compared to the control cohort, patients showed a decrease in the upper lumbar/ lower lumbar while the lower lumbar/pelvis joint showed an increase in contribution pre- and post-surgery. A significant decrease in the angle distribution was seen for all patients in the coronal and transverse planes to become within the motion patterns exhibited by the control group.

Conclusion: Quantifying the kinematics of the spine in patients undergoing posterior spine fusion is essential to understand the effect of spine motion on the incidence of spine pathologies and the effect of surgery on the kinematic outcome. The findings of this study could be expanded on in the future to understand the changes in segment coordination due to pathology and understand the effect of fusion level on the risk of complication following surgery.

Introduction:

As the percentage of elderly people in the population increases, the number of patients presenting with spinal pathologies such as low back pain (LBP) and adult spine deformity (ASD) is expected to increase¹⁹⁰. In the case of ASD, surgical interventions such as posterior spine fusion (PSF) have been linked to improved clinical results compared to conservative treatments¹⁹¹. PSF surgeries can be differentiated into short fusion surgeries that involve the fusion of 1–2-disc levels or long fusion surgeries entailing the fixation of more than 2-disc levels³⁹. However, complications following PSF surgeries are quite frequent, especially following long PSF^{2,191}. Of these, proximal junctional kyphosis is a common complication that could require reoperation². Various studies have investigated the risk factors leading to the onset of PJK and have suggested approaches to try and diminish its incidence^{191–193}. Limited investigations have analysed the effect of patients' dynamic activities on the development of PJK¹⁹¹.

Researchers now agree that impairments to the posture and movement of the patient contribute to the onset and recurrence of both LBP and ASD^{20,21,88}. To measure these impairments conventional radiographic assessments before surgery is not enough^{18,191}. Additionally, the assessment of a patient's mobility in the clinical setting is currently done using quality of life questionnaires that could not be considered an objective quantifying tool¹⁸. Motion capture can be used as an objective tool to assess spine function, characterize the motion of the spine before and after surgery, reveal the motion characteristics related to PJK and help in surgical planning^{23,88,191}. Gait analysis has been previously used to investigate the dynamic parameters that could lead to the onset of PJK where an increase in anterior pelvic tilt was linked to a higher chance of developing PJK following PSF surgery¹⁹¹. However, the effect of alterations to spine kinematics on the onset of PJK have not been yet investigated.

Using a multi-segmental spine measurement protocol, the distinct motion patterns of the spine can be investigated to measure the intersegmental angles between the spine segments, the angles between the spine segments and the pelvis, the range of motion of the spinal segments and the coordination between the segments. All of these parameters could help in understanding the changes in spine characteristics influencing the onset of PJK.

The purpose of this study was to quantify the motion of the spine in patients with ASD before and after PSF surgery. Using the spine motion analysis protocol developed in Chapter 2, the study aimed at:

1. Assessing the difference in spine kinematics in patients undergoing short or long PSF surgeries.
2. Analysing the changes in spine kinematics before and after surgery for PSF surgeries.
3. Investigating the overall changes in spine kinematics between patients and the control group.

Methods:

Participants:

Thirty patients (Table 13) undergoing both long (n=10) and short (n=20) PSF surgeries were recruited for the study. Patient recruitment was done through the National Centre for Spinal Disorders, Hungary. Patients were measured one day before surgery and then 6 months following surgery. Of the 30 patients recruited, 23 returned for their postoperative measurement (7 from the long fusion cohort and 15 from the short fusion cohort).

Twenty-two healthy participants (Table 13) were also enrolled in the study as asymptomatic controls. General exclusion criteria for both groups were injury or pain to any body part that could affect spine kinematics. Ethics approval was obtained from the National Ethics Committee of Hungary (OGYÉI/163-4/2019). The measurement was explained to all the participants before getting their signed consent.

Table 13 Participant Characteristics

	Long Fusion Mean (SD)	Short Fusion Mean (SD)	Healthy Participants Mean (SD)
Gender	7F, 2M	8F, 12M	12M, 10F
Age (years)	54.9 (10.7)	46.4 (11.9)	26(4)
Height (m)	1.68 (0.10)	1.72 (0.08)	1.75(0.07)
Weight (kg)	85.9 (23.9)	84.9 (16.5)	71(14)
BMI (kg/m²)	30 (6.48)	28.4 (3.9)	23(3.3)

Radiographic Evaluation:

Standing x-rays were recorded of the patients a day before surgery and then at the 6-months follow up appointment. The spinopelvic alignment parameters of each patient were calculated using the Surgimap software (Nemaris Inc, New York, NY, USA) to evaluate the outcome of the PSF. Both lumbar and thoracic spine parameters were measured to report on Pelvic

Incidence (PI), Pelvic Tilt (PT), Sacral Slope (SS), Lumbar Lordosis (LL), L4-S1 Lordosis, PI-LL mismatch, Thoracic Kyphosis (TK), T9 Spinopelvic Inclination (T9SPi), T1 Spinopelvic Inclination (T1SPi), T1 Slope, Cervical Lordosis (CL) and the Global Tilt (GT) ^{49,194}. The global alignment and proportion score (GAP) was then calculated ¹⁹⁵. Additionally, the sagittal vertical axes (SVA) of C7-S1 and C2-C7 were reported.

Motion Data Collection:

The spine and lower limb kinematics were acquired using a 3D motion capture system (6-camera VICON MXT40, Vicon, Oxford, UK) operating at 100Hz. The marker setup used to track the motion of the participants has priorly been described in Chapter 2. In summary, markers were placed on anatomical landmarks of the trunk at C7, T3, T7, T12, L3 and the virtual sacrum marker in addition to the clavicle, xiphoid process, and shoulders markers. The lower limb markers followed the Davis marker setup ¹⁷⁹. All markers were placed by the same investigator using hypoallergenic tape. A reference static standing posture was recorded for each participant before starting with the motion tasks. Participants were asked to complete 2 activities of daily living, and these were:

- Sit-to-Stand (STS) transition (stool with adjustable height $h=47-69\text{cm}$, increased in case a patient could not stand up without support)
- Ball Pickup and return ($m=3\text{kg}$, $\text{radius}=6.75\text{cm}$, ball placed on the adjustable height stool)

The tasks were practised by each participant before recording 3 repetitions.

Data Analysis:

Spine Kinematics Analysis:

Spine Marker trajectories were filtered using a 10Hz Woltring filter. The data was then processed using a custom-built MATLAB (MathWorks, Inc, Natick, USA). Spine kinematics were measured following the protocol developed in Chapter 2. As such, the spine was divided into different segments: upper thoracic (T3-T7), lower thoracic (T7-T12), upper lumbar (T12-L3) and lower lumbar (L3-Sacrum). The 3D joint angles of the spinal segments (intersegmental joint angles) and pelvis (pelvis-segment joint angles) were defined following the Grood and Suntay ¹⁸³ convention in accordance with ISB recommendations ¹⁶¹. The STS motion task was divided into the standing and sitting phases.

To define and normalize the task durations, the motion synchronization technique developed in Chapter 2 was used again where:

- The start and end of each motion task were defined using 1) the C7 marker displacement for STS and ball pickup, 2) the heel strike instance detected by the force plate for the walking trials.
- Three turning points were assigned per task that conveyed the moment key events happened in the motion. These turning points were based on the first derivative of each joint angle.

This approach was performed on each patients' joint angles in the 3 repetitions and then time-stretched to match the median turning points of the individual UT/Pelvis joint motion. For healthy participants, both inter and intrasubject synchronisation was performed and then joint angles were time-stretched to match the median turning points of the overall UT/pelvis joint. The kinematic data of all participants was time normalized to 100 points.

From the synchronisation method, the timing of the motion peaks was reported for all joint angles and tasks.

From the intersegmental and the segment-pelvis joint angles, angular outcomes were calculated for all tasks:

- The ROM in the plane of motion is calculated as the difference between maximal and minimal angles.
- Percent contribution of the joint to the overall motion of the shoulders with respect to the pelvis: $\frac{Joint\ ROM}{ShoulderPelvis\ ROM} * 100$.

Both timed and angular outcomes were generated for each patient before and after the surgery and the healthy control group. Comparisons were then made between:

1. The long fusion versus the short fusion cohorts before the surgery
2. The before and after measurement of each patient
3. The healthy participants vs the patient cohorts.

Additionally, in the case of the comparison between the healthy population and the patient cohort, pairwise comparisons of the joint angle distributions at each of the 100-time were completed in all three planes of motion using independent t-tests.

Results:

Radiographic Evaluation:

Looking at the GAP score calculated, in the long fusion cohort before the surgery, 8 patients had a severely disproportioned GAP score (≥ 7). Two patients had a score between 3 and 6 equivalent to a moderately disproportioned spine. Following the surgery, 6 patients in the long fusion cohort had full standing x-rays allowing for the measurement of the GAP score again. Only one patient had no change in their GAP score, 3 patients had a 1–3-point decrease in the GAP score however it was still equivalent to a severely disproportioned spine. Two patients had a significant decrease in their GAP score to become equal to 3 and equivalent to a moderately disproportioned spine.

For the short fusion cohort, before the surgery, of the 14 patients with full standing x-rays, 10 had GAP scores equivalent to proportioned spines (0-2) while 3 had GAP scores equivalent to a moderately disproportioned spine and only one patient had a severe disproportion. Following the surgery, 10 of the 14 patients had follow up full spine x-rays and all 10 patients had a GAP score ≤ 2 equivalent to a proportioned spine.

Chapter 3: Multi-Segment Spine Motion of Patients before and following Posterior Spine Fusion

Table 14 Spinopelvic Parameters to evaluate spine parameters pre- and post-surgery of Long Fusion patients.

Spinopelvic Parameter	Time of Measurement	Long Fusion Patient									
		1	2	3	4	5	6	7	8	9	10
PT (°)	PreOp	21.2	21.4	21.5	36.9	23.6	25.9	31.4	-2.1	27.1	20.9
	PostOp	19.7	18.7	25.7	28.1	23.0	28.3	19.4	0.5	-	-
PI (°)	PreOp	55.1	40.9	39.5	55.0	50.1	42.9	45.1	31.7	54.7	52.5
	PostOp	53.7	41.2	39.7	52.0	50.3	50.8	45.5	31.7	-	-
SS (°)	PreOp	33.8	19.6	18.0	18.1	26.5	16.9	13.7	33.8	27.6	31.5
	PostOp	33.9	22.5	17.0	23.8	27.3	22.5	26.1	31.3	-	-
LL (°)	PreOp	32.8	32.1	11.7	20.2	31.3	17.5	2.0	81.6	31.4	56.3
	PostOp	48.5	31.9	17.1	45.9	37.2	43.7	51.6	53.5	-	-
L4-S1	PreOp	25.1	26.6	32.9	34.8	31.1	22.3	11.2	55.9	28.8	46.0
	PostOp	45.8	34.6	32.5	42.8	41.4	30.2	33.8	52.2	-	-
PI-LL (°)	PreOp	22.3	8.8	27.8	34.8	18.7	25.4	43.1	-50.0	23.3	-3.8
	PostOp	5.1	9.3	22.6	6.1	13.2	7.1	-6.1	-21.5	-	-
TK (°)	PreOp	19.3	24.9	15.8	50.8	46.9	26.9	18.7	83.8	32.7	71.7
	PostOp	-	-	38.2	52.1	49.0	48.6	46.8	47.4	-	-
T9SPi (°)	PreOp	-6.2	-13.2	-11.6	-14.8	-7.6	-10.1	-8.8	-18.7	-10.2	-16.5
	PostOp	-	-	-15.0	-19.7	-12.1	-18.1	-18.4	-12.8	-	-
T1SPi (°)	PreOp	-0.9	-6.6	-2.1	2.8	5.4	0.0	-0.1	-1.1	-1.7	1.5
	PostOp	-	-	-3.4	-6.0	1.7	-7.0	-9.6	-1.4	-	-
T1Slope (°)	PreOp	30.0	12.7	24.6	43.8	37.0	28.9	41.2	30.6	30.6	52.2
	PostOp	-	-	25.2	25.7	32.0	23.0	30.5	22.7	-	-
CL (°)	PreOp	31.3	8.6	2.0	36.3	51.5	37.3	33.8	10.4	5.7	25.7
	PostOp	-	-	0.5	19.9	14.4	9.0	12.6	8.4	-	-
C2-C7 SVA (mm)	PreOp	21.4	17.1	24.7	26.5	-3.6	-8.0	19.8	16.4	50.5	40.7
	PostOp	-	-	30.2	4.9	30.7	11.6	28.7	11.8	-	-
C7-S1 SVA (mm)	PreOp	59.0	-21.6	46.0	127.4	122.9	80.7	94.4	6.6	75.3	81.7
	PostOp	-	-	46.9	20.6	99.7	15.6	-25.1	3.9	-	-
GT (°)	PreOp	26.4	17.2	26.0	51.7	37.2	33.9	41.1	-3.5	33.8	31.3
	PostOp	-	-	30.2	28.5	31.6	28.0	14.5	-0.9	-	-
GAP Score	PreOp	7	8	11	12	11	12	13	4	12	6
	PostOp	-	-	11	11	10	8	3	3	-	-

Chapter 3: Multi-Segment Spine Motion of Patients before and following Posterior Spine Fusion

Table 15 Spinopelvic Parameters to evaluate spine alignment pre- and post-surgery in Short Fusion Patients

		Short Fusion Patients																			
Spinopelvic Parameter	Time of Measurement	SFP1	SFP2	SfP3	SFP4	SFP5	SFP6	SFP7	SFP8	SFP9	SFP10	SFP11	SFP12	SFP13	SFP14	SFP15	SFP16	SFP17	SFP18	SFP19	SFP20
PT (°)	PreOp	8.3	3.8	15.5	27.7	35.4	10.4	25.8	-	16.6	8.7	6.0	24.5	-	15.6	12.9	13.9	19.5	-	24.8	16.9
	PostOp	18.6	7.1	16.2	21.3	25.4	4.4	26.7	-	11.9	11.6	5.4	-	15.2	9.6	-	13.5	21.0	8.6	24.7	-
PI (°)	PreOp	50.5	52.0	54.9	66.5	77.0	46.5	86.6	-	53.6	49.8	41.4	81.4	-	49.7	55.5	42.6	64.3	-	82.4	63.6
	PostOp	51.5	50.9	56.0	66.3	77.2	46.0	85.6	-	53.6	50.5	41.5	-	42.6	49.4	-	41.6	65.9	45.6	82.1	-
SS (°)	PreOp	42.1	48.2	39.4	38.8	41.7	36.1	60.8	-	37.0	41.0	35.4	56.8	-	34.2	42.6	28.7	44.8	-	57.6	46.6
	PostOp	32.9	43.8	39.8	45.0	51.8	41.6	58.9	-	41.7	38.9	36.0	-	27.5	39.9	-	28.0	45.0	37.0	57.4	-
LL (°)	PreOp	63.3	59.5	50.7	64.1	53.6	42.3	61.5	-	66.7	47.4	52.6	65.1	-	50.0	61.5	35.4	56.0	-	73.5	65.4
	PostOp	48.3	57.7	51.0	77.6	65.8	56.6	63.9	-	67.6	56.7	57.8	-	35.8	63.3	-	42.2	61.0	57.7	66.3	-
L4-S1	PreOp	45.7	42.2	34.4	28.7	19.5	30.3	29.2	-	35.3	34.6	30.5	21.4	-	29.7	43.6	16.0	30.2	-	41.4	33.6
	PostOp	47.6	37.2	41.8	44.7	35.6	33.6	31.3	-	39.7	44.8	34.3	-	25.0	42.2	-	19.1	33.5	31.2	29.7	-
PI-LL (°)	PreOp	-12.8	-7.5	4.2	2.4	23.5	4.2	25.0	-	-13.1	2.4	-11.2	16.3	-	-0.3	-5.9	7.1	8.3	-	9.0	-1.8
	PostOp	3.2	-6.8	5.0	-11.2	11.3	-10.7	21.8	-	-14.0	-6.2	-16.3	-	6.8	-13.9	-	-0.7	4.9	-12.2	15.8	-
TK (°)	PreOp	47.1	31.7	-	54.7	28.0	33.8	-	-	63.2	-	43.2	31.2	-	45.3	43.4	37.9	25.6	-	29.8	54.7
	PostOp	-	31.6	-	70.8	32.9	-	21.7	-	58.5	31.0	40.4	-	34.6	50.6	-	31.5	42.4	33.6	31.0	-
T9SPi (°)	PreOp	-11.3	-4.6	-	-15.3	-10.9	-4.5	-	-	-15.1	-	0.0	-1.9	-	-8.4	-11.3	-8.8	-7.9	-	-11.6	-10.3
	PostOp	-	-7.0	-	-18.6	-10.1	-	-4.7	-	-13.4	-11.3	-11.3	-	-8.4	-12.4	-	-11.9	-10.3	-11.4	-6.6	-
T1SPi (°)	PreOp	-2.8	-0.4	-	-6.8	-7.7	3.7	-	-	-3.1	-	-2.8	1.0	-	0.4	-2.9	-4.0	-3.7	-	11.6	-0.9
	PostOp	-	-3.1	-	-8.0	-6.2	-	-1.5	-	-3.2	-5.3	-6.2	-	-0.9	-4.2	-	-6.9	-4.0	-8.2	-1.3	-
T1Slope (°)	PreOp	35.4	32.3	-	30.9	15.1	26.2	-	-	48.2	-	31.8	34.0	-	30.3	20.3	29.2	22.1	-	19.9	32.3
	PostOp	-	22.5	-	32.6	19.4	-	17.0	-	39.0	16.4	19.4	-	29.2	26.9	-	27.1	33.5	13.7	28.3	-
CL (°)	PreOp	46.2	34.9	-	22.2	4.9	44.1	-	-	35.3	-	15.0	8.2	-	23.9	14.2	13.5	6.6	-	11.7	10.0
	PostOp	-	21.0	-	20.6	2.4	-	7.3	-	28.8	6.9	4.5	-	21.4	17.0	-	7.5	13.4	5.4	24.2	-
C2-C7 SVA (mm)	PreOp	9.4	3.3	-	25.3	17.8	-12.8	-	-	27.9	-	20.1	33.9	-	12.2	14.1	31.5	23.1	-	0.7	39.1
	PostOp	-	4.8	-	26.0	20.1	-	17.3	-	32.4	19.1	13.3	-	6.8	16.6	-	42.3	21.4	12.1	-1.1	-
C7-S1 SVA (mm)	PreOp	14.7	22.9	-	21.1	19.1	79.0	-	-	27.6	-	6.8	76.7	-	58.0	13.4	9.9	20.5	-	-4.8	47.2
	PostOp	-	2.2	-	-7.7	6.8	-	56.9	-	21.3	-14.1	2.2	-	49.7	-1.1	-	-23.2	24.0	-49.6	56.1	-
GT (°)	PreOp	8.5	5.7	-	29.2	36.0	18.1	-	-	16.9	-	5.7	32.1	-	21.3	12.2	13.1	20.2	-	22.6	20.7
	PostOp	-	6.3	-	18.4	25.3	-	32.1	-	12.2	8.4	0.5	-	19.3	7.7	-	9.5	22.1	2.1	29.5	-
GAP Score	PreOp	0	1	-	5	7	4	-	-	0	-	0	2	-	1	1	3	0	-	0	0
	PostOp	-	0	-	1	0	-	2	-	0	0	0	-	3	0	-	2	0	0	1	-

Patient Cohorts Comparisons:

Before surgery the patient cohorts were seen to exhibit different ROM ranges. In particular, the median ROM of the joints defined was seen to be higher for the patients of the short fusion cohort during the ball pickup task. This increase was also seen for the segment/pelvis angles of the standing and sitting tasks. On the other hand, the shoulder/UT joint ROM was seen to remain the same for both cohorts during the STS tasks. More detail of the ROM median and 25th-75th percentile distributions could be seen in Figure 14.

In regard to the timing parameter which relates to the timing of the motion peak, no differences were seen between the cohorts and this could be seen in more detail in Figure 15.

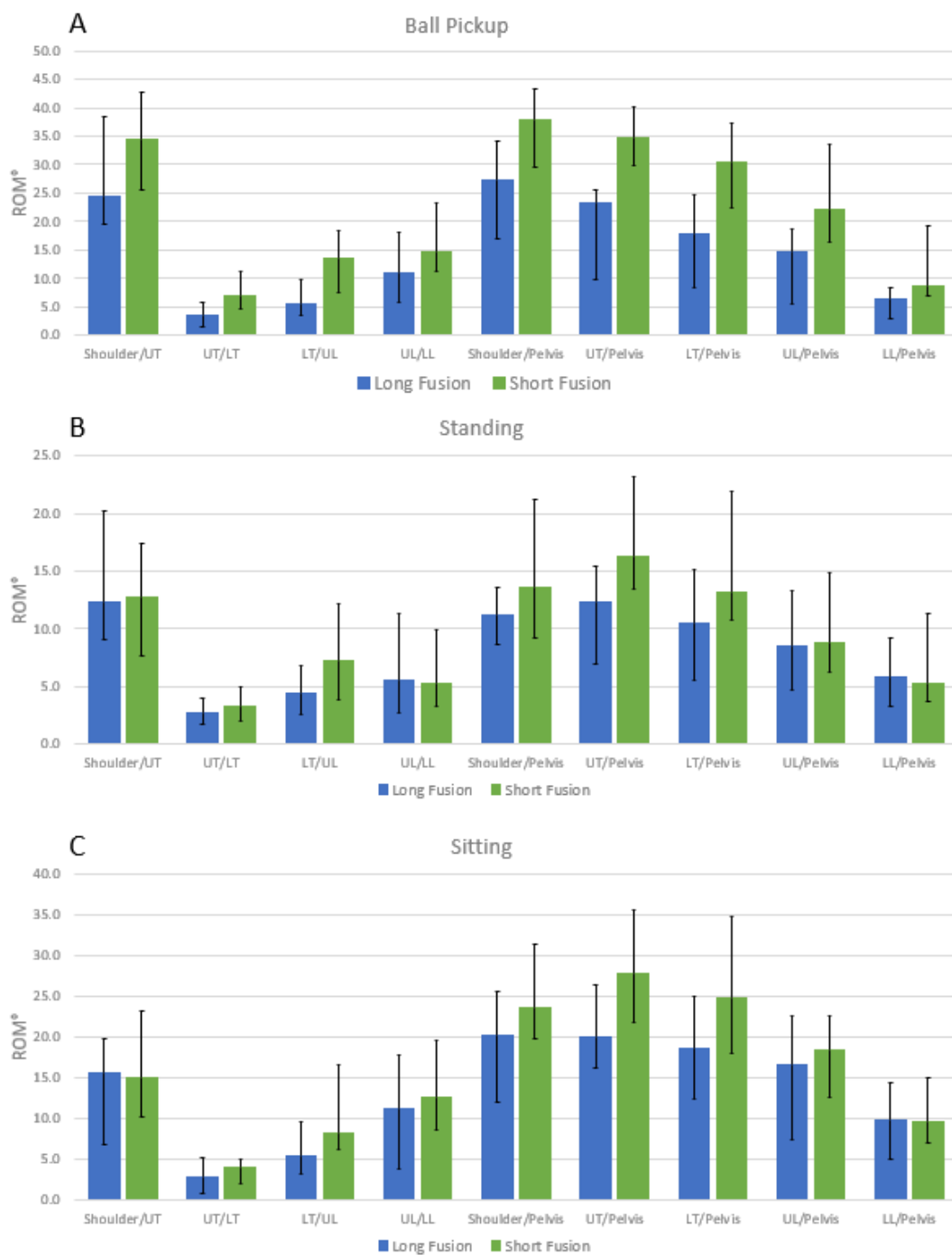


Figure 14 Differences in Ranges of motion between the two patient cohorts pre-surgery for all segments defined during Ball Pickup (A), Standing (B) and Sitting (C).

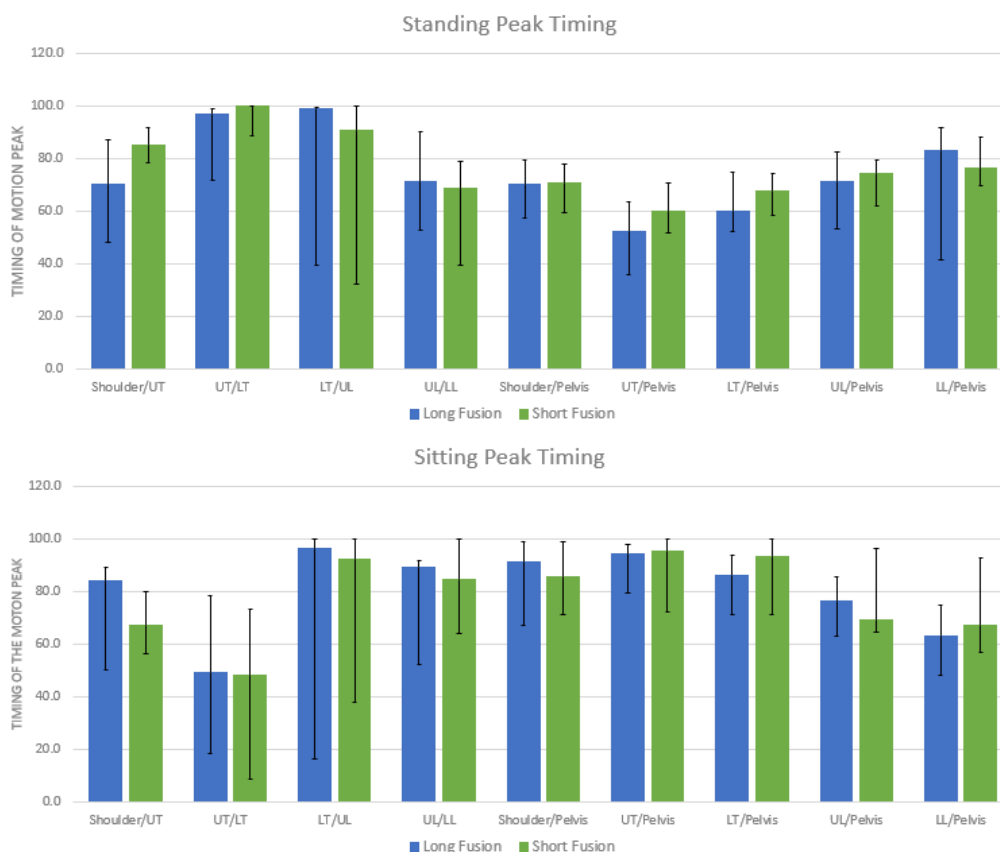


Figure 15 Peak motion timing values of the two patient cohorts pre-surgery for the standing and sitting tasks.

Before and After Surgery Comparison:

Long Fusion Cohort:

In terms of the individual changes pre-and post-surgery of the long cohort patients, the intersegmental angles of UT/LT, LT/UL and UL/LL saw the least change following surgery for all 8 participants with a mean difference less than 9°. In contrast, the angle of the Shoulder/UT exhibited higher degree differences pre-and post-surgery with a median decrease of 12° for the ball pickup motion. For the standing and sitting tasks, the difference was not as apparent where the shoulder/UT angle increased for some patients and decreased for others. Nonetheless, the difference for all patients was less than 4°. More detail on the ROMs of patients 4 and 7 in particular could be seen in Figure 16.

Looking in more detail at the changes in motion for the 10 patients of the long fusion cohort; two observations were recorded:

- The first for patients whose GAP score remained severely disproportionate (P3, P4, P5 and P6) (P4 in Figure 16). The shoulder/UT and Shoulder/Pelvis ROM decreased by 12° and 17° respectively during ball pickup while the ROM of these joints increased by a median of 5° during the sitting task. This same increase was seen during sitting for

the UL/LL joint. On the other hand, the UT/Pelvis, LT/Pelvis, UL/Pelvis and LL/Pelvis joints showcased an increase in ROM following surgery for all tasks.

- The second observation related to patients whose GAP score decreased significantly to become equivalent to a moderately disproportioned spine (P7 and P8) (P7 in Figure 16). For these patients the ROM of all joints was seen to overall decrease following the surgery for all tasks. Only an increase of 8° was seen for the Shoulder/UT joint during the sitting task post-surgery.

Looking at the timing parameter, the motion peak timing did not show significant differences pre- and post-surgery for the sitting and standing tasks. However, a median 10% decrease in the timing of the second motion peak was seen during ball pickup for all 8 participants.

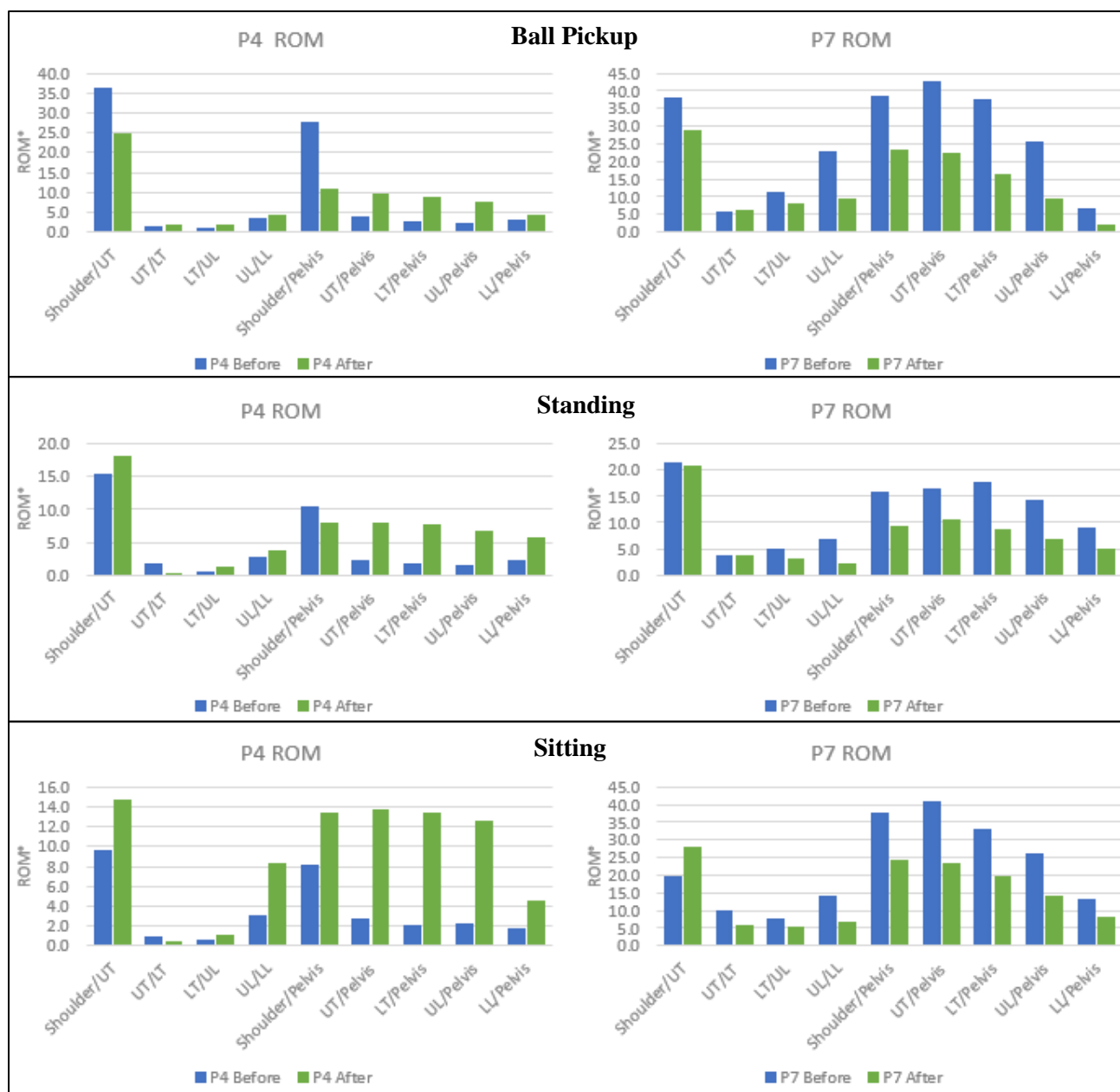


Figure 16 Changes in ROM before and after surgery for patients in the long fusion cohort for ball pickup, standing and sitting. (p=patient)

Short Fusion Cohort:

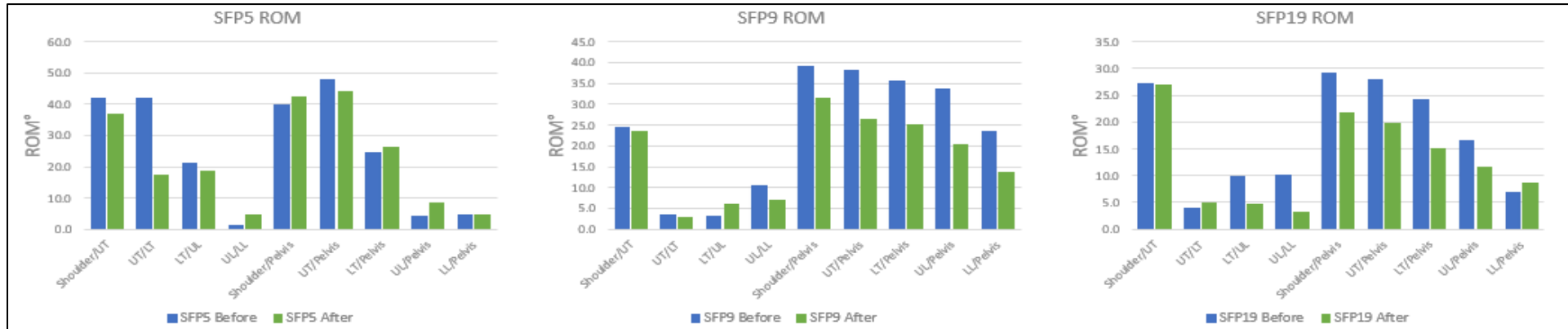
Looking at the angular parameters of the short fusion cohort, in particular the ROM values of the joints defined, different results were seen for the different tasks completed.

As to be expected, during ball pickup, a decrease in ROM was seen in patients for all joints defined. This difference was more apparent in some patients than others especially for patients with an initial GAP score less than 3 (such as Sfp9 and Sfp19 in Figure 17). These patients also showed a median decrease of 8.5° in the segment/pelvis joints post-surgery. In contrast, for patients with a GAP score more than 3, large differences in the ROM values were not apparent pre- and post-surgery (sfp5 in Figure 17).

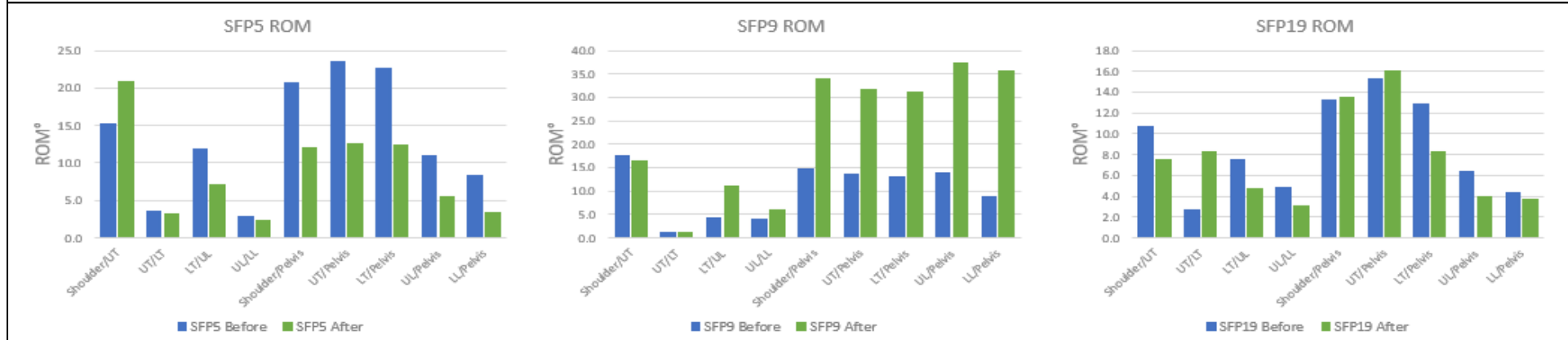
On the other hand, during the standing and sitting tasks, most patients showed a decrease in the ROM of the joints defined, especially at the level of the segment/pelvis joints. For more than 50% of the patients this difference was equal to 6° of decrease. In the case of 2 patients, the ROM of the segment/pelvis joints were seen to increase rather than decrease (such as Sfp9 in Figure 17).

Looking at the timed parameter, again no change in the peak timing of all patients of this cohort was recorded.

Ball Pickup



Standing



Sitting

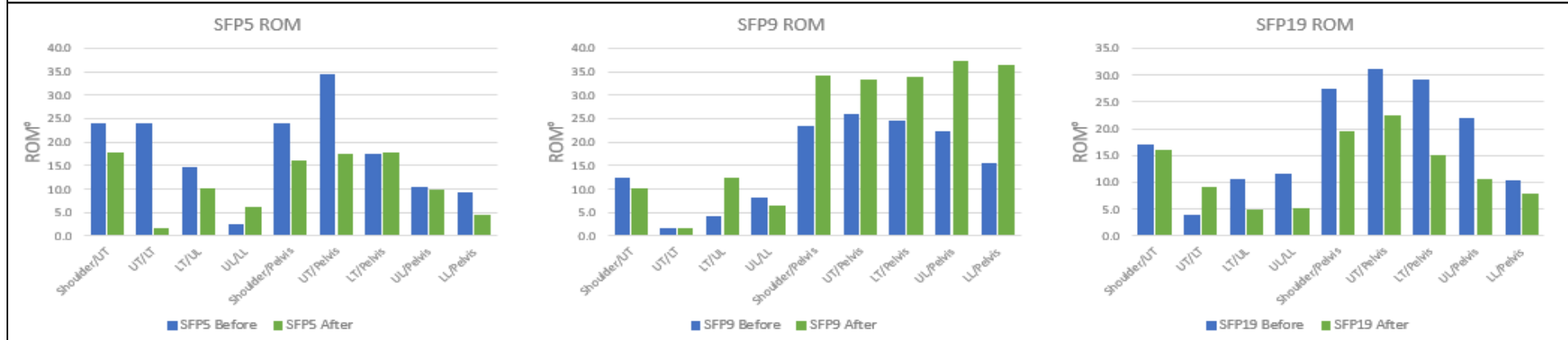


Figure 17 Changes in ROM before and after surgery for patients in the short fusion cohort for ball pickup, standing and sitting. (sfp=short fusion patient)

Healthy Participants and Patient cohorts' comparisons:

When comparing the angular parameters of the patient cohorts to those of the healthy, two consistent observations were recorded across all tasks.

- The UL/LL intersegmental angle was seen to have a decreased contribution to the motion for both cohorts.
- In contrast, the LL/pelvis segment was seen to exhibit an increased contribution to the motion during ball pickup and STS for both cohorts when compared to the healthy population.

Details of the contribution of each cohort before and after surgery can be found in Table 16.

Differences in the timing of the motion peak remained limited and were too small to be statistically compared.

Table 16 Percent Contributions of segments defined for both patient cohorts pre- and post-surgery and the control cohort for the three tasks completed.

Task	Segment	Percent Contribution						
		Participant Cohort						
		Healthy	All Patients		Long Fusion		Short Fusion	
Before	After		Before	After	Before	After		
Ball Pickup	Shoulder/UT	89	91.0	96.5	100.0	165.5	87	95
	UT/LT	10	18	21.5	15	20.5	20	21.5
	LT/UL	31	31	33.5	25	23.5	34.5	34
	UL/LL	48	40	34	45	41	37	32
	UT/Pelvis	90	97	94.5	92	91.5	98.5	95.5
	LT/Pelvis	90	82	77.5	79	78	82.5	77
	UL/Pelvis	59	64	55	58	55	66.5	55
Standing	LL/Pelvis	18	25	20	21	20	26	21
	Shoulder/UT	142	92	89	129	169.5	84.5	83
	UT/LT	23	22	23	20	26	24.5	23
	LT/UL	35	36	41	33	15.5	38.5	48
	UL/LL	44	37	36	44	36.5	34.5	36
	UT/Pelvis	107	113	113	109	113	114.5	113
	LT/Pelvis	95	104	100.5	99	108	104	100.5
Sitting	UL/Pelvis	65	76	84	84	99.5	73.5	82
	LL/Pelvis	38	48	64	50	74	44.5	48.5
	Shoulder/UT	76	68	65	84	87.5	63.5	64
	UT/LT	10	13	13	12	6.5	13	14.5
	LT/UL	19	35	30.5	21	13	36.5	42.5
	UL/LL	55	49	40	37	45	50	40
	UT/Pelvis	98	111	107	109	104	114	108
LT/Pelvis	97	106	99.5	91	104	106.5	99	
UL/Pelvis	81	80	75.5	73	93.5	81	71.5	
LL/Pelvis	32	40	38	42	37	39.5	38.5	

In terms of the distribution of the angle of motion across joints defined. Significant differences were seen in the sagittal plane between each individual patient and the healthy motion band distributions at the time at which peak motion is achieved. This agrees with the decrease in ROM that was seen in patient joint angles. Incidentally, significant changes were seen in the coronal and transverse angles pre- and post-surgery when compared to the healthy cohort. Post-surgery, all patients exhibited joint angle distributions within the angle distributions of the healthy population.

Discussion:

As the average life expectancy is increase due to advancements in healthcare ^{2,33}, we're seeing an increase in spine pathologies such as ASD ¹⁹, disc degeneration disease (DDD) ³⁴ and LBP ³⁵. Spine kinematics have been linked to the prevalence and recurrence of spine pathologies ^{20,21,88} hence it is of great interest to analyse spine motion in order to unravel parameters that lead to these pathologies. Through this study we aimed to assess spine kinematics of patients undergoing PSF surgeries of the spine using a comprehensive motion analysis protocol. First the kinematics of the pathological spine were described pre-surgery in two cohorts: long fusion and short fusion. Second the change in spine kinematics was assessed pre- and post-surgery for the 23 patients that returned for their assessment. Finally, the kinematics pre- and post-surgery of all the patients were compared to those of healthy participants.

To understand how the severity of the pathology affects the motion of the spine, we first looked at the ROM of the patients from the two cohorts before the surgery. Patients undergoing long fusion surgeries are those who have pathologies affecting more than one functional spine unit (FSU) ³⁹. To provide the patient with pain relief and re-establish sagittal alignment in the spine ³⁸, long PSF surgeries are required where more than 3 vertebral levels are fused together using transpedicular screws and rods. In contrast short PSF surgeries entail the fusion of 1-2 vertebral levels ³⁹. To assess if the extent of the spine pathology affected the spine kinematics of the patient pre-surgery, the angular and timed parameters defined in this study were compared between the two patient cohorts recruited. Patients in the long fusion cohort exhibited a decreased ROM for all joints defined, both intersegmental and segment/pelvis, except for the Shoulder/UT joint in STS and the LL/pelvis joint for all 3 tasks. Pain especially due to LBP plays a big role in this case to limit the motion of the painful FSU ³⁸. Back pain has been seen to significantly decrease the motion of the lumbar spine in particular in all motion directions ¹⁹⁶. In a study by Laird et al. ¹⁹⁷, lower ROM values were measured for patients with LBP in both thoracic and lumbar spine especially during flexion; this decrease was less apparent when

patients completed STS motions. Endo et al.¹⁹⁸ went on to elaborate that the ROM of the lumbar spine when returning from flexion is strongly affected by back pain and affecting also postural balance. Additionally, they found a link between the severity of the pain and the decreased ROM¹⁹⁸. In contrast in a study by Sullivan et al.¹⁹⁹, when comparing the ROM of different spine patient groups, no stronger impairment to the ROM was found due to pathology. However, if we were to look at studies relating to the fusion of the cervical spine, single level fusions do in fact affect the motion of the spine although multilevel fusion decreases the ROM by 7.8° per segment of fusion²⁰⁰. Besides pain, in patients with ASD, the deformity occurring in the spine also serves to limit the ROM of the lumbar spine in the sagittal plane²⁰¹. This notion is also supported in a study by Glavis et al.²⁰² who found that the deformation to the spine causes a decrease in mobility at the curve apex however, an increased mobility is seen above and below the apex of deformation. The decrease in ROM seen in this study especially in the long fusion cohort agrees with previous studies when considering the effect of pain and deformity on the motion of these patients^{198,201}. To understand the similarity in ROM of the LL/pelvis between the two cohorts, we need to understand the motion abilities of the L4-L5 FSU and the L5-S1 FSU. In a study by Basques et al.²⁰³, the L4-L5 FSU is found to be a hypermobile joint that compensates for the motion loss in the upper lumbar segment, while, the L5-S1 joint exhibits high translational motion which could explain the limited effect of pathological severity on the ROM of the LL/pelvis joint.

When assessing the changes to spine kinematics pre- and post-surgery in the two cohorts defined, overall, we saw a decrease in ROM due to the fusion of vertebral levels. However, the extent of this decrease differed between the two cohorts and within cohorts themselves. Looking first at the long fusion cohort, limited ROM differences was seen in the intersegmental angles from UT to LL pre- and post-surgery. This is to be expected because when looking at the thoracic spine in particular, we find that the ROM in the UT and LT segments are smaller than the rest of the spine due to the decreased disc height and the rib cage²⁰⁴. For the patients with a GAP score still equivalent to a severe disproportion, we saw an increase in the UT/Pelvis, LT/Pelvis, UL/Pelvis and LL/Pelvis. This finding agrees with the findings of Kuwahara et al.⁸⁹ who found that patients exhibited an increase in the max ROM of the lumbar spine post-surgery during the stance phase of gait. Looking into more detail on the reasons for this ROM increase even though the spine has been fused, we need to understand the effect back pain and spine deformity had on the initial motion of the spine. Shum et al.²⁰⁵ found a significant decrease in lumbar spine mobility in severe back pain patients who use different compensation techniques to achieve motion tasks. One of these compensation techniques was

seen this long fusion cohort where the Shoulder/UT segment contributed increasingly to the ball pickup motion of the spine pre-surgery. For patients with a moderate spine disproportion following surgery, we saw a decrease in ROM for all joints and tasks which is a finding that agrees with the Konz et al.⁹⁸ study who found a decrease in ROM for all spine segments. This connection between post-surgery GAP score and ROM values was also found in the short fusion cohort. For ball pickup, post-surgery proportioned spines showed a decrease of ROM for all joints; the contrary was seen for patients with moderately disproportioned spines. On the other hand, for the STS task, the change in ROM for joints was not consistent for all participants. This inconsistency could be explained by understanding the sporadic motion related to a diseased spine where the increases and decreases in ROM depends on the individual case²⁰⁶. Additionally, the mechanical stiffness of a degenerated disc contributes to the change in spine kinematics²⁰⁷. In a study by Widmer et al.²⁰⁷, two different flexion-patterns were seen in patients; one presented as a decrease in ROM especially when disc degeneration is in an advanced stage while the second showed an initial increase in ROM during flexion to then decrease as the motion progressed due to the overcompensation mechanism of the spine.

The final comparison carried out in this study related to the changes between the healthy control population and the patients recruited. In the case of this assessment, we tried to carry out the comparison without dividing the patient cohort into two groups to check if this separation correctly conveyed the distinct spine kinematics of each group. Two common observations were seen for all patients before and after surgery when compared to the control cohort. First, the UL/LL joint contributed less to the motion of patients to that of the control. On the contrary the LL/Pelvis joint contributed more to the motion of patients when compared to the control group. These findings are supported by the fact that greater disturbances to spine kinematics are seen when the lumbar spine segments are involved causing changes to the lumbar ROM²⁰³. Additionally, the decrease in motion in the UL/LL motion is again attributed to the hypermobility of the L4-L5 segment when compared to the motion of the L2-L3 segments^{203,208}. Beyond the differences in motion contributions, when assessing the angle distributions of each joint and comparing the patient angles to those of the healthy cohort, two consistent significant differences were found. The first related to the sagittal plane, where a significant decrease in the angle distribution was found for patients pre- and post-surgery when peak motion is achieved. This difference agrees with the decrease in ROM seen in patients that remained pre- and post-surgery. The second significant difference was found in the coronal and transverse planes, wherein the angle distribution of the patients decreased in magnitude post-surgery to be within the range the healthy cohort exhibits. This incidental finding agrees

with various studies in the literature. Symptomatic spine patients have been found to have an increased axial rotation especially in the lower lumbar levels ²⁰³. In a study by Patel et al. ¹⁰⁶, a significant decrease in thoracic rotation was seen in patients following spine surgery to match the values reported by the healthy population.

There are limitations to consider when interpreting the findings of this study. The first concerns the sample size, seeing that only 10 patients were included in the long fusion cohort and only 8 returned to their post-surgery measurement. Second, due to patients getting measured a day before surgery, a large number did not have a full standing x-ray of their spine which affected the measurement of the GAP score. Third, although the patients were differentiated into a long fusion and a short fusion cohort, they were not categorized based on their pathology which could have provided us with more accurate values and a better cohort analysis. Finally, although the marker setup developed aimed to be readily used in a clinical setting, it is still more applicable to healthy subjects as patients with spine deformity would have differing anatomical landmarks ²⁰⁹ and as such a marker based approach that is more individual to the patient would help in identifying the changes to motion around the deformity.

Conclusion:

In conclusion, this study focused on quantifying the motion of the spine in patients undergoing posterior spine fusion pre- and post-surgery, in addition to a control cohort. The patients recruited were divided into the long fusion and the short fusion cohorts. Radiographic evaluation of patient x-rays showed an improvement in spine alignment for all patients. Patients in the long fusion cohort showed a greater decrease in spine ROM when compared to the short fusion cohort pre-surgery. Post-surgery, intersegmental joints showcased a limited change in ROM while segment/pelvis joints showed a decreased ROM except for patients with severely disproportionate GAP scores who had sporadic changes to their ROMs post-surgery. For all patients, the UL/LL segment was seen to contribute less to the overall motion of the spine pre- and post-surgery when compared to the control group. The LL/Pelvis segment showed an increase in contribution in patients compared to the control group. Following surgery, patients showed a significant decrease in coronal and transverse plane motion to become within the motion patterns exhibited by the control group.

Chapter 4: The use of 3D virtual and printed models to plan deformity correction surgeries

From the journal paper:

Fayad J, Turbucz M, Hajnal B, Bereczki F, Bartos M, Bank A, Lazary A and Eltes PE, *Complicated Postoperative Flat Back Deformity Correction with the Aid of Virtual and 3D Printed Anatomical Models: Case Report*. Front. Surg. 2021. doi: 10.3389/fsurg.2021.662919

Abstract

Introduction: The number of patients with iatrogenic spinal deformities is increasing due to the increase in instrumented spinal surgeries globally. Correcting a deformity could be challenging due to the complex anatomical and geometrical irregularities caused by previous surgeries and spine degeneration. Virtual and 3D printed models have the potential to illuminate the unique and complex anatomical-geometrical problems found in these patients.

Case Presentation: We present a case report with a 6-months follow-up (FU) of a 71-year-old female patient with severe sagittal and coronal malalignment due to repetitive discectomy, decompression, laminectomy, and stabilization surgeries over the last 39 years. The patient suffered from severe low back pain (VAS = 9, ODI = 80). Deformity correction by performing asymmetric 3-column pedicle subtraction osteotomy (PSO) and stabilization was decided as the required surgical treatment. To better understand the complex anatomical condition, a patient-specific virtual geometry was defined by segmentation based on the preoperative CT. The geometrical accuracy was tested using the Dice Similarity Index (DSI). A complex 3D virtual plan was created for the surgery from the segmented geometry in addition to 3D printed model.

Discussion: The segmentation process provided a highly accurate geometry (L1 to S2) with a DSI value of 0.92. The virtual model was shared in the internal clinical database in 3DPDF format. The printed physical model was used in the preoperative planning phase, patient education/communication and during the surgery. The surgery was performed successfully, and no complications were registered. The measured change in the sagittal vertical axis was 7 cm, in the coronal plane, the distance between the C7 plumb line and the central sacral vertical

line was reduced by 4 cm. A 30° degree correction was achieved for the lumbar lordosis due to the PSO at the L4 vertebra. The patient ODI was reduced to 20 points at the 6-months FU.

Conclusions: The printed physical model was considered advantageous by the surgical team in the pre-surgical phase and during the surgery as well. The model was able to simplify the geometrical problems and potentially improve the outcome of the surgery by preventing complications and reducing surgical time.

Introduction:

As the number of instrumented spinal operations increases globally, the group of patients with iatrogenic spinal deformities is growing¹⁹. Loss of lordosis, development of segmental or global kyphosis after a shorter or longer thoracolumbar stabilization are the most common form of iatrogenic (so-called “flat back”) deformities²⁷. Beyond the consequent spinal canal stenosis, the disturbance of global balance can result in severe disability and pain where only surgical correction of the spinal alignment can provide significant functional improvement²⁷. The common sagittal balance problem in some cases is complicated by coronal imbalance, making the surgical correction procedure more complex. Further anatomical and geometrical irregularities caused by the previous surgeries (e.g., lack of anatomical landmarks, segmental bony deformations) makes the situation more challenging. In such cases, meticulous preoperative planning and proper implementation of the surgical plan are the keys to success and advanced scientific tools are needed to support the process and improve the outcome.

Here, we present the case of an elderly female patient with severe sagittal and coronal malalignment due to repetitive spine surgical interventions for over 39 years. Virtual and 3D printed patient-specific models were used to understand the unique and complex anatomical-geometrical problem and to plan the proper surgical correction.

Case Presentation:

Medical history

A 71-year-old female patient was admitted to our institution. She suffered from severe low back pain, irradiating to the left leg, and an inability to walk more than 50 m due to fatigue in both lower extremities. There were some significant, treated comorbidities in her medical history: chronic hypertension, non-insulin-dependent (type II) diabetes, and ischemic heart disease. Previously, the patient’s back problems were treated in other hospitals. The first discectomy surgery at the level of L4/S1 was performed 39 years ago, since then a mild L5 sensory-motor deficit persisted on the right side. 16 years later, an L4/5 discectomy was performed followed by an L3/4 discectomy a year later. A repeated discectomy was done at the L4/5 level 4 years ago, followed by a discectomy/decompression at the L2/3 level due to signs of cauda syndrome. The last surgical intervention in another hospital was done a year later (3 years ago) when an L2-L4 posterior stabilization and L3 laminectomy without intervertebral fusion was performed.

Evaluation and analysis

Physical examination showed severe sagittal and coronal imbalance, compromised gait, tenderness in the lower back area and spastic muscles. She suffered from mild distal motor weakness in both lower extremities and numbness of the left leg. Based on her examination and imaging studies (full spine X-ray, lumbar CT (Figure 21) and MRI (Figure 22)), severe lumbar sagittal and coronal malalignment was identified as the primary source of pain. Beside the deformity, non-union and partial implant loosening at the L2-L4 segment, and degenerative instability at the L1/2 and L3/4 segments were diagnosed. The patient's pain was assessed by the Visual Analogue Scale (VAS=9 preoperatively), and disability was measured using the Oswestry Disability Index (ODI=80% preoperatively) ²¹⁰. Surgical treatment was indicated considering the spinal pathology, severe pain, disability, and life quality deterioration.

Analysis of spinopelvic alignment in terms of surgical correction

Global balance and spinopelvic alignment were analysed to determine the objective of the correction. Parameters describing the spinopelvic alignment were calculated from standing x-ray using the Surgimap software (Nemaris Inc, New York, NY, USA). Pelvic incidence (PI), pelvic tilt (PT), sacral slope (SS), lumbar lordosis (LL) and thoracic kyphosis (TK) were measured ⁴⁹ (Figure 18). Global sagittal alignment parameters such as the sagittal vertical axis (SVA), T1 spino pelvic inclination (T1SPi), T9 spino pelvic inclination (T9SPi), and T1 pelvic angle (TPA) were also calculated ¹⁹⁴. The Global Alignment and Proportion (GAP) Score was calculated according to the method published by Yilgor et al ¹⁹⁵. The coronal alignment was assessed by measuring the distance between the centre of the C7 vertebral body and the central sacral vertical line (CSVL) ²¹¹. The measurements are summarized in Table 17.

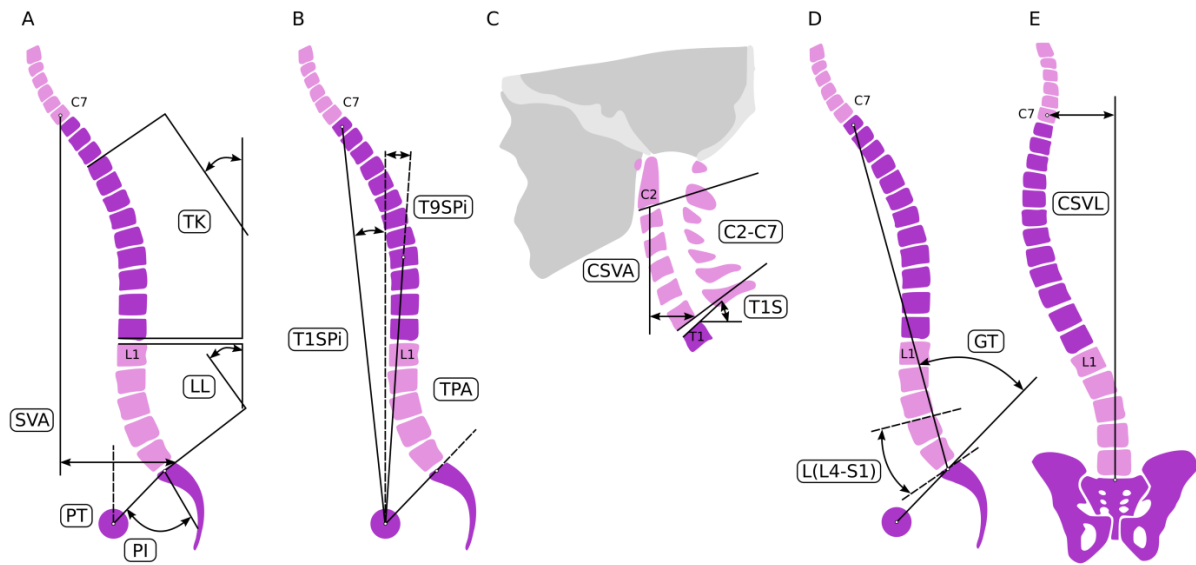


Figure 18 Spinal alignment evaluation. Sagittal spino-pelvic parameters (A, B, C) for the assessment of the alignment (A, B, C adopted from Lafage et al 2015); pelvic parameters measured were PI, PT, and SS. Regional spinal parameters included PI-LL mismatch, LL, and TK. Global alignment was assessed linearly by SVA and the angular measurements of T1SPl, T9SPl, and TPA. Cervical parameters were composed of T1 slope, C2–C7 cervical lordosis, and C2–C7 SVA. D for the GAP score L4-S1 lordosis L(L4-S1) and the global tilt (GT) were defined. E coronal alignment is assessed by measuring the distance between the centre of the C7 vertebral body and the CSVL.

The central origin of the patient’s complaint was the loss of lordosis at the lumbar spine due to the degenerative and iatrogenic processes. The patient’s global balance was characterized as an imbalance both in the sagittal and coronal planes. The GAP score was 8 preoperatively, corresponding to severely disproportioned alignment. Therefore, the aim of the surgical correction was the 3D correction of the lumbar alignment. To calculate the degree of the desired lordosis correction, different approaches were sequentially applied. First, we used the formula published by LeHuec et al²¹² to calculate the ideal lumbar lordosis (ILL) corresponding to the pelvic anatomy of the patient. According to their formula ($LL=0.54*PI+27.6^\circ$), the ILL was 57° . Second, the ILL was adjusted by the patient’s age to avoid overcorrection and to decrease surgical invasiveness^{49,213,214}. In the age group of 65–74-year-old, the threshold of spinopelvic alignment parameters to avoid significant disability ($ODI>40\%$) are $SVA=9\text{cm}$, $PI-LL=18^\circ$, $PT=26^\circ$. The threshold values for minimal disability ($ODI<20\%$) are $SVA=5\text{cm}$, $PI-LL=6^\circ$, $PT=23^\circ$. According to these data²¹⁴, target values of SVA between 5 and 9cm, PI-LL between $6-18^\circ$ and PT between $23-25^\circ$ were determined for the alignment correction. A LL between 37° and 49° corresponded to these parameters, therefore the desired total lordosis correction was 20 to 32° . Considering all of the surgical issues, and the optimal lordosis distribution, an L1/L2 and L3/L4 transforaminal lumbar interbody fusions (TLIF) and alignment correction by performing an asymmetric pedicle subtraction osteotomy (PSO) of about 20° at the LIV level

as well as stabilisation from Th9 to the iliac bone with posterior fusion was decided as the required surgical intervention to treat the patient.

Virtual and 3D printed models of the surgery

To better understand the complex, anatomical condition at the lower lumbar level, especially in the neuro foraminal and central spinal canal area, patient-specific virtual and physical models were created based on the pre-op CT (Figure 19). The CT data were exported from the hospital PACS in DICOM file format. To comply with the ethical approval and the patient data protection policies, anonymisation of the DICOM data was performed using Clinical Trial Processor software (CTP, RSNA, USA) ²¹⁵. The segmentation process was performed on the 2D CT images ²¹⁶. The thresholding algorithm and manual segmentation tools (erase, paint, fill etc.) were used in 3D Slicer 4.1.1 free software (Brigham and Women's Hospital, Boston, MA, USA) ²¹⁷, Figure 19.

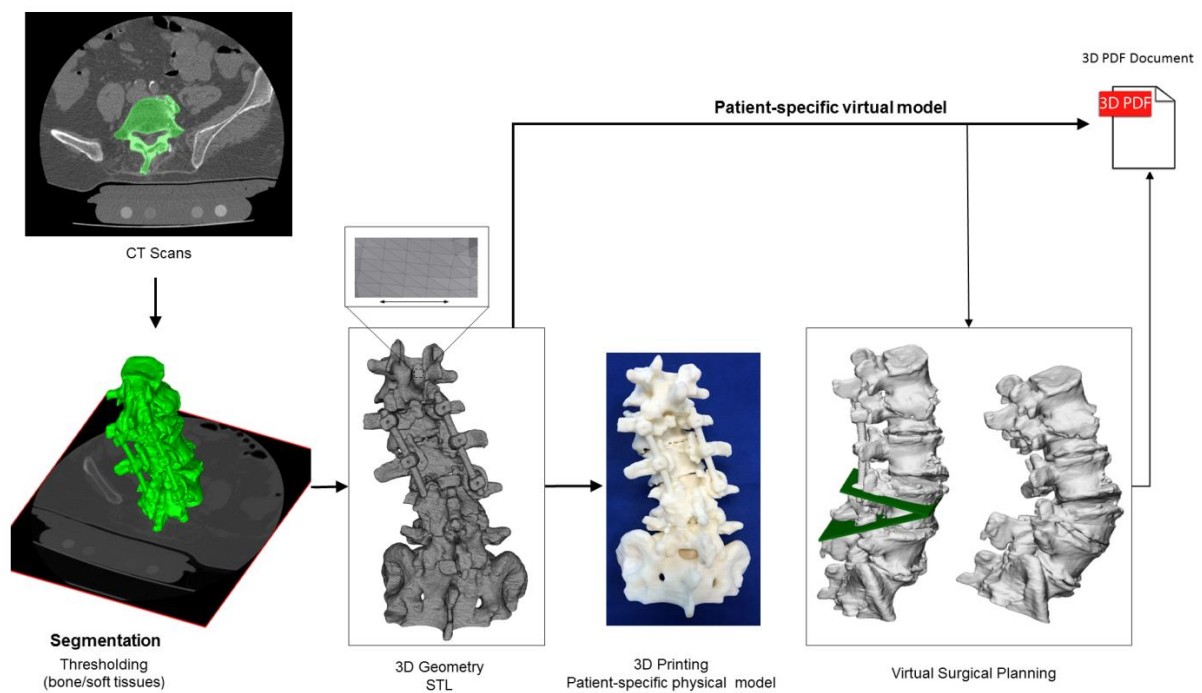


Figure 19 Definition of virtual 3D geometry from CT scan. During the segmentation process, the bone volume is first separated from the surrounding soft tissue by thresholding of the greyscale levels of the CT images. The resulting mask (green) voxels represent the 3D volume of the L1-S1 spine segment. Then, from the mask, a triangulated surface mesh is generated in STL format. The STL file serves as an input for 3D printing, with FDM technology. The virtual patient-specific geometry can be edited in CAD software to perform virtual surgical intervention (L4 PSO). The virtual geometries are then integrated into the clinical communication as a 3DPDF document.

To evaluate the accuracy of the segmentation process, the Dice Similarity Index (DSI) was calculated ²¹⁸, obtaining a value of 0.92 and thus providing a highly accurate geometry. Inspection and correction of the 3D geometry were performed with MeshLab1.3.2 free

software (CNR, Pisa, Italy) ²¹⁹ and universal remeshing with contour preservation was applied. The virtual geometry of the patient spine (triangulated surface mesh, STereoLithography (STL) format) was printed with a *Fused Deposition Modelling* (FDM) device (Dimension 1200es 3D Printer; Stratasys, Israel, / filament type: *ABSplus* in ivory, / scaffold: Soluble Support Technology, SST). In parallel to the printing process, a complex 3D virtual plan was created for the surgery in Autodesk Fusion 360 (Autodesk Inc., California, U.S.A.) Computer-Aided Design (CAD) software. First, the STL model was converted into a solid body, and then virtually we cut out from the L4 vertebra for an asymmetric 3-column pedicle subtraction osteotomy (PSO) with 20° correction in the sagittal plane. The virtual model and virtual surgical plan were imported in STL format to MeshLab1.3.2 and subsequently saved as a Universal 3D File (U3D). A 3D Portable Document Format (3DPDF) file, containing the U3D mesh, was created using Adobe Acrobat (version 10 Pro Extended) 3D tools with default activation settings. The 3D visualization parameters were set as follows: CAD optimized lights, white background, solid rendering style and default 3D conversion settings. The 3DPDF file was then incorporated in the institutional web browser-based SQL database (Oracle Database 12c) as previously described in the literature ²⁹. The document was accessible by clinicians from any institutional desktop PC or mobile device.

Surgical treatment and outcome

The surgery was successfully performed by the senior surgeon (AL) without any complications (OR time: 270 min, blood loss: 750 ml). The patient was discharged from the hospital in good condition, 4 days after surgery. Thirty degrees of lumbar lordosis correction was achieved, the majority at the L4-S1 level (17°) (Figure 20, Table 17). The measured change in the sagittal vertical axis (SVA) was 7cm. In the coronal plane, the C7 to CSVL distance was reduced by 4 cm. The GAP score decreased significantly from 8 to 3. ODI decreased at the 6-months FU to 20 points from 80, the VAS for the LBP decreased to 3 from 9 ²²⁰.

Table 17 Parameters for the evaluation of the spinal alignment pre and postoperatively.

PARAMETER	PREOP	POSTOP
PI (°)	55	55
PT (°)	27	21
SS (°)	28	34
LL (°)	17	47
PI-LL (°)	38	8
TL (°)	2	5

TK (°)	16	30
T9SPI (°)	0	6
T1SPI (°)	7	1
TPA (°)	34	22
T1S (°)	41	31
CL (°)	39	32
GT	12	28
L(L4-S1)	14	31
C2-C7 SVA (MM)	12	20
SVA C7-S1 (MM)	156	82
C7 TO CSVL DISTANCE (MM)	48	5
GAP SCORE	8	3

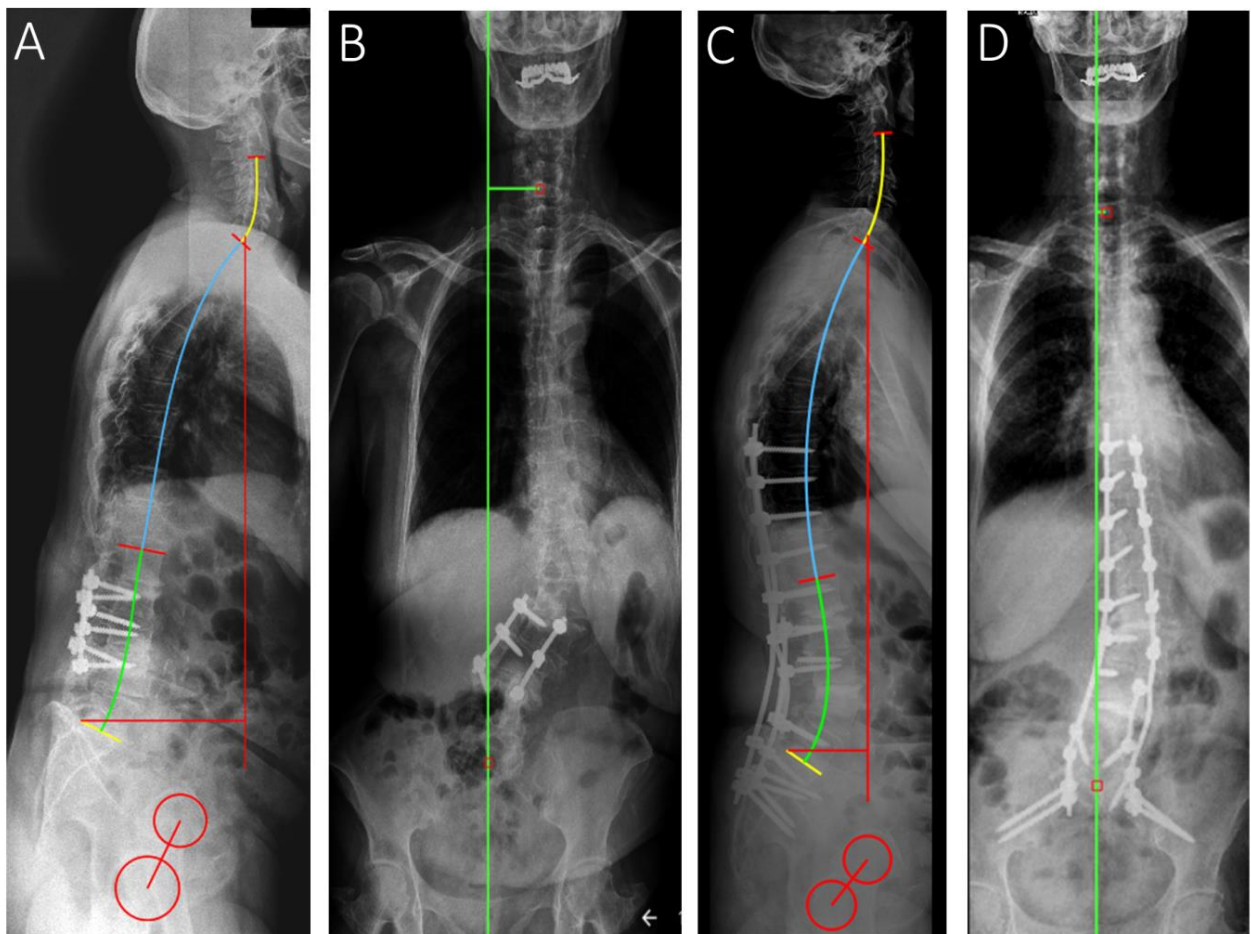


Figure 20 Standing x-rays for spinal alignment evaluation Preoperative (A, B) and postoperative (C, D) standing x-rays for sagittal (A, C) and coronal (B, D) spinal alignment evaluation, using the Surgimap software sagittal alignment tools. In the sagittal plane, the SVA was reduced by 7.4 cm compared to the preoperative x-rays due to the Th9-Ileum fixation, correction with the L3-L4 intervertebral fusion (TLIF) and the 3-column osteotomy at the L4 level. The coronal alignment was corrected by reducing the distance between C7 to CSVL from 4.8 cm pre-op (B) to 0.5 cm post-op (D).

Discussion:

Clinical studies about the benefits of new visualization and 3D printing techniques are still very rare worldwide ¹⁶². Patient-specific tangible, 3D printed physical models can improve surgical performance and outcome compared to the sole on-screen inspection of the virtual models ²²¹. 3D printed physical models through haptic perception improve understanding of 3D shapes compared to visual perception only ²²²⁻²²⁴. In a survey-based study among the members of AOSpine ²²⁵, a high interest among spine surgeons in the incorporation of 3D technologies (virtual or 3D printed models) into clinical practice was recorded. The Radiological Society of North America (RSNA) 3D printing Special Interest Group (SIG) published ²²⁶ guidelines for medical 3D printing and appropriateness for clinical scenarios. The recommended scenarios do not include the iatrogenic adolescent spinal deformity, although this case demonstrates the benefits.

In a recent systematic review ⁵² by Lopez et. al., in adult spinal deformity, the usage of 3D printing in preoperative planning and the manufacturing of surgical guides are associated with increased screw accuracy and favourable deformity correction outcomes. In our study, the physical model not only guided the preoperative planning phase but also aided the surgeon in understanding the complex anatomy during the surgery.

It is challenging in the surgical management of adult spinal deformity to determine the degree of planned correction, particularly in patients with severe preoperative malalignment. Less aggressive correction may constitute a reasonable compromise between radiographic alignment goals and perioperative and postoperative risk ²¹³. The Surgimap software allowed the measurement of pre-and postoperative x-rays with ease and speed, providing a vast array of opportunities for assessment of spinal deformity and surgical planning. The aid of 3D virtual, printed models and x-ray-based planning software allowed us to achieve a LL of 47° after the surgery providing the restoration of global balance shown by the improvement of GAP score. The well-planned, surgical correction of the lumbar alignment provided the restoration of the global spino-pelvic balance resulting in the reduction in pain and disability as well as improvement in health-related quality of life. The improved global parameter (GAP score of 3) corresponds to a moderately disproportioned alignment, with a low chance for postoperative mechanical complication ¹⁹⁵.

The limitation of the described approach is that currently, it is uncommon for medical centres to have access to a 3D printing facility or lack the know-how for image processing needed for

model preparation. The time needed for the presented visualisation, printing, and planning is also a limitation as it is not always available before surgery.

Conclusion:

A patient-specific 3D virtual and printed physical geometry, as well as computer-aided surgical planning, were used to develop the optimal surgical plan for the deformity correction in a complicated iatrogenic adult spinel deformity case. The surgery was successfully implemented providing the planned correction of the lumbar alignment. The printed physical model was considered advantageous by the surgical team in the pre-surgical phase and during the surgery as well. The chosen FDM technology provided an accurate, robust, and affordable physical model. The model not only clarifies the geometrical problems but can also improve the outcome of the surgery by preventing complications and reducing surgical time.

Supplementary Materials

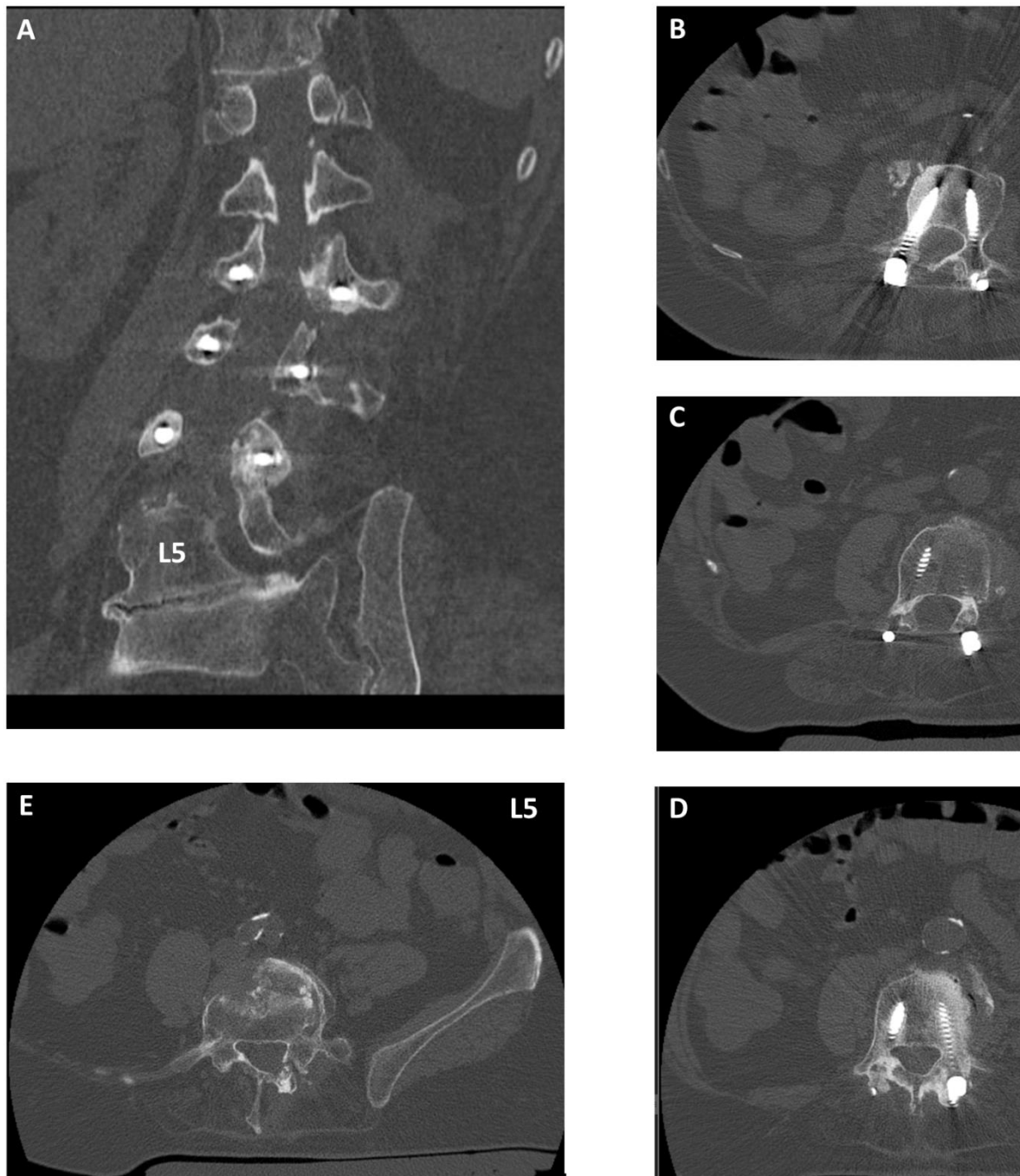


Figure 21 Supplementary Figure 1

Supplementary Figure 1. Preoperative computed tomography (CT) images of the lumbar spine.

A coronal CT scan image at the pedicle level (L2, L3, L4), L5 vertebral body is marked as a landmark. B Axial CT scan image at the L2 pedicle. C axial CT scan image at the L3 pedicle. D axial CT scan image at the L4 pedicle. E axial CT scan image at the L5 pedicle



Figure 22 Supplementary Figure 2

Supplementary Figure 2. Preoperative magnetic resonance imaging (MRI) of the lumbar spine.

A sagittal MRI scan image at the pedicle level (L2, L3, L4), L5 vertebral body is marked as a landmark. B axial MRI scan image at the L2 pedicle. C axial MRI scan image at the L3 pedicle. D axial MRI scan image at the L4 pedicle. E axial MRI scan image at the L5 pedicle

Chapter 5: The effect of PEEK rods on the biomechanics of proximal junctional kyphosis

This chapter is part of the manuscript:

Mate Turbucz, MSc*, Jennifer Fayad, MSc*, Agoston J. Pokorni, MSc, Peter E. Eltes, MD, PhD, Aron Lazary, MD, PhD. *Biomechanical comparison of rigid and semi-rigid fixation techniques for the assessment of proximal junctional kyphosis - a finite element study* to be submitted to the *Journal of Neurosurgery: Spine*

Abstract:

Introduction: Proximal junctional kyphosis (PJK) is a common complication seen following posterior spine fusion. Various risk factors have been associated with PJK. One of these is a biomechanical risk factor linked to the sudden change in rigidity between the spine and implant. Currently different biomechanical considerations are being assessed to decrease the rigidity of the instrumentation. The purpose of this study was to assess the effect of using polyetheretherketone (PEEK) auxiliary rods in spine fusion on the onset of PJK.

Methods: Three T7-L5 finite element (FE) models were developed: 1) intact spine; 2) fused spine from T8 to L5 referred to as RIGID; 3) PEEK rods from T8 to L5 combined with posterior fusion from T9 to L5. A modified protocol was developed to investigate the effect of the instrumentation on 4 motion tasks: flexion, extension, lateral bending, and axial rotation. The protocol applied a pure bending moment of 5 Nm to measure the intervertebral rotation (IVR) angles. A displacement load was then applied to the two instrumented FE models, where the pedicle screw load and stress distribution at the upper instrumented vertebra (UIV) were compared.

Results: PEEK exhibited higher IVR values than the RIGID model at the UIV for the 4 motion tasks. Looking at the stresses in the screw, RIGID gave the largest values at the UIV level while PEEK reduced the stresses by 27.7%, 36.6%, 34.2% and 59.8% for flexion, extension, lateral bending, and axial rotation. Looking at the stress distribution in the UIV, RIGID again exhibited the highest stress patterns for all motions.

Conclusions: The PEEK fixation technique increased the mobility of the UIV and provided a less rigid transition in IVR values between the UIV and the proximal spine segment. This

semi-rigid fixation led to a decrease in screw loads and in the stresses at the UIV which could help in decreasing the prevalence of PJK. Additional research on the fixation levels and material properties of the auxiliary rods is however needed for this semi-rigid fixation to be of clinical benefit.

Introduction

Adult spinal deformities (ASD) are becoming increasingly prevalent in today's ageing society^{2,3}. Proximal junctional kyphosis (PJK) is a complication seen in ASD patients following posterior spine fusion^{2,10,11}, the prevalence rates are quite high ranging between 5% and 40%¹². PJK is a slow-developing symptom showing a forward bending occurring at the uppermost instrumented vertebrae (UIV)^{2,12-14}. A majority of patients affected by PJK are asymptomatic with some experts debating that it is a simple radiographic diagnosis with no clinical impact^{14,48}. Nevertheless, evidence exists to suggest PJK can significantly impact clinical outcomes resulting in pain, neurological deficits, progressive sagittal plane deformities and a need for revision surgery^{11,14,48}. PJK most commonly develops in ASD patients within three months following surgery, with 80% of affected patients developing it within 18 months of surgery¹².

Various risk factors have been associated with the development of PJK⁴⁷. Older age, high body mass index, decrease in bone mineral density, overcorrection of sagittal alignment and fusion to the sacrum have all been reported as risk factors for PJK^{13,14,48}. Conflicting evidence exists to suggest that the choice of UIV and the number of vertebrae fused influence the prevalence of PJK^{13,48}. The aetiology of PJK is complex^{2,48}, suggested failure mechanisms include altered biomechanics of the spine due to the change in rigidity between the UIV and the cranial spine segments^{9,14}, recurrence of the deformity due to the process of natural ageing in ASD patients⁴⁸, surgical disruption to the spinal muscles and ligaments at the UIV level^{9,13,48}.

Different biomechanical considerations have been assessed in the literature to reduce the overall rigidity of the instrumentation used^{14,176}. Metal rods used for spine fusion exhibit high stiffness creating a mismatch between the spine and the instrumentation, a locality of high-stress concentration at the level of the UIV and redistributing the motion of the spine¹⁷⁶. More flexible instrumentations have been investigated using multiple rods, hooks, elastic tethers and polyetheretherketone (PEEK) rods^{14,176}. PEEK rods have an elastic modulus between that of cancellous and cortical bone and exhibit smaller bending stiffness properties when compared to metal rods thus resembling the physiological environment of the spine^{176,177}.

The purpose of this study was to evaluate the effect of using PEEK rods on the intervertebral rotation, pedicle screw loads, and stress distribution at the UIV using finite element models of

an intact and fused spine, to ultimately assess the changes in biomechanical properties leading to the onset of PJK.

Materials and Methods

Intact T7-L5 Model:

The FE model of the T7-L5 spine was developed by segmenting CT scans of a healthy 24-year-old male adult including the vertebral bodies and intervertebral discs in Materialise Mimics (Mimics Research, Mimics Innovation Suite v23.0, Materialize, Leuven, Belgium). The geometries created were imported into Materialise 3Matic (Mimics Research, Mimics Innovation Suite v21.0, Materialize, Leuven, Belgium) to create the surface meshes and define the various segments of the vertebrae and intervertebral disc. The thoracic spine segment (T7-T12) and the lumbar spine segment (L1-L5) were registered to the same coordinate system using rigid surface registration to create the T7-L5 overall model (Figure 23).

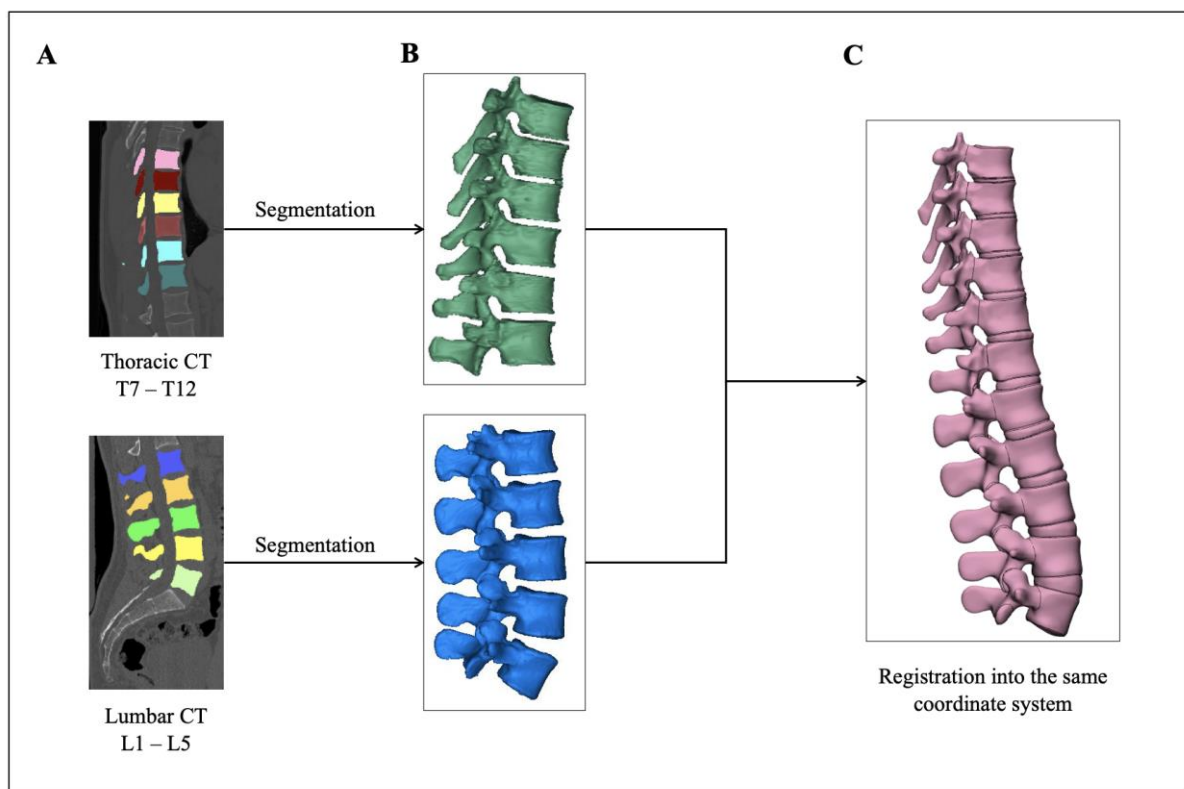


Figure 23 T7-L5 Modelling steps

(A) Segmentation of the thoracic and lumbar spines. (B) 3D models of the thoracic and lumbar spines. (C) Overall T7-L5 intact model is registered in the same coordinate system.

In Materialise 3Matic (Mimics Research, Mimics Innovation Suite v21.0, Materialize, Leuven, Belgium) each vertebra was divided into the cortical shell, trabecular core, vertebral endplates and the posterior elements^{227,228}. The facet joints between the posterior bony elements of the

vertebrae were modelled with a 0.5mm gap between the opposing joints. Facet joints were modelled following a Neo Hooke hyperelastic mode ^{229,230}. Following this step, the final geometry of the intact model was further developed in HyperWorks (Altair Engineering, Inc., Troy, Michigan, United States). The intervertebral discs (IVD) included the nucleus pulposus, the annulus fibrosis (AF) and the cartilaginous endplate ²³¹. The AF was made up of the ground substance (GS) and fibres. The AF fibres were modelled as two-node truss elements at alternating 30°/150° with the horizontal. The nucleus pulposus made up 45% of the IVD and was positioned more posteriorly ^{232,233}. The nucleus pulposus and annulus ground substance were modelled following a Mooney-Rivlin hyperelastic model. The spine ligaments were also created in HyperWorks (Altair Engineering, Inc., Troy, Michigan, United States) and these were: anterior longitudinal ligament (ALL), posterior longitudinal ligament (PLL), Ligamentum Flavum (FL), Capsular ligaments (CL), Intratransverse ligament (ITL), Intraspinous ligament (ISL) and the Supraspinous ligament (SSL). The material properties of all the defined elements were modelled using prior published studies (Table 18). The developed model was then exported to ABAQUS (Simulia Corp., USA) for further analysis.

Table 18 Components, element types and material properties of the developed model

Component	Young's Modulus	Poisson Ratio	Element Type	Reference
Trabecular Bone	100	0.2	C3D4	Shirazi-Adl et al., 1986 ²³⁴
Cortical Bone	10,000	0.3	C3D4	Rohlmann et al., 2006b ²³⁵
Posterior Elements	3,500	0.25	C3D4	Shirazi-Adl et al., 1986 ²³⁴
Vertebral Endplate	1,200	0.29	C3D4	Li et al., 2015 ²³⁶
Facet Joint	2 material parameters C10=5.36 and D1=0.04		C3D6	Finley et al., 2018 ²³⁷
Nucleus Pulposus	3 material parameters C10=0.12 and C01=0.03		C3D8H	Schmidt et al., 2007 ²³⁸
Annulus Fibrosis ground substance	Lumbar: 2 material parameters C10= 0.18 and C01=0.045		C3D8H	Schmidt et al., 2006 ²³⁹ Schmidt et al., 2007 ²³⁸
	Thoracolumbar: calibrated stress-strain relationship			
Annulus Fibrosis Fibres	Lumbar: weighted non-linear stress-strain relationship		T3D2	Shirazi-Adl et al., 1986 ²³⁴ Schmidt et al.,
	Thoracolumbar: calibrated stress-strain relationship			

				2006 ²³⁹ Lu et al. 2013 ²⁴⁰
Cartilaginous endplate	23.8	0.42	C3D6, C3D8	Finley et al., 2018 ²³⁷
Ligaments	Nonlinear stress-strain relationship		SPRINGA	Rohlmann et al., 2006a ²⁴¹
Titanium Rods	110,000	0.3	C3D4	Li et al., 2015 ²³⁶
PEEK Rods	3,600	0.3	C3D4	

Model Validation:

Before analysing the IVR of the spine segments, the FE model needed to be validated. A pure bending moment was applied to assess flexion-extension, lateral bending, and axial rotation. Two validations were carried out by applying a 7.5Nm load on 5 separated motion segments of the thoracic spine (T7/T8, T8/T9, T9/T10, T10/T11, T11/T12) and the lumbar spine (L1-L5). A third validation was done by applying a 5 Nm bending load on a T11-L3 model to measure the IVR of T12/L1. All FE models were loaded at the most proximal endplate and fixed at the most distal one²⁴²⁻²⁴⁴.

Instrumented models:

To test the effect of PEEK rods on the onset of PJK two fused spine models were modified and evaluated in addition to the intact T7-L5 model (Figure 24):

- 1- RIGID: posterior fusion of the spine from T8 to L5 using pedicle screws and 5.5 mm titanium rods
- 2- PEEK: 5.5 mm PEEK rods between T8 and T9 in addition to a posterior fusion of the spine from T9 to L5 using pedicle screws and 5.5 mm titanium rods.

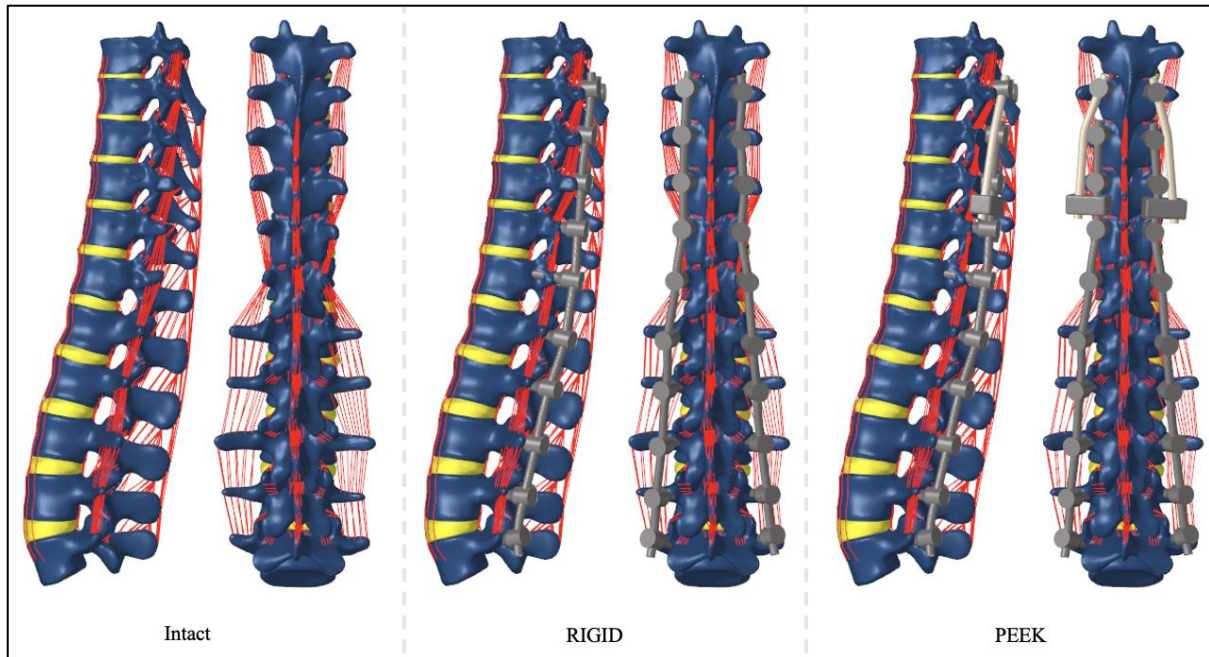


Figure 24 Developed FE models in lateral and posterior view.

Data analysis:

The IVR, maximum Von Mises stress in the screw bodies and the stress distribution in the UIV were investigated and compared for the three spine models developed. For the 3 models, the load was applied at the upper endplate of the T7 vertebrae while the L5 vertebrae. To do so, a modified protocol was applied for biomechanical evaluation ²⁴⁵. The protocol consisted of 2 steps:

- 1) Load-controlled step: The intact T7-L5 and the two instrumented FE models were loaded with a 5 Nm pure bending moment in flexion-extension, lateral bending, and axial rotation ¹⁴. The IVR response of the 3 models was recorded and compared. In the case of lateral bending and axial rotation, as the load was symmetrical on the left and right, the average IVR value was used for the analysis.
- 2) Displacement-controlled step: in this step, the instrumented PEEK model was loaded to match the IVR results of the RIGID model measured in the first step. Maximum von Mises stress values in the screw bodies were then obtained and compared between the two models. Again, for lateral bending and axial rotation, the average values were only reported. In addition, the stress distributions in the UIV in the axial cross-section were also visualized and compared.

Results:

Model validation:

The IVR values for the validation matched the range of the established in-vitro measurements for all loads except for lateral bending, especially at the T9-T10 level (Figure 25, B). In flexion-extension (Figure 25, A) and axial rotation (Figure 25, C), the IVR values were very close to the in vitro mean values. However, lateral bending exhibited smaller IVRs in the INTACT model when compared to the in-vitro results.

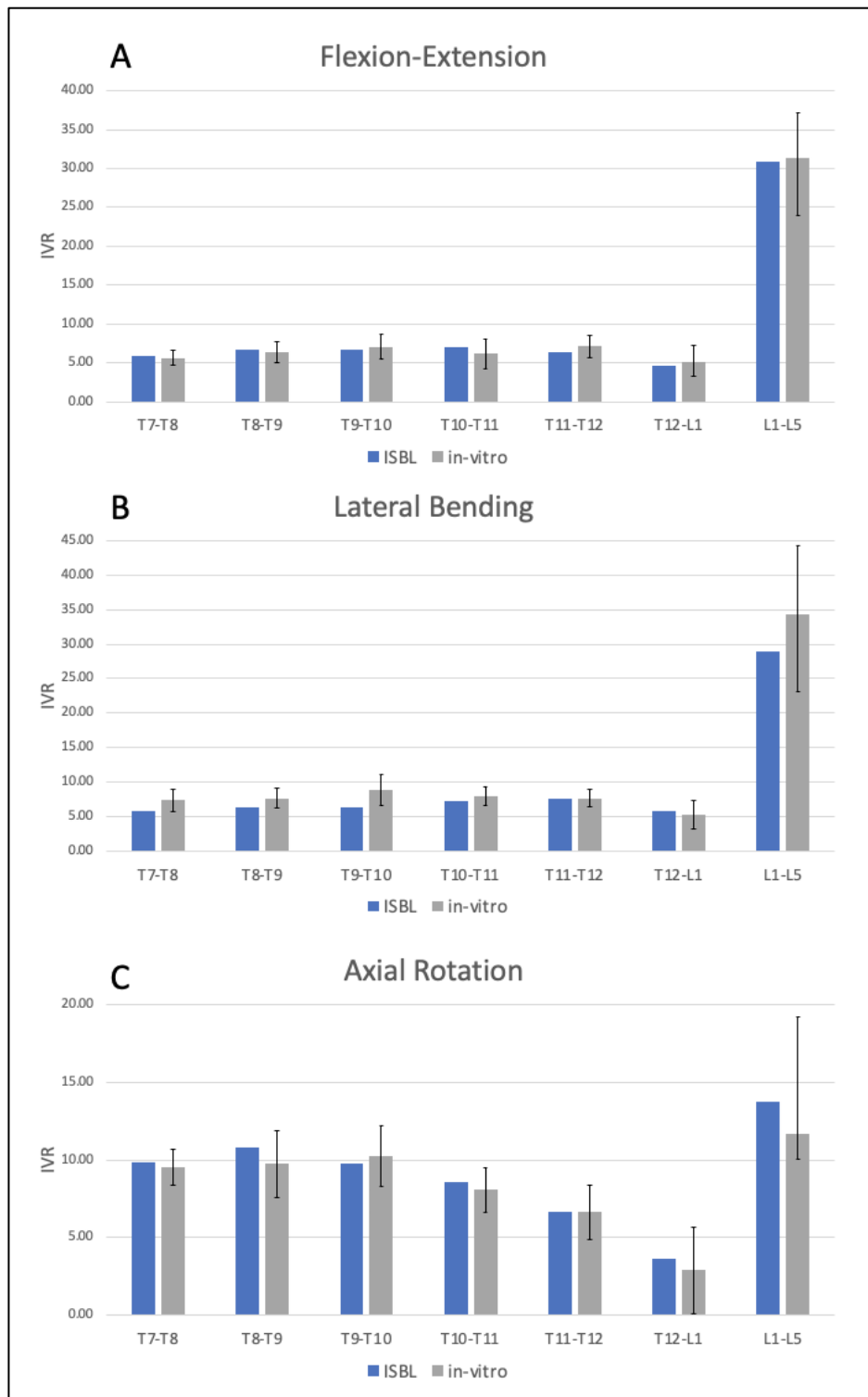


Figure 25 Validation of IVR values of the developed Intact model compared to in-vitro values (A) Flexion-Extension IVR values for the intact model and the in-vitro results for the different spine segments assessed. (B) Lateral bending IVR values for the intact model and the in-vitro results for the different spine segments assessed. (C) Axial rotation IVR values for the intact model and the in-vitro results for the different spine segments assessed.

Intervertebral Rotations:

PEEK exhibited particularly different IVR values to those of the RIGID model at the UIV level. Below the UIV, the differences between the two models were minimal.

At the UIV level, IVR values for RIGID and PEEK were 0.12° and 0.24° for flexion (Figure 26, A), 0.14° and 0.26° for extension (Figure 26, B). For lateral bending, PEEK exhibited a three-fold increase in IVR compared to the RIGID model.

Below the UIV, a 2.7% decrease in IVR was detected for both fixations when compared to the INTACT model (Figure 26, C). The highest IVR values were detected during axial rotation, equal to 0.23° and 1.6° for RIGID and PEEK (Figure 26, D).

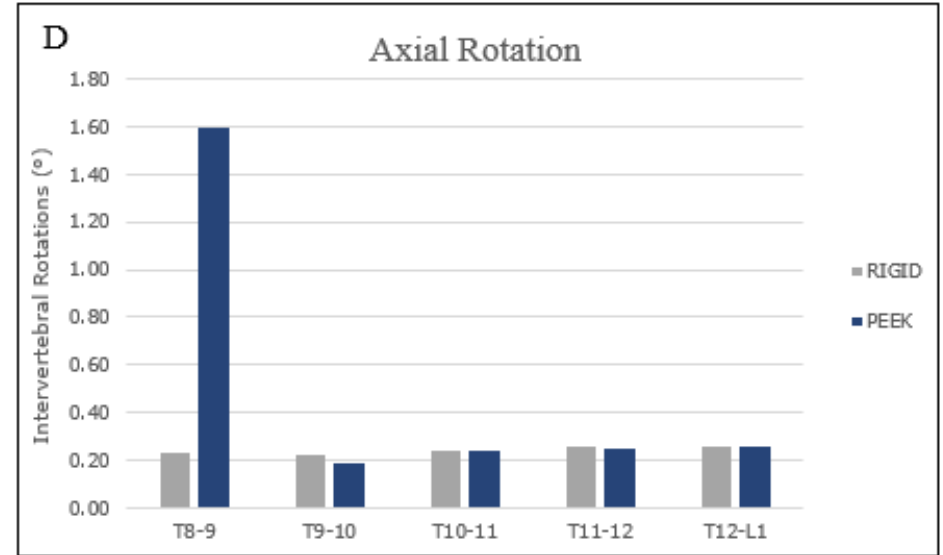
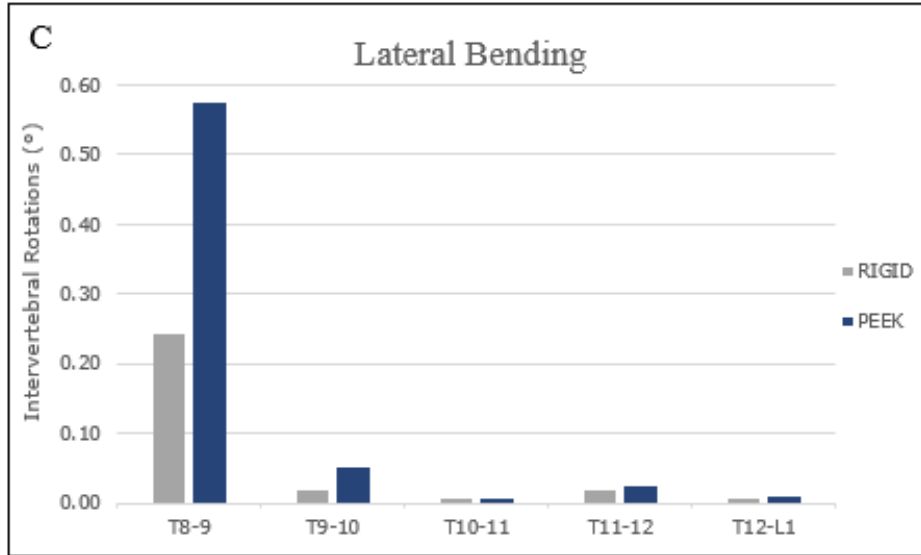
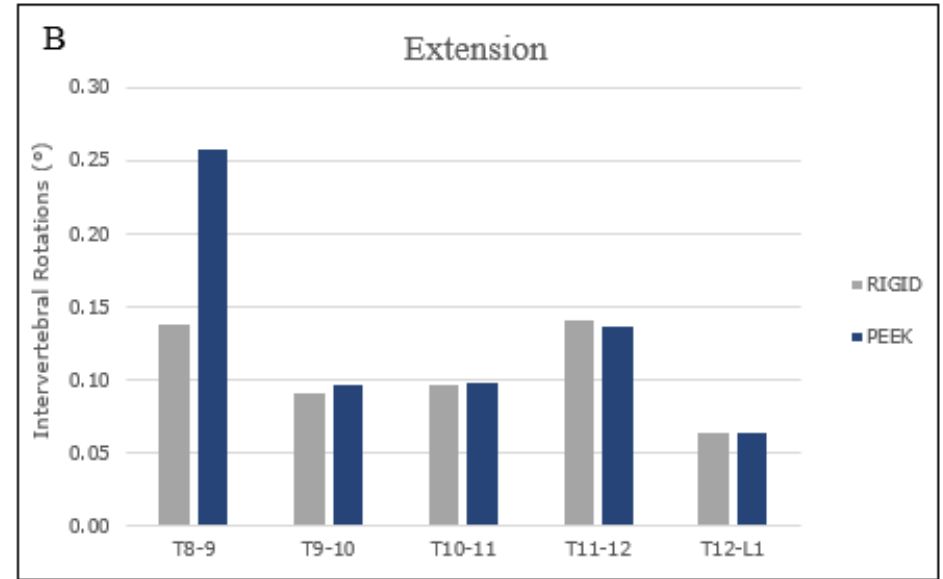
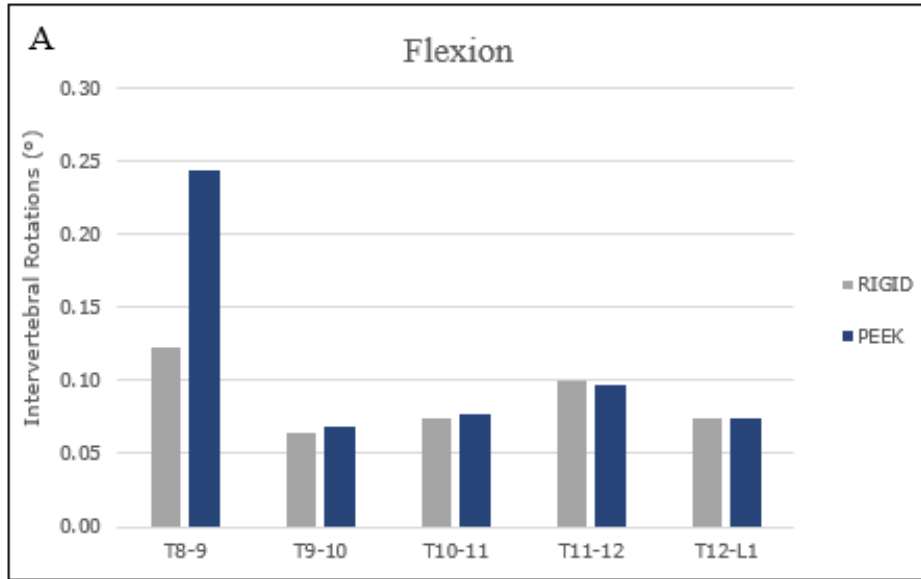


Figure 26 IVR values of the RIGID and PEEK models under a 5Nm load. (A) Flexion, (B) Extension, (C) Lateral bending: showing the mean value for left and right bending, (D) Axial rotation: showing the mean value for left and right rotation.

Von Mises Stress in Screw Bodies:

The RIGID model exhibited the largest Von Mises stress values for all levels. Looking in particular at the UIV level, screw stress values were equal to 37.26 MPa, 42.13 MPa, 44.4 MPa, and 44.59 MPa in flexion, extension, lateral bending and axial rotation. In contrast, PEEK showed a reduced maximum stress values by 27.72% for flexion (Figure 27,A), 36.67% for extension (Figure 27,B), 34.26% for lateral bending (Figure 27,C) and by 59.81% for axial rotation (Figure 27,D). In the case of axial rotation, stress levels were not reduced below the UIV (Figure 27, D)

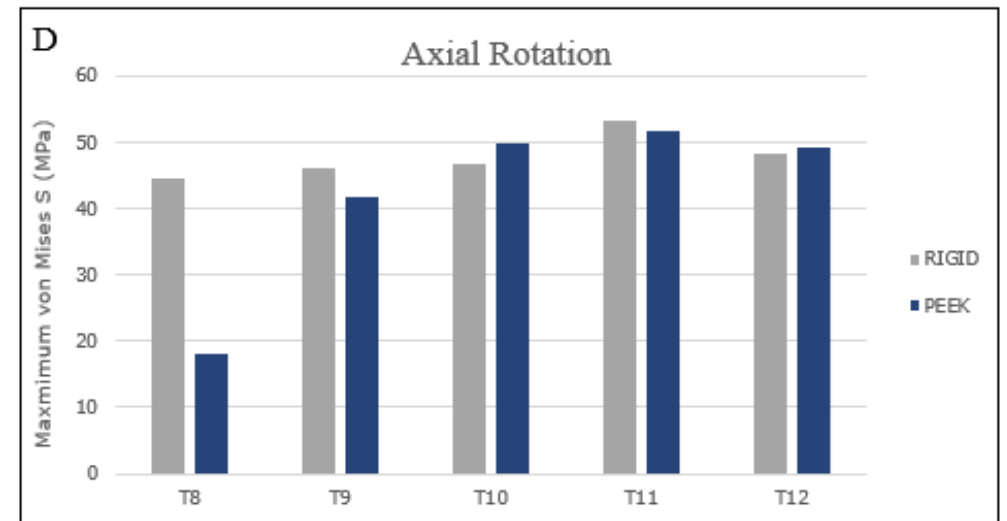
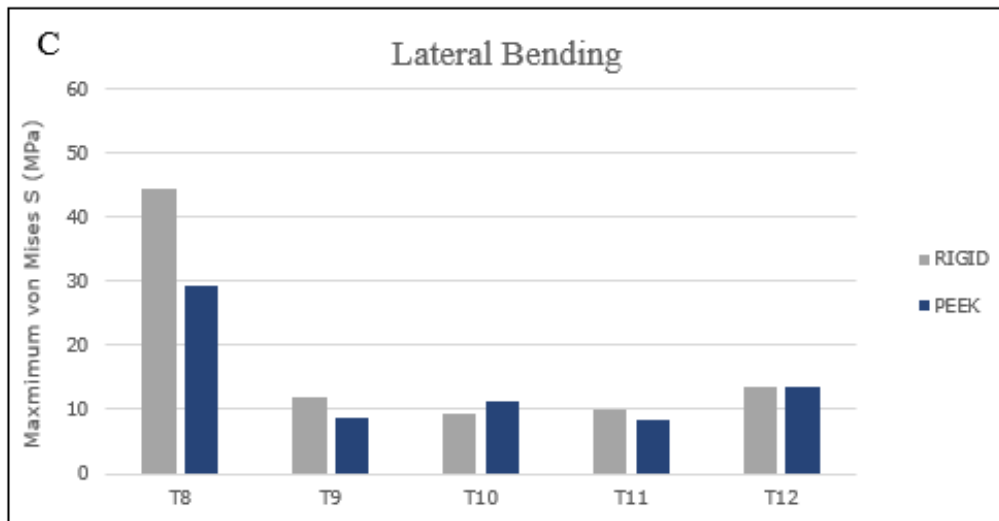
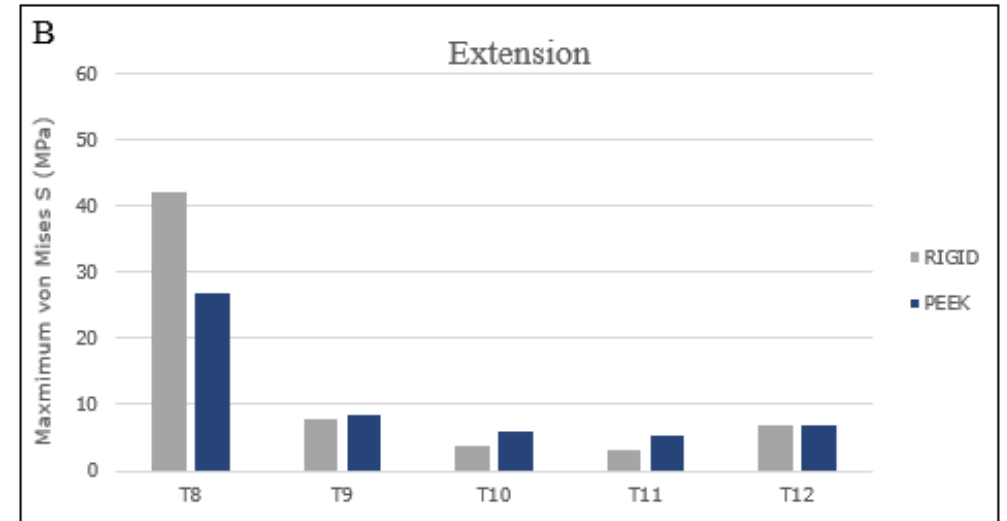
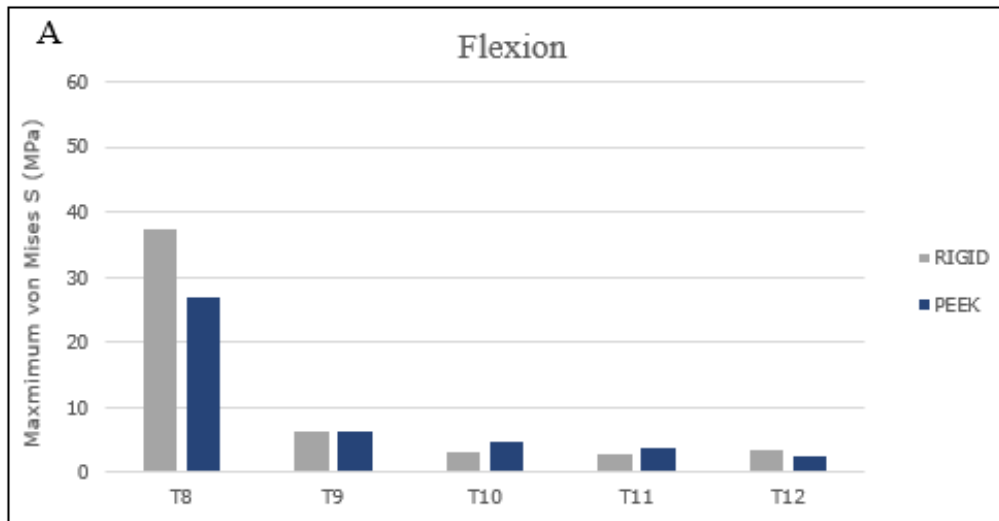


Figure 27 Maximum Von Mises stress values in screw bodies in the RIGID and PEEK models. (A) Flexion, (B) Extension, (C) Lateral bending: showing the mean value for left and right bending, (D) Axial rotation: showing the mean value for left and right rotation

Stress Distribution in the UIV:

Using an axial cross-section of the FE model at the UIV level, the equivalent stress distributions were visualized. The RIGID model exhibited the highest stress areas with some sections exhibiting more than 10MPa of stress (Figure 28, A-D). For the PEEK model, large stress values only appeared in the screw bodies for right and left lateral bending (Figure 28, C) and axial rotation (Figure 28, D). In contrast, larger stress values appeared at the outer edge of the screw bodies in the RIGID model for axial rotation and lateral bending (Figure 28, D).

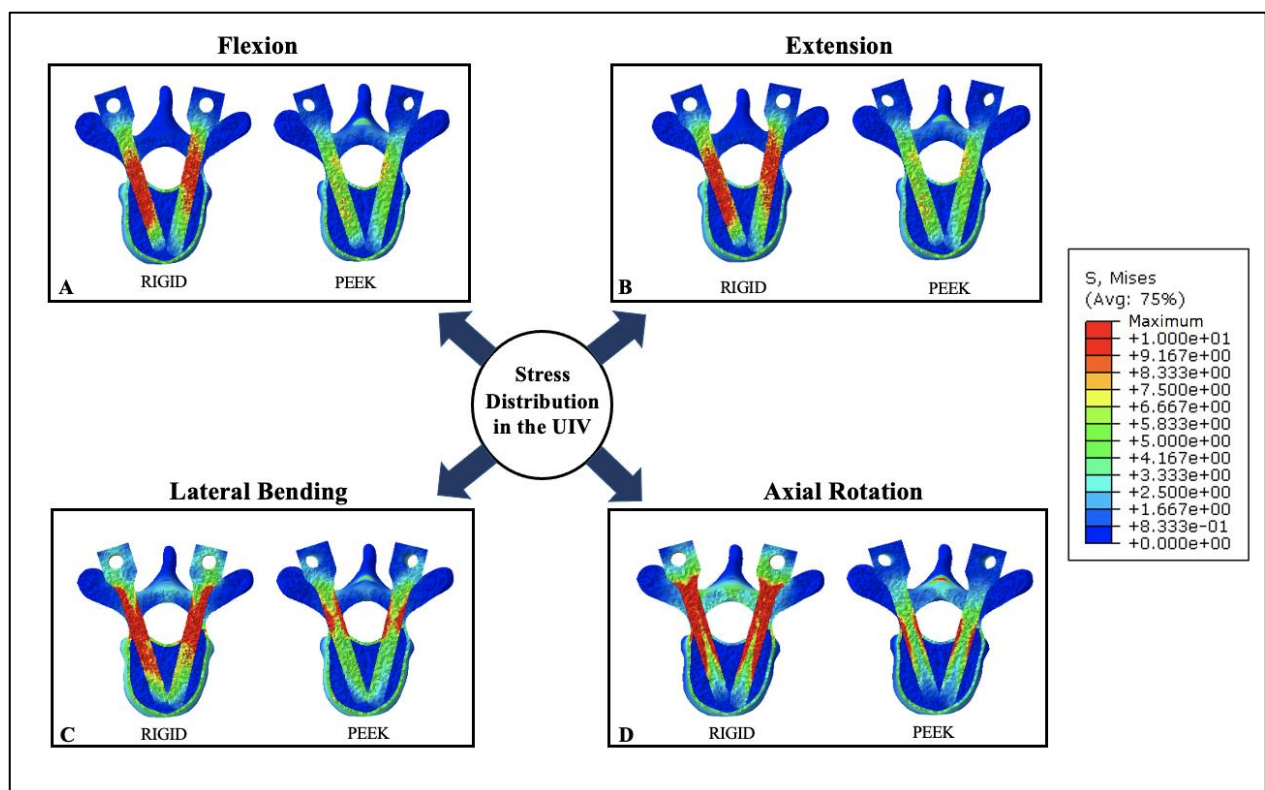


Figure 28 Stress distribution in the UIV of the RIGID and PEEK models. (A) Flexion, (B) Extension, (C) Left Lateral bending, (D) Right Axial rotation. The stress distribution map varied from blue colour depicting 0MPa stress values, green depicting stress values ≈ 5 MPa and red colour depicting stress values >10 MPa.

Discussion

Proximal junctional kyphosis is a surgical complication appearing following posterior spine fusion². The incidence rate of PJK in ASD patients ranges between 9.8% to 61.7%^{10,173,246,247}. PJK manifests as an abnormal kyphotic bending just above the uppermost instrumented vertebra (UIV)^{2,248}. This failure most commonly occurs in the thoracolumbar spine with the highest risk of PJK manifestation occurring when the UIV is at the T10 level^{14,249}. Due to PJK being multifactorial and affected by various risk factors (surgical approach, amount of

alignment correction, type of instrumentation, age, and osteoporosis), this surgical complication remains a problematic issue that still needs to be fully understood^{13,14,48}.

Different surgical approaches have been suggested in the literature to relieve the impact of PJK on the patient including preserving the posterior ligament structures³¹, vertebral augmentation at the UIV to decrease the risk of endplate fracture²⁵⁰, and the use of less rigid fixation instrumentation through transition rods²⁵¹, posterior tethers^{14,30,173}, and transverse process hooks^{14,173,252}. Looking in particular at the rigidity of the instrumentation, researchers have hypothesized that the change in rigidity between instrumentation and spine causes a locality of high stresses in the UIV that could be a leading cause in the occurrence of PJK¹⁷⁶.

In the case of the current study, the use of auxiliary polyetheretherketone (PEEK) rods was investigated to decrease the overall rigidity of the fusion construct and as such provide a transition zone between the instrumented vs the non-instrumented spine. PEEK has a rigidity closer to the physiological material properties of the vertebral bone and can thus form a more homogenous environment around the UIV^{176,177}. The use of such transition rods could provide a solution to limit the incidence of PJK^{14,30,173,251}. We used a finite element model of the thoracolumbar spine to assess the use of auxiliary PEEK rods. FEA was chosen to investigate the instrumentation as opposed to cadaveric specimens as the latter is limited by the increased variability between the specimens and the changes to the tissue hydration due to the fixatives added^{31,163,164}. Using FEA, comparisons between different testing conditions can directly be completed and thus allow for the estimation of the intervertebral rotations, intradiscal pressure, instrumentation stresses and the stress distributions in the vertebrae that could not be easily measured in an experimental setting^{14,31}.

While FEA has been extensively used for the modelling of the lumbar spine^{32,169}, fewer standards are found for the modelling of the thoracolumbar spine^{14,31,32,170,171}. Due to the limited investigations, validations of the thoracolumbar FE models are vital to providing results depicting the actual physiological response¹⁶³. In this study, to account for the lack of in-vitro intervertebral rotation data for the thoracolumbar spine, different smaller segments had to be created. However, it would be recommended to have in-vitro IVR values of the thoracolumbar spine. Nonetheless, the IVR values of the intact model were within the ranges found for in-vitro in the literature²⁴²⁻²⁴⁴. The only outlier was found in lateral bending, especially in the T9-T10 motion segment. This disagreement could be due to a difference in the stiffness of the Intratransverse ligament or due to the limited motion of the IVD in the coronal plane¹⁶⁹.

Looking at the instrumented spine variations developed, the intact thoracolumbar spine model was modified to create a 1) RIGID model where a posterior spine fusion was added from T8

to L5 and 2) PEEK model where auxiliary PEEK rods were added from T8 to T9 followed by a PSF from T9 to L5. Using these two developed instrumented models, the intervertebral rotations, Von Mises stress in the screw body and stress distribution at the UIV were compared. We hypothesized that PEEK would allow for greater intervertebral rotations as is it more flexible while also allowing for a decrease in the stress at the level of the UIV due to its lower rigidity. Consequently, this could decrease the occurrence of PJK.

For the intervertebral rotations, PEEK did indeed allow for greater intervertebral motion most notably at the level of the T8-T9 motion segment which was the UIV (Figure 26). The RIGID model exhibited diminished IVR values at the UIV equal to almost half of the values measured for the PEEK in flexion, extension, and lateral bending. For axial rotation, the difference was greater between the two models indicating the considerable effect a rigid titanium rod has on the motion of the spine, especially at the UIV. This change in segment motion between the UIV and the UIV+1 induces high strain values in the instrumented segment. These differences were also seen in models using posterior tethers to decrease the rigidity of the implant construct where the range of motion at the level of the UIV was measured to be almost 90% of the original intact model¹⁴.

The maximum Von Mises stresses in the screw bodies was seen to be the highest in the rigid model for all bending moment directions. In general, axial rotation induced the most stresses for all screw bodies in both models when compared to flexion, extension, and lateral bending. In addition, the highest differences in the stresses between the two models were seen during axial rotation at the level of the UIV. This increase in screw stresses during axial rotation has also been noted in studies published by Song et al.²⁵³ and Li et al.²³⁶. When maximum von mises stress greatly increase in the screw body, screw breakage is to be expected²⁵³.

Looking at the stress distribution, an axial cross-section of the UIV was used to compare the changes between the two instrumented models. The PEEK model exhibited notably fewer stresses in the UIV for all 4 bending moment directions. For both models, the highest stresses were seen in the screw bodies. This finding agrees with the finding of Zhu et al.²⁵⁴ who found significant increases in the maximum stress (more than 10Mpa) in the UIV of a fused spine compared to an intact model.

The measurements reported for the two instrumented models agreed with our hypothesis that the auxiliary PEEK rods would allow for greater motion in the fused segment and decrease the stresses in both the screw bodies and the vertebra at the UIV level.

The present study does have some limitations. First, the finite element model used in this study is a simplified model that does not account for the soft tissues surrounding the spine and the

rib cage and the segmental it induces on the spine. Second, although PEEK rods did increase IVR values and decreased maximum stresses, these findings cannot guarantee the decrease of PJK. An extensive clinical study is needed to assert the usefulness of auxiliary rods and their advantage in decreasing PJK.

Conclusion

The incidence of PJK could be diminished by using auxiliary PEEK rods during posterior spine fusion surgeries. Using finite element analysis, PEEK rods were found to increase intervertebral rotations while also helping decrease the maximum stresses in the screw bodies and allowing for a decrease in the stress distribution at the UIV level. This semi-rigid fixation approach allowed for the creation of a transitional zone between the instrumented segment of the spine and the unfused segment.

Chapter 6: Gait analysis and mapping bony fusion to analyse the outcome of the Closed loop reconstruction technique

Parts of this chapter have been published in:

Peter Endre Eltes, Mate Turbucz, Jennifer Fayad, Ferenc Bereczki, György Szőke, Tamás Terebessy, Damien Lacroix, Peter Pal Varga and Aron Lazary, *A novel three-dimensional computational method to assess rod contour deformation and to map bony fusion in a lumbopelvic reconstruction after en-bloc sacrectomy*. *Front. Surg.* 2022. doi: 10.3389/fsurg.2021.698179

**As a co-author on this paper, I was Investigator 3 and was responsible for the gait analysis*

Abstract

Introduction: Total ‘en bloc’ sacrectomy is a complex surgical procedure needed for the resection of tumours in the sacral region. This procedure has major consequences on the load-bearing ability and mobility of patients after surgery due to the delicate anatomy of the region affected. The stabilization technique used to reconnect the spine to the pelvis plays a major role in restoring the load-bearing ability of the lumbopelvic region. The purpose of this study is to computationally evaluate the biomechanics of the closed loop lumbopelvic reconstruction technique concerning the resulting mobility of the patient, the construct used and the extent of bony fusion.

Materials and Methods: A 42-year-old patient underwent a total sacrectomy with a closed loop reconstruction. Following the surgery, 12 CT scans were collected from the patient over 6 years. To measure the patient's mobility and assess the cyclic loading of the implant, a gait analysis session was recorded 6 years following surgery. To measure the extent of implant deformation, 3D geometries of the construct in the 12 CT scans were defined and registered to a common coordinate system. The distance between the proximal and the distal parts of the implant was measured over the years. To assess bony fusion, a voxel-based mesh was defined

as a particular region of interest. The Hounsfield values were used to assign bone mineral density values for all the mesh elements ranging from 0 to 1,12 g/cm³.

Results: The patient was able to walk independently following the surgery with minor gait alteration. A bending forward was detected at the level of the pelvis. This bending forward was also seen in the implant deformation where a significant correlation was found between the sagittal plane deformation and the number of days following surgery. Bony fusion was detected at the 2-year follow up where BMD values= 0.98cm³ increasing to 2.3cm³ at the 6-year mark.

Conclusion: The closed loop technique minimally affected the patient's mobility, achieved bony fusion, and provided a non-rigid fixation allowing for implant deformation. The surgical assessment developed here can be used to understand the biomechanics of complex surgical spine procedures.

Introduction

Primary bone tumours of the sacrum are very rare ²⁵⁵. The most common of these is chordoma representing 40% of all sacral neoplasms ²⁵⁶. Chordoma is a slow-growing low malignancy tumour characterized by a high recurrence rate ²⁵⁵ (Figure 29, A). Due to the mild symptoms, it usually is diagnosed in advanced stages making surgical interventions the first treatment of choice for large sacral chordomas ²⁵⁷. Aiming at optimal oncological results, wide surgical margins are preferred for the resection of the tumour, known as en-bloc sacrectomy. However, this approach leads to the loss of the connection between the spine and pelvis and of the sacral nerve roots (Figure 29, B), causing problems with incontinence, sexual dysfunction, and mobility ^{258–260}.

Beyond the main aim of the surgery to remove the tumour and provide successful oncological results, the spinopelvic connection needs to be re-established ²⁵⁸. Different reconstruction techniques following sacrectomy currently exist, aiming to achieve a stable fixation between the pelvis and lumbar spine, using implants to achieve bony fusion ²⁵⁷. These reconstruction techniques have been linked to complication rates with no gold standard being available ^{261,262}. The closed loop technique (CLT) developed by Varga et al (2009) ²⁶³ (Figure 29, C), is a reconstruction technique used following en-bloc sacrectomy. This technique allows for the establishment of the spinopelvic junction using a single U-shaped rod attached using iliac and transpedicular screws ²⁵⁸.

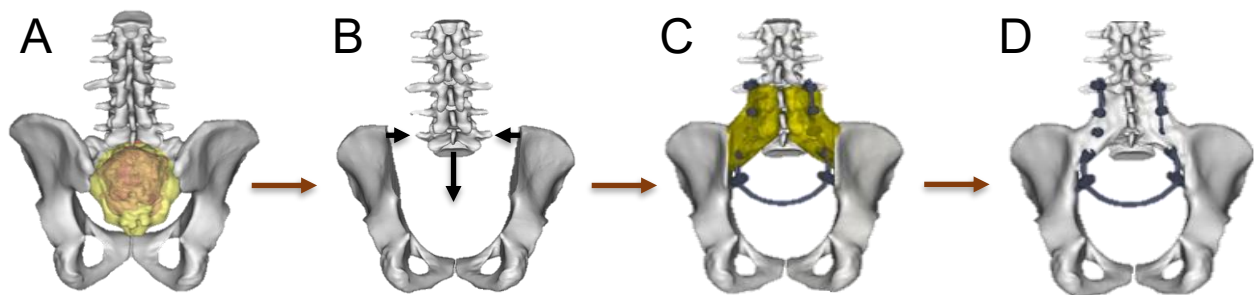


Figure 29 The Closed Loop reconstruction technique following en bloc sacrectomy. (A) Chordoma tumour affecting the sacrum. (B) Removal of the tumour through sacrectomy. (C) The closed loop reconstruction technique uses the U-shaped rod. (D) adapted from Eltes et al. (2022) ²⁶⁴

The CLT technique provides a non-rigid fixation allowing for implant deformation and continuous bone remodelling ²⁶⁵ (Figure 29, D). The aims of this study could be separated into three main points:

- 1- Assessing the mobility of the patient 6 years after the en bloc sacrectomy and the CLT reconstruction was to assess the mobility,

- 2- Mapping the bony fusion and measuring the changes in bone mass density (BMD) at the spinopelvic junction over the 6-year follow up period
- 3- Measuring the extent of implant deformation in the sagittal plane and its effect on the biomechanics of the CLT construct.

Methods:

Clinical Case:

A 42-year-old male presented with mild and non-specific low back pain for 4-5 years. Upon radiological examination, a tumour mass was discovered affecting the whole sacrum extending up to L3 on the right side. The diagnosis confirmed the presence of a chordoma tumour (Figure 30). The surgeons agreed that a total “en bloc” sacrectomy is needed to remove the tumour combined with soft tissue and spinopelvic reconstruction (closed loop reconstruction) using a poster only approach. The removal of the tumour leads to the loss of the cranial and ventral ligaments of S1 and the cutting of the nerve roots below L5. The surgery is available on the Open Operating Theatre (OOT) platform of the European Spine Journal ^{266,267}. To anchor the U-shaped rod (5.5mm rod, CD Horizon©LEGACY™ 5.5, Medtronic Sofamor Danek, Memphis, Tennessee, United States) of CLT to the iliac and lumbar spine, two pairs of transpedicular screws were used in addition to pedicle screws going up to L2. To achieve bony fusion, an artificial bone substitute was used (ACTIFUSE®, Baxter International Inc., Deerfield, Illinois, United States) and placed between the body of L5 and the iliac crest bilaterally. Following the surgery, the gait abilities of the patient and analysis of CT data over the 6-year follow up period were performed. The study got approval from the National Ethics Committee of Hungary, the National Institute of Pharmacy and Nutrition (reference number: OGYÉI/163-4/2019). The patient provided signed consent.

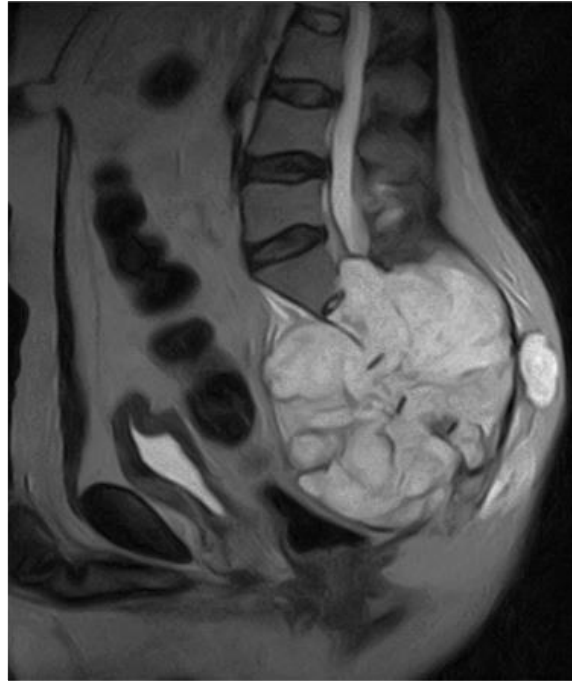


Figure 30 Preop MRI of the Chordoma tumour in the sagittal plane

Post-Surgical Evaluation:

Gait Analysis:

The patient was able to walk with crutches at the 3rd month FU, and without any assisting device at the 12th month FU. At the 6-year FU, the patient (48 years of age, w: 90.5kg, h:185cm) underwent a gait analysis session. The patient was requested to walk back and forth along a straight path, mounting a full-body plug-in-gait marker setup.

Marker trajectories were acquired using a 6-camera motion analysis system (VICON MXT40, UK), and ground reaction forces (GRF) using a force platform (AMTI OR6, USA) mounted halfway along the path.

The patient completed five trials in total. Spatio-temporal parameters were calculated. Gait speed was normalized to body height (BH) and stance time was calculated as a percentage of the total stride time. Joint kinematics and kinetics were calculated from marker trajectory and ground reaction forces using Vicon's Nexus-plug-in-gait protocol. Mean and standard deviation of data per gait cycle were calculated over the 5 available repetitions per side and compared to normative data ²⁶⁸.

Radiographic acquisitions:

To quantify the deformation of the construct and the degree of bony fusion, the patient underwent 12 CT scans in the 6-year FU period. The scans were acquired using the same CT machine over the years (Hitachi Presto, Hitachi Medical Corporation, Tokyo, Japan). The CT

data were exported from the hospital's PACS system as a DICOM file. This data was then anonymized using the Clinical Trial Processor Software (Radiological Society of North America) ²¹⁵. 5 CT scans were taken in the 1st year, 2 in the 2nd year, one in the 3rd, 4th and 5th years and lastly 2 were taken in the 6th year.

3D Geometry Definition:

To define the geometry of the closed loop instrumentation, segmentation of the CT data was required. No signs of implant failure were detected in any of the CT scans taken. The segmentation was performed using Materialise Mimics (Mimics Research, Mimics Innovation Suite v21.0, Materialise, Leuven, Belgium) where the closed loop instrumentations and the left pelvic bone were separated in each of the 12 CT scans acquired. From the generated mask, a triangulated surface mesh was generated. The accuracy of the segmentation process was evaluated using the Dice Similarity Index (DSI) ²⁶⁹; where two investigators (I_1 and I_2) segmented the implant and pelvic bone geometries to calculate the DSI by comparing I_2 's segmentation to that of I_1 ²⁹. DSI values range between 0 and 1.

Implant Geometry alignment:

To measure the extent of the implant deformation over the 6-year FU, the 12 segmented CT scans needed to be aligned in the same coordinate system. Here, the left pelvic bone of the 1st CT scan was used as the reference geometry. Using 8 points placed on anatomical landmarks of the pelvic bone, a point-based registration was performed in Mimics. Using this method, the 12 geometries taken from the CT scans were superimposed and aligned altogether (Figure 31). To evaluate the accuracy of this registration approach, the Hausdorff distance (HD) was measured in MeshLab 1.3.2 software ²¹⁹ (<http://www.meshlab.net>). The HD measurement was done on each postop scan where the geometries of the 2-12th scan were compared to that of the 1st scan. The HD values were also calculated for the left transpedicular screws over the 12 CT scans as these were found to be colinear following registration.

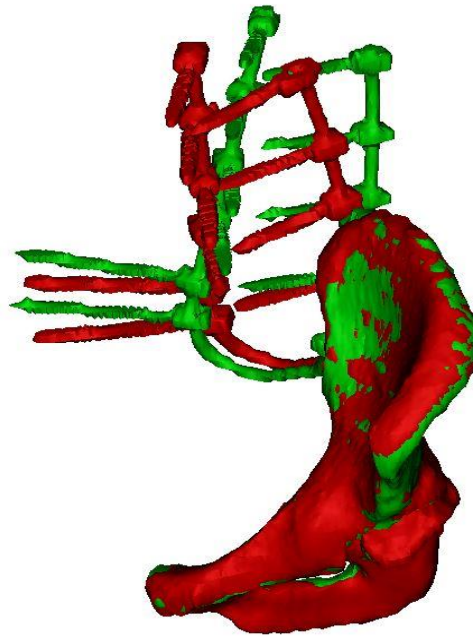


Figure 31 Alignment of 1st and 12th CT scan.
Implant deformation can be seen following registration, where Green= 1st CT scan and Red= 12th CT scan. Adapted from Eltes et al. (2022) ²⁶⁴

Measuring Implant Deformation:

Following registration, the implant deformation over the years could be measured. To achieve this, the centreline of the geometry was first defined in Mimics (Figure 32). From this centreline, the tip of the L2 pedicle screw (mobile point) and the tip of the caudal iliac screw (fixed point) were selected as the basis for the measurement. The distance between these two points was measured in the 3 anatomical planes using Materialise 3-Matic (Mimics Innovation Suite v21.0, Materialise, Leuven, Belgium). Again, to test the accuracy of the measurement, the segmentation of the implant, the centreline definition, and the distance between the 2 points was completed by 3 investigators (I₁, I₂, and I₃). The three-dimensional distance was also calculated using the coronal (X_d), sagittal (Y_d) and axial (Z_d) plane distances following the formula $3D_d = \sqrt{X_d^2 + Y_d^2 + Z_d^2}$.

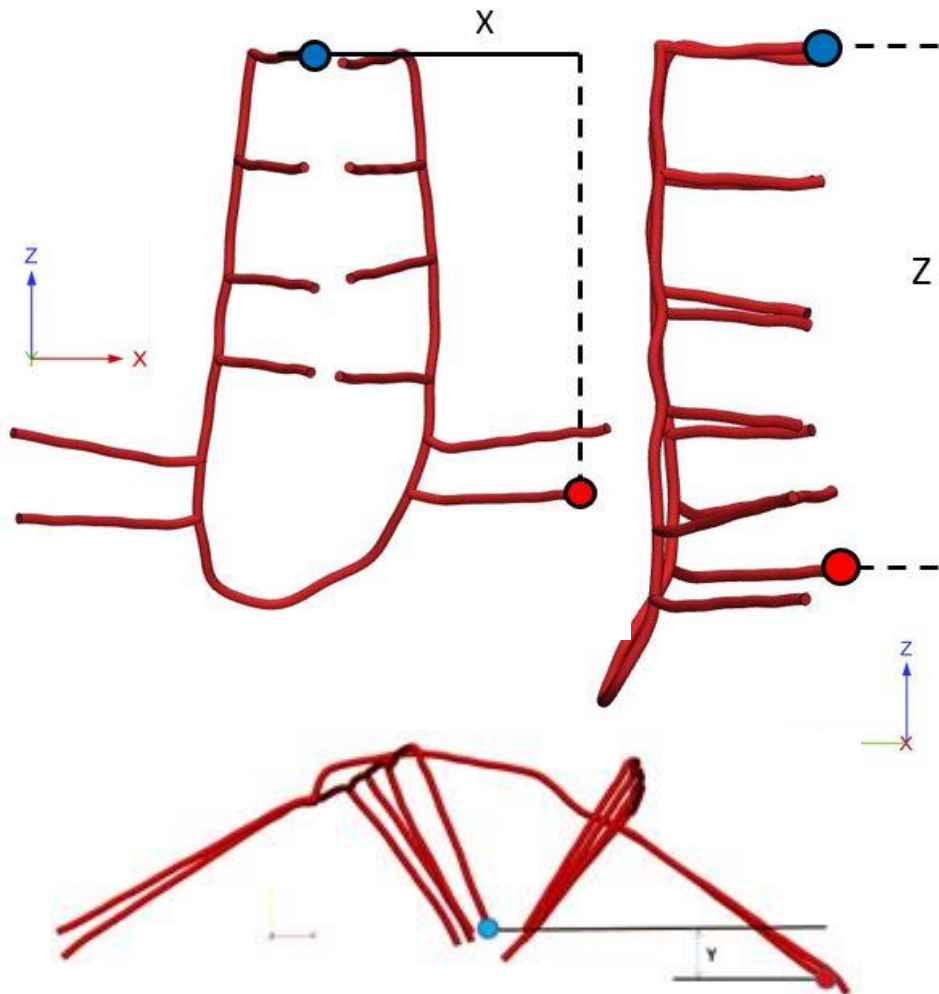


Figure 32 Simplified implant construct and deformation measurement Distance measurement in the three anatomical planes where X= coronal distance, Z= axial distance and Y= sagittal distance. The blue dot corresponds to the tip of the right L2 pedicle screw, the red dot corresponds to the tip of the caudal trans iliac screw. Adapted from Eltes et al. (2022)²⁶⁴

Mapping Bony fusion:

To measure bony fusion over the FU period, a single axial slice was selected from each CT scan of the same anatomical region corresponding to the midplane between the L4 and L5 pedicle screws. This region of interest was segmented again to include the bone tissue and fat. From this mask, a voxel-based finite element model was created using Mimics. Due to the patients' CT scans being acquired without a calibration phantom, QCT scans were selected from the hospital's PACS system that were acquired in the same months as the 12 CT scans. The QCT scans were from male subjects who had the same body mass indices as the patient (BMI=28±2). From these QCT scans, the Hounsfield units were converted into bone mass density values using the calibration phantom (Hitachi Presto, Hitachi Medical Corporation, Tokyo, Japan). This conversion followed prior studies to have: $BMD = \rho_{QCT} = a + b * HU$, where ρ_{QCT} [g/cm³] is bone density. Following the conversion, in the FE mesh, each element was colour coded using 10 colours corresponding to the different BMD values.

Statistical Analysis:

To demonstrate the reproducibility of the study, the reliability and repeatability of the method developed were assessed. Non-parametric tests were used throughout due to the small sample size. Using intraclass correlation coefficient (ICC) at the 95% confidence interval (CI), the inter-rater (I₁ vs I₂ vs I₃) reliability was determined based on a mean rating of 3, absolute agreement and a 2-way mixed-effects model. Intra-rater reliability (I₁T₁ vs I₁T₂, I₂T₁ vs I₂T₂, I₃T₁ vs I₃T₂) was assessed using ICC at 95%CI based on a single measurement, absolute agreement and the 2way mixed-effects models. Using Spearman’s rank correlation, the relationship between implant deformation in the 3 anatomical planes and the number of postop days was assessed in addition to the relationship between the volume change in the BMD categories²⁷⁰. The statistical tests were performed using SPSS® Statistics 23 software (SPSS Inc, Chicago, IL).

Results

Gait Analysis:

The patients’ gait speed was reduced compared to the control on both sides while the stride time increased. Stance time in percentage of the gait cycle lasted longer than in the control, particularly on the left side, showing an asymmetric gait (Table 19).

Table 19 Gait Characteristics

Mean (SD) temporospatial gait characteristics of the right and left leg compared to healthy subjects.

	Control	Right Leg	Left Leg
Gait Speed/BH (%BH/s)	71.36 (10.23)	40.25 (3.05)	39.27 (2.34)
Stride Time (s)	1.10 (0.10)	1.37 (0.06)	1.36 (0.06)
Stance Time (%GC)	62.64 (1.97)	65.34 (3.80)	71.66 (2.40)

Kinematic analysis of gait showed a forward-leaning of approximately 20° of the pelvis and the trunk throughout the gait cycle, resulting in the disappearance of hip extension on both sides during the final part of the stance phase (push-off). An increased rise of the pelvis could be observed associated with increased adduction of the hip, particularly on the right side. A pivoting behaviour was also demonstrated by an increased anterior rotation of the left pelvis during stance. Alterations in the kinematics of lower limbs were minor, with a lack of knee flexion peak and increased ankle extension at the beginning of the stance phase and increased flexion of the knee during the swing phase (Figure 33)

GRF components were reduced in the antero-posterior and medial-lateral directions, particularly on the right side. At the hip, the initial flexion moment peak almost disappeared on both sides resulting in an extended and maintained extension moment, which significantly increased on the left side. Adduction moments increased on both sides, particularly on the left. Joint moments were, on the other hand, decreased at the knee, particularly on the left side, while differences were minor at the ankle (Figure 34)

Power analysis showed a significantly reduced power generation at the ankle during push off on both sides, associated with a power absorption peak as opposed to a normal power generation peak at the hip. The knee power absorption peak was slightly increased at the beginning of the stance phase (Figure 35).

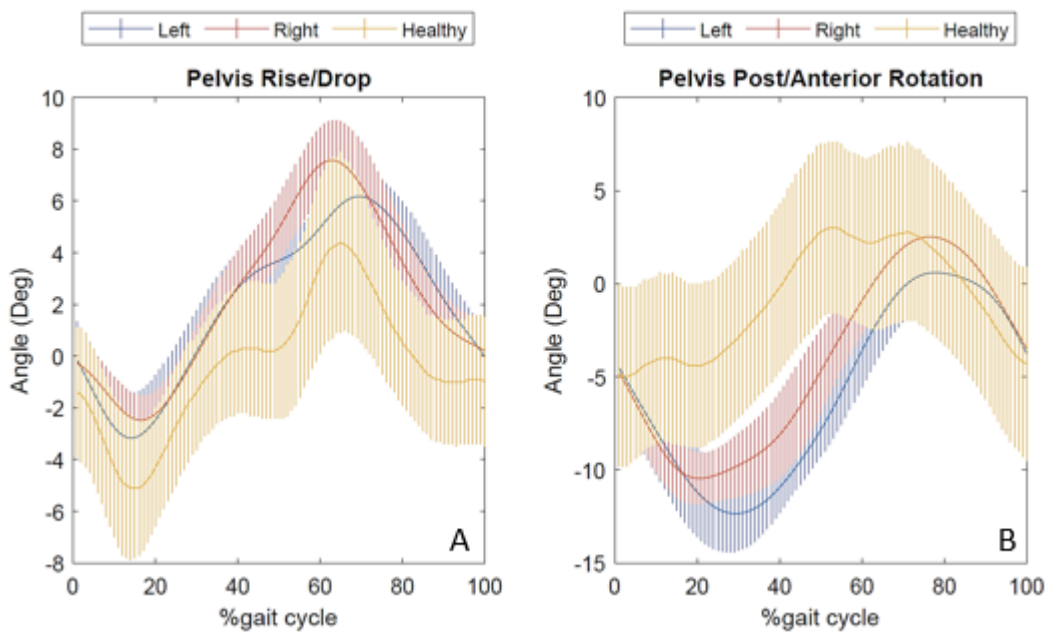


Figure 33 Time series Kinematics of the pelvis

In the coronal (A) and frontal (B) planes. Data were normalised to 100% of the gait cycle. The graphs show the left (blue) and right (red) legs of the patient compared to healthy subjects (yellow).

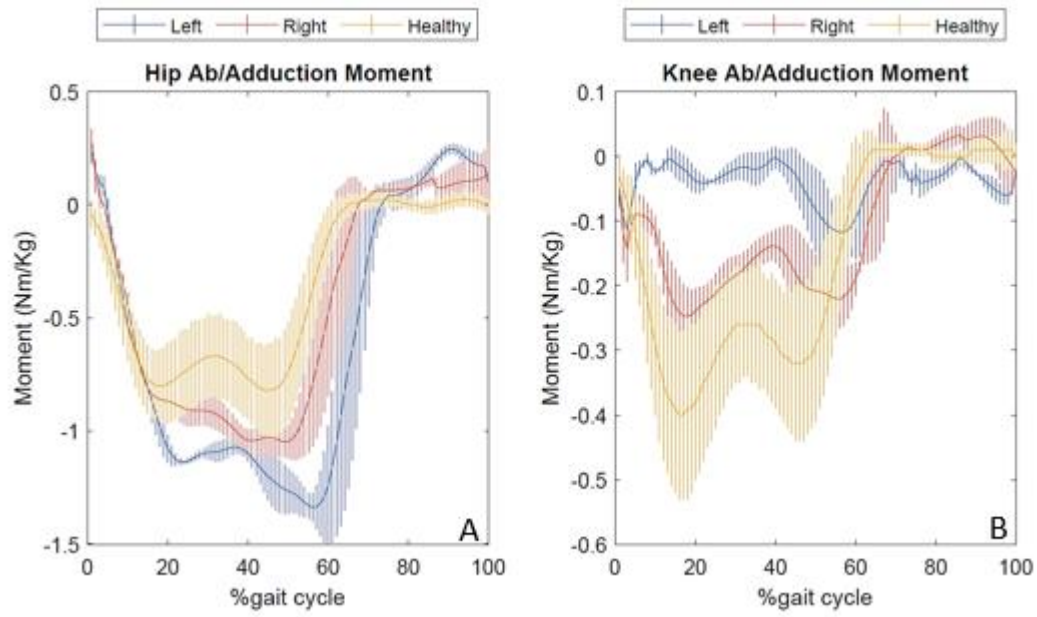


Figure 34 Time series kinetics of the hip (A) and knee (B) during abduction/adduction

Data were normalised to body weight. The graphs show the left (blue) and right (red) legs of the patient compared to healthy subjects (yellow).

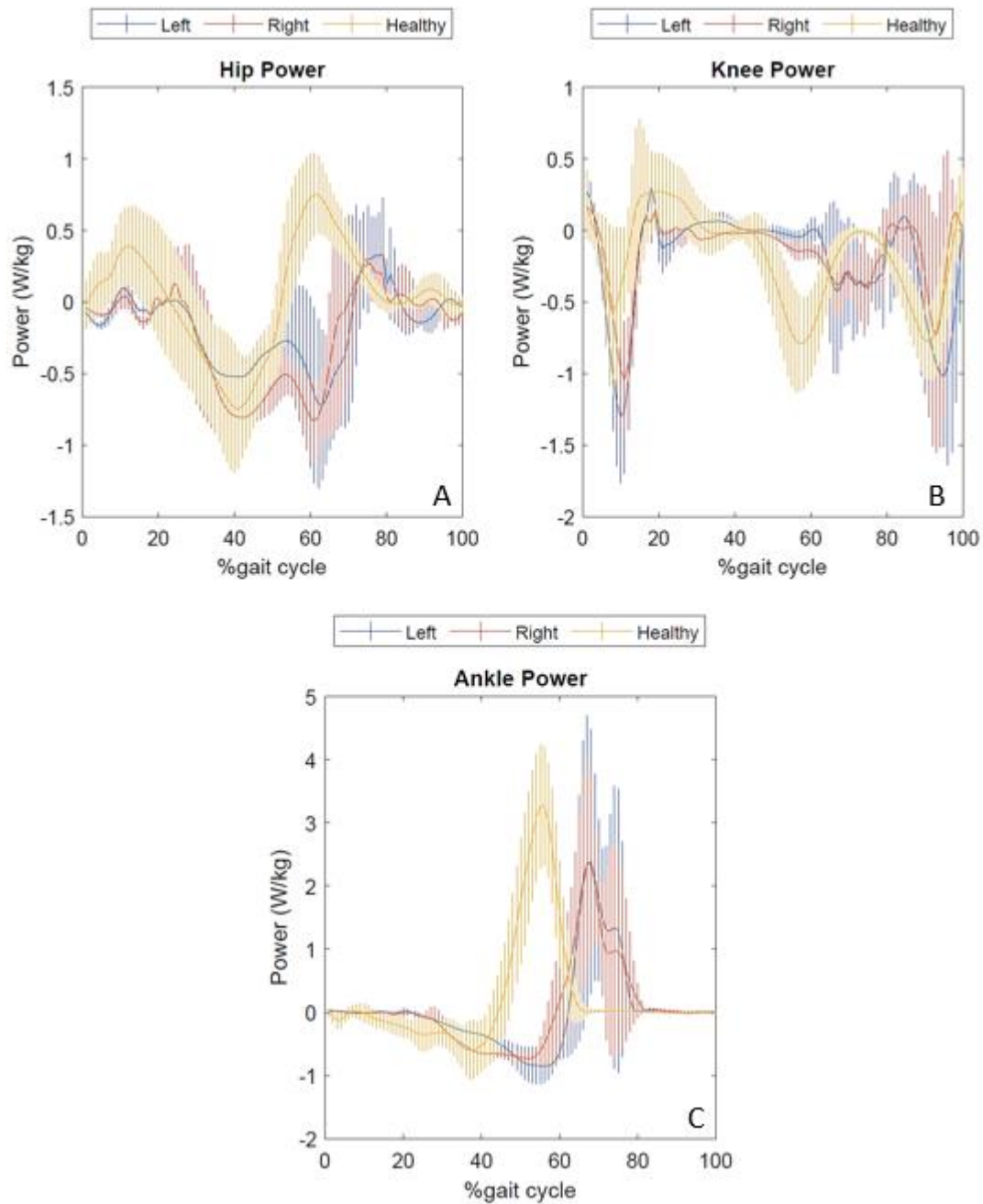


Figure 35 Joint powers during flexion-extension of the hip (A), knee (B), and ankle (C) in the sagittal plane. Joint powers were normalised to body weight. The graphs show the left (blue) and right (red) legs of the patient compared to healthy subjects (yellow).

Segmentation Accuracy:

The DSI values of the segmentation done by I_1 and I_2 were very high equal to 0.97 ± 0.02 for the implant geometry and 0.96 ± 0.05 for the pelvic geometry. These values indicate negligible variance due to investigator bias, indicating the high accuracy of the segmentation method ²⁷¹.

Evaluation of implant alignment:

The HD values calculated for the pelvic bone and the iliac screw bodies were equal to 0.63 ± 0.14 mm and 0.95 ± 0.10 mm respectively. Indicating that the registered geometries were indeed adequately fitted²⁷². The trans iliac screw bodies did not deform or change position for all 12 CT scans in the common coordinate system.

Implant Deformation:

The average implant displacement over the 12CT scans compared to the first postop CT was $\Delta X_d = 7.27 \pm 2.80$ mm in the frontal plane, $\Delta Y_d = 8.24 \pm 2.51$ mm in the coronal plane, and $\Delta Z_d = 10.15 \pm 2.97$ mm in the sagittal plane. In terms of measurement reproducibility and accuracy, ICC values showed high reliability for both inter- and intra-rater measurements except for the I_1T_1 vs I_1T_2 intra-rater reliability equal to 0.768 corresponding to good reliability²⁷³. The deformation of the implant construct was the most significant in the sagittal plane showing a forward bending tendency of the implant. A strong negative correlation was found between Y_d and the number of days after surgery ($\rho = -0.664$, $p = 0.018$).

Mapping of the bony fusion:

Bone material density (BMD) was measured in the region of interest for the fusion process over the 6-year FU period. Solid fusion between the lumbar spine, L4 vertebrae and the iliac bones was detected at the 2-year FU (Figure 36). Looking at the spearman rank correlation, the relationship between the 10 BMD categories' volumetric change and the days after surgery was significantly positive showing a strong correlation ($\rho > 0.800$, $p < 0.050$).

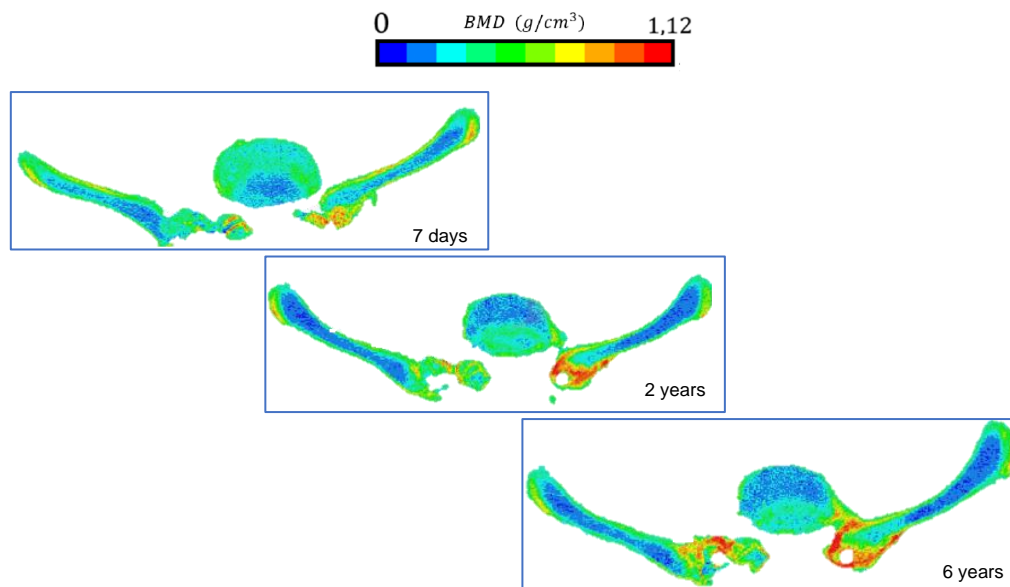


Figure 36 Map of the fusion and remodelling process at the ROI at the 7 days, 2 years, and 6 years FU. The BMD values are represented in 10 colour codes from 0 to 1.12 g/cm³ on an RGB scale. The red colour represents the strongest bone tissue. The provided scale bar's length is 2 cm. Adapted from Eltes et al. (2022)²⁶⁴

Discussion

The non-rigid fixation abilities of the CLT method were investigated in this study to restore the lumbopelvic junction following sacrectomy. The method aimed to assess the implant deformation, bony fusion and patient mobility over a 6-year follow up period. The method succeeded in measuring the extent of implant deformation over the years and mapping bone remodelling at the fixation site. A significant correlation was found between the implant deformation and the number of postop days indicating a forward bending tendency of the construct. Looking at the patients' mobility, CLT provided excellent locomotor outcomes after the en bloc sacrectomy which agreed with similar results published by Smith *et al.*²⁵⁷. The patients' ability to walk independently further helped in the cyclic loading of the construct promoting bony fusion²⁷⁴. The notion of cyclic loading during gait was highlighted by Clark *et al.*²⁷⁵ where they compared 3 spinopelvic reconstruction techniques under gait loading and their effect on sagittal implant failure. However, their study only assessed cadaveric specimens without taking into consideration the process of bony fusion.

Following surgery, the patient was able to walk independently, with minor gait alterations for compensating the lost neural function. The resulting gait was slow and slightly asymmetric with increased support on the left leg and right pivoting and a reduced propulsion power at the hip and ankle. On the other hand, joint mobility was close to normal at all the joints, distally in particular. The forward-leaning of the pelvis and the trunk could serve as a compensation technique to guarantee progression, exploit gravity, and reduce muscle force requirements of the hip and knee extensors. The observed gait alterations can be related to the impaired function in the hip muscles resulting from loss of the sacral nerve roots after sacrectomy, although EMG analysis is required to better support this hypothesis.

Looking at bony growth or loss following fixation surgeries, the effect of a construct stiffness on the healing of bone has already been widely investigated^{276,277} showing that stiffer constructs would lead to non-union²⁷⁸⁻²⁸¹. For spine fixations, fixation using rods and screws results in a decrease in the load on the vertebral level thus reducing the strain throughout the stabilized segment and leading to BMD loss^{282,283}. In this study, the effect of rod stiffness on the fusion process was further highlighted as the high value of BMD correlated to the forward bending tendency of the construct. The notion of implant deformation in-vivo due to upper body weight and motion is a well-known phenomenon however it has not been investigated priorly in lumbopelvic reconstruction surgeries²⁸⁴⁻²⁸⁶. The measurements completed in this

study could thus be used to measure the deformation of large constructs in other surgical procedures for scientific and clinical analysis. Regions of interest in the constructs where the highest deformation occurs would need to be identified to help in surgical planning and prevent implant failure.

In terms of mapping the bony fusion, the voxel-based method used in this study successfully created an FE mesh of the region of interest. The application of this method to a larger participant cohort would be desirable to assess the accuracy of the meshes for different pathologies. Currently, a gold standard approach to map bony fusion doesn't exist however, experts agree on the need to investigate the surgical case retrospectively over a long FU period (more than 2 years) using CT scans to better understand complex surgical problems.

We introduced the centrelines to avoid artefacts in the CT scans, even so, the resolution of the clinical CT affects the straightness of the centreline. In the future, after applying the method to a larger patient cohort, we plan to perform a curvature analysis methodologically similar to Hay et al.'s work ²⁸⁷, in which the centreline would be a technical advantage. Through this approach, FE models can be validated to assess the effect of the construct's stiffness on the process of bony fusion ²⁸⁸. Additionally, the data collected over the long FU period can be used for implant design, especially when associated with 3D printed patient-specific implants ²⁸⁹.

Concerning the limitation of this study, first, the method developed was only applied in the case of one patient however implementing it on a larger cohort would be of great interest. To measure implant deformation, the study only reported on the distance between the uppermost pedicle screw at L2 and the fixed iliac screw body to quantify the extent of implant deformation. Based on this measurement approach, distinguishing between the mechanical factors affecting the deformation is not possible (such as axial or shear load, sagittal or lateral bending and axial torsion). Finally, the retrospective nature of the study limited testing of the repeatability of the CT scans by repositioning the patient and thus measuring the accuracy of the BMD mapping and the implant deformation.

Conclusion

In conclusion, the current postsurgical assessment provided vital information regarding the biomechanics of the spine following sacrectomy and the closed loop reconstruction technique. Through this assessment, the extent of implant deformation following surgery was quantified. Using the voxel-based BMD mapping approach bony fusion at the surgical site was successfully described over the 6 years follow up period. Lastly, using gait analysis, the

patient's mobility following the surgery was measured to assess the ability of the CLT technique to withstand cyclic gait loading.

Conclusions

This PhD project provided insights on the use of various techniques to help surgeons plan and assess the outcome of spine surgeries.

The first part of the thesis focused on the use of stereophotogrammetric motion analysis to measure the kinematics of the spine. A review of the currently available protocols for spine motion analysis was first completed to investigate what is missing in the literature and why a gold standard for spine kinematics does not exist. The review assessed papers in terms of their reliability, suitability to be used in a clinical setting and the clinical significance of the outcome measurements reported. Subsequently, from the data collected in the review, a comprehensive protocol to measure multi-segmental kinematics was developed. The protocol suggested in this thesis was 1) assessed on its reliability, especially in terms of marker misplacement, 2) able to measure the multiple segments of the spine during activities of daily living and 3) able to provide data on the range of motion of spine segments and the coordination between segments. Through this protocol as well, a spine motion synchronisation technique was developed to limit the effect of the individuals' speed on the reported joint angles and was based on finding key events in the motion of the spine.

When applied in a clinical setting, the motion analysis protocol was indeed able to measure the motion of patients before and after surgery while also comparing the measurement to healthy controls. The protocol developed was found to be applicable in a clinical setting requiring minimal changes to conventional laboratory gait protocols, limiting the complexity of the marker setup, and providing comparable outcome measurement between groups.

Looking at the second technique investigated in this thesis, 3D printing of spine models was found to provide positive outcomes in terms of operation success, the confidence of the surgeon before starting the surgery and patient communication. Through haptic feedback, the surgeons were able to hold the printed anatomy in their hands to get a better idea of the optimal surgical correction needed. Using these computer-aided tools, surgeons were also able to simulate the vertebral osteotomy and assess the degree of correction required. The developed methodology was found to be applicable in a clinical setting especially as it uses FDM technology allowing for faster printing and limiting the cost of the printed anatomy.

Through FEA, the effect of auxiliary PEEK rods on the onset of PJK was assessed. From this investigation, we found that semi-rigid fixations of the spine do indeed increase the intervertebral rotations and decrease the stress in the vertebral and screw bodies, especially at

the UIV. PEEK allowed for the creation of a transition zone between the instrumented and non-instrumented segments of the spine. These results indicate that rod rigidity could be considered a risk factor for the onset of PJK. The developed methodology could be used in the future to model different thoracolumbar fixation techniques and could be used for patient-specific surgical planning.

In terms of surgical outcome assessment, different computer-based approaches were found to help provide a biomechanical evaluation of spine surgery. In particular, the methodology developed in this thesis was able to 1) map the bony fusion between spine and instrumentation and as such allow surgeons to confirm the success of the surgical fusion, 2) measure the extent of instrumentation deformation over the years to investigate the changes induced by the body load and chance of implant failure, 3) assess the mobility of the patient following such a complex surgery to confirm that the patient had minimal changes to their gait. The methodology developed could be used to assess the biomechanical effect of various complex spine surgeries and to improve spine reconstruction techniques.

In conclusion, this PhD provided various approaches to help surgeons in their decision-making process before surgery but also tools to assess surgical outcomes. All the techniques investigated were assessed on their reliability and their ease of use in a clinical setting. The results reported in this work could be a basis for future work to incorporate these techniques into the everyday clinical assessment of surgeons.

List of Figures

Figure 1 Posterior Spine fusion instrumentation showing an FSU with transpedicular screws and rods.	13
Figure 2 Patient with PJK requires 2 revision surgeries to address the mechanical complication	14
Figure 3 Sagittal spino-pelvic parameters.....	15
Figure 4 PRISMA flow chart representing the review process.	24
Figure 5 Quality Assessment Score of Articles included in the review.....	25
Figure 6 Quality Assessment Questionnaire.....	25
Figure 7 Steps needed for the fabrication of a 3D printed anatomical model of the heart.	51
Figure 8 FE model of the lumbar spine.....	55
Figure 9 Marker Setup on spine anatomical landmarks.....	61
Figure 10 Turning points identified in the UT/pelvis joint angle for each motion task.....	64
Figure 11 Joint angle curves between the segments defined and between the segments and the pelvis.....	69
Figure 12 Segment to Pelvis ROM in the sagittal plane during the standing and sitting tasks.	70
Figure 13 Percent Contribution of the UT/LT and UL/LL segments with the reference for the overall motion being the Shoulder/Pelvis joint. ¹⁸⁴	71
Figure 14 Differences in Ranges of motion between the two patient cohorts pre-surgery for all segments defined during Ball Pickup (A), Standing (B) and Sitting (C).	86
Figure 15 Peak motion timing values of the two patient cohorts pre-surgery for the standing and sitting tasks.	87
Figure 16 Changes in ROM before and after surgery for patients in the long fusion cohort for ball pickup, standing and sitting. (p=patient)	89
Figure 17 Changes in ROM before and after surgery for patients in the short fusion cohort for ball pickup, standing and sitting. (sfp=short fusion patient)	91
Figure 18 Spinal alignment evaluation.	101
Figure 19 Definition of virtual 3D geometry from CT scan.	102
Figure 20 Standing x-rays for spinal alignment evaluation	104
Figure 21 Supplementary Figure 1.....	107
Figure 22 Supplementary Figure 2.....	108
Figure 23 T7-L5 Modelling steps	112
Figure 24 Developed FE models in lateral and posterior view.....	115
Figure 25 Validation of IVR values of the developed Intact model compared to in-vitro values	117
Figure 26 IVR values of the RIGID and PEEK models under a 5Nm load.....	119
Figure 27 Maximum Von Mises stress values in screw bodies in the RIGID and PEEK models.	121
Figure 28 Stress distribution in the UIV of the RIGID and PEEK models.....	122
Figure 29 The Closed Loop reconstruction technique following en bloc sacrectomy.....	128
Figure 30 Preop MRI of the Chordoma tumour in the sagittal plane	130
Figure 31 Alignment of 1 st and 12 th CT scan.....	132
Figure 32 Simplified implant construct and deformation measurement.....	133
Figure 33 Time series Kinematics of the pelvis.....	135
Figure 34 Time series kinetics of the hip (A) and knee (B) during abduction/adduction.....	136
Figure 35 Joint powers during flexion-extension of the hip (A), knee (B), and ankle (C) in the sagittal plane.....	137
Figure 36 Map of the fusion and remodelling process at the ROI at the 7 days, 2 years, and 6 years FU.....	138

List of Tables

Table 1 Search Strings used on each database	21
Table 2 Quality Assessment questionnaire used to evaluate the quality of the studies included in the review.	21
Table 3 Standardised extraction form used to extract relevant information from the studies collected.....	22
Table 4 Characteristics of included studies as retrieved from the data extraction form.	26
Table 5 Characteristics of studies extracted from the literature search with marker setups adapted from papers in Table 4.....	29
Table 6 Study participants sample size and characteristics	33
Table 7 Range of Motion of the spine segments during the various tasks reported in the studies extracted.....	37
Table 8 Marker Setup.....	60
Table 9 Motion Capture Systems in the 3 laboratories used.....	62
Table 10 Segments of the spine defined	62
Table 11 TPs defined for each motion task from the first derivative of the joint angles.....	64
Table 12 Angle Distribution around the median of the intersegmental joints over the 3 ROM tasks between the 2 marker placement approaches. Significant differences are indicated with (*)	66
Table 13 Participant Characteristics	79
Table 14 Spinopelvic Parameters to evaluate spine parameters pre- and post-surgery of Long Fusion patients.....	83
Table 15 Spinopelvic Parameters to evaluate spine alignment pre- and post-surgery in Short Fusion Patients.....	84
Table 16 Percent Contributions of segments defined for both patient cohorts pre- and post-surgery and the control cohort for the three tasks completed.....	92
Table 17 Parameters for the evaluation of the spinal alignment pre and postoperatively.	103
Table 18 Components, element types and material properties of the developed model.....	113
Table 19 Gait Characteristics	134

Acronyms

PEEK: Polyetheretherketone	XP: Xiphoid Process
LBP: Low Back Pain	IJ: Clavicle
PSF: Posterior Spine Fusion	RASIS/LASIS: Right/Left Anterior Superior Iliac Spine
PJK: Proximal Junctional Kyphosis	RPSIS/LPSIS: Right/Left Posterior Superior Iliac Spine
CT: Computed Tomography	RTHI/LTHI: Right/Left Thigh
MRI: Magnetic Resonance Imaging	RTIB/LTIB: Right/Left Tibia
FE: Finite Element	RKNE/LKNE: Right/Left Knee
3D: Three Dimensional	RANK/LANK: Right/Left Ankle
ASD: Adult Spine Deformity	RTOE/LTOE: Right/Left Toe
ASF: Anterior Spine Fusion	RHEE/LHEE: Right/Left Heel
FSU: Functional Spine Unit	TP: Turning Point
UIV: Upper Instrumented Vertebra	STS: Sit-to-Stand
PI: Pelvic Incidence	ODI: Oswestry Disability Index
PT: Pelvic Tilt	VAS: Visual Analogue Scale
SS: Sacral Slope	FU: Follow-up
LL: Lumbar Lordosis	PSO: Pedicle Subtraction Osteotomy
TK: Thoracic Kyphosis	ILL: Ideal Lumbar Lordosis
SVA: Sagittal Vertical Alignment	TLIF: transforaminal lumbar interbody fusions
T1SPi: T1 Spinopelvic Inclination	STL: Stereolithography
T9SPi: T9 Spinopelvic Inclination	GAP: Global Alignment and Proportion
TPA: T1 Pelvic Angle	IVR: Intervertebral Rotation
T1S: T1 Slope	AF: Annulus Fibrosis
CSVL: Central Sacral Vertical Line	GS: Ground Substance
ROM: Range of Motion	ALL: Anterior Longitudinal Ligament
UT: Upper Thoracic	PLL: Posterior Longitudinal Ligament
LT: Lower Thoracic	FL: Flavum Ligament
UL: Upper Lumbar	CL: Capsular Ligament
LL: Lower Lumbar	ITL: Intratransverse Ligament
ADL: Activities of Daily Living	ISL: Intraspinous Ligament
CLBP: Chronic Low Back Pain	SSL: Supraspinous Ligament
AIS: Adolescent Idiopathic Scoliosis	CLT: Close Loop Technique
DDD: Disc Degeneration Disease	BMD: Bone Mass Density
CAD: Computer-Aided Design	OOT: Open Operating Theatre
FDM: Fused Deposition Modelling	GRF: Ground Reaction Forces
DLP: Digital Light Processing	BH: Body Height
SLS: Selective Laser Sintering	HD: Hausdorff Distance
DSI: Dice Similarity Index	QCT: Quantitative Computed Tomography
FEA: Finite Element Analysis	ICC: Intraclass Correlation
IDP: Intradiscal Pressure	
IVD: Intervertebral Disc	
SACR: Sacrum	

Acknowledgements

There are so many people that I'd like to thank for their contributions, help and support. First, I want to express my sincere gratitude to all of the participants that agreed to take part in this study. Without your help part of this thesis literally could never be completed.

Second, a huge thank you to everyone at the University of Bologna.

Luca, thank you for giving me the opportunity and for your patience during this whole PhD.

Rita, thank you for your constant guidance, help, and feedback.

To the biomechanics team in Bologna, you are a great group. Special thanks to Samuele, Edoardo, Valentina and Amy who made the last few months a blast.

To the Budapest team, I cannot thank you enough you really are a dream team.

To Peter, thank you for constantly being there, for your support, guidance, and nonstop push to make this thesis complete. Working with you was a great experience.

Thank you to Aron for all your help and support to make this project work.

My sincere gratitude goes to everyone at the In Silico biomechanics lab, Mate thank you for being a great colleague and for all the conversations and discussions in the office. Feri, I cannot thank you enough for becoming the most overqualified translator just so I could complete all the measurements. Agoston and Beni, thank you for the interesting talks, for being experts in so many software and for providing so much help. Finally, a huge thank you to Julia, who took so much care of me throughout my Budapest stay.

To the Spinner team, I cannot express my thanks enough. These bi-monthly meetings we had were a safe space to talk, complain and support each other. Chloe, Cameron, Denata, Marco and Jose thank you for always being there and I wish we could have met more in person.

To Chloe, I don't know where to start. Through these 3 years, I gained a friend, not just a colleague who was always there to listen and give advice. We only lived in the same city for a few months at a time, but this only made our friendship tighter.

Finally, to my friends and family, I couldn't have finished this work without your support. To my parents, thank you for always being there. To Joe, thank you for answering any question I had, giving amazing advice and for hopping on a plane whenever I moved to a new city. To Eliane, Christy and Remi, you've helped me so much these last 3 years, listened to any frustration I had and proofread all of my writings. To Jon who visited me any chance he had. To Gemini, Tonia, Noha, Jason, Kevin, Nandini thank you for being an amazing group that I call friends.

Bibliography

1. Reid PC, Morr S, Kaiser MG. State of the union: A review of lumbar fusion indications and techniques for degenerative spine disease. *J Neurosurg Spine*. 2019;31(1):1-14. doi:10.3171/2019.4.SPINE18915
2. Cerpa M, Sardar Z, Lenke L. Revision surgery in proximal junctional kyphosis. *Eur Spine J*. 2020;29(s1):78-85. doi:10.1007/s00586-020-06320-y
3. Jia F, Wang G, Liu X, Li T, Sun J. Comparison of long fusion terminating at L5 versus the sacrum in treating adult spinal deformity: a meta-analysis. *Eur Spine J*. 2020;29(1):24-35. doi:10.1007/s00586-019-06187-8
4. Fekete TF, Loibl M, Jeszenszky D, et al. How does patient-rated outcome change over time following the surgical treatment of degenerative disorders of the thoracolumbar spine? *Eur Spine J*. 2018;27(3):700-708. doi:10.1007/s00586-017-5358-2
5. Jacobs WCH, Rubinstein SM, Koes B, Van Tulder MW, Peul WC. Evidence for surgery in degenerative lumbar spine disorders. *Best Pract Res Clin Rheumatol*. 2013;27(5):673-684. doi:10.1016/j.berh.2013.09.009
6. Meyer B, Rauschmann M. *Spine Surgery*. (Meyer B, Rauschmann M, eds.). Springer International Publishing; 2019. doi:10.1007/978-3-319-98875-7
7. Buser Z, Ortega B, D'Oro A, et al. Spine Degenerative Conditions and Their Treatments: National Trends in the United States of America. *Glob Spine J*. 2018;8(1):57-67. doi:10.1177/2192568217696688
8. Deyo RA, Nachmesonn A, Mirza SK. Spinal Fusion Sugery-The case for Restraint. *J Bone Jt Surg Am Vol*. 2004;4:138-142.
9. Lee J, Park Y-S. Proximal Junctional Kyphosis: Diagnosis, Pathogenesis, and Treatment. *Asian Spine J*. 2016;10(3):593-600. doi:10.4184/asj.2016.10.3.593
10. Glattes RC, Bridwell KH, Lenke LG, Kim YJ, Rinella A, Edwards C. Proximal Junctional Kyphosis in Adult Spinal Deformity Following Long Instrumented Posterior Spinal Fusion. *Spine (Phila Pa 1976)*. 2005;30(14):1643-1649. doi:10.1097/01.brs.0000169451.76359.49
11. Iyer S, Lovecchio F, Elysée JC, et al. Posterior Ligamentous Reinforcement of the Upper Instrumented Vertebrae +1 Does Not Decrease Proximal Junctional Kyphosis in Adult Spinal Deformity. *Glob Spine J*. 2020;10(6):692-699. doi:10.1177/2192568219868472

12. Decker S, Lafage R, Krettek C, et al. Is sacral extension a risk factor for early proximal junctional kyphosis in adult spinal deformity surgery? *Asian Spine J.* 2020;14(2):212-219. doi:10.31616/ASJ.2018.0314
13. Diebo BG, Shah N V., Stroud SG, Paulino CB, Schwab FJ, Lafage V. Realignment surgery in adult spinal deformity. *Orthopade.* 2018;(February):301-309. doi:10.1007/s00132-018-3536-5
14. Bess S, Harris JE, Turner AWL, et al. The effect of posterior polyester tethers on the biomechanics of proximal junctional kyphosis: a finite element analysis. *J Neurosurg Spine.* 2017;26(1):125-133. doi:10.3171/2016.6.SPINE151477
15. Pigge RR, Scheerder FJ, Smit TH, Mullender MG, van Royen BJ. Effectiveness of preoperative planning in the restoration of balance and view in ankylosing spondylitis. *Neurosurg Focus.* 2008;24(1):1-5. doi:10.3171/FOC/2008/24/1/E7
16. El Rahal A, Solla F, Fiere V, Toquart A, Barrey CY. Sagittal Balance and Preoperative Planning. In: Meyer B, Rauschmann M, eds. *Spine Surgery: A Case-Based Approach.* Springer International Publishing; 2019:447-458. doi:10.1007/978-3-319-98875-7_54
17. Harada GK, Siyaji ZK, Younis S, Louie PK, Samartzis D, An HS. Imaging in Spine Surgery: Current Concepts and Future Directions. *Spine Surg Relat Res.* 2020;4(2):99-110. doi:10.22603/ssrr.2020-0011
18. Diebo BG, Shah N V., Pivec R, et al. From static spinal alignment to dynamic body balance: Utilizing motion analysis in spinal deformity surgery. *JBJS Rev.* 2018;6(7):1-12. doi:10.2106/JBJS.RVW.17.00189
19. Diebo BG, Shah N V, Boachie-Adjei O, et al. Adult spinal deformity. *Lancet.* 2019;394(10193):160-172. doi:10.1016/S0140-6736(19)31125-0
20. Gombatto SP, Brock T, DeLork A, Jones G, Madden E, Rinere C. Lumbar spine kinematics during walking in people with and people without low back pain. *Gait Posture.* 2015;42(4):539-544. doi:10.1016/j.gaitpost.2015.08.010
21. Mitchell K, Porter M, Anderson L, et al. Differences in lumbar spine and lower extremity kinematics in people with and without low back pain during a step-up task: A cross-sectional study. *BMC Musculoskelet Disord.* 2017;18(1):1-9. doi:10.1186/s12891-017-1721-z
22. Haddas R, Ju KL, Belanger T, Lieberman IH. The use of gait analysis in the assessment of patients afflicted with spinal disorders. *Eur Spine J.* Published online 2018. doi:10.1007/s00586-018-5569-1
23. Ignasiak D, Rüeger A, Ferguson SJ. Multi-segmental thoracic spine kinematics

- measured dynamically in the young and elderly during flexion. *Hum Mov Sci.* 2017;54(September 2016):230-239. doi:10.1016/j.humov.2017.05.011
24. Pelegrinelli ARM, Silva MF, Guenka LC, Carrasco AC, Moura FA, Cardoso JR. Low back pain affects coordination between the trunk segments but not variability during running. *J Biomech.* 2020;101:109605. doi:10.1016/j.jbiomech.2020.109605
 25. Mason DL, Preece SJ, Bramah CA, Herrington LC. Reproducibility of kinematic measures of the thoracic spine, lumbar spine and pelvis during fast running. *Gait Posture.* 2014;43:96-100. doi:10.1016/j.gaitpost.2013.11.007
 26. Negrini S, Piovanelli B, Amici C, Cappellini V. Trunk motion analysis: a systematic review from a clinical and methodological perspective. *Eur J Phys Rehabil Med.* 2016;52(4):3-5.
 27. Potter BK, Lenke LG, Kuklo TR. Prevention and Management of Iatrogenic Flatback Deformity. *JBJS.* 2004;86(8).
https://journals.lww.com/jbjsjournal/Fulltext/2004/08000/Prevention_and_Management_of_Iatrogenic_Flatback.27.aspx
 28. Fayad J, Turbucz M, Hajnal B, et al. Complicated Postoperative Flat Back Deformity Correction With the Aid of Virtual and 3D Printed Anatomical Models: Case Report. *Front Surg.* 2021;8(May):1-7. doi:10.3389/fsurg.2021.662919
 29. Eltes PE, Kiss L, Bartos M, et al. Geometrical accuracy evaluation of an affordable 3D printing technology for spine physical models. *J Clin Neurosci.* 2020;72:438-446. doi:10.1016/j.jocn.2019.12.027
 30. Yagi M, Nakahira Y, Watanabe K, Nakamura M, Matsumoto M, Iwamoto M. The effect of posterior tethers on the biomechanics of proximal junctional kyphosis: The whole human finite element model analysis. *Sci Rep.* 2020;10(1):1-8. doi:10.1038/s41598-020-59179-w
 31. Cahill PJ, Wang W, Asghar J, et al. The use of a transition rod may prevent proximal junctional kyphosis in the thoracic spine after scoliosis surgery: A finite element analysis. *Spine (Phila Pa 1976).* 2012;37(12):687-695. doi:10.1097/BRS.0b013e318246d4f2
 32. M.a. T, V. B, P.E. M, D. O. Generation of a finite element model of the thoracolumbar spine. *Acta Bioeng Biomech.* 2007;9(1):35-46.
<http://ovidsp.ovid.com/ovidweb.cgi?T=JS&PAGE=reference&D=emed8&NEWS=N&AN=2008045577>
 33. Aebi M, Gunzburg R, Szpalski M. The Aging Spine. In: Aebi M, Gunzburg R,

- Szpalski M, eds. *European Spine Journal*. Springer Berlin Heidelberg; 2003.
doi:10.1007/b139015
34. Sato M, Sainoh T, Orita S, et al. Posterior and Anterior Spinal Fusion for the Management of Deformities in Patients with Parkinson's Disease. *Case Rep Orthop*. 2013;2013:1-6. doi:10.1155/2013/140916
 35. Allegri M, Montella S, Salici F, et al. Mechanisms of low back pain: a guide for diagnosis and therapy. *F1000Research*. 2016;5:1530.
doi:10.12688/f1000research.8105.2
 36. Koes BW, van Tulder MW, Thomas S. Diagnosis and treatment of low back pain. *BMJ*. 2006;332(7555):1430-1434. doi:10.1136/bmj.332.7555.1430
 37. Barreto TW, Lin KW. Noninvasive Treatments for Low Back Pain. *Am Fam Physician*. 2017;96(5):324-327.
 38. Youssef JA, Orndorff DO, Patty CA, et al. Current Status of Adult Spinal Deformity. *Glob Spine J*. 2013;3(1):051-062. doi:10.1055/s-0032-1326950
 39. Deyo RA, Mirza SK, Martin BI, Kreuter W, Goodman DC, Jarvik JG. Trends, major Medical complications, and charges associated with surgery for lumbar spinal stenosis in older adults. *JAMA - J Am Med Assoc*. 2010;303(13):1259-1265.
doi:10.1001/jama.2010.338
 40. Phan K, Xu J, Maharaj MM, et al. Outcomes of Short Fusion versus Long Fusion for Adult Degenerative Scoliosis: A Systematic Review and Meta-analysis. *Orthop Surg*. 2017;9(4):342-349. doi:10.1111/os.12357
 41. Ghandhari H, Ameri E, Nikouei F, Haji Agha Bozorgi M, Majdi S, Salehpour M. Long-term outcome of posterior spinal fusion for the correction of adolescent idiopathic scoliosis. *Scoliosis Spinal Disord*. 2018;13(1):10-14. doi:10.1186/s13013-018-0157-z
 42. Deniz Olgun Z, Yazici M. Posterior instrumentation and fusion. *J Child Orthop*. 2013;7(1):69-76. doi:10.1007/s11832-012-0456-5
 43. Frymoyer JW. Low back pain. The role of spine fusion. *Neurosurg Clin N Am*. 1991;2(4):933-954. doi:10.1016/S1042-3680(18)30711-3
 44. Ferrara LA, Secor JL, Jin BH, Wakefield A, Inceoglu S, Benzel EC. A biomechanical comparison of facet screw fixation and pedicle screw fixation: Effects of short-term and long-term repetitive cycling. *Spine (Phila Pa 1976)*. 2003;28(12):1226-1234.
doi:10.1097/00007632-200306150-00005
 45. Wang Y, Fei Q, Qiu G, et al. Anterior spinal fusion versus posterior spinal fusion for

- moderate lumbar/thoracolumbar adolescent idiopathic scoliosis: a prospective study. *Spine (Phila Pa 1976)*. 2008;33(20):2166-2172. doi:10.1097/BRS.0b013e318185798d
46. Daniels CJ, Wakefield PJ, Bub GA, Toombs JD. A Narrative Review of Lumbar Fusion Surgery With Relevance to Chiropractic Practice. *J Chiropr Med*. 2016;15(4):259-271. doi:10.1016/j.jcm.2016.08.007
 47. Kim HJ, York PJ, Elysee JC, et al. Cervical, Thoracic, and Spinopelvic Compensation After Proximal Junctional Kyphosis (PJK): Does Location of PJK Matter? *Glob Spine J*. 2020;10(1):6-12. doi:10.1177/2192568219879085
 48. Nguyen N-LM, Kong CY, Hart RA. Proximal junctional kyphosis and failure—diagnosis, prevention, and treatment. *Curr Rev Musculoskelet Med*. 2016;9(3):299-308. doi:10.1007/s12178-016-9353-8
 49. Lafage R, Ferrero E, Henry JK, et al. Validation of a new computer-assisted tool to measure spino-pelvic parameters. *Spine J*. 2015;15(12):2493-2502. doi:10.1016/j.spinee.2015.08.067
 50. Kondo R, Yamato Y, Nagafusa T, et al. Effect of corrective long spinal fusion to the ilium on physical function in patients with adult spinal deformity. *Eur Spine J*. 2017;26(8):2138-2145. doi:10.1007/s00586-017-4987-9
 51. Elsig JPJ, Kaech DL. Imaging-based planning for spine surgery. *Minim Invasive Ther Allied Technol*. 2006;15(5):260-266. doi:10.1080/13645700600958457
 52. Lopez CD, Boddapati V, Lee NJ, et al. Three-Dimensional Printing for Preoperative Planning and Pedicle Screw Placement in Adult Spinal Deformity: A Systematic Review. *Glob Spine J*. Published online 2020. doi:10.1177/2192568220944170
 53. Dagdia L, Kokabu T, Ito M. Classification of adult spinal deformity: Review of current concepts and future directions. *Spine Surg Relat Res*. 2019;3(1):17-26. doi:10.22603/ssrr.2017-0100
 54. Hoy D, March L, Brooks P, et al. The global burden of low back pain: Estimates from the Global Burden of Disease 2010 study. *Ann Rheum Dis*. 2014;73(6):968-974. doi:10.1136/annrheumdis-2013-204428
 55. Wu A, March L, Zheng X, et al. Global low back pain prevalence and years lived with disability from 1990 to 2017: estimates from the Global Burden of Disease Study 2017. *Ann Transl Med*. 2020;8(6):299-299. doi:10.21037/atm.2020.02.175
 56. Schwab F, Dubey A, Gamez L, et al. Adult scoliosis: Prevalence, SF-36, and nutritional parameters in an elderly volunteer population. *Spine (Phila Pa 1976)*. 2005;30(9):1082-1085. doi:10.1097/01.brs.0000160842.43482.cd

57. Barreto MVA, De Rezende Pratali R, Barsotti CEG, Dos Santos FPE, De Oliveira CEAS, Nogueira MP. Incidence of spinal deformity in adults and its distribution according srs-schwab classification. *Coluna/ Columna*. 2015;14(2):93-96. doi:10.1590/S1808-185120151402147624
58. Daniell JR, Osti OL. Failed back surgery syndrome: A review article. *Asian Spine J*. 2018;12(2):372-379. doi:10.4184/asj.2018.12.2.372
59. Christe G, Redhead L, Legrand T, Jolles BM, Favre J. Multi-segment analysis of spinal kinematics during sit-to-stand in patients with chronic low back pain. *J Biomech*. 2016;49(10):2060-2067. doi:10.1016/j.jbiomech.2016.05.015
60. Christe G, Rochat V, Jolles BM, Favre J. Lumbar and thoracic kinematics during step-up: Comparison of three-dimensional angles between patients with chronic low back pain and asymptomatic individuals. *J Orthop Res*. 2020;38(6):1248-1256. doi:10.1002/jor.24575
61. Miura K, Kadone H, Koda M, et al. Thoracic kyphosis and pelvic anteversion in patients with adult spinal deformity increase while walking: analyses of dynamic alignment change using a three-dimensional gait motion analysis system. *Eur Spine J*. 2020;29(4):840-848. doi:10.1007/s00586-020-06312-y
62. Hidalgo B, Gilliaux M, Poncin W, Detrembleur C. Reliability and validity of a kinematic spine model during active trunk movement in healthy subjects and patients with chronic non-specific low back pain. *J Rehabil Med*. 2012;44(9):756-763. doi:10.2340/16501977-1015
63. Pumberger M, Schmidt H, Putzier M. Spinal Deformity Surgery: A Critical review of Alignment and Balance. *Asian Spine J*. 2018;12(4):775-783.
64. Wong KWN, Luk KDK, Leong JCY, Wong SF, Wong KKY. Continuous dynamic spinal motion analysis. *Spine (Phila Pa 1976)*. 2006;31(4):414-419. doi:10.1097/01.brs.0000199955.87517.82
65. Balkovec C, Veldhuis JH, Baird JW, Brodland GW, McGill SM. A videofluoroscopy-based tracking algorithm for quantifying the time course of human intervertebral displacements. *Comput Methods Biomech Biomed Engin*. 2017;20(7):794-802. doi:10.1080/10255842.2017.1302435
66. Mellor FE, Thomas P, Breen A. Moving back: The radiation dose received from lumbar spine quantitative fluoroscopy compared to lumbar spine radiographs with suggestions for dose reduction. *Radiography*. 2014;20(3):251-257. doi:10.1016/j.radi.2014.03.010

67. Hadelsberg UP, Harel R. Hazards of Ionizing Radiation and its Impact on Spine Surgery. *World Neurosurg.* 2016;92:353-359.
doi:<https://doi.org/10.1016/j.wneu.2016.05.025>
68. Lee S, Wong KWN, Chan M, Yeung H, Chiu JLF, Leong JCY. Development and validation of a new technique for assessing lumbar spine motion. *Spine (Phila Pa 1976).* 2002;27(8):E215-20.
69. Leardini A, Biagi F, Belvedere C, Benedetti MG. Quantitative comparison of current models for trunk motion in human movement analysis. *Clin Biomech.* 2009;24(7):542-550. doi:10.1016/j.clinbiomech.2009.05.005
70. Leardini A, Biagi F, Merlo A, Belvedere C, Grazia M, Benedetti MG. Multi-segment trunk kinematics during locomotion and elementary exercises. *Clin Biomech.* 2011;26(6):562-571. doi:10.1016/j.clinbiomech.2011.01.015
71. Needham R, Stebbins J, Chockalingam N. Three-dimensional kinematics of the lumbar spine during gait using marker-based systems: A systematic review. *J Med Eng Technol.* 2016;40(4):172-185. doi:10.3109/03091902.2016.1154616
72. Needham R, Naemi R, Healy A, Chockalingam N. Multi-segment kinematic model to assess three-dimensional movement of the spine and back during gait. *Prosthet Orthot Int.* Published online 2015:1-12. doi:10.1177/0309364615579319
73. Baker R, Esquenazi A, Benedetti MG, Desloovere K. Gait analysis: clinical facts. *Eur J Phys Rehabil Med.* 2016;52(4):560-574.
<http://www.ncbi.nlm.nih.gov/pubmed/27618499>
74. Ferrari A, Benedetti MG, Pavan E, et al. Quantitative comparison of five current protocols in gait analysis. *Gait Posture.* 2008;28(2):207-216.
doi:10.1016/j.gaitpost.2007.11.009
75. Wu G, Helm FCT Van Der, Veeger HEJD, et al. ISB recommendation on definitions of joint coordinate systems of various joints for the reporting of human joint motion — Part II : shoulder , elbow , wrist and hand. 2005;38:981-992.
doi:10.1016/j.jbiomech.2004.05.042
76. Papi E, Bull AMJ, McGregor AH. Is there evidence to use kinematic/kinetic measures clinically in low back pain patients? A systematic review. *Clin Biomech.* 2018;55(April):53-64. doi:10.1016/j.clinbiomech.2018.04.006
77. Intolo P, Milosavljevic S, Baxter DG, Carman AB, Pal P, Munn J. The effect of age on lumbar range of motion: A systematic review. *Man Ther.* 2009;14(6):596-604.
doi:10.1016/j.math.2009.08.006

78. Pourahmadi MR, Ebrahimi Takamjani I, Jaberzadeh S, et al. Kinematics of the Spine During Sit-to-Stand Movement Using Motion Analysis Systems: A Systematic Review of Literature. *J Sport Rehabil.* 2019;28(1):77-93. doi:10.1123/jsr.2017-0147
79. Maaswinkel E, Griffioen M, Perez RSGM, van Dieën JH. Methods for assessment of trunk stabilization, a systematic review. *J Electromyogr Kinesiol.* 2016;26:18-35. doi:https://doi.org/10.1016/j.jelekin.2015.12.010
80. Page MJ, McKenzie JE, Bossuyt PM, et al. The PRISMA 2020 statement: An updated guideline for reporting systematic reviews. *PLOS Med.* 2021;18(3):e1003583. doi:10.1371/journal.pmed.1003583
81. Bishop C, Paul G, Thewlis D. Recommendations for the reporting of foot and ankle models. *J Biomech.* 2012;45(13):2185-2194. doi:10.1016/j.jbiomech.2012.06.019
82. Severijns P, Overbergh T, Thauvoye A, et al. A subject-specific method to measure dynamic spinal alignment in adult spinal deformity. *Spine J.* 2020;20(6):934-946. doi:10.1016/j.spinee.2020.02.004
83. Seerden SFL, Dankaerts W, Swinnen TW, Westhovens R, De Vlam K, Vanwanseele B. Differences in multi-segmental spine kinematics between patients with different stages of axial spondyloarthritis and healthy controls. *Musculoskelet Sci Pract.* 2021;53(April 2020):102368. doi:10.1016/j.msksp.2021.102368
84. Al-eisa E, Egan D, Deluzio K, Wassersug R. Effects of Pelvic Asymmetry and Low Back Pain on Trunk Kinematics During Sitting : A Comparison With Standing. 2006;31(5):135-143.
85. Christe G, Kade F, Jolles BM, Favre J. Chronic low back pain patients walk with locally altered spinal kinematics. *J Biomech.* 2017;60:211-218. doi:10.1016/j.jbiomech.2017.06.042
86. Gombatto SP, Arpa ND, Landerholm S, et al. Differences in kinematics of the lumbar spine and lower extremities between people with and without low back pain during the down phase of a pick up task , an observational study. *Musculoskelet Sci Pract.* 2017;28:25-31. doi:10.1016/j.msksp.2016.12.017
87. Hemming R. Non-specific chronic low back pain : differences in spinal kinematics in subgroups during functional tasks. *Eur Spine J.* 2018;27(1):163-170. doi:10.1007/s00586-017-5217-1
88. Hernandez A, Gross K, Gombatto S. Clinical Biomechanics Differences in lumbar spine and lower extremity kinematics during a step down functional task in people with and people without low back pain. *Clin Biomech.* 2017;47(June 2016):46-52.

- doi:10.1016/j.clinbiomech.2017.05.012
89. Kuwahara W, Deie M, Fujita N, et al. Characteristics of thoracic and lumbar movements during gait in lumbar spinal stenosis patients before and after decompression surgery. *Clin Biomech.* 2016;40:45-51.
doi:10.1016/j.clinbiomech.2016.10.016
 90. Schmid S, Studer D, Hasler CC, et al. Quantifying spinal gait kinematics using an enhanced optical motion capture approach in adolescent idiopathic scoliosis. *Gait Posture.* 2016;44:231-237. doi:10.1016/j.gaitpost.2015.12.036
 91. Crosbie J, Vachalathiti R, Smith R. Patterns of spinal motion during walking. *Gait Posture.* 1997;5(1):6-12. doi:10.1016/S0966-6362(96)01066-1
 92. Deane JA, Papi E, Phillips ATM, McGregor AH. Reliability and minimal detectable change of the 'Imperial Spine' marker set for the evaluation of spinal and lower limb kinematics in adults. *BMC Res Notes.* 2020;13(1):1-8. doi:10.1186/s13104-020-05295-9
 93. Frigo C, Carabalon R, Dalla Mura M, et al. The upper body segmental movements during walking by young females. *Clin Biomech (Bristol, Avon).* 2003;18(5):419-425. doi:10.1016/S0268-0033(03)00028-7
 94. Gilleard WL. Trunk motion and gait characteristics of pregnant women when walking: Report of a longitudinal study with a control group. *BMC Pregnancy Childbirth.* 2013;13:71. doi:10.1186/1471-2393-13-71
 95. Holewijn RM, Kingma I, de Kleuver M, Keijsers NLW. Posterior spinal surgery for adolescent idiopathic scoliosis does not induce compensatory increases in distal adjacent segment motion: a prospective gait analysis study. *Spine J.* 2018;0031. doi:10.1016/j.spinee.2018.05.010
 96. Ignasiak D, Rüeger A, Sperr R, Ferguson SJ. Thoracolumbar spine loading associated with kinematics of the young and the elderly during activities of daily living. *J Biomech.* 2018;70:175-184. doi:10.1016/j.jbiomech.2017.11.033
 97. Kakar RS, Li Y, Brown CN, Oswald TS, Simpson KJ. Spine and Lower Extremity Kinematics Exhibited During Running by Adolescent Idiopathic Scoliosis Patients With Spinal Fusion. *Spine Deform.* 2019;7(2):254-261. doi:10.1016/j.jspd.2018.08.015
 98. Konz RJ, Fatone S, Stine RL, Ganju A, Gard SA, Ondra SL. A kinematic model to assess spinal motion during walking. *Spine (Phila Pa 1976).* 2006;31(24):E898-906. doi:10.1097/01.brs.0000245939.97637.ae
 99. Kuai S, Guan X, Zhou W, et al. Continuous lumbar spine rhythms during level

- walking, stair climbing and trunk flexion in people with and without lumbar disc herniation. *Gait Posture*. 2018;63(May):296-301. doi:10.1016/j.gaitpost.2018.05.006
100. Lin H, Seerden S, Zhang X, Fu W, Vanwanseele B. Inter-segmental coordination of the spine is altered during lifting in patients with ankylosing spondylitis A cross-sectional study. *Med (United States)*. 2020;99(5). doi:10.1097/MD.00000000000018941
 101. List R, Gülay T, Stoop M, Lorenzetti S. Kinematics of the Trunk and the Lower During Restricted and Unrestricted Squats. *J Strength Cond Res*. 2013;27(6):1529-1538.
 102. Müller J, Müller S, Engel T, Reschke A, Baur H, Mayer F. Stumbling reactions during perturbed walking: Neuromuscular reflex activity and 3-D kinematics of the trunk - A pilot study. *J Biomech*. 2016;49(6):933-938. doi:10.1016/j.jbiomech.2015.09.041
 103. Noamani A, Vette AH, Preuss R, Popovic MR, Rouhani H. Quantification of multi-segment trunk kinetics during multi-directional trunk bending. *Gait Posture*. 2018;64(June):205-212. doi:10.1016/j.gaitpost.2018.06.027
 104. Papi E, Bull AMJ, McGregor AH. Spinal segments do not move together predictably during daily activities. *Gait Posture*. 2019;67(July 2018):277-283. doi:10.1016/j.gaitpost.2018.10.031
 105. Papi E, Bull AMJ, McGregor AH. Alteration of movement patterns in low back pain assessed by Statistical Parametric Mapping. *J Biomech*. 2020;100:109597. doi:10.1016/j.jbiomech.2019.109597
 106. Patel A, Pivec R, Shah N V., et al. Motion analysis in the axial plane after realignment surgery for adolescent idiopathic scoliosis. *Gait Posture*. 2018;66(August):181-188. doi:10.1016/j.gaitpost.2018.08.015
 107. Pesenti S, Prost S, Pomero V, et al. Does static trunk motion analysis reflect its true position during daily activities in adolescent with idiopathic scoliosis? *Orthop Traumatol Surg Res*. Published online 2020. doi:10.1016/j.otsr.2019.12.023
 108. Pollock R, Heneghan P, Riches PE. Under-arm partial body weight unloading causes spinal elongation and vibration attenuation during treadmill walking. *Gait Posture*. 2008;28(2):271-277. doi:10.1016/j.gaitpost.2007.12.074
 109. Preuss RA, Popovic MR. Three-dimensional spine kinematics during multidirectional , target-directed trunk movement in sitting. *J Electromyogr Kinesiol*. 2010;20(5):823-832. doi:10.1016/j.jelekin.2009.07.005
 110. Rouhani H, Mahallati S, Preuss R, Masani K, Popovic MR. Sensitivity of Intersegmental Angles of the Spinal Column to Errors Due to Marker Misplacement. *J*

- Biomech Eng.* 2015;137(7). doi:10.1115/1.4030406
111. Rozumalski A, Schwartz MH, Wervey R, Swanson A, Dykes DC, Novacheck T. The in vivo three-dimensional motion of the human lumbar spine during gait. *Gait Posture.* 2008;28(3):378-384. doi:10.1016/j.gaitpost.2008.05.005
 112. Ryan N, Bruno P. Analysis of 3D multi-segment lumbar spine motion during gait and prone hip extension. *J Electromyogr Kinesiol.* 2017;33:111-117. doi:10.1016/j.jelekin.2017.02.005
 113. Saad WAA, Mat Dzahir MA, Yamamoto S, et al. Differences of spinal kinematics contribution between cervical and multi-segmental thoracic spine during Sit-To-Stand (STS) & Stand-To-Flexion (STF). *IOP Conf Ser Mater Sci Eng.* 2020;788(1). doi:10.1088/1757-899X/788/1/012026
 114. Sayers MGL, Bachem C, Schütz P, et al. The effect of elevating the heels on spinal kinematics and kinetics during the back squat in trained and novice weight trainers. *J Sports Sci.* 2020;38(9):1000-1008. doi:10.1080/02640414.2020.1738675
 115. Schinkel-ivy A, Drake JDM. Which motion segments are required to sufficiently characterize the kinematic behavior of the trunk? *J Electromyogr Kinesiol.* 2015;25(2):239-246. doi:10.1016/j.jelekin.2014.12.008
 116. Schmid S, Studer D, Hasler CC, et al. Using skin markers for spinal curvature quantification in main thoracic adolescent idiopathic scoliosis: An explorative radiographic study. *PLoS One.* 2015;10(8):1-12. doi:10.1371/journal.pone.0135689
 117. Seay J, Selbie WS, Hamill J. In vivo lumbo-sacral forces and moments during constant speed running at different stride lengths. 2008;(October 2014):37-41. doi:10.1080/02640410802298235
 118. Seerden SFL, Dankaerts W, Swinnen TW, Westhovens R, de Vlam K, Vanwanseele B. Multi-segment spine and hip kinematics in asymptomatic individuals during standardized return from forward bending versus functional box lifting. *J Electromyogr Kinesiol.* 2019;49(August):102352. doi:10.1016/j.jelekin.2019.102352
 119. Simonet E, Winteler B, Frangi J, et al. Walking and running with non-specific chronic low back pain: What about the lumbar lordosis angle? *J Biomech.* 2020;108:109883. doi:10.1016/j.jbiomech.2020.109883
 120. Stoll J, Rector M, Baur H, et al. Influence of load on three-dimensional segmental trunk kinematics in one-handed lifting: A pilot study. *J Appl Biomech.* 2016;32(5):520-525. doi:10.1123/jab.2015-0227
 121. Sung PS, Danial P, Lee DC. Comparison of the different kinematic patterns during

- lateral bending between subjects with and without recurrent low back pain. *Clin Biomech.* 2016;38:50-55. doi:10.1016/j.clinbiomech.2016.08.006
122. Sung PS, Park MS. Lumbar spine coordination during axial trunk rotation in adolescents with and without right thoracic idiopathic scoliosis. *Hum Mov Sci.* 2020;73(September):102680. doi:10.1016/j.humov.2020.102680
 123. Swain CTV V, Whyte DG, Ekegren CL, et al. Multi-segment spine kinematics: relationship with dance training and low back pain. *Gait Posture.* 2018;68:274-279. doi:10.1016/j.gaitpost.2018.12.001
 124. Tojima M, Ogata N, Yozu A, Sumitani M, Haga N. Novel 3-Dimensional Motion Analysis Method for Measuring the Lumbar Spine Range of Motion. *Spine (Phila Pa 1976).* 2013;38(21):E1327-E1333. doi:10.1097/BRS.0b013e3182a0dbc5
 125. Wilk B, Karol LA, Johnston II CE, et al. The effect of scoliosis fusion on spinal motion: A comparison of fused and nonfused patients with idiopathic scoliosis. *Spine (Phila Pa 1976).* 2006;31(3):309-314. doi:10.1097/01.brs.0000197168.11815.ec
 126. Zwambag DP, Beaudette SM, Gregory DE, Brown SHM. Development of a Novel Technique to Record 3D Intersegmental Angular Kinematics During Dynamic Spine Movements. *Ann Biomed Eng.* 2018;46(2):298-309. doi:10.1007/s10439-017-1970-x
 127. Preece SJ, Bramah C, Mason D. A marker set for measuring the kinematics of the lumbar spine and thoracic spine during running: a technical note. *J Hum Sport Exerc.* 2016;11(3):390-396. doi:10.14198/jhse.2016.113.07
 128. Ghasemi M, Arjmand N. Spinal segment ranges of motion, movement coordination, and three-dimensional kinematics during occupational activities in normal-weight and obese individuals. *J Biomech.* 2021;123:110539. doi:10.1016/j.jbiomech.2021.110539
 129. Glover NA, Kakar RS, Chaudhari AMW. Effects of spinal coupling and marker set on tracking of spine models during running. *J Biomech.* 2021;116:110217. doi:10.1016/j.jbiomech.2020.110217
 130. Alijanpour E, Abbasi A, Needham RA, Naemi R. Spine and pelvis coordination variability in rowers with and without chronic low back pain during rowing. *J Biomech.* 2021;120:110356. doi:10.1016/j.jbiomech.2021.110356
 131. Arshad R, Angelini L, Zander T, Di Puccio F, El-Rich M, Schmidt H. Spinal loads and trunk muscles forces during level walking – A combined in vivo and in silico study on six subjects. *J Biomech.* 2018;70:113-123. doi:10.1016/j.jbiomech.2017.08.020
 132. Hagins M, Swain CTV, Orishimo KF, Kremenic IJ, Liederbach M. Motion of the multi-segmented spine in elite dancers during passé and arabesque. *Gait Posture.*

- 2021;88(June):198-202. doi:10.1016/j.gaitpost.2021.05.032
133. Niggli LA, Eichelberger P, Bangerter C, Baur H, Schmid S. Between-session reliability of skin marker-derived spinal kinematics during functional activities. *Gait Posture*. 2021;85(February):280-284. doi:10.1016/j.gaitpost.2021.02.008
 134. Beaudette SM, Zwambag DP, Graham RB, Brown SHM. Discriminating spatiotemporal movement strategies during spine flexion-extension in healthy individuals. *Spine J*. 2019;19(7):1264-1275. doi:10.1016/j.spinee.2019.02.002
 135. Breloff SP, Chou L-S. a Multi-Segmented Approach To the Quantification of Trunk Movement During Gait. *J Musculoskelet Res*. 2015;18(02):1550009. doi:10.1142/S0218957715500098
 136. Choi AR, Kim YJ, Rim YH, et al. Development of a spine kinematic model for the clinical estimation of abnormal curvature. *IFMBE Proc*. 2007;14:2892-2895.
 137. Claus AP, Hides JA, Moseley GL, Hodges PW. Thoracic and lumbar posture behaviour in sitting tasks and standing: Progressing the biomechanics from observations to measurements. *Appl Ergon*. 2016;53:161-168. doi:10.1016/j.apergo.2015.09.006
 138. Sugaya T, Sakamoto M, Nakazawa R, Wada N. Relationship between spinal range of motion and trunk muscle activity during trunk rotation. *J Phys Ther Sci*. 2016;28(2):589-595. doi:10.1589/jpts.28.589
 139. Peharec S, Jerković R, Bacić P, Azman J, Bobinac D. Kinematic measurement of the lumbar spine and pelvis in the normal population. *Coll Antropol*. 2007;31(4):1039-1042. <http://www.ncbi.nlm.nih.gov/pubmed/18217455>
 140. Alemi MM, Burkhart KA, Lynch AC, et al. The Influence of Kinematic Constraints on Model Performance During Inverse Kinematics Analysis of the Thoracolumbar Spine. *Front Bioeng Biotechnol*. 2021;9(July):1-15. doi:10.3389/fbioe.2021.688041
 141. Frigo C, Carabalon R, Dalla Mura M, et al. The upper body segmental movements during walking by young females. *Clin Biomech (Bristol, Avon)*. 2003;18(5):419-425. doi:10.1016/S0268-0033(03)00028-7
 142. Kudo S, Fujimoto M, Sato T, Nagano A. Quantitative evaluation of linked rigid-body representations of the trunk. *Gait Posture*. 2018;63:119-123. doi:10.1016/j.gaitpost.2018.04.046
 143. Marich A V., Hwang CT, Salsich GB, Lang CE, Van Dillen LR. Consistency of a lumbar movement pattern across functional activities in people with low back pain. *Clin Biomech*. 2017;44:45-51. doi:10.1016/j.clinbiomech.2017.03.004

144. Papi E, Bull AMJ, McGregor AH. Spinal segments do not move together predictably during daily activities. *Gait Posture*. 2019;67:277-283.
doi:10.1016/j.gaitpost.2018.10.031
145. Seerden S, Dankaerts W, Vanwanseele B. Reliability of a multi-segmental kinematic model to analyse 3D movement in the lumbar spine. *Gait Posture*. 2016;49:53.
doi:10.1016/j.gaitpost.2016.07.117
146. Bagheri R, Takamjani IE, Dadgoo M, et al. A protocol for clinical trial study of the effect of core stabilization exercises on spine kinematics during gait with and without load in patients with non-specific chronic low back pain. *Chiropr Man Ther*. 2017;25(1):1-8. doi:10.1186/s12998-017-0162-y
147. Hooker QL, Lanier VM, van Dillen LR. Consistent differences in lumbar spine alignment between low back pain subgroups and genders during clinical and functional activity sitting tests. *Musculoskelet Sci Pract*. 2021;52(October 2020):102336.
doi:10.1016/j.msksp.2021.102336
148. Knechtle D, Schmid S, Suter M, et al. Fear-avoidance beliefs are associated with reduced lumbar spine flexion during object lifting in pain-free adults. *Pain*. 2021;162(6):1621-1631. doi:10.1097/j.pain.0000000000002170
149. Marich A V., Hwang CT, Sorensen CJ, van Dillen LR. Examination of the Lumbar Movement Pattern during a Clinical Test and a Functional Activity Test in People with and without Low Back Pain. *PM R*. 2020;12(2):140-146. doi:10.1002/pmrj.12197
150. Leardini A, Berti L, Begon M, Allard P. Effect of trunk sagittal attitude on shoulder, thorax and pelvis three-dimensional kinematics in able-bodied subjects during gait. *PLoS One*. 2013;8(10):1-7. doi:10.1371/journal.pone.0077168
151. Connolly M, Middleton K, Spence G, Cant O, Reid M. Effects of Lumbar Spine Abnormality and Serve Types on Lumbar Kinematics in Elite Adolescent Tennis Players. *Sport Med - Open*. 2021;7(1). doi:10.1186/s40798-020-00295-2
152. Tack P, Victor J, Gemmel P, Annemans L. 3D-printing techniques in a medical setting: A systematic literature review. *Biomed Eng Online*. 2016;15(1):1-21.
doi:10.1186/s12938-016-0236-4
153. Sun, Lau, Wong, Yeong. Personalized Three-Dimensional Printed Models in Congenital Heart Disease. *J Clin Med*. 2019;8(4):522. doi:10.3390/jcm8040522
154. Stefan P, Pfandler M, Lazarovici M, et al. Three-dimensional-Printed Computed Tomography-Based Bone Models for Spine Surgery Simulation. *Simul Healthc*. 2020;15(1):61-66. doi:10.1097/SIH.0000000000000417

155. Eltes PE, Kiss L, Bartos M, et al. Geometrical accuracy evaluation of an affordable 3D printing technology for spine physical models. *J Clin Neurosci*. 2020;72:438-446. doi:10.1016/j.jocn.2019.12.027
156. Tan LA, Yerneni K, Tuchman A, et al. Utilization of the 3D-printed spine model for freehand pedicle screw placement in complex spinal deformity correction. *J Spine Surg*. 2018;4(2):319-327. doi:10.21037/jss.2018.05.16
157. Bücking TM, Hill ER, Robertson JL, Maneas E, Plumb AA, Nikitichev DI. From medical imaging data to 3D printed anatomical models. *PLoS One*. 2017;12(5):1-10. doi:10.1371/journal.pone.0178540
158. Tejo-Otero A, Buj-Corral I, Fenollosa-Artés F. 3D Printing in Medicine for Preoperative Surgical Planning: A Review. *Ann Biomed Eng*. 2020;48(2):536-555. doi:10.1007/s10439-019-02411-0
159. Garg B, Mehta N. Current status of 3D printing in spine surgery. *J Clin Orthop Trauma*. 2018;9(3):218-225. doi:10.1016/j.jcot.2018.08.006
160. Senkoylu A, Daldal I, Cetinkaya M. 3D printing and spine surgery. *J Orthop Surg*. 2020;28(2):1-7. doi:10.1177/2309499020927081
161. Wu AM, Lin JL, Kwan KYH, Wang XY, Zhao J. 3D-printing techniques in spine surgery: the future prospects and current challenges. *Expert Rev Med Devices*. 2018;15(6):399-401. doi:10.1080/17434440.2018.1483234
162. Wilcox B, Mobbs RJ, Wu A-M, Phan K. Systematic review of 3D printing in spinal surgery: the current state of play. *J spine Surg (Hong Kong)*. 2017;3(3):433-443. doi:10.21037/jss.2017.09.01
163. Jones AC, Wilcox RK. Finite element analysis of the spine: Towards a framework of verification, validation and sensitivity analysis. *Med Eng Phys*. 2008;30(10):1287-1304. doi:10.1016/j.medengphy.2008.09.006
164. Little JP. *The Spine: Biomechanics and Subject-Specific Finite Element Models*. Elsevier Inc.; 2019. doi:10.1016/B978-0-12-816713-7.00022-2
165. Wang B, Ke W, Hua W, Zeng X, Yang C. Biomechanical Evaluation and the Assisted 3D Printed Model in the Patient-Specific Preoperative Planning for Thoracic Spinal Tuberculosis: A Finite Element Analysis. *Front Bioeng Biotechnol*. 2020;8(July):1-12. doi:10.3389/fbioe.2020.00807
166. Aroeira RMC, Pertence AE de M, Kemmoku DT, Greco M. Three-dimensional geometric model of the middle segment of the thoracic spine based on graphical images for finite element analysis. *Res Biomed Eng*. 2017;33(2):97-104.

- doi:10.1590/2446-4740.08916
167. Fagan MJ, Julian S, Mohsen AM. Finite element analysis in spine research. *Proc Inst Mech Eng Part H J Eng Med*. 2002;216(5):281-298. doi:10.1243/09544110260216568
 168. Zhang Z, Fogel GR, Liao Z, Sun Y, Liu W. Biomechanical analysis of lumbar interbody fusion cages with various lordotic angles: a finite element study. *Comput Methods Biomech Biomed Engin*. 2018;21(3):247-254. doi:10.1080/10255842.2018.1442443
 169. Dreischarf M, Zander T, Shirazi-Adl A, et al. Comparison of eight published static finite element models of the intact lumbar spine: Predictive power of models improves when combined together. *J Biomech*. 2014;47(8):1757-1766. doi:10.1016/j.jbiomech.2014.04.002
 170. Couvertier M, Germaneau A, Saget M, et al. Biomechanical analysis of the thoracolumbar spine under physiological loadings: Experimental motion data corridors for validation of finite element models. *Proc Inst Mech Eng Part H J Eng Med*. 2017;231(10):975-981. doi:10.1177/0954411917719740
 171. Wang T, Cai Z, Zhao Y, et al. Development of a three-dimensional finite element model of thoracolumbar kyphotic deformity following vertebral column decancellation. *Appl Bionics Biomech*. 2019;2019. doi:10.1155/2019/5109285
 172. Bridwell KH, Lenke LG, Cho SK, et al. Proximal junctional kyphosis in primary adult deformity surgery: Evaluation of 20 degrees as a critical angle. *Neurosurgery*. 2013;72(6):899-906. doi:10.1227/NEU.0b013e31828bacd8
 173. Buell TJ, Bess S, Xu M, et al. Optimal tether configurations and preload tensioning to prevent proximal junctional kyphosis: A finite element analysis. *J Neurosurg Spine*. 2019;30(5):574-584. doi:10.3171/2018.10.SPINE18429
 174. Mar DE, Burton DC, McIff TE. Biomechanics of Prophylactic Tethering for Proximal Junctional Kyphosis: Comparison of Posterior Tether Looping Techniques. *Spine Deform*. 2019;7(2):197-202. doi:10.1016/j.jspd.2018.07.001
 175. Park WM, Choi DK, Kim K, Kim YJ, Kim YH. Biomechanical effects of fusion levels on the risk of proximal junctional failure and kyphosis in lumbar spinal fusion surgery. *Clin Biomech*. 2015;30(10):1162-1169. doi:10.1016/j.clinbiomech.2015.08.009
 176. Bylski-Austrow DI, Glos DL, Bonifas AC, Carvalho MF, Coombs MC, Sturm PF. Flexible growing rods: A biomechanical pilot study of polymer rod constructs in the stability of skeletally immature spines. *Scoliosis Spinal Disord*. 2016;11(1). doi:10.1186/s13013-016-0087-6

177. Selim A, Mercer S. Polyetheretherketone (PEEK) rods for lumbar fusion: A systematic review and meta-analysis. *Int J Spine Surg*. 2018;12(2):190-200. doi:10.14444/5027
178. Rast FM, Graf ES, Meichtry A, Kool J, Bauer CM. Between-day reliability of three-dimensional motion analysis of the trunk: A comparison of marker based protocols. *J Biomech*. 2016;49(5):807-811. doi:10.1016/j.jbiomech.2016.02.030
179. Davis RB, Ounpuu S, Tyburski D, Gage JR. A Gait Analysis Data Collection and Reduction Technique. *Hum Mov Sci*. 1991;10:575-597.
180. Zemp R, List R, Gulay T, et al. Soft Tissue Artefacts of the Human Back : Comparison of the Sagittal Curvature of the Spine Measured Using Skin Markers and an Open Upright MRI. *PLoS One*. 2014;9(4):1-8. doi:10.1371/journal.pone.0095426
181. Lewis CL, Foch E, Luko MM, Loverro KL, Khuu A. Differences in Lower Extremity and Trunk Kinematics between Single Leg Squat and Step Down Tasks. Published online 2015:1-15. doi:10.1371/journal.pone.0126258
182. Szeto GPY, Wong KT, Law KY, Lee EWC. International Journal of Industrial Ergonomics A study of spinal kinematics in community nurses performing nursing tasks. *Int J Ind Ergon*. 2013;43(3):203-209. doi:10.1016/j.ergon.2013.02.003
183. Grood ES, Suntay WJ. A Joint Coordinate System for the Clinical Description of Three-Dimensional Motions: Application to the Knee. *J Biomech Eng*. 1983;105(2):136. doi:10.1115/1.3138397
184. Andriacchi TP, Alexander EJ. Studies of human locomotion: Past, present and future. *J Biomech*. 2000;33(10):1217-1224. doi:10.1016/S0021-9290(00)00061-0
185. Severijns P, Overbergh T, Schmid S, Moke L, Scheys L. Spinal Palpation Error and Its Impact on Skin Marker-Based Spinal Alignment Measurement in Adult Spinal Deformity. *Front Bioeng Biotechnol*. 2021;9(June):1-9. doi:10.3389/fbioe.2021.687323
186. Visscher RMS, Freslier M, Moissenet F, et al. Impact of the Marker Set Configuration on the Accuracy of Gait Event Detection in Healthy and Pathological Subjects. *Front Hum Neurosci*. 2021;15(September):1-7. doi:10.3389/fnhum.2021.720699
187. Della Croce U, Leardini A, Chiari L, Cappozzo A. Human movement analysis using stereophotogrammetry Part 4: Assessment of anatomical landmark misplacement and its effects on joint kinematics. *Gait Posture*. 2005;21(2):226-237. doi:10.1016/j.gaitpost.2004.05.003
188. Scalona E, Di Marco R, Castelli E, et al. Inter-laboratory and inter-operator reproducibility in gait analysis measurements in pediatric subjects. *Int Biomech*.

- 2019;6(1):19-33. doi:10.1080/23335432.2019.1621205
189. Kaufman K, Miller E, Kingsbury T, et al. Reliability of 3D gait data across multiple laboratories. *Gait Posture*. 2016;49:375-381. doi:10.1016/j.gaitpost.2016.07.075
 190. Acaroglu E. Decision-making in the treatment of adult spinal deformity. *EFORT Open Rev*. 2016;1(5):167-176. doi:10.1302/2058-5241.1.000013
 191. Ham DW, Han H, Kim HJ, Park SM, Chang BS, Yeom JS. Risk factors for acute proximal junctional kyphosis after adult spinal deformity surgery in preoperative motion analysis. *Eur Spine J*. 2021;30(5):1215-1225. doi:10.1007/s00586-021-06830-3
 192. Yagi M, Akilah KB, Boachie-Adjei O. Incidence, risk factors and classification of proximal junctional kyphosis: surgical outcomes review of adult idiopathic scoliosis. *Spine (Phila Pa 1976)*. 2011;36(1):E60-8. doi:10.1097/BRS.0b013e3181eeae2
 193. Kim DK, Kim JY, Kim DY, Rhim SC, Yoon SH. Risk factors of proximal junctional kyphosis after multilevel fusion surgery: More than 2 years follow-up data. *J Korean Neurosurg Soc*. 2017;60(2):174-180. doi:10.3340/jkns.2016.0707.014
 194. Protosaltis TS, Schwab FJ, Smith JS, et al. The T1 pelvic angle (TPA), a novel radiographic parameter of sagittal deformity, correlates strongly with clinical measures of disability. *Spine J*. 2013;13(9):S61.
 195. Yilgor C, Sogunmez N, Yavuz Y, et al. Global alignment and proportion (GAP) score: development and validation of a new method of analyzing spinopelvic alignment to predict mechanical complications after adult spinal deformity surgery. *Spine J*. 2017;17(10):S155-S156.
 196. Wong TKT, Lee RYW. Effects of low back pain on the relationship between the movements of the lumbar spine and hip. *Hum Mov Sci*. 2004;23(1):21-34. doi:10.1016/j.humov.2004.03.004
 197. Laird RA, Keating JL, Ussing K, Li P, Kent P. Does movement matter in people with back pain? Investigating “atypical” lumbo-pelvic kinematics in people with and without back pain using wireless movement sensors. *BMC Musculoskelet Disord*. 2019;20(1):1-15. doi:10.1186/s12891-018-2387-x
 198. Endo T, Shirado O, Tominaga R, et al. Maximum gait speed and lumbar spinal mobility can affect quality of life in elderly women with lumbar kyphosis. *North Am Spine Soc J*. 2022;9(December 2021):100100. doi:10.1016/j.xnsj.2022.100100
 199. Sullivan MS, Shoaf LD, Riddle DL. The relationship of lumbar flexion to disability in patients with low back pain. *Phys Ther*. 2000;80(3):240-250. doi:10.1093/ptj/80.3.240

200. Lee SH, Lee JC, Tauchi R, Daniel Riew K. Influence of the Number of Cervical Fusion Levels on Cervical Spine Motion and Health-Related Quality of Life. *Spine (Phila Pa 1976)*. 2016;41(8):E474-E480. doi:10.1097/BRS.0000000000001299
201. Eyvazov K, Samartzis D, Cheung JPY. The association of lumbar curve magnitude and spinal range of motion in adolescent idiopathic scoliosis: a cross-sectional study. *BMC Musculoskelet Disord*. 2017;18(1):1-9. doi:10.1186/s12891-017-1423-6
202. Galvis S, Burton D, Barnds B, et al. The effect of scoliotic deformity on spine kinematics in adolescents. *Scoliosis spinal Disord*. 2016;11:42. doi:10.1186/s13013-016-0103-x
203. Basques BA, Espinoza Orías AA, Shifflett GD, et al. The Kinematics and Spondylosis of the Lumbar Spine Vary Depending on the Levels of Motion Segments in Individuals With Low Back Pain. *Spine (Phila Pa 1976)*. 2017;42(13):E767-E774. doi:10.1097/BRS.0000000000001967
204. Liebsch C, Jonas R, Wilke HJ. Thoracic spinal kinematics is affected by the grade of intervertebral disc degeneration, but not by the presence of the ribs: An in vitro study. *Spine J*. 2020;20(3):488-498. doi:10.1016/j.spinee.2019.10.006
205. Shum GLK, Crosbie J, Lee RYW. Movement coordination of the lumbar spine and hip during a picking up activity in low back pain subjects. *Eur Spine J*. 2007;16(6):749-758. doi:10.1007/s00586-006-0122-z
206. Johnson JM, Mahfouz M, Battaglia N V., Sharma A, Cheng JS, Komistek RD. Clinical and statistical correlation of various lumbar pathological conditions. *J Biomech*. 2013;46(4):683-688. doi:10.1016/j.jbiomech.2012.11.043
207. Widmer J, Fornaciari P, Senteler M, Roth T, Snedeker JG, Farshad M. Kinematics of the Spine Under Healthy and Degenerative Conditions: A Systematic Review. *Ann Biomed Eng*. 2019;47(7):1491-1522. doi:10.1007/s10439-019-02252-x
208. Zhang BL, Huang W, Xia H, Feng X. Kinematic characteristics of lumbar spinous processes during axial rotation in patients with lumbar degenerative disc disease lateral lumbar interbody fusion and intervention. *BMC Musculoskelet Disord*. 2017;18(1):1-9. doi:10.1186/s12891-017-1504-6
209. Overbergh T, Severijns P, Beaucage-Gauvreau E, et al. Subject-Specific Spino-Pelvic Models Reliably Measure Spinal Kinematics During Seated Forward Bending in Adult Spinal Deformity. *Front Bioeng Biotechnol*. 2021;9(September):1-11. doi:10.3389/fbioe.2021.720060
210. Valasek T, Varga PP, Szövérfi Z, Kümin M, Fairbank J, Lazary A. Reliability and

- validity study on the Hungarian versions of the Oswestry Disability Index and the Quebec Back Pain Disability Scale. *Eur Spine J.* 2013;22(5):1010-1018.
211. Bess S, Protopsaltis TS, Lafage V, et al. Clinical and radiographic evaluation of adult spinal deformity. *J Spinal Disord Tech.* 2016;29(1):6-16.
 212. Le Huec JC, Thompson W, Mohsinaly Y, Barrey C, Faundez A. Sagittal balance of the spine. *Eur Spine J.* 2019;28(9):1889-1905. doi:10.1007/s00586-019-06083-1
 213. Ailon T, Smith JS, Shaffrey CI, et al. Degenerative spinal deformity. *Neurosurgery.* 2015;77(suppl_1):S75-S91.
 214. Lafage R, Schwab F, Challier V, et al. Defining Spino-pelvic alignment thresholds: should operative goals in adult spinal deformity surgery account for age? *Spine (Phila Pa 1976).* 2016; 41 (1): 62–8.
 215. Aryanto KYE, Oudkerk M, van Ooijen PMA. Free DICOM de-identification tools in clinical research: functioning and safety of patient privacy. *Eur Radiol.* 2015;25(12):3685-3695. doi:10.1007/s00330-015-3794-0
 216. Bozic KJ, Keyak JH, Skinner HB, Bueff HU, Bradford DS. Three-dimensional finite element modeling of a cervical vertebra: an investigation of burst fracture mechanism. *J Spinal Disord.* 1994;7(2):102-110.
 217. Kikinis R, Pieper SD, Vosburgh KG. 3D Slicer: A Platform for Subject-Specific Image Analysis, Visualization, and Clinical Support. In: *Intraoperative Imaging and Image-Guided Therapy.* Springer New York; 2014:277-289. doi:10.1007/978-1-4614-7657-3_19
 218. Zou KH, Warfield SK, Bharatha A, et al. Statistical Validation of Image Segmentation Quality Based on a Spatial Overlap Index. *Acad Radiol.* 2004;11(2):178-189. doi:10.1016/S1076-6332(03)00671-8
 219. Cignoni P, Callieri M, Corsini M, Dellepiane M, Ganovelli F, Ranzuglia G. Meshlab: an open-source mesh processing tool. In: *Eurographics Italian Chapter Conference.* Vol 2008. ; 2008:129-136.
 220. Rocchi MBL, Sisti D, Benedetti P, Valentini M. Critical comparison of nine different self-administered questionnaires for the evaluation of disability caused by low back pain. *Eur J Phys Rehabil Med.* 2005;41(4):275.
 221. Zheng Y, Yu D, Zhao J, Wu Y, Zheng B. 3D Printout Models vs. 3D-Rendered Images: Which Is Better for Preoperative Planning? *J Surg Educ.* 2016;73(3):518-523. doi:10.1016/J.JSURG.2016.01.003
 222. Wijntjes MWA, Volcic R, Pont SC, Koenderink JJ, Kappers AML. Haptic perception

- disambiguates visual perception of 3D shape. *Exp brain Res*. 2009;193(4):639-644.
223. Norman JF, Norman HF, Clayton AM, Lianekhammy J, Zielke G. The visual and haptic perception of natural object shape. *Percept Psychophys*. 2004;66(2):342-351.
224. Norman JF, Clayton AM, Norman HF, Crabtree CE. Learning to perceive differences in solid shape through vision and touch. *Perception*. 2008;37(2):185-196.
225. Eltes PE, Kiss L, Bartos M, et al. Attitude of spine surgeons towards the application of 3D technologies-a survey of AOSpine members. *Ideggyogy Sz*. 2019;72(7-8):227-235.
226. Chepelev L, Wake N, Ryan J, et al. Radiological Society of North America (RSNA) 3D printing Special Interest Group (SIG): guidelines for medical 3D printing and appropriateness for clinical scenarios. *3D Print Med*. 2018;4(1):1-38.
227. Shirazi-Adl SA, Shrivastava SC, Ahmed AM. Stress analysis of the lumbar disc-body unit in compression. A three-dimensional nonlinear finite element study. *Spine (Phila Pa 1976)*. 1984;9(2):120-134. doi:10.1097/00007632-198403000-00003
228. Baroud G, Nemes J, Heini P, Steffen T. Load shift of the intervertebral disc after a vertebroplasty: a finite-element study. *Eur spine J Off Publ Eur Spine Soc Eur Spinal Deform Soc Eur Sect Cerv Spine Res Soc*. 2003;12(4):421-426. doi:10.1007/s00586-002-0512-9
229. Remus R, Lipphaus A, Neumann M, Bender B. Calibration and validation of a novel hybrid model of the lumbosacral spine in ArtiSynth–The passive structures. *PLoS One*. 2021;16(4):e0250456. doi:10.1371/JOURNAL.PONE.0250456
230. Zeng ZL, Zhu R, Wu YC, et al. Effect of Graded Facetectomy on Lumbar Biomechanics. *J Healthc Eng*. 2017;2017. doi:10.1155/2017/7981513
231. Park WM, Kim K, Kim YH. Effects of degenerated intervertebral discs on intersegmental rotations, intradiscal pressures, and facet joint forces of the whole lumbar spine. *Comput Biol Med*. 2013;43(9):1234-1240. doi:10.1016/j.combiomed.2013.06.011
232. Noailly J, Wilke HJ, Planell JA, Lacroix D. How does the geometry affect the internal biomechanics of a lumbar spine bi-segment finite element model? Consequences on the validation process. *J Biomech*. 2007;40(11):2414-2425. doi:10.1016/J.JBIOMECH.2006.11.021
233. White AA, Panjabi MM. *Clinical Biomechanics of the Spine*. Lippincott; 1990.
234. Shirazi-Adl A, Ahmed AM, Shrivastava SC. Mechanical response of a lumbar motion segment in axial torque alone and combined with compression. *Spine (Phila Pa 1976)*. 1986;11(9):914-927. doi:10.1097/00007632-198611000-00012

235. Rohlmann A, Zander T, Schmidt H, Wilke HJ, Bergmann G. Analysis of the influence of disc degeneration on the mechanical behaviour of a lumbar motion segment using the finite element method. *J Biomech.* 2006;39(13):2484-2490.
doi:10.1016/J.JBIOMECH.2005.07.026
236. Li J, Shang J, Zhou Y, Li C, Liu H. Finite Element Analysis of a New Pedicle Screw-Plate System for Minimally Invasive Transforaminal Lumbar Interbody Fusion. *PLoS One.* 2015;10(12). doi:10.1371/journal.pone.0144637
237. Finley SM, Brodke DS, Spina NT, et al. FEBio finite element models of the human lumbar spine. *Comput Methods Biomech Biomed Engin.* 2018;21(6):444-452.
doi:10.1080/10255842.2018.1478967
238. Schmidt H, Heuer F, Drumm J, Klezl Z, Claes L, Wilke H-JJ. Application of a calibration method provides more realistic results for a finite element model of a lumbar spinal segment. *Clin Biomech.* 2007;22(4):377-384.
doi:10.1016/j.clinbiomech.2006.11.008
239. Schmidt H, Heuer F, Simon U, et al. Application of a new calibration method for a three-dimensional finite element model of a human lumbar annulus fibrosus. *Clin Biomech.* 2006;21(4):337-344. doi:10.1016/j.clinbiomech.2005.12.001
240. Lu Y, Rosenau E, Paetzold H, et al. Strain changes on the cortical shell of vertebral bodies due to spine ageing: A parametric study using a finite element model evaluated by strain measurements. *Proc Inst Mech Eng Part H J Eng Med.* 2013;227(12):1265-1274. doi:10.1177/0954411913501293
241. Rohlmann A, Bauer L, Zander T, Bergmann G, Wilke HJ. Determination of trunk muscle forces for flexion and extension by using a validated finite element model of the lumbar spine and measured in vivo data. *J Biomech.* 2006;39(6):981-989.
doi:10.1016/J.JBIOMECH.2005.02.019
242. Wilke HJ, Herkommer A, Werner K, Liebsch C. In vitro analysis of the segmental flexibility of the thoracic spine. *PLoS One.* 2017;12(5).
doi:10.1371/JOURNAL.PONE.0177823
243. Couvertier M, Germaneau A, Saget M, et al. Biomechanical analysis of the thoracolumbar spine under physiological loadings: Experimental motion data corridors for validation of finite element models. *Proc Inst Mech Eng Part H J Eng Med.* 2017;231(10):975-981. doi:10.1177/0954411917719740
244. Rohlmann A, Neller S, Claes L, Bergmann G, Wilke H. Influence of a follower load on intradiscal pressure and intersegmental rotation of the lumbar spine. *Spine (Phila*

- Pa 1976*). 2001;26(24):557-561.
245. Panjabi MM. Hybrid multidirectional test method to evaluate spinal adjacent-level effects. *Clin Biomech*. 2007;22(3):257-265.
doi:10.1016/J.CLINBIOMECH.2006.08.006
 246. Kim YJ, Bridwell KH, Lenke LG, Glattes CR, Rhim S, Cheh G. Proximal junctional kyphosis in adult spinal deformity after segmental posterior spinal instrumentation and fusion: Minimum five-year follow-up. *Spine (Phila Pa 1976)*. 2008;33(20):2179-2184.
doi:10.1097/BRS.0b013e31817c0428
 247. Bess S, Harris JE, Turner AWL, et al. The effect of posterior polyester tethers on the biomechanics of proximal junctional kyphosis: A finite element analysis. *J Neurosurg Spine*. 2017;26(1):125-133. doi:10.3171/2016.6.SPINE151477
 248. Yagi M, Akilah KB, Boachie-Adjei O. Incidence, risk factors and classification of proximal junctional kyphosis: Surgical outcomes review of adult idiopathic scoliosis. *Spine (Phila Pa 1976)*. 2011;36(1). doi:10.1097/BRS.0b013e3181eeae2
 249. Annis P, Lawrence B, Spiker W, et al. Predictive Factors for Acute Proximal Junctional Failure after Adult Deformity Surgery with Upper Instrumented Vertebrae in the Thoracolumbar Spine. *Evid Based Spine Care J*. 2014;05(02):160-162.
doi:10.1055/s-0034-1386755
 250. Ghobrial GM, Eichberg DG, Kolcun JPG, et al. Prophylactic vertebral cement augmentation at the uppermost instrumented vertebra and rostral adjacent vertebra for the prevention of proximal junctional kyphosis and failure following long-segment fusion for adult spinal deformity. *Spine J*. 2017;17(10):1499-1505.
doi:10.1016/j.spinee.2017.05.015
 251. Guevara-Villazón F, Boissiere L, Hayashi K, et al. Multiple-rod constructs in adult spinal deformity surgery for pelvic-fixated long instrumentations: an integral matched cohort analysis. *Eur Spine J*. 2020;29(4):886-895. doi:10.1007/s00586-020-06311-z
 252. Cammarata M, Aubin CÉ, Wang X, Mac-Thiong JM. Biomechanical risk factors for proximal junctional kyphosis: A detailed numerical analysis of surgical instrumentation variables. *Spine (Phila Pa 1976)*. 2014;39(8):E500-E507.
doi:10.1097/BRS.0000000000000222
 253. Song M, Sun K, Li Z, et al. Stress distribution of different lumbar posterior pedicle screw insertion techniques: a combination study of finite element analysis and biomechanical test. *Sci Rep*. 2021;11(1):1-15. doi:10.1038/s41598-021-90686-6
 254. Zhu W-Y, Zang L, Li J, Guan L, Hai Y. A biomechanical study on proximal junctional

- kyphosis following long-segment posterior spinal fusion. *Brazilian J Med Biol Res = Rev Bras Pesqui medicas e Biol.* 2019;52(5):e7748. doi:10.1590/1414-431X20197748
255. Varga PP, Lazary A. Chordoma of the sacrum: “En bloc” high partial sacrectomy. *Eur Spine J.* 2010;19(6):1037-1038. doi:10.1007/s00586-010-1459-x
 256. Disler DG, Miklic D. Imaging findings in tumors of the sacrum. *AJR Am J Roentgenol.* 1999;173(6):1699-1706. doi:10.2214/ajr.173.6.10584822
 257. Smith JA, Tuchman A, Huoh M, Kaiser AM, Schooler WG, Hsieh PC. Locomotor biomechanics after total sacrectomy: A case report. *Spine (Phila Pa 1976)*. Published online 2014. doi:10.1097/BRS.0000000000000594
 258. Varga PP, Szövérfi Z, Lazary A. Surgical treatment of primary malignant tumors of the sacrum. *Neurol Res.* Published online 2014. doi:10.1179/1743132814y.0000000366
 259. Fourney DR, Rhines LD, Hentschel SJ, et al. En bloc resection of primary sacral tumors: classification of surgical approaches and outcome. *J Neurosurg Spine.* 2005;3(2):111-122. doi:10.3171/spi.2005.3.2.0111
 260. Zoccali C, Skoch J, Patel AS, Walter CM, Maykowski P, Baaj AA. Residual neurological function after sacral root resection during en-bloc sacrectomy: a systematic review. *Eur Spine J.* 2016;25(12):3925-3931. doi:10.1007/s00586-016-4450-3
 261. Varga PP, Szoverfi Z, Lazary A. Surgical resection and reconstruction after resection of tumors involving the sacropelvic region. *Neurol Res.* 2014;36(6):588-596. doi:10.1179/1743132814Y.0000000370
 262. Zileli M, Hoscokun C, Brastianos P, Sabah D. Surgical treatment of primary sacral tumors: complications associated with sacrectomy. *Neurosurg Focus.* 2003;15(5):E9.
 263. Varga PP, Bors I, Lazary A. 1. Varga PP, Bors I, Lazary A. Sacral Tumors and Management. *Orthop Clin North Am.* 2009;40(1):105-123. doi:10.1016/J.OCL.2008.09.010 Sacral Tumors and Management. *Orthop Clin North Am.* 2009;40(1):105-123. doi:10.1016/J.OCL.2008.09.010
 264. Eltes PE, Turbucz M, Fayad J, et al. A Novel Three-Dimensional Computational Method to Assess Rod Contour Deformation and to Map Bony Fusion in a Lumbopelvic Reconstruction After En-Bloc Sacrectomy. *Front Surg.* 2022;8(January):1-13. doi:10.3389/fsurg.2021.698179
 265. Varga PP, Szoverfi Z, Lazary A. Surgical resection and reconstruction after resection of tumors involving the sacropelvic region. *Neurol Res.* Published online 2014.

- doi:10.1179/1743132814y.0000000370
266. Aebi M, Gunzburg R. OOT: The Open Operating Theatre. *Eur Spine J*. 2011;20(6):825-825. doi:10.1007/s00586-011-1832-4
 267. Varga PP, Lazary A. Chordoma of the sacrum: “en bloc” total sacrectomy and lumbopelvic reconstruction. *Eur Spine J*. 2010;19(6):1039-1040. doi:10.1007/s00586-010-1460-4
 268. Bovi G, Rabuffetti M, Mazzoleni P, Ferrarin M. A multiple-task gait analysis approach: Kinematic, kinetic and EMG reference data for healthy young and adult subjects. *Gait Posture*. 2011;33(1):6-13. doi:10.1016/j.gaitpost.2010.08.009
 269. Zou KH, Warfield SK, Bharatha A, et al. Statistical validation of image segmentation quality based on a spatial overlap index1: scientific reports. *Acad Radiol*. 2004;11(2):178-189. doi:https://doi.org/10.1016/S1076-6332(03)00671-8
 270. Evans JD. *Straightforward Statistics for the Behavioral Sciences*. Thomson Brooks/Cole Publishing Co; 1996.
 271. Yao J, Burns JE, Forsberg D, et al. A multi-center milestone study of clinical vertebral CT segmentation. *Comput Med Imaging Graph*. 2016;49:16-28. doi:10.1016/j.compmedimag.2015.12.006
 272. Hayashi T, Chen H, Miyamoto K, et al. A computerized scheme for localization of vertebral bodies on body CT scans. In: *Medical Imaging 2011: Image Processing*. Vol 7962. International Society for Optics and Photonics; 2011:796238.
 273. Koo TK, Li MY. A Guideline of Selecting and Reporting Intraclass Correlation Coefficients for Reliability Research. *J Chiropr Med*. 2016;15(2):155-163. doi:10.1016/j.jcm.2016.02.012
 274. Soh SH, Rafferty K, Herring S. Cyclic loading effects on craniofacial strain and sutural growth in pigs. *Am J Orthod Dentofac Orthop*. 2018;154(2):270-282. doi:10.1016/j.ajodo.2017.11.036
 275. Clark AJ, Tang JA, Leasure JM, et al. Gait-simulating fatigue loading analysis and sagittal alignment failure of spinal pelvic reconstruction after total sacrectomy: comparison of 3 techniques. *J Neurosurg Spine*. 2014;20(4):364-370.
 276. Perren SM. Evolution of the internal fixation of long bone fractures: the scientific basis of biological internal fixation: choosing a new balance between stability and biology. *J Bone Joint Surg Br*. 2002;84(8):1093-1110.
 277. Bottlang M, Doornink J, Lujan TJ, et al. AAOS Supplement Selected Scientific Exhibits: Effects of Construct Stiffness on Healing of Fractures Stabilized with

- Locking Plates. *J Bone Jt Surgery Am Vol.* 2010;92(Suppl 2):12.
278. Potter BK. From Bench to Bedside: How stiff is too stiff? Far-cortical locking or dynamic locked plating may obviate the question. *Clin Orthop Relat Res.* 2016;474(7):1571-1573.
279. Henderson CE, Lujan TJ, Kuhl LL, Bottlang M, Fitzpatrick DC, Marsh JL. 2010 mid-America Orthopaedic Association Physician in Training Award: healing complications are common after locked plating for distal femur fractures. *Clin Orthop Relat Res.* 2011;469(6):1757-1765.
280. Holzman MA, Hanus BD, Munz JW, O'Connor DP, Brinker MR. Addition of a medial locking plate to an in situ lateral locking plate results in healing of distal femoral nonunions. *Clin Orthop Relat Res.* 2016;474(6):1498-1505.
281. Rodriguez EK, Zurakowski D, Herder L, et al. Mechanical construct characteristics predisposing to non-union after locked lateral plating of distal femur fractures. *J Orthop Trauma.* 2016;30(8):403-408.
282. Yoshihara H. Rods in spinal surgery: a review of the literature. *Spine J.* 2013;13(10):1350-1358.
283. Craven TG, Carson WL, Asher MA, Robinson RG. The effects of implant stiffness on the bypassed bone mineral density and facet fusion stiffness of the canine spine. *Spine (Phila Pa 1976).* 1994;19(15):1664-1673.
284. Luca A, Ottardi C, Sasso M, et al. Instrumentation failure following pedicle subtraction osteotomy: the role of rod material, diameter, and multi-rod constructs. *Eur Spine J.* 2017;26(3):764-770.
285. La Barbera L, Brayda-Bruno M, Liebsch C, et al. Biomechanical advantages of supplemental accessory and satellite rods with and without interbody cages implantation for the stabilization of pedicle subtraction osteotomy. *Eur spine J.* 2018;27(9):2357-2366.
286. La Barbera L, Wilke H-J, Liebsch C, et al. Biomechanical in vitro comparison between anterior column realignment and pedicle subtraction osteotomy for severe sagittal imbalance correction. *Eur Spine J.* 2020;29(1):36-44.
287. Hay O, Dar G, Abbas J, et al. The lumbar lordosis in males and females, revisited. *PLoS One.* 2015;10(8):1-17. doi:10.1371/journal.pone.0133685
288. Anderson DD, Thomas TP, Marin AC, Elkins JM, Lack WD, Lacroix D. Computational techniques for the assessment of fracture repair. *Injury.* 2014;45:S23-S31.

289. Huang S, Ji T, Guo W. Biomechanical comparison of a 3D-printed sacrum prosthesis versus rod-screw systems for reconstruction after total sacrectomy: A finite element analysis. *Clin Biomech.* 2019;70:203-208.